Ultrafast spin dynamics in ferromagnetic thin films

Jerome Hurst

UNIVERSITÉ DE STRASBOURG

ÉCOLE DOCTORALE **Physique et Chimie-Physique (ED182)**

Institut de Physique et Chimie des Matériaux de Strasbourg

UMR 7504

THÈSE présentée par :

Jérôme HURST

soutenue le : **17 mai 2017**

pour obtenir le grade de : **Docteur de l'université de Strasbourg**

Discipline/ Spécialité : Physique de la matière condensée

Ultrafast spin dynamics in ferromagnetic thin films

THÈSE dirigée par :

M. HERVIEUX Paul-Antoine	Professeur, Université de Strasbourg - IPCMS
M. MANFREDI Giovanni	Directeur de recherche, IPCMS

RAPPORTEURS :

M. OPPENEER Peter	Professeur, Université de Uppsala
M. PONS Bernard	Professeur, Université de Bordeaux - CELIA

AUTRES MEMBRES DU JURY :

M. MERDJI Hamed	Ingénieur de recherche, CEA - LIDYL
M. HERTEL Ricardo	Directeur de recherche, IPCMS

Résumé en Français de la thèse

Dans cette thèse, on s'intéresse à la modélisation théorique et à la simulation numérique de la dynamique de charges et de spins dans des nano-structures métalliques. Ces dernières années, la physique des nano-structures métalliques a connu un intérêt scientifique croissant, aussi bien d'un point de la physique fondamentale que d'un point de vue des applications technologiques. Des nano-structures métalliques sont utilisées aujourd'hui dans le domaine de la nano-photonique, de la chime et même de la biologie et de la médecine. Il est donc essentiel d'avoir des modèles théoriques nous permettant de décrire correctement de tels objets. Cette thèse comporte deux études distinctes. La première, constituée des chapitres 1 à 4, porte sur la dynamique ultra-rapide de spins dans des films ferromagnétiques de Nickel. Ces derniers sont en interaction avec un champ laser intense sur des échelles de temps très courtes de l'ordre de la dizaine - centaine de femtosecondes. De telles études ont déjà été réalisées auparavant sur des films de Sodium, mais en considérant uniquement les interactions électrostatiques. Dans ces travaux, on souhaiterait également inclure les aspects magnétiques en tenant compte du spin et des couplages qu'il induit sur la dynamique électronique. Un exemple bien connu d'un tel couplage est le couplage spin-orbite. La seconde partie, constituée du chapitre 5, porte sur sur la dynamique de charge (sans spin) d'électrons confinés dans des nano-particules d'Or ou bien encore par des potentiels anisotropes. On s'intéresse particulièrement à la réponse dipolaire induite par une excitation laser auto-résonante.

Chapitre 1

Le premier chapitre de ma thèse est constitué de cinq parties et constitue une introduction aux différents modèles physiques permettant d'étudier la dynamique quantique non-linéaire d'un système d'électrons en interaction. Ce chapitre ne concerne que la dynamique de charge, le spin est volontairement mis de coté et sera traité dans le second chapitre.

Dans la première partie, je décris les différentes grandeurs physiques qui caractérisent les électrons de conduction dans les métaux. Ces dernières sont: La fréquence plasma $\omega_p = \sqrt{e^2 n/m\epsilon_0}$ dont l'inverse correspond au temps typique de mouvement des électrons, la densité de charge n qui est directement relié au rayon de Wigner-Seitz r_s et la longueur d'onde de DeBroglie $\lambda_{\text{DB}} = \hbar/p$ qui est relié à l'extension spatiale des fonctions d'ondes électroniques. Dans la table 1, on donne

r_s	$0.16\,\mathrm{nm}$
n	$5.9 \times 10^{28}\,\mathrm{m}^{-3}$
T	$300\,\mathrm{K}$
ω_p^{-1}	$0.5\,\mathrm{fs}$
T_F	$64000\,\mathrm{K}$
v_F	$1.4 \times 10^6\,\mathrm{m/s}$
λ_F	$0.11\,\mathrm{nm}$
γ_q	5.5

TABLE 1: Paramètres physiques pour les électrons de conduction de l'Or ($T = 300\,\mathrm{K}$)

une application numérique pour les électrons de conduction de l'Or. La conclusion principale de cette partie est que les électrons dans les métaux doivent être traité comme un plasma quantique confiné par le potentiel des ions. Les ions n'ont pas de dynamique orbitale car on travaille sur des échelles de temps de l'ordre de la femtoseconde (10^{-15} s) alors que le temps typique de mouvement des ions est de l'ordre de la picoseconde (10^{-12} s).

Dans la seconde partie du chapitre, je présente le formalisme de Schrödinger de la mécanique quantique et je discute de l'approximation du champ moyen. Cette dernière étant utilisée dans la suite de la thèse. Je présente notamment les équations de Hatree et les équations de Hartre-Fock. Une discussion sur le traitement de l'échange et des corrélations ainsi que sur des modèles plus sophistiqués du type DFT/TDDFT figure également dans cette partie.

La troisième partie de la thèse est une introduction à la formulation de Wigner de la mécanique quantique ou encore appelé formulation de la mécanique quantique dans l'espace des phases. Dans cette partie j'introduis la transformation de Weyl qui permet d'associer à chaque opérateur de la mécanique quantique une fonction des variables $\boldsymbol{r}$ (position) et $\boldsymbol{p}$ (impulsion) définit dans l'espace des phase. Dans ce formalisme la fonction de Wigner, notée f, est la transformée de Weyl de l'opérateur densité. Elle s'exprime de la manière suivante:

$$f\left(\boldsymbol{r},\boldsymbol{p},t\right)=\frac{1}{\left(2\pi\hbar\right)^3}\sum_{\alpha=1}^{N}p_\alpha\int d\lambda\exp\left(\frac{i\boldsymbol{p}\cdot\boldsymbol{\lambda}}{\hbar}\right)\Psi_\alpha^*\left(\boldsymbol{r}+\frac{\boldsymbol{\lambda}}{2},t\right)\Psi_\alpha\left(\boldsymbol{r}-\frac{\boldsymbol{\lambda}}{2},t\right), \quad (1)$$

où les quantités $\Psi_\alpha\left(\boldsymbol{r},t\right)$ correspondent aux différentes fonctions d'ondes du système d'électrons en interaction et traités dans l'approximation du champ moyen. La fonction de Wigner obéit à l'équation d'évolution suivante:

$$i\hbar\frac{\partial f}{\partial t}=\left\{\mathcal{H},f\right\}_\star, \quad (2)$$

où $\mathcal{H}$ est la fonction dans l'espace des phases associée à l'opérateur Hamiltonien

du système. L'équation (2) est appelée équation de Wigner. L'équation de Wigner est l'analogue de l'équation d'évolution de la matrice densité: $i\hbar\partial_t\widehat{\rho} = \left[\widehat{\mathcal{H}}, \widehat{\rho}\right]$ et également appelée équation de Von Neumann. Le terme de droite de l'équation précédente correspond au crochet de Moyal. Ce dernier a l'avantage de pouvoir s'écrire en une série de termes en puissance de $\hbar$. En particulier, le terme d'ordre zero correspond au crochet de Poisson qui est utilisé en mécanique classique. On montre dans cette partie que dans la limite classique ($\hbar \to 0$), l'équation de Wigner (2) se réduit à l'équation de Vlasov:

$$\frac{\partial f}{\partial t} + \boldsymbol{v} \cdot \boldsymbol{\nabla} f + \frac{e}{m} \boldsymbol{\nabla} V_{\mathrm{H}} \cdot \boldsymbol{\nabla}_{\boldsymbol{p}} f = 0, \tag{3}$$

où V_{H} est le potentiel d'Hartree qui est solution de l'équation de Poisson. Cette partie comporte également une discussion sur l'incorporation d'un champ magnétique dans l'équation de Wigner et du problème de l'invariance de jauge. En particulier, on montre qu'il faut redéfinir le crochet de Moyal et la fonction de Wigner afin d'avoir une équation de Wigner qui soit indépendante de la jauge électromagnétique.

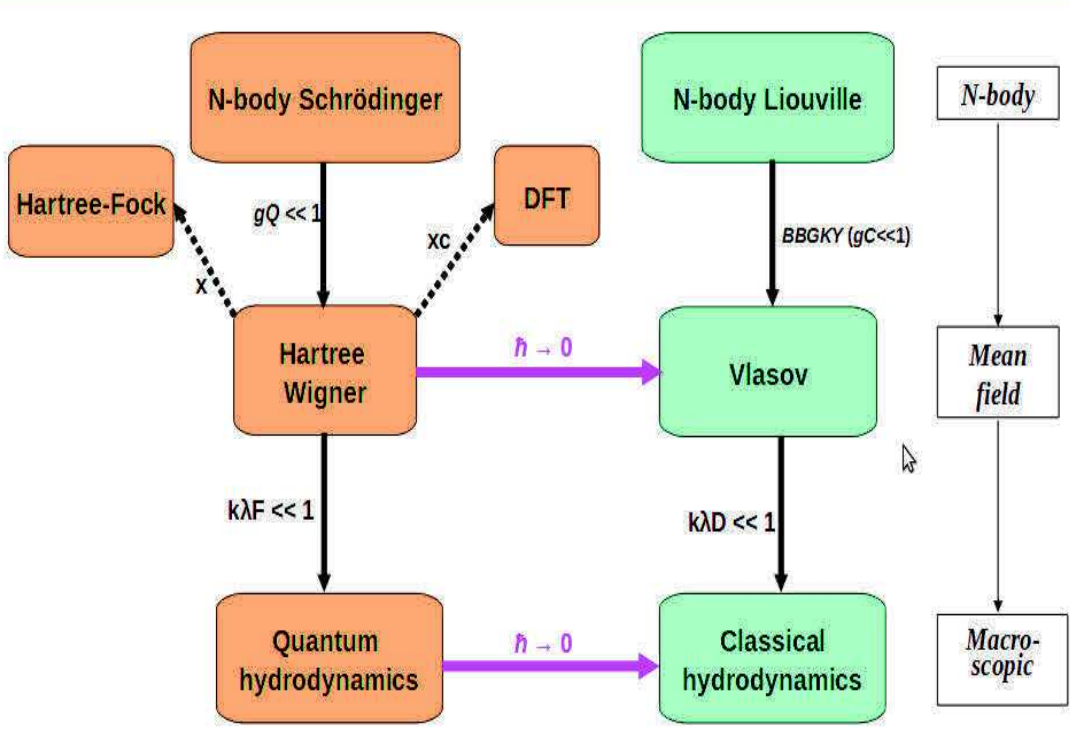

FIGURE 1: Schéma des différents modèles physiques décrivant la dynamique d'un gaz d'électrons en interaction, ainsi que les limites de validité des différents modèles. Les paramètres gC et gQ représentent, respectivement, les paramètres de couplage classiques et quantiques d'un plasma.

La quatrième partie du chapitre 1 porte sur la construction de modèles fluides

classiques et quantiques à partir des équations de Vlasov et de Wigner. Les équations fluides décrivent l'évolution de variables hydrodynamiques tels que la densité de charge: $n = \int f d\boldsymbol{v}$, la vitesse moyenne des électrons: $\boldsymbol{j} = \int \boldsymbol{v} f d\boldsymbol{v}/n$ ou encore le tenseur de pression: $p_{ij} = \int w_i w_j f d\boldsymbol{v}$ ($\boldsymbol{w} = \boldsymbol{v} - \boldsymbol{u}$). D'un point de vue théorique, les équations cinétiques de Wigner/Vlasov sont équivalentes à une infinité d'équations fluides. Afin de construire un modèle fluide raisonnable, il nous faut donc trouver un moyen de fermer ces équations. Dans cette partie, on montre que sous certaines conditions spécifiques les équations fluides peuvent être fermées et s'écrivent de la manière suivante:

$$\begin{cases} \dfrac{\partial n}{\partial t} + \boldsymbol{\nabla} \cdot (n\boldsymbol{u}) = 0, \\ \dfrac{\partial u_i}{\partial t} + u_j(\partial_j u_i) = \dfrac{\hbar^2}{2m^2}\partial_i \left[\dfrac{\boldsymbol{\nabla}^2\sqrt{n}}{\sqrt{n}}\right] - \dfrac{1}{nm}\partial_j \left(P_C\right)_{ij} + \dfrac{1}{m}\partial_i V_{\mathrm{H}}. \end{cases} \tag{4}$$

Dans le modèle fluide ci-dessus, le terme P_C correspond à la pression classique des électrons. Cette dernière peut s'exprimer de la manière suivante:

$$\left(P_C\right)_{ij} = \frac{\left(3\pi^2\right)^{2/3}\hbar^2}{5m} n_0^{5/3}\delta_{ij}, \tag{5}$$

dans le cas d'un système d'électrons complètement dégénérés.

La dernière partie du premier chapitre est une analyse des conditions de validité des modèles fluides à travers l'étude des relations de dispersion. En particulier, on compare la relation de dispersion de l'équation de Wigner à celle provenant du modèle fluide (4). La conclusion principale de ce chapitre est que les modèles fluides sont valides dans la limite des grandes longueurs d'onde. De manière plus précise, il faut que la condition suivante: $\lambda k << 1$ soit valide, où k est le vecteur d'onde de l'excitation et λ représente la longueur d'écrantage de l'interaction électromagnétique. La figure 1 résume les différents modèles présentés dans le chapitre 1 ainsi que leurs domaines de validité.

Chapitre 2

Dans le second chapitre de ma thèse, je présente les méthodes théoriques que j'ai développé au cours de ma thèse sur la dynamique de spin dans l'espace des phases. Ce chapitre est constitué de trois parties distinctes.

Dans la première partie, je décrit de manière générale comment traiter le spin en mécanique quantique. En partant de l'équation de Dirac je montre comment on peut, grâce à la transformation de Foldy–Wouthuysen, inclure les effets de spin dans le Hamiltonien de Pauli. Je prend en compte deux effets de spin qui sont

l'interaction Zeeman et le couplage spin-orbite.

La seconde partie du deuxième chapitre concerne la généralisation des équations de Wigner en présence du spin. Dans un premier temps je propose d'étendre la fonction de Wigner à une matrice à deux dimensions, notée $\mathcal{F}$, afin d'inclure les différentes composantes du spin de l'électron. Ainsi la fonction de Wigner avec spin s'écrit:

$$\mathcal{F}\left(\boldsymbol{r},\boldsymbol{v},t\right)=\left(\frac{1}{2\pi\hbar}\right)^{3}\int d\boldsymbol{\lambda}\exp\left[\frac{i\boldsymbol{\lambda}}{\hbar}\cdot\left(m\boldsymbol{v}-e\int_{-1/2}^{1/2}d\tau\boldsymbol{A}\left(\boldsymbol{r}+\tau\boldsymbol{\lambda}\right)\right)\right]\rho(\boldsymbol{r}-\boldsymbol{\lambda}/2,\boldsymbol{r}+\boldsymbol{\lambda}/2,t) \tag{6}$$

où $\mathcal{F}$ est une matrice 2×2 et ρ est la matrice densité du système:

$$\mathcal{F}=\begin{pmatrix}f^{\uparrow\uparrow} & f^{\uparrow\downarrow}\\ f^{\downarrow\uparrow} & f^{\downarrow\downarrow}\end{pmatrix}\quad\text{et}\quad\rho=\begin{pmatrix}\rho^{\uparrow\uparrow} & \rho^{\uparrow\downarrow}\\ \rho^{\downarrow\uparrow} & \rho^{\downarrow\downarrow}\end{pmatrix}. \tag{7}$$

Les composantes de la matrices densité $\rho^{\eta\eta'}(\boldsymbol{r},\boldsymbol{r}',t)$, où $\eta=\{\uparrow,\downarrow\}$ désignent respectivement les composantes de spin "up" et de spin "down", sont données par la relation suivante:

$$\rho^{\eta\eta'}(\boldsymbol{r},\boldsymbol{r}')=\sum_{\mu}\Psi_{\mu}^{\eta}(\boldsymbol{r},t)\Psi_{\mu}^{\eta'*}(\boldsymbol{r}',t). \tag{8}$$

Afin d'étudier les propriétés macroscopiques du système, je définit quatre nouvelles fonctions de distribution f_0, f_i ($i=\{x,y,z\}$) de la manière suivante:

$$f_0=Tr\left\{\mathcal{F}\right\}=f^{\uparrow\uparrow}+f^{\downarrow\downarrow},\quad\boldsymbol{f}=Tr\left(\mathcal{F}\boldsymbol{\sigma}\right). \tag{9}$$

D'après ces définitions, la densité de particule ainsi que la densité de moment magnétique de spin du système d'électrons en interaction s'expriment de la manière suivante:

$$n(\boldsymbol{r},t)=\int f_0(\boldsymbol{r},\boldsymbol{v},t)d\boldsymbol{v},\quad\boldsymbol{S}(\boldsymbol{r},t)=\frac{\hbar}{2}\int\boldsymbol{f}(\boldsymbol{r},\boldsymbol{v},t)d\boldsymbol{v}. \tag{10}$$

Dans cette représentation, les quatre fonctions de Wigner ont une signification physique précise: f_0 représente la densité d'électrons dans l'espace des phases, tandis que f_i ($i=x,y,z$) représente la densité de spins polarisés dans la direction i dans l'espace des phases. Ensuite, on dérive les équations d'évolution de ces quatre fonctions de distribution. Après des calculs complexes, détaillés en Annexe, on obtient les équations d'évolution suivantes pour un système d'électrons en interaction avec

spin:

$$\begin{aligned}
&\frac{\partial f_0}{\partial t}+\frac{1}{m}\left(\boldsymbol{\pi}+\boldsymbol{\Delta\widetilde{\pi}}\right)\cdot\boldsymbol{\nabla}f_0-\frac{e}{m}\left[m\widetilde{\boldsymbol{E}}+\left(\boldsymbol{\pi}+\boldsymbol{\Delta\widetilde{\pi}}\right)\times\widetilde{\boldsymbol{B}}\right]_i\partial_{\pi_i}f_0\\
&-\mu_{\mathrm{B}}\boldsymbol{\nabla}\left(\widetilde{\boldsymbol{B}}-\frac{1}{2mc^2}\boldsymbol{\pi}\times\widetilde{\boldsymbol{E}}\right)_i\cdot\boldsymbol{\nabla}_{\boldsymbol{\pi}}f_i+\frac{\mu_{\mathrm{B}}}{4mc^2}\left[\left(\boldsymbol{E}_+ +\boldsymbol{E}_-\right)\times\boldsymbol{\nabla}\right]\cdot\boldsymbol{f}\\
&-\frac{\mu_{\mathrm{B}}e}{2mc^2}\left[\widetilde{\boldsymbol{E}}\times\left[\widetilde{\boldsymbol{B}}\times\boldsymbol{\nabla}_{\pi}\right]\right]\cdot\boldsymbol{f}-\frac{\mu_{\mathrm{B}}}{2mc^2}\frac{i}{\hbar}\left[\boldsymbol{\Delta\widetilde{\pi}}\times\left(\boldsymbol{E}_+ -\boldsymbol{E}_-\right)\right]\cdot\boldsymbol{f}=0, \qquad (11)
\end{aligned}$$

$$\begin{aligned}
&\frac{\partial f_k}{\partial t}+\frac{1}{m}\left(\boldsymbol{\pi}+\boldsymbol{\Delta\widetilde{\pi}}\right)\cdot\boldsymbol{\nabla}f_k-\frac{e}{m}\left[m\widetilde{\boldsymbol{E}}+\left(\boldsymbol{\pi}+\boldsymbol{\Delta\widetilde{\pi}}\right)\times\widetilde{\boldsymbol{B}}\right]_i\partial_{\pi_i}f_k\\
&-\mu_{\mathrm{B}}\boldsymbol{\nabla}\left(\widetilde{\boldsymbol{B}}-\frac{1}{2mc^2}\boldsymbol{\pi}\times\widetilde{\boldsymbol{E}}\right)_k\cdot\boldsymbol{\nabla}_{\boldsymbol{\pi}}f_0+\frac{\mu_{\mathrm{B}}}{4mc^2}\left[\left(\boldsymbol{E}_+ +\boldsymbol{E}_-\right)\times\boldsymbol{\nabla}\right]_k f_0\\
&-\frac{\mu_{\mathrm{B}}e}{2mc^2}\left[\widetilde{\boldsymbol{E}}\times\left[\widetilde{\boldsymbol{B}}\times\boldsymbol{\nabla}_{\pi}\right]\right]_k f_0-\frac{\mu_{\mathrm{B}}}{2mc^2}\frac{i}{\hbar}\left[\boldsymbol{\Delta\widetilde{\pi}}\times\left(\boldsymbol{E}_+ -\boldsymbol{E}_-\right)\right]_k f_0\\
&-\frac{e}{2m}\left[\left(\boldsymbol{B}_+ +\boldsymbol{B}_- -\frac{1}{2mc^2}\left(\boldsymbol{\pi}+\boldsymbol{\Delta\widetilde{\pi}}\right)\times\left(\boldsymbol{E}_+ +\boldsymbol{E}_-\right)\right)\times\boldsymbol{f}\right]_k\\
&+\frac{\mu_{\mathrm{B}}}{2mc^2}\frac{i}{2}\left[\left(\left(\boldsymbol{E}_+ -\boldsymbol{E}_-\right)\times\left(\boldsymbol{\nabla}-e\widetilde{\boldsymbol{B}}\times\boldsymbol{\nabla}_{\boldsymbol{\pi}}\right)\right)\times\boldsymbol{f}\right]_k=0. \qquad (12)
\end{aligned}$$

Où $\boldsymbol{\Delta\widetilde{\pi}}$ dépend du champ magnétique et correspond à une correction quantique sur la variable vitesse:

$$\boldsymbol{\Delta\widetilde{\pi}}=-i\hbar e\boldsymbol{\nabla}_{\boldsymbol{\pi}}\times\left[\int_{-1/2}^{1/2}d\tau\tau\boldsymbol{B}\left(\boldsymbol{r}+i\hbar\tau\boldsymbol{\nabla}_{\boldsymbol{\pi}}\right)\right], \qquad (13)$$

$\widetilde{\boldsymbol{E}}$ et $\widetilde{\boldsymbol{B}}$ sont des corrections quantiques et s'écrivent en fonction des champs électromagnétiques classiques:

$$\widetilde{\boldsymbol{E}}=\int_{-1/2}^{1/2}d\tau\boldsymbol{E}\left(\boldsymbol{r}+i\hbar\tau\boldsymbol{\nabla}_{\boldsymbol{\pi}}\right),\quad\widetilde{\boldsymbol{B}}=\int_{-1/2}^{1/2}d\tau\boldsymbol{B}\left(\boldsymbol{r}+i\hbar\tau\boldsymbol{\nabla}_{\boldsymbol{\pi}}\right). \qquad (14)$$

Les indices $\pm$ signifient que les quantités concernées sont évaluées en $\boldsymbol{r}\pm i\hbar\boldsymbol{\nabla}_{\boldsymbol{\pi}}/2$. Les equations (11)-(12) sont une généralisation de l'équation de Wigner (2) en tenant compte du spin de l'électron à travers l'effet Zeeman et le couplage spin-orbite. Les champs électriques et magnétiques apparaissant dans les équations de Wigner (11)-(12) ont différentes origines. Une partie de ces champs représente l'interaction entre le système d'éléctrons et un champ laser externe. Mais ils peuvent également représenter les champs électromagnétiques créés par les particules elles mêmes. Dans ce cas les champs électriques et magnétiques sont solutions des équations de

Maxwell suivantes:

$$\begin{cases} \boldsymbol{\nabla}\cdot\boldsymbol{E} &= \dfrac{\rho}{\epsilon_0} - \dfrac{\boldsymbol{\nabla}\cdot\boldsymbol{P}}{\epsilon_0}, \\ \boldsymbol{\nabla}\cdot\boldsymbol{B} &= 0, \\ \boldsymbol{\nabla}\times\boldsymbol{E} &= -\dfrac{\partial\boldsymbol{B}}{\partial t}, \\ \boldsymbol{\nabla}\times\boldsymbol{B} &= \mu_0\boldsymbol{j} + \mu_0\epsilon_0\dfrac{\partial\boldsymbol{E}}{\partial t} + \mu_0\dfrac{\partial\boldsymbol{P}}{\partial t} + \mu_0\boldsymbol{\nabla}\times\boldsymbol{M}. \end{cases} \tag{15}$$

Où, les termes sources sont reliés aux fonctions de distribution de Wigner de la manière suivante:

$$\rho = -e\int f_0 d\boldsymbol{v}, \tag{16}$$

$$\boldsymbol{j} = -e\left[\int \boldsymbol{v} f_0 d\boldsymbol{v} + \frac{\boldsymbol{E}\times\boldsymbol{M}}{2mc^2}\right], \tag{17}$$

$$\boldsymbol{M} = -\mu_{\mathrm{B}}\int \boldsymbol{f} d\boldsymbol{v}, \tag{18}$$

$$\boldsymbol{P} = -\frac{\mu_{\mathrm{B}}}{2c^2}\int \boldsymbol{v}\times\boldsymbol{f} d\boldsymbol{v}. \tag{19}$$

Dans les équations précédentes on a introduit de nouveaux termes sources telles que la magnétisation de spin $\boldsymbol{M}$, la "polarisation de spin" $\boldsymbol{P}$ ainsi qu'une contribution au courant de charge provenant du spin-orbite. Ces modifications doivent être apportées pour des raisons d'auto-consistance. En effet les équations de Wigner ont été obtenues en effectuant un développement semi-relativiste de l'équation de Dirac. Il nous faut donc également effectuer le même développement sur les termes sources apparaissant dans les équations de Maxwell-Dirac.
Les équations de Wigner (11)-(12) couplées aux équations de Maxwell forment un modèle auto-consistant pour étudier la dynamique quantique de charges et de spins d'un système d'électrons en interaction dans l'approximation du champ moyen.
On montre également dans cette section comment inclure les effets d'échange et de corrélations à travers des champs électriques et magnétiques dans les équations de Wigner. Ceci nous permet d'apporter des corrections à l'approximation du champ moyen. Un traitement de l'échange et des corrélations pour décrire le magnétisme non colinéaire est également décrit.
On présente ensuite la limite semi-classique des équations de Wigner avec spin. En prenant en compte uniquement les termes d'ordre 0 et 1 en $\hbar$, on montre ainsi que

les équations de Wigner avec spin se réduisent aux équations suivantes:

$$\frac{\partial f_0}{\partial t} + \boldsymbol{v}\cdot\boldsymbol{\nabla} f_0 - \frac{e}{m}\left(\boldsymbol{E}+\boldsymbol{v}\times\boldsymbol{B}\right)\cdot\boldsymbol{\nabla}_{\boldsymbol{v}} f_0 + \frac{\mu_{\mathrm{B}}}{2mc^2}\left(\boldsymbol{E}\times\boldsymbol{\nabla}\right)_i f_i$$
$$-\frac{\mu_{\mathrm{B}}}{m}\boldsymbol{\nabla}\left[B_i - \frac{1}{2c^2}\left(\boldsymbol{v}\times\boldsymbol{E}\right)_i\right]\cdot\boldsymbol{\nabla}_{\boldsymbol{v}} f_i - \frac{\mu_{\mathrm{B}} e}{2m^2c^2}\left[\boldsymbol{E}\times\left(\boldsymbol{B}\times\boldsymbol{\nabla}_{\boldsymbol{v}}\right)\right]_i f_i = 0, \tag{20}$$

$$\frac{\partial f_i}{\partial t} + \boldsymbol{v}\cdot\boldsymbol{\nabla} f_i - \frac{e}{m}\left(\boldsymbol{E}+\boldsymbol{v}\times\boldsymbol{B}\right)\cdot\boldsymbol{\nabla}_{\boldsymbol{v}} f_i + \frac{\mu_{\mathrm{B}}}{2mc^2}\left(\boldsymbol{E}\times\boldsymbol{\nabla}\right)_i f_0$$
$$-\frac{\mu_{\mathrm{B}}}{m}\boldsymbol{\nabla}\left[B_i - \frac{1}{2c^2}\left(\boldsymbol{v}\times\boldsymbol{E}\right)_i\right]\cdot\boldsymbol{\nabla}_{\boldsymbol{v}} f_0 - \frac{\mu_{\mathrm{B}} e}{2m^2c^2}\left[\boldsymbol{E}\times\left(\boldsymbol{B}\times\boldsymbol{\nabla}_{\boldsymbol{v}}\right)\right]_i f_0$$
$$-\frac{2\mu_{\mathrm{B}}}{\hbar}\left\{\left[\boldsymbol{B} - \frac{1}{2c^2}\left(\boldsymbol{v}\times\boldsymbol{E}\right)\right]\times\boldsymbol{f}\right\}_i = 0, \tag{21}$$

où le facteur $\hbar$ est caché dans la défintion du magnéton de Bohr $\mu_{\mathrm{B}} = e\hbar/(2m)$. Les équations ci-dessus sont des équations de Vlasov avec spin. On remarque que les différentes fonctions de distribution sont couplées entre elles à travers des effets semi-relativistes liés au spin (Zeeman + spin-orbite). De plus, il n'y a pas de corrections quantiques sur la dynamique orbitale des électrons, ces dernières sont au minimum des corrections de second ordre en $\hbar$. On en conclut donc que les équations de Vlasov avec spin (20)-(21), couplées aux équations de Maxwell (15) forment un modèle semi-classique qui décrit la dynamique d'un système d'électrons en interaction où le spin est pris en compte mais où la dynamique orbitale des électrons est classique. On démontre que les quantités suivantes sont conservées au cours du temps:

$$M_{tot} = m\int f_0 d\boldsymbol{v}d\boldsymbol{r}, \tag{22}$$

$$\boldsymbol{P}_{tot} = m\int \boldsymbol{v} f_0 d\boldsymbol{v}d\boldsymbol{r} + \int \boldsymbol{D}\times\boldsymbol{B}d\boldsymbol{r}, \tag{23}$$

$$E_{tot} = \frac{m}{2}\int \boldsymbol{v}^2 f_0 d\boldsymbol{v}d\boldsymbol{r} + \mu_{\mathrm{B}}\int \boldsymbol{f}\cdot\boldsymbol{B}d\boldsymbol{v}d\boldsymbol{r} + \frac{\epsilon_0}{2}\int \boldsymbol{E}^2 d\boldsymbol{r} + \frac{1}{2\mu_0}\int \boldsymbol{B}^2 d\boldsymbol{r}, \tag{24}$$

$$\boldsymbol{J}_{tot} = m\int \left(\boldsymbol{r}\times\boldsymbol{v}\right) f_0 d\boldsymbol{r}d\boldsymbol{v} + \frac{\hbar}{2}\int \boldsymbol{f}d\boldsymbol{r}d\boldsymbol{v} + \int \boldsymbol{r}\times\left(\boldsymbol{D}\times\boldsymbol{B}\right)d\boldsymbol{r}. \tag{25}$$

Où l'on a introduit les champs électriques et magnétiques dans la matière: $\boldsymbol{D} = \epsilon_0\boldsymbol{E}+\boldsymbol{P}$ et $\boldsymbol{H} = \boldsymbol{B}-\mu_0\boldsymbol{M}$. Le premier terme correspond à la masse total du système. Le second terme représente l'impulsion totale du système, une partie de l'impulsion provient des particules tandis que l'autre partie correspond à l'impulsion du champ électromagnétique. Le troisième terme est l'énergie total du système, elle s'écrit comme une somme de l'énergie cinétique des particules, l'énergie Zeeman et l'énergie du champ électromagnétique. Enfin, le dernier terme représente le moment cinétique total du système. Il s'écrit comme une somme de trois termes, le moment orbital des particules, le moment cinétique de spin et le moment cinétique du champ.

En terme de simulations numériques, les équations de Vlasov sont plus simple à traiter que les équations de Wigner. Ceci s'explique par le fait que les équations de Wigner sont non-local dans l'espace des phases. Les équations de Vlasov sont valides lorsque la condition suivante est satisfaite: $L >> \lambda_{\mathrm{DB}}$, où L est la taille typique du système (distance typique de variation des gradients de densité) et $\lambda_{\mathrm{DB}} = \hbar/mv$ est la longueur d'onde de DeBroglie.

La dernière partie du second chapitre concerne la dérivation de modèles fluides avec spin. En partant des équation de Vlasov avec spin (20)-(21), on construit différents modèles fluides. Les variables fluides apparaissant dans ces équations hydrodynamiques, en plus de la densité n et de la magnétisation m définit précédemment (10), sont:

$$\begin{aligned}
\boldsymbol{u} &= \frac{1}{n}\int \boldsymbol{v} f_0 d\boldsymbol{v}, && (26)\\
J^S_{i\alpha} &= \frac{\hbar}{2}\int v_i f_\alpha d\boldsymbol{v}, && (27)\\
P_{ij} &= m\int w_i w_j f_0 d\boldsymbol{v}, && (28)\\
\Pi_{ij\alpha} &= \frac{\hbar}{2} m\int v_i v_j f_\alpha d\boldsymbol{v}, && (29)\\
Q_{ijk} &= m\int w_i w_j w_k f_0 d\boldsymbol{v}, && (30)
\end{aligned}$$

où l'on a séparé la vitesse moyenne des électrons $\boldsymbol{u}$ de ses fluctuations $\boldsymbol{w} \equiv \boldsymbol{v} - \boldsymbol{u}$. Dans les équations précédentes P_{ij} and Q_{ijk} sont respectivement le tenseur de pression et de flux d'énergie. Le courant de spin $J^S_{i\alpha}$ représente la vitesse moyenne fluide le long de la direction i d'électrons polarisés en spin dans la direction α. La quantité $\Pi_{ij\alpha}$ représente un terme de pression de spin. Les équations d'évolution des quantités fluides précédentes s'obtiennent en considérant différents moments de l'équation de Wigner. Ainsi, on obtient les équations fluides suivantes:

$$\begin{aligned}
&\frac{\partial n}{\partial t} + \boldsymbol{\nabla}\cdot(n\boldsymbol{u}) = 0, && (31)\\
&\frac{\partial S_\alpha}{\partial t} + \partial_i J^S_{i\alpha} + \frac{e}{m}\left(\boldsymbol{S}\times\boldsymbol{B}\right)_\alpha = 0, && (32)\\
&\frac{\partial u_i}{\partial t} + u_j(\partial_j u_i) + \frac{1}{nm}\partial_j P_{ij} + \frac{e}{m}\left[E_i + (\boldsymbol{u}\times\boldsymbol{B})_i\right] + \frac{e}{nm^2}S_\alpha\left(\partial_i B_\alpha\right) = 0, && (33)\\
&\frac{\partial J^S_{i\alpha}}{\partial t} + \partial_j \Pi_{ij\alpha} + \frac{eE_i}{m}S_\alpha + \frac{e}{m}\epsilon_{jki}B_k J^S_{j\alpha} + \frac{e}{m}\epsilon_{jk\alpha}B_k J^S_{ij} + \frac{\mu_{\mathrm{B}}\hbar}{2m}\left(\partial_i B_\alpha\right) n = 0, && (34)\\
&\frac{\partial P_{ij}}{\partial t} + u_k\partial_k P_{ij} + P_{jk}\partial_k u_i + P_{ik}\partial_k u_j + P_{ij}\partial_k u_k + \partial_k Q_{ijk} + \frac{e}{m}\big[\epsilon_{lki}B_k P_{jl}\\
&\qquad + \epsilon_{lkj}B_k P_{il}\big] + \frac{e}{m^2}\sum_\alpha\left[\partial_i B_\alpha\left(J^S_{j\alpha} - S_\alpha u_j\right) + \partial_j B_\alpha\left(J^S_{i\alpha} - S_\alpha u_i\right)\right] = 0. && (35)
\end{aligned}$$

Comme pour tous système d'équations fluides, il convient de choisir une relation de

fermeture adaptée. Dans cette partie du chapitre, nous allons utiliser une méthode général basée sur le principe de maximisation de l'entropie (MEP). Cette dernière repose sur le faite que la fonction distribution d'équilibre correspond à la configuration microscopique la plus probable, c'est à dire celle qui maximise l'entropie tout en étant assujetti à certaines contraintes. Ces contraintes sont généralement exprimées sous forme de moments de la fonction de distribution. D'un point de vue mathématique cette procédure se réduit à un problème de maximisation d'une fonctionnelle. Afin d'illustrer la MEP, on écrit le Hamiltonien du système de la manière suivante:

$$\mathcal{H} = h_0(\boldsymbol{r}, \boldsymbol{v})\sigma_0 + \boldsymbol{h}(\boldsymbol{r}, \boldsymbol{v}) \cdot \boldsymbol{\sigma}, \tag{36}$$

où h_0 et $\boldsymbol{h}$ sont des fonctions de la position $\boldsymbol{r}$ et de la vitesse $\boldsymbol{v} \equiv (\boldsymbol{p} + e\boldsymbol{A})/m$. Dans notre cas (sans spin-orbite), on a

$$h_0 = m\frac{|\boldsymbol{v}|^2}{2} + V, \quad \boldsymbol{h} = \mu_B \boldsymbol{B}. \tag{37}$$

Dans le but de simplifier les notations, on écrit les moments fluides de la manière suivante:

$$\boldsymbol{m}_i(\boldsymbol{r}) = Tr \int \boldsymbol{\chi}_i \mathcal{F} d\boldsymbol{v}, \tag{38}$$

où $\mathcal{F}$ est définit par l'équation (7) et χ_i est associée à la i^{eme} quantité fluide:

$$\boldsymbol{m} = \begin{pmatrix} n \\ \boldsymbol{S} \\ \boldsymbol{u} \\ J^S_{i\alpha} \\ \vdots \end{pmatrix}; \qquad \boldsymbol{\chi} = \begin{pmatrix} 1 \\ \frac{\hbar}{2}\boldsymbol{\sigma} \\ \boldsymbol{v} \\ \frac{\hbar}{2} v_i \sigma_\alpha \\ \vdots \end{pmatrix}. \tag{39}$$

La densité d'entropie est définit de la manière suivante:

$$s(\mathcal{F}) = \begin{cases} k_B\, Tr\left\{\mathcal{F}\log\mathcal{F} - \mathcal{F}\right\} & \text{(M–B)} \\ k_B\, Tr\left\{\mathcal{F}\log\mathcal{F} + (1-\mathcal{F})\log(1-\mathcal{F})\right\} & \text{(F–D),} \end{cases} \tag{40}$$

où l'on fait la distinction entre une statistique de Maxwell-Boltzmann (M–B) et de Fermi-Dirac (F–D). Le principe de maximisation de l'entropie suppose qu'à l' équilibre la fonction de distribution $\mathcal{F}$ est un extremum de l'énergie libre:

$$\mathcal{E} \;=\; Tr \int \left[Ts(\mathcal{F}) + \mathcal{H}'\mathcal{F}\right] d\boldsymbol{v}d\boldsymbol{r} - \int \lambda_i(\boldsymbol{r}) m_i(\boldsymbol{r}) d\boldsymbol{r}, \tag{41}$$

où $\mathcal{H}' = \mathcal{H} + \lambda_i(\boldsymbol{r})\boldsymbol{\chi}_i$, T est la température et les fonctions λ_i sont des multiplicateurs de Lagrange. Ces derniers forment un ensemble de paramètres indépendants qui vont servir à paramétriser la fonction de distribution à l'équilibre. Une des difficultés majeur de la MEP est d'exprimer les fonctions λ_i en fonction des différents

moments fluides $\boldsymbol{m}$. La variation total de l'énergie libre s'écrit:

$$\delta\mathcal{E} \quad = \quad \delta\lambda_i \frac{\delta}{\delta\lambda_i}\mathcal{E} + \delta\mathcal{F}\frac{\delta}{\delta\mathcal{F}}\mathcal{E}, \tag{42}$$

où la distribution d'équilibre $\mathcal{F}^{eq}$ correspond à l'extremum de l'énergie libre $\delta\mathcal{E}(\mathcal{F}^{eq}) = 0$. À partir des équations (40) et (41)-(42), on en déduit que la fonction d'équilibre s'écrit de la manière suivante:

$$\mathcal{F}^{eq} = \begin{cases} a\exp\left(-\beta\mathcal{H}'\right) & \text{(M–B)} \\ a\left[\exp\left(\beta\mathcal{H}'\right)+1\right]^{-1} & \text{(F–D),} \end{cases} \tag{43}$$

où a est une constante et $\beta = 1/(k_B T)$. Les équations (43) constituent un résultat très général qui est valide pour n'importe quel nombre de contraintes sur les moments. Différentes applications de la MEP sont faites dans cette partie. Par exemple dans le cas d'une fermeture du type Fermi-Dirac avec des contraintes sur la densité de charge et de spin ainsi que sur la vitesse moyenne des charges. Dans ce cas on trouve le modèle fluide suivant:

$$\frac{\partial n}{\partial t} + \boldsymbol{\nabla}\cdot(n\boldsymbol{u}) = 0, \tag{44}$$

$$\frac{\partial S_\alpha}{\partial t} + \partial_i J^S_{i\alpha} + \frac{e}{m}\left(\boldsymbol{S}\times\boldsymbol{B}\right)_\alpha = 0, \tag{45}$$

$$\frac{\partial u_i}{\partial t} + u_j(\partial_j u_i) + \frac{1}{nm}\partial_j P_{ij} + \frac{e}{m}\left[E_i + (\boldsymbol{u}\times\boldsymbol{B})_i\right] + \frac{e}{nm^2}S_\alpha\left(\partial_i B_\alpha\right) = 0, \tag{46}$$

où le courant de spin se factorise de la manière suivante: $J^S_{i\alpha} = u_i S_\alpha$. Cela signifie que l'on néglige certaines corrélations entre la vitesse des électrons et leurs spins. Pour la pression on obtient la forme suivante:

$$P \quad = \quad \frac{\hbar^2}{5m}\frac{(6\pi^2)^{2/3}}{2^{5/3}}\left[\left(n-\frac{2}{\hbar}|\boldsymbol{S}|\right)^{5/3} + \left(n+\frac{2}{\hbar}|\boldsymbol{S}|\right)^{5/3}\right], \tag{47}$$

où l'on voit clairement apparaître l'effet des deux populations de spin (spin "up" et spin "down").
Dans les équations fluides présentées ci-dessus on a négligé le couplage spin-orbite. Dans cette même partie, on présente un système d'équations fluides fermées avec des corrections dues aux effets de couplage spin-orbite.

Chapitre 3

Dans le troisième chapitre de la thèse, on effectue une analyse linéaire du modèle de Vlasov avec spin. Le but de cette analyse est d'identifier une dépendance en spin dans la relation de dispersion du mode plasmon. Pour cela on étudie la propagation d'une faible perturbation sur un système infini d'électrons polarisés en spin.

La perturbation correspond à une excitation sinusoïdale, elle s'écrit de la manière suivante:

$$\delta f_{0,i} = \delta_{0,i} \cos(\boldsymbol{k} \cdot \boldsymbol{r}). \tag{48}$$

La perturbation ci-dessus représente une fluctuation periodique, avec un vecteur d'onde $\boldsymbol{k}$, de la densité de charges et de spins. Dans ce cas la réponse linéaire est caractérisée par une fonction diélectrique $\epsilon(\omega, \boldsymbol{k})$. De plus, les zéros de cette fonction correspondent aux différents modes propres du système. La réponse linéaire sans spin, associée au système Vlasov-Poisson, a été décrite pour la première fois en 1938. Le principale mode d'oscillation est le mode plasmon. Ce dernier oscille à la fréquence plasma $\omega_p = e^2 n_0 / m\epsilon_0$ et correspond à une oscillation collective des électrons par rapport au fond ionique fixe, voir Fig. 2. Dans le cas général, il peut s'avérer être compliqué de trouver la relation de dispersion du système. Dans notre cas, nous avons simplifié le problème en supposant un état d'équilibre homogène à une dimension (x) et en considérant une polarisation de spin uniquement selon l'axe z (approximation du magnétisme colinéaire). Dans ce cas les fonctions de distribution à l'équilibre s'écrivent:

$$f_0^{(0)} = f_0^{(0)}(v) = \mathcal{G}\left(mv^2/2 + \mu_B B\right) + \mathcal{G}\left(T, m\boldsymbol{v}^2/2 - \mu_B B\right), \tag{49}$$

$$f_z^{(0)} = f_z^{(0)}(v) = \mathcal{G}\left(mv^2/2 + \mu_B B\right) - \mathcal{G}\left(T, mv^2/2 - \mu_B B\right). \tag{50}$$

où $\mathcal{G}$ est soit une distribution de Maxwell-Boltzmann, soit une distribution de Fermi-Dirac. Sous couvert des approximations précédentes, on cherche à linéariser le

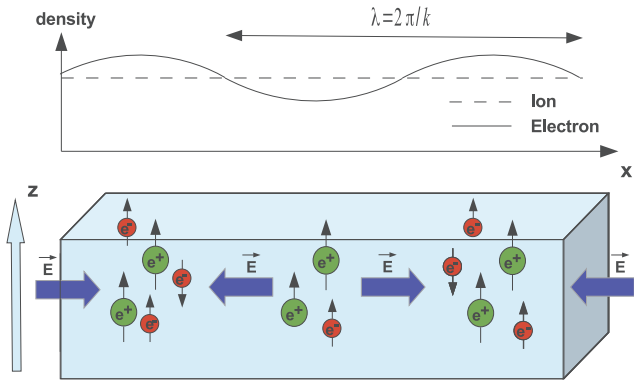

FIGURE 2: Schéma d'une excitation électrique longitudinale dans la direction x ainsi que les densités d'électrons et d'ions associées. Les spins sont polarisés dans la direction z.

système d'équations suivant:

$$\frac{\partial f_0}{\partial t} + v\,\partial_x f_0 - \frac{1}{m}\partial_x\left(-e\phi + V_{XC}\right)\partial_v f_0 - \frac{\mu_B}{m}\partial_x\left(B_{XC} + B_z\right)\partial_v f_z = 0, \tag{51}$$

$$\frac{\partial f_z}{\partial t} + v\,\partial_x f_z - \frac{1}{m}\partial_x\left(-e\phi + V_{XC}\right)\partial_v f_z - \frac{\mu_B}{m}\partial_x\left(B_{XC} + B_z\right)\partial_v f_0 = 0, \tag{52}$$

$$\frac{\partial^2\phi}{\partial x^2} = \frac{e}{\epsilon_0}\left(\int f_0 dv - n_0\right), \qquad \frac{\partial B_z}{\partial x} = -\mu_B\mu_0\frac{\partial}{\partial x}\left(\int f_z dv\right), \tag{53}$$

où la variable vitesse $v \equiv v_x$ désigne la composante x du vecteur vitesse.

Dans la première partie de ce chapitre, on utilise la transformée de Fourrier-Laplace pour déterminer la réponse linéaire du système d'équations précèdent (51)-(53). On trouve la fonction diélectrique suivante:

$$\begin{aligned}\epsilon\left(p,k\right) = 1 &+ \frac{\omega_p^2}{kn_0}\mathcal{I}_0 - \frac{k\mu_B^2\mu_0}{m}\mathcal{I}_0 + \frac{k}{m}\left[\left(\partial_n V_{XC} + \mu_B\partial_m B_{XC}\right)\mathcal{I}_0 + \left(\partial_m V_{XC} + \mu_B\partial_n B_{XC}\right)\mathcal{I}_z\right] \\ &+ \frac{\mu_B k^2}{m^2}\left[\left(\partial_n V_{XC}\right)\left(\partial_m B_{XC}\right) - \left(\partial_n B_{XC}\right)\left(\partial_m V_{XC}\right)\right]\left[\mathcal{I}_0^2 - \mathcal{I}_z^2\right] \\ &+ \left[-\frac{\omega_p^2\mu_B^2\mu_0}{n_0 m} + \frac{\mu_B\omega_p^2}{n_0 m}\partial_m B_{XC} - \frac{k^2\mu_B^2\mu_0}{m^2}\partial_n V_{XC}\right]\left(\mathcal{I}_0^2 - \mathcal{I}_z^2\right),\end{aligned} \tag{54}$$

où, les intégrales I_0 et I_z sont définit par les relations suivantes:

$$I_{0,z} = -i\int \frac{\partial_v f_{0,z}^{(0)}}{p + ikv} dv. \tag{55}$$

La fonction diélectrique du système (54) dépend uniquement de l'état d'équilibre du système (49)-(50) à travers les intégrales I_0 et I_z.

Dans la seconde partie de ce chapitre, on cherche à trouver les zéros de la fonction diélectrique $\omega(k)$ pour un état d'équilibre polarisé en spin et décrit par une statistique de Fermi-Dirac. Malheureusement, il s'avère que cette étude n'a pas aboutit en raison d'un problème mathématique complexe. En effet d'un point de vue générale, la variable ω étant une quantité complexe, il faut évaluer les intégrales I_0 et I_z par une intégrale dans le plan complexe. Cette intégrale se fait sans trop de difficultés grâce à la méthode des contours de Landau. Cependant une condition nécessaire pour utiliser cette méthode est que les fonctions suivantes: $\partial f_{0,z}^{(0)}(v)/\partial v$ soient des fonctions analytiques de la variable complexe v. Or dans le cas d'une distribution d'équilibre du type Fermi-Dirac ceci n'est pas le cas, on ne peut donc pas utiliser la méthode des contours de Landau.

Dans la troisième partie du chapitre, on étudie la relation de dispersion du plasmon avec spin en considérant une distribution d'équilibre du type Maxwell-Boltzmann. Dans ce cas on peut appliquer la méthode des contours de Landau et on obtient la

fonction diélectrique suivante:

$$\epsilon(\omega,k) = 1 - \frac{1}{v_T^2}\left[\frac{\omega_p^2}{k^2} - \frac{\mu_B^2\mu_0 n_0}{m} + 2\frac{n_0}{m}\left(\partial_n V_X + \alpha\partial_m V_X\right)\right] Z'\left(\frac{\omega}{kv_T}\right) + \left(\frac{n_0}{mv_T^2}\right)^2 \left[(\partial_n V_X)^2 - (\partial_m V_X)^2\right]\left[1-\alpha^2\right] Z'\left(\frac{\omega}{kv_T}\right)^2 + \left(\frac{n_0}{kv_T^2}\right)^2 \left[\frac{\mu_B\omega_p^2}{n_0 m}\partial_n V_X - \frac{\omega_p^2\mu_B^2\mu_0}{n_0 m} - \frac{k^2\mu_B^2\mu_0}{m^2}\partial_n V_X\right]\left[1-\alpha^2\right] Z'\left(\frac{\omega}{kv_T}\right)^2, \quad (56)$$

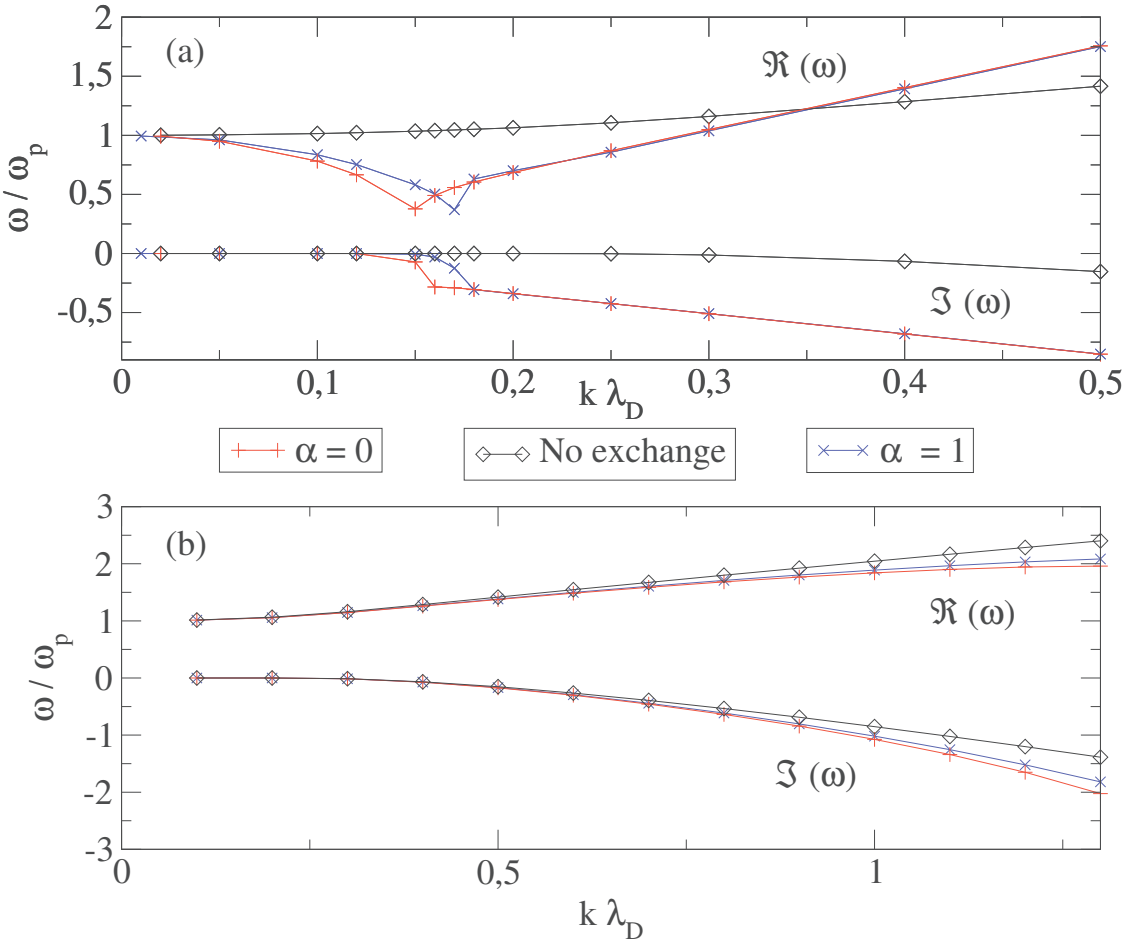

FIGURE 3: Relation de dispersion du plasmon $\omega(k)$ pour deux différents systèmes physiques. Les lignes du haut correspondent à la partie réelle de la fréquence tandis que les lignes du bas correspondent à la partie imaginaire de la fréquence. Les lignes noires correspondent aux cas sans interaction d'échange tandis que les lignes colorées correspondent aux cas avec interaction d'échange. Les lignes bleus représentent un système complètement polarisé en spin et les lignes rouges à un système non polarisé en spin. Dans la figure (a), on considère des électrons avec une densité: $n_0 = 10^{22}\,\mathrm{m}^{-3}$ et une température $T = 300\,\mathrm{K}$. Dans la figure (b), on considère des électrons avec la densité suivante: $n_0 = 5.9\times10^{28}\,\mathrm{m}^{-3}$ et à $T = 64000\,\mathrm{K}$ ($v_T = v_\mathrm{F}$). Dans les deux cas, on a: $m = 1\,\mathrm{a.u}$ et $\epsilon_0 = 1/4\pi\,\mathrm{a.u}$.

où $Z'(\varrho) = -2\varrho Z(\varrho) - 2$ est reliée à la fonction de dispersion plasma $Z(\varrho)$. Ce résultat est une généralisation de la fonction diélectrique du plasmon en tenant compte des effets de spin. Afin de trouver les zéros de cette fonction diélectrique, nous utilisons le programme ZEAL. Ce dernier permet de trouver tous les zéros d'une fonction analytique dans une certaine région du plan complexe. Les zéros de la fonction diélectrique forment la relation de dispersion du système. Ces derniers dépendent de la densité, de la température et de la magnétisation du système à l'équilibre. On a étudié deux cas différents dans cette partie. Dans un premier temps on a considéré une densité d'électrons métalliques: $n_0 = 5.9 \times 10^{28}\,\mathrm{m}^{-3}$ (Or). La température du système doit être artificiellement élevés car on considère une statistique de Maxwell-Boltzmann et non une statistique de Fermi-Dirac. On prend donc $T = 65000\ \mathrm{K}$ afin d'avoir des électrons à la vitesse de Fermi. Dans la figure 3 (b), on représente la relation de dispersion dans le cas de l'Or. On remarque que les effets de spin n'influent presque pas sur la relation de dispersion du plasmon (différence entre la courbe noir et les courbes colorées). Dans le second cas (idéaliste), on considère une densité électronique égale à $n_0 = 10^{22}\,\mathrm{m}^{-3}$. Pour un tel système, l'approximation de Maxwell-Boltzmann est justifié car la température de Fermi est de l'ordre de $2\,\mathrm{K}$. Dans ce cas, on observe une forte influence des effets de spin. En effet le fréquence plasmon décroit pour des faibles valeurs de k au lieu de croître dans le cas sans spin. Néanmoins cette situation correspond à un cas idéaliste que l'on ne trouve pas dans des régimes de la physique du solide. On en conclut donc que les effets de spin sur la relation de dispersion plasmon existent, cependant ils n'apparaissent pas dans les régimes habituels de température et de densité que l'on rencontre en matière condensée.

Chapitre 4

Le quatrième chapitre de ma thèse est une application des équations de Vlasov sur l'étude de la dynamique de charges et de spins dans des films ferromagnétiques de Nickel. En particulier on s'intéresse à l'interaction entre un pulse laser femtoseconde et les électrons dans le film. Le résultat principale de ce chapitre est la création d'un courant de spin oscillant dans la direction normal du film. On considère un film infiniment fin ($L \sim 5\,\mathrm{nm}$) dans la direction x, de telle sorte que l'on a un problème unidimensionnel à résoudre selon l'axe x (voir Fig. 4). Pour modéliser la distribution des ions, on utilise un modèle du type jellium avec une densité ionique continue: $n^i(x) = n_0\left[1 + \exp\left[(|x| - L/2)\,\sigma\right]\right]^{-1}$, où L est l'épaisseur du film, σ un paramètre modélisant la surface du film ($\sigma \sim 0.5 - 1$ Å) et $n_0 = (4\pi r_s/3)^{-1}$ est la densité du Nickel dans l'état solide ($r_s = 2.6\ u.a$).
La structure électronique du Nickel est la suivante: [Ni] = [Ar] $3d^8\ 4s^2$. Dans mon modèle, je considère que les électrons de la couche $4s$ sont délocalisés et sont responsables du magnétisme itinérant. Tandis que les électrons de la couche $3d$ restent localisés autour de l'atome de Nickel et forment un spin ionique.

Le moment magnétique total du Nickel $\boldsymbol{M}^{tot} = \boldsymbol{M}^{i} + \boldsymbol{M}^{e}$ est égal à $0.606\ \mu_{\mathrm{B}}$ par atome. On doit donc spécifier la proportion de moments magnétiques portés par les différent types d'électrons. Le moment magnétique des électrons de la couche $3d$, définit par $\boldsymbol{M}^{i} = -g\mu_B \boldsymbol{S}^{i}$, est égale à $0.54\ \mu_{\mathrm{B}}$ par atome à zero kelvin. On en déduit donc que le moment magnétique porté par les électrons $4s$, définit par $\boldsymbol{M}^{e}$, est égale à $0.066\ \mu_{\mathrm{B}}$ par atome.
En plus des différentes interactions électrostatiques entre les ions et les électrons, on considère également une interaction d'échange entre le spin des ions avec un constante de couplage J et une interaction d'échange entre le spin localisé des ions et le spin délocalisé des électrons avec une constante de couplage K (voir figure 5).
La dynamique de spin et de charge des électrons itinérant est modélisé avec le modèle semi-classique des équations de Vlasov avec spin. Pour des raisons numériques, on considère uniquement l'interaction Zeeman. Ceci nous permet de réduire l'espace des phases à un espace à deux dimensions $(x, v_x = v)$. Cependant, avec cette approximation on ne peut pas traiter le couplage spin-orbite. Les électrons sont donc décrit par les fonctions de distribution f_0 et f_i qui évoluent de la manière suivante:

$$\frac{\partial f_0}{\partial t} + v \cdot \partial_x f_0 - \frac{1}{m}\frac{\partial V}{\partial x}\frac{\partial f_0}{\partial v} - \frac{\mu_{\mathrm{B}}}{m}\frac{\partial B_i}{\partial x}\frac{\partial f_i}{\partial v} = 0, \tag{57}$$

$$\frac{\partial f_i}{\partial t} + v \cdot \partial_x f_i - \frac{1}{m}\frac{\partial V}{\partial x}\frac{\partial f_i}{\partial v} - \frac{\mu_{\mathrm{B}}}{m}\frac{\partial B_i}{\partial x}\frac{\partial f_0}{\partial v} - \frac{e}{m}\left[\boldsymbol{B} \times \boldsymbol{f}\right]_i = 0. \tag{58}$$

Ces fonctions de distribution nous permettent de reconstruire des quantités macroscopiques telles que la densité d'électron $n_e = \int f_0 dv$ ou de magnétisation $\boldsymbol{M}_e = -\mu_B \int \boldsymbol{f} dv / n_0$. Le potentiel électrique $V = -eV_{\mathrm{H}} + V_{xc} + V_{ext}$ et le champ magnétique

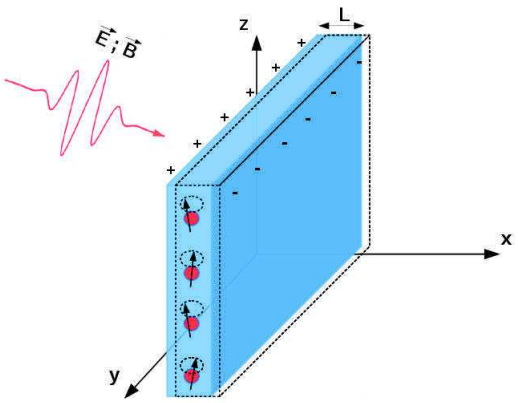

FIGURE 4: Géométrie d'un film de Nickel.

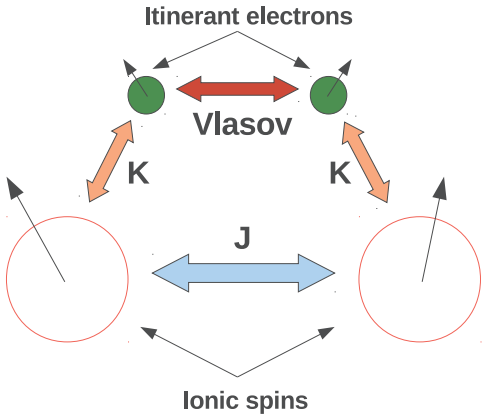

FIGURE 5: Schéma des différentes intéractions d'échange entre les ions ($3d^8$) et les électrons ($4s^2$), K et J sont des constantes d'échange.

$\boldsymbol{B} = \boldsymbol{B}_{sd}+\boldsymbol{B}_{xc}+\boldsymbol{B}_{ext}$ présents dans les equations (57)-(58). Ces derniers ont plusieurs origines. V_H est le potentiel d'Hartree, il obéit à l'équation de Poisson:

$$\partial_x^2 V_H = \frac{e}{\epsilon_0}\left[\int f_0 dv - n_i\right]. \tag{59}$$

$\boldsymbol{B}_{sd} = -Kn_i\boldsymbol{S}_i/2\mu_{\mathrm{B}}$ désigne un champ magnétique local qui représente l'interaction d'échange entre le spin des ions et le spin des électrons. Les quantités V_{xc} et $\boldsymbol{B}_{xc}$ représentent les effets d'échange-corrélation et V_{ext} et $\boldsymbol{B}_{ext}$ représentent les champs externes (lasers pulsés).
Les spins des ions ont un mouvement de précession qui est décrit par une équation de Landau-Lifchitz continue:

$$\frac{\partial \boldsymbol{S}^i}{\partial t} = \frac{a^2 J}{\hbar}\boldsymbol{S}^i \times \frac{\partial^2 \boldsymbol{S}^i}{\partial x^2} - \gamma \boldsymbol{S}^i \times \boldsymbol{B}_{eff}, \tag{60}$$

où $\gamma = g\mu_B/\hbar$ est le facteur de Landé de l'électron, $a = 2r_s$ est la distance inter-particule et $\boldsymbol{B}_{eff} = \boldsymbol{B}_{ext}+K\boldsymbol{M}^e/2g\mu_B^2$ est un champ magnétique effectif. En résumé, les équations (57)-(58) et (60) constituent un modèle auto-consistant permettant de décrire la dynamique électronique de charges et de spins dans un film ferromagnétique de Nickel.

Dans la seconde partie du chapitre, on cherche à caractériser l'état stationnaire du système ($f_0^{(0)}$ et $f_z^{(0)}$) pour lequel les spins sont orientés dans la direction transverse du film (z). En ce qui concerne les électrons, les solutions stationnaires des équations de Vlasov avec spin (57)-(58) s'écrivent:

$$f_0^{(0)} = \mathcal{F}_{\mathcal{D}}(H^+) + \mathcal{F}_{\mathcal{D}}(H^-), \quad f_z^{(0)} = \mathcal{F}_{\mathcal{D}}(H^+) - \mathcal{F}_{\mathcal{D}}(H^-), \tag{61}$$

où $\mathcal{F}_{\mathcal{D}}$ est une fonction de distribution de Fermi-Dirac longitudinale:

$$\mathcal{F}_{\mathcal{D}}(H) = \frac{2\pi k_{\mathrm{B}} T}{m}\left(\frac{m}{2\pi\hbar}\right)^3 \ln\left[1+\exp\left[\left(\mu - H\right)/k_{\mathrm{B}}T\right]\right].$$

Les quantités μ et $H^{\pm} = \frac{m}{2}v^2 + V \pm \mu_{\mathrm{B}}B_z$ représentent respectivement le potentiel chimique et le Hamiltonien des spins "up" et "down".
En ce qui concerne les ions, l'état stationnaire de l'équation (60) est obtenu en prenant une moyenne statistique dans l'ensemble canonique:

$$\langle S_z^i\rangle = S\mathcal{B}_S\left[\frac{S}{k_B T}\left(2J\langle S_z^i\rangle - \frac{K}{2\mu_{\mathrm{B}}}M_z^e\right)\right], \tag{62}$$

où $S = 0.54/2$ est la valeur du spin ionique à zero kelvin et $\mathcal{B}_S$ est la fonction de Brillouin .
Les états stationnaires précédents sont obtenus en résolvant un problème auto-consistant.

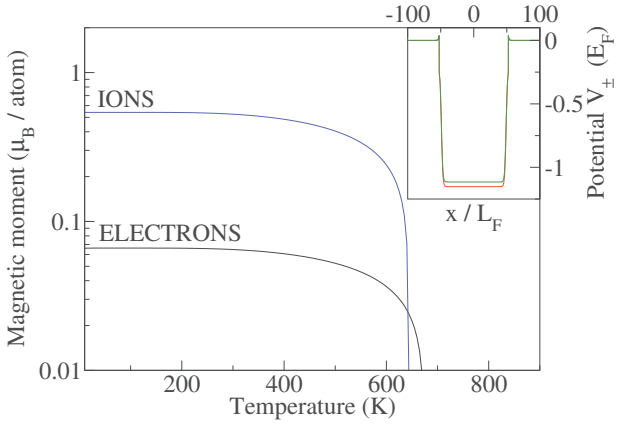

FIGURE 6: État fondamental d'un film de Nickel ($L = 100$ L_F et $\sigma = 1$ L_F). Figure principale: Magnétisation des ions (bleu) et des électrons (noir) en fonction de la température. Figure secondaire: Potentiel de confinement des spins "up" V_+ (rouge) et des spins "down" V_- (vert).

En effet pour déterminer $f_0^{(0)}$, $f_z^{(0)}$ et $\langle S_z^i \rangle$, on doit d'abord calculer les champs internes V_H et B_{sd} qui dépendent eux mêmes de $f_0^{(0)}$ et $\langle S_z^i \rangle$. On choisit donc des fonctions de distribution initiales $f_0^{(0)}$ et $f_z^{(0)}$, ensuite on calcule les champs autoconsistants puis on recalcule les nouvelles fonctions de distribution. On recommence ce processus jusqu'à avoir convergence des résultats. Cette procédure dépend de deux paramètres d'échange (K et J). Afin de trouver ces paramètres, on se place à température nulle, puis on choisit K pour obtenir la bonne valeur pour le moment magnétique des électrons. Ensuite on règle J pour avoir la bonne température de Curie. Dans la figure 6, on représente l'évolution du moment magnétique des électrons et des ions en fonction de la température. On retrouve un bon comportement pour la magnétisation du Nickel en prenant les valeurs suivantes: $J = 0.022\,\mathrm{eV}$ et $K = 0.014\ \mathrm{eV.nm^3}$ pour les constantes d'échange. On remarque également que les spins "up" sont plus confinés que les spins "down". Ceci est dû au champ magnétique d'échange entre les ions et les électrons. Ce dernier peut atteindre des valeurs très importantes de l'ordre de 6.10^3 Tesla.

Dans la troisième partie du chapitre 4, on réalise des simulations numériques des équations de Vlasov avec spin (57)-(58). On excite la dynamique électronique en introduisant un déplacement en vitesse Δv des fonctions de distribution électroniques f_0 et f_z. Dans la figure 7, on représente une simulation réalisée avec une excitation $\Delta v = 0.05\ v_F$. Comme on s'y attendait, on observe la création d'un dipôle électrique: $\langle X \rangle_e = \int x f_0 dx dv$. On observe également la création d'un dipôle magnétique (équivalent à un courant de spin): $\langle X \rangle_m \equiv \int x f_z dx dv$. Ceci est plus surprenant car on a uniquement excité la dynamique de charges et non la dynamique de spins. Ce courant de spin est progressivement créé au cours des premières oscillations du plasmon et oscille à une fréquence beaucoup plus basse que celle du plasmon ($0.043\ \omega_p$). Cette fréquence est très proche de la fréquence balistique $\omega_b = (2L/v_F)^{-1}$ qui est l'inverse

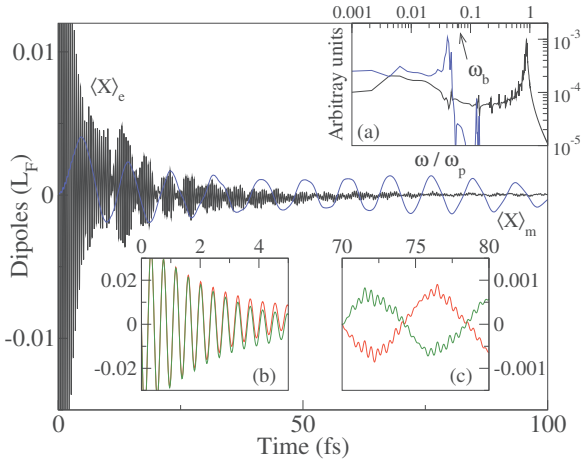

FIGURE 7: Simulations réalisées sur des films de Nickel ($L = 50\ L_{\mathrm{F}}$ et $\sigma = 1\ L_{\mathrm{F}}$). Figure principale: Évolution temporelle des dipôles électriques (noir) et magnétiques (bleu). Figure (a): Spectre de Fourrier des dipôles électriques et magnétiques. Figures (b)-(c): Évolution temporelle des dipôles "up" (rouge) et "down" (vert).

du temps de vol des électrons parcourant le film d'une surface à l'autre à la vitesse de Fermi. Dans le cas d'un film de taille $L = 50\ L_{\mathrm{F}}$, la fréquence balistique vaut $\omega_b = 0.063\ \omega_p$. On propose l'explication suivante pour comprendre l'origine de la création de ce courant de spin. A l'équilibre, les spins "up" sont plus confinés que les spins "down". Lorsque l'on va exciter les électrons, les spins "down" vont atteindre en moyenne la surface du film avant les spins "up". À la surface du film le champ électrique est le plus fort en raison des forts gradients de densité. La présence des spins "down" à la surface du film va modifier le champ électrique à la surface. Si bien que les électrons de spin "up", arrivant un peu pus tard, vont ressentir un champ électrique différent que celui ressentit par les spins "down". La conséquence de cette effet est que les spins "up" vont être repoussés plus rapidement que les spins "down" vers l'intérieur du film. De l'autre coté du film c'est la situation opposée qui se produit, à savoir que ce sont les électrons de spin "up" qui modifient le champ à la surface et que ce sont les électrons de spin "down" qui sont repoussés vers l'intérieur du film plus rapidement. Cette effet s'amplifie après chaque oscillations du plasmon jusqu'à arriver à la situation où les deux populations de spin oscillent en opposition de phase. Ceci explique l'origine de la création du dipôle magnétique ou du courant de spin.

Dans la dernière partie du chapitre 4, on modélise une situation plus réaliste dans laquelle les électrons sont excités par un champ laser femtoseconde. Ce dernier est modélisé par le champ électrique suivant: $\boldsymbol{E}(x) = E_0 \exp\left[-\left[(t-t_0)/\Delta t\right]^2\right] \cos(\omega_l t)\, \widehat{e}_x$, où E_0 est l'amplitude du laser, Δt la durée du pulse et ω_l la fréquence centrale du pulse. Dans la figure 8, on excite les électrons avec un pulse laser dans le régime du visible $\lambda_l = 2\pi c/\omega_l = 800$ nm, $\Delta t = 5\ fs$ et $E_0 = 10^{10}$ V/m. Dans la partie (a) de la figure, on représente l'évolution temporelle sur 100 fs des dipôles électriques et

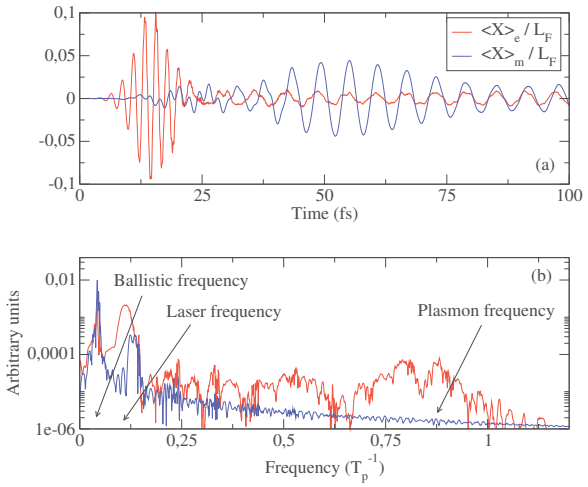

FIGURE 8: Simulations réalisées sur des film de Nickel: $L = 50\ L_{\mathrm{F}}$ et $\sigma = 1\ L_{\mathrm{F}}$. Les électrons sont excités par un pulse laser: $\Delta t = 5$ fs, $\lambda_L = 800$ nm, $E_0 = 10^{10}$ V/m et $t_0 = 3\ \Delta t$. Figure (a): Evolution temporelle des dipôles électriques (rouge) et magnétiques (bleu). Figure (b): Spectre de Fourrier des deux dipôles.

magnétiques. On remarque que le dipôle électrique est créé par le pulse laser sur des temps très courts ($t < 25$ fs), tandis que le dipôle magnétique est créé plus "lentement". Après que le pulse laser ait disparu les deux dipôles continuent à osciller avec des amplitudes similaires. On observe donc toujours la création d'un courant de spin même avec une excitation laser réaliste et dans le régime non linéaire.

Chapitre 5

Dans le chapitre 5, on s'intéresse à la dynamique de charges des électrons dans des nano-structures métalliques. Ce sont de petits objets métalliques de l'ordre du nanomètre contenant entre plusieurs dizaine et plusieurs milliers d'électrons. De tels objets sont intéressant à étudier car ils mettent en jeu des effets électroniques collectifs qui permettent d'exalter certaines propriétés telle que la génération d'harmoniques. Ils sont utilisés dans de nombreux domaines de la science telle que la nano-photonique, la biologie et également la médecine.

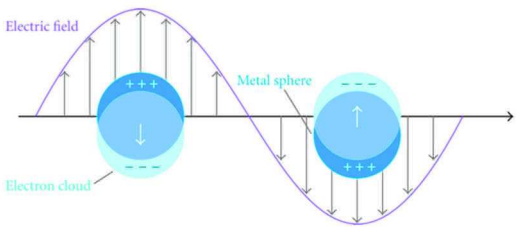

FIGURE 9: Illustration de l'oscillation d'un plasmon.

Dans la première partie du chapitre 5, on étudie la dynamique des électrons confinés dans des nano-particules d'Or. On considère des nano-particules ayant un rayon de 1 à 2 nanomètre. On s'intéresse en particulier à deux modes d'oscillations du nuage électronique. Le premier mode est le mode plasmon, ce dernier correspond à une oscillation collective des électrons autour du fond ionique fixe (voir figure 9). C'est un mode de surface car les charges sont localisées à la surface de la nano-particule. La fréquence typique de l'oscillation du plasmon est donnée par la fréquence plasma: $\omega_p = \sqrt{e^2 n_0/m\epsilon_0}$, où $n_0 = 5.9 \times 10^{28}\ \mathrm{m}^{-3}$ est la densité électronique de l'Or. Le second mode est un mode de respiration de la densité électronique. Ce dernier correspond à une oscillation isotrope du nuage électronique. C'est un mode de volume car une différence de charge apparaît également à l'intérieur de la nano-particule.
On modélise la dynamique électronique grâce à des équations d'hydrodynamiques quantiques:

$$\begin{cases} \dfrac{\partial n}{\partial t} + \nabla n\boldsymbol{u} &= 0 \\ \dfrac{\partial \boldsymbol{u}}{\partial t} + \boldsymbol{u}\nabla\boldsymbol{u} &= \nabla V_H - \nabla V_X - \dfrac{\nabla P}{n} + \dfrac{1}{2}\nabla\left[\dfrac{\nabla^2\sqrt{n}}{\sqrt{n}}\right] \\ \nabla^2 V_H &= 4\pi(n - n_i) \end{cases} \tag{63}$$

La première équation est une équation de continuité qui traduit la conservation du nombre d'électrons dans le système. La seconde équation est une équation d'Euler qui donne l'évolution de la vitesse moyenne des électrons en fonction des différentes forces agissant sur le système. Ces différentes forces sont représentées par le potentiel d'Hartree V_{H} qui obéit à l'équation de Poisson, la pression de Fermi $P = (3\pi^2)^{2/3}\, n^{5/3}/5$ et le potentiel d'échange-corrélation:

$$V_X = \frac{\delta E_x[n]}{\delta n} \qquad E_X[n] = -\frac{3(3\pi^2)^{1/3}}{4\pi}\int n^{4/3} d\boldsymbol{r} - \beta\int \frac{(\nabla n)^2}{n^{4/3}} d\boldsymbol{r}. \tag{64}$$

Enfin le dernier terme de l'équation d'Euler est un terme d'origine quantique qui est relié au potentiel de Bohm.
La résolution numérique des équations hydrodynamiques précédentes s'avère être difficile à réaliser numériquement. On choisit donc d'utiliser une approche variationnel pour résoudre ces équations hydrodynamiques. Dans un premier temps, on montre que le système d'équations fluides ci-dessus est équivalent à la densité

Lagrangienne suivante:

$$\begin{aligned}\mathcal{L} &= n\left(\frac{\partial S}{\partial t}+\frac{(\nabla S)^2}{2}\right)+\frac{(\nabla n)^2}{8n}+\frac{3}{10}\left(3\pi^2\right)^{2/3}n^{5/3}\\ &\quad -\frac{3}{4\pi}\left(3\pi^2\right)^{1/3}n^{4/3}-\beta\frac{(\nabla n)^2}{n^{4/3}}-\frac{(\nabla V_H)^2}{8\pi}-(n-n_i)V_H. \end{aligned} \tag{65}$$

Cette densité Lagrangienne dépend de trois champs scalaires: la densité électronique $n(\boldsymbol{r},t)$, le champ $S(\boldsymbol{r},t)$ qui est relié à la vitesse moyenne des électrons ($\boldsymbol{u}=\nabla S$) et le potentiel d'Hartree V_{H}. Ensuite le principe de la méthode variationnel est de faire un "Ansatz" sur le profil spatial de la densité électronique. Dans notre cas, on choisit la densité suivante:

$$n(\boldsymbol{r},t)=\frac{A}{1+\exp\left(\left[\frac{s(\boldsymbol{r},t)}{\sigma(t)}\right]^3-\left[\frac{r_c}{\sigma_0}\right]^3\right)}, \tag{66}$$

où $s=\sqrt{x^2+y^2+(z-d(t))^2}$ est une variable de coordonnées déplacées. On a introduit dans la densité électronique deux variables dynamiques $d(t)$ et $\sigma(t)$. La première représente le centre de masse du nuage d'électrons et nous permet de décrire le mode dipolaire. Tandis que la seconde représente le débordement de la densité électronique aux bords de la nano-particule ("spill-out effect") et nous permet de décrire le mode de respiration. A partir de "l'Ansatz" sur la densité électronique, il est possible en utilisant respectivement l'équation de continuité et l'équation de Poisson de trouver un profile spatial pour la vitesse moyenne des

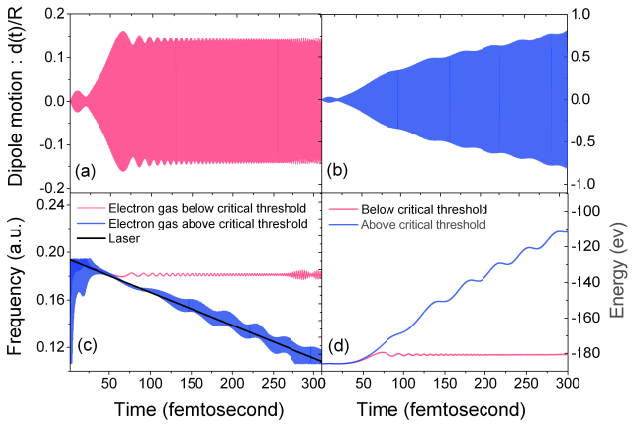

FIGURE 10: Excitation auto-résonante d'une nano-particule d'Or ($N=200$) pour deux valeurs d'intensité du champ laser: $I=4.5\,10^{10}$ W/cm^2 (courbe rouge) et $I=5.4\,10^{10}$ W/cm^2 (courbe bleu). Les figures du haut montrent l'évolution temporelles du dipôle électrique $d(t)$ en-dessous du seuil (a) et au-dessus du seuil (b). (c): Fréquence laser (noir) et fréquences instantanées des dipôles. (d): Énergies absorbées par les électrons au cours du temps.

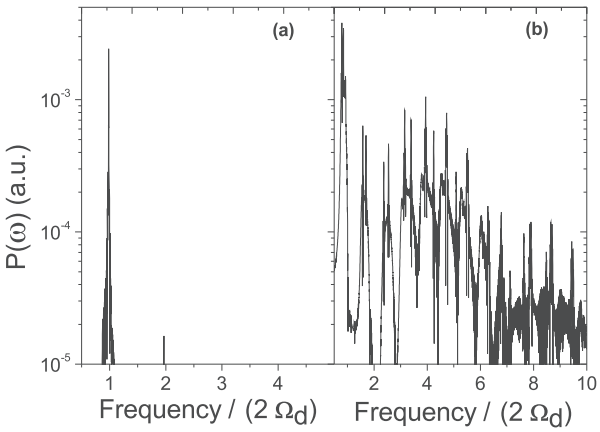

FIGURE 11: Spectre en fréquence du rayonnement électromagnétique généré par le dipôle électrique en-dessous du seuil d'auto-résonance (a) et au-dessus du seuil (b).

électrons et le potentiel d'Hartree. On peut ensuite calculer le Lagrangien du système, ce dernier s'obtient en intégrant la densité Lagrangienne sur tout l'espace: $L\left(d,\sigma,\dot{d},\dot{\sigma}\right) = \frac{-1}{N}\int \mathcal{L}\left(d,\sigma,\boldsymbol{r}\right)d\boldsymbol{r}$. Puis en utilisant les équations d'Euler-Lagrange, on obtient un système d'équations différentielles décrivant la dynamique du plasmon et du mode de respiration:

$$\left\{\begin{array}{lcl} M(a)\ddot{\sigma} & = & -\frac{dU(\sigma)}{d\sigma} + F\left(\sigma\right)d^2 - G\left(\sigma\right)d^4 \\ \ddot{d} & = & -\Omega_d^2\sigma)d + 4K(\sigma)d^3 \end{array}\right. \tag{67}$$

Sans rentrer dans les détails des différents termes, on remarque que l'on a un système de deux équations non-linéaires couplées. A partir de ces équations, on peut extraire les fréquences de résonance des modes d'oscillations. Pour le mode dipolaire on trouve Ω_d et pour le mode de respiration on trouve $\Omega_\sigma = \sqrt{dU(\sigma_0)/d\sigma}/M(a)$. On montre également que ces deux modes dépendent correctement du nombre d'électrons dans le système. Ceci nous permet de valider notre approche variationnel. Ensuite nous allons exciter le système avec un champ électrique auto-résonant, ce dernier s'écrit de la manière suivante:

$$\boldsymbol{E}(t) = E_0\cos\left(\left[\Omega_d + \frac{1}{2}\alpha(t-t_0)\right](t-t_0)\right)\widehat{e}_z \tag{68}$$

La particularité d'une excitation auto-résonante est d'avoir une fréquence qui varie dans le temps. Dans notre cas la fréquence décroit linéairement avec un taux α. Ce type d'excitation peut être réalisé expérimentalement à l'aide d'un laser "chirpé". Le principe de l'auto-résonance est d'avoir un blocage de phase entre le système et l'excitation. Autrement dit la condition de résonance est toujours satisfaite même dans le régime non-linéaire. Ceci n'est évidement pas la cas si on excite le système à une fréquence constante car lorsque le système entre dans le régime non-linéaire sa fréquence instantanée est modifiée et la condition de résonance est perdu. Afin

que l'auto-résonance fonctionne il faut que la condition suivante soit satisfaite: $E_0 > \xi_c$ ($\xi_c \propto |\alpha|^{3/4}$). C'est à dire qu'il faut que la variation de la fréquence soit suffisamment lente pour que le système ait le temps de s'adapter et de se mettre en phase avec l'excitation. Dans la figure 10, on représente l'évolution temporelle du mode dipolaire dans un cas où l'auto-résonance ne fonctionne pas (Fig.10(a)) puis dans un cas où l'auto-résonance fonctionne (Fig.10(b)). Dans le cas ou l'auto-résonance fonctionne, on remarque que l'on arrive à exciter fortement le dipôle électrique en utilisant une intensité laser à peine plus élevée que dans le cas (Fig.10(a)). En effet dans la figure 10(a) l'intensité laser vaut $I = 4.5\ 10^{10}\ \mathrm{W/cm^2}$ alors que dans la figure 10(b) elle vaut $I = 5.4\ 10^{10}\ \mathrm{W/cm^2}$. Cette dynamique, au cours de laquelle les électrons sont excités de manière cohérente par le champ laser, conduit à la création d'un dipôle électrique dans le régime non-linéaire. Or un dipôle électrique qui oscille émet un rayonnement électromagnétique. Dans la figure 11, on représente le spectre en puissance de ce rayonnement. On montre que dans le cas d'une excitation auto-résonante, le spectre est riche en harmoniques de la fréquence dipolaire linéaire. En principe une excitation auto-résonante pourrait donc être utilisé pour faire de la génération d'harmoniques sur des nano-particules métalliques.

Dans la seconde partie du chapitre 5, j'étudie par une approche variationnel la dynamique d'un gaz d'électrons confiné dans un potentiel anisotrope et anharmonique. Je met en évidence un lien entre la dynamique non-linéaire des électrons, étudié à travers les sections de Poincaré, et la génération d'harmoniques.

"Life is like riding a bicycle. To keep your balance, you must keep moving."

Albert Einstein

Contents

List of Abbreviations

DFT	**D**ensity **F**unctional **T**heory
TDDFT	**T**ime-**D**ependent **D**ensity **F**unctional **T**heory
LSDA	**L**ocal-**S**pin **D**ensity **A**pproximation
HF	**H**artree-**F**ock
QHD	**Q**uantum **H**ydro**D**ynamic
SIC	**S**elf-**I**nteraction **C**orrection
M-B	**M**axwell-**B**oltzmann
F-D	**F**ermi-**D**irac
DMS	**D**iluted **M**agnetic **S**emi-conductors
RKKY	**R**undermann-**K**ittel- **K**asuya-**Y**osida
PIC	**P**article **I**n **C**ells
CFL	**C**ourant **F**riedrichs **L**ewy
MEP	**M**aximum **E**ntro**p**y method
HHG	**H**igh **H**armonic **G**eneration
a.u.	**a**tomic **u**nits

Physical Constants

Speed of Light	$c = 2.99792458\ 10^{8}\ m.s^{-1}$	(Meter per second)
Charge of the electron	$e = 1.602177\ 10^{-19}\ \mathrm{c}$	(Coulomb)
Mass of the electron	$m = 9.109384\ 10^{-31}\ \mathrm{kg}$	(Kilogramme)
Reduced Planck constant	$\hbar = 1.054572\ 10^{-31}\ \mathrm{J.s}$	(Joule per second)
Bohr magneton	$\mu_B = 9.274010\ 10^{-24}\ \mathrm{A.m^2}$	(Ampere per square meter)
Vacuum permittivity	$\epsilon_0 = 8.854188\ 10^{-12}\ \mathrm{F.m^{-1}}$	(Faraday per meter)
Permeability constant	$\mu_0 = 4\pi\ 10^{-7}\ \mathrm{H.m^{-1}}$	(Henry per meter)
Boltzmann constant	$k_B = 1.380649\ 10^{-7}\ \mathrm{J.K^{-1}}$	(Joule per Kelvin)

List of Symbols

T	Temperature	(K)
q	Electric charge	(c)
r_S	Wigner-Seitz radius	(m)
ω_p	Plasma frequency	(s^{-1})
T_p	Plasma period	(s)
ω_b	Ballistic frequency	(s^{-1})
T_b	Ballistic period	(s)
γ	Classical coupling parameter	(No units)
γ_q	Quantum coupling parameter	(No units)
g	Landé g-factor	(No units)
γ_g	Gyromagnetic ratio of an electron	$s^{-1}.T^{-1}$
λ_D	Debye length	(m)
λ_F	Thomas–Fermi screening length	(m)
λ_{DB}	Thermal de Broglie wavelength	(m)
ν_{ee}	Electron-electron collision rate	(s^{-1})
v_F	Fermi velocity	($m.s^{-1}$)
T_F	Fermi temperature	(K)
E_F	Fermi energy	(J)
μ	Chemical potential	(J)
v_T	Thermal speed	($m.s^{-1}$)
$\mathcal{U}_B$	Bohm potential	(J)
t	Time variable	(s)
$\boldsymbol{r}$	Position variable	(m)
$\boldsymbol{v}$	Velocity variable	($m.s^{-1}$)
$\boldsymbol{p}$	Impulsion variable	($kg.m.s^{-1}$)
$\boldsymbol{\pi}$	Generalized impulsion	($kg.m.s^{-1}$)
$\mathcal{F}$	Wigner/Vlasov distribution function (2×2 matrix)	($s^3.m^{-6}$)
f	Wigner/Vlasov distribution function without spin	($s^3.m^{-6}$)
$f^{(0)}$	Equilibrium Wigner/Vlasov distribution function	($s^3.m^{-6}$)
δf	Perturbed Wigner/Vlasov distribution function	($s^3.m^{-6}$)
f_0	Wigner/Vlasov distribution function for the charges	($s^3.m^{-6}$)
$\boldsymbol{f}$	Wigner/Vlasov distribution function for the spins	($s^3.m^{-6}$)
n	Electron density	(m^{-3})
$n^{\uparrow}$	Spin-up density	(m^{-3})
$n^{\downarrow}$	Spin-down density	(m^{-3})

$\boldsymbol{m}$	Electron spin density	(m^{-3})
ξ	Spin polarization	(No units)
$\langle X \rangle_e$	Electric dipole Electron spin density	(m)
$\langle X \rangle^{\uparrow}$	Spin-up dipole Electron spin density	(m)
$\langle X \rangle^{\downarrow}$	Spin-down dipole Electron spin density	(m)
$\langle X \rangle_m$	Magnetic dipole	(m)
n_0	Equilibrium electron density	(m^{-3})
m_0	Equilibrium electron magnetization density	(m^{-3})
n^i	Ion density	(m^{-3})
n_0^i	Ion bulk density (Nickel)	(m^{-3})
$\boldsymbol{S}$	Electron spin density	$(\mathrm{J.s.m}^{-3})$
$\boldsymbol{S}^i$	Ion spin	(No units)
$\boldsymbol{S}_0^i$	Equilibrium ion spin	(No units)
$\boldsymbol{M}$	Electron spin magnetic moment density	$([\mu_\mathrm{B}]\,.\mathrm{m}^{-3})$
$\boldsymbol{M}^i$	Ion spin magnetic moment	$([\mu_\mathrm{B}])$
$\boldsymbol{j}$	Electron current density	$(\mathrm{c.s}^{-1}.\mathrm{m}^{-2})$
$\boldsymbol{u}$	Mean electron velocity	$(\mathrm{s}^{-1}.\mathrm{m}^{-2})$
$\overline{\boldsymbol{u}}$	Mean electron velocity with spin-orbit correction	$(\mathrm{s}^{-1}.\mathrm{m}^{-2})$
$\boldsymbol{P}$	″Spin″ polarization	$(\mathrm{c.m}^{-2})$
$J_{i\alpha}^S$	Spin current density	$(\mathrm{J.m}^{-2})$
$\overline{J}_{i\alpha}^S$	Spin current density with spin-orbit correction	$(\mathrm{J.m}^{-2})$
P_{ij}	Pressure tensor	$(\mathrm{J.m}^{-3})$
$\Pi_{ij\alpha}^S$	Spin pressure tensor	$(\mathrm{J.s}^{-1}.\mathrm{m}^{-1})$
Q_{ijk}	Generalized energy flux tensor	$(\mathrm{J.s}^{-1}.\mathrm{m}^{-2})$
$\boldsymbol{E}$	Electric field	$(\mathrm{V.m}^{-1})$
$\boldsymbol{B}$	Magnetic field	(T)
$\boldsymbol{D}$	Electric displacement field	$(\mathrm{c.m}^{-2})$
ϕ	Scalar potential	(V)
$\boldsymbol{A}$	Vector potential	$(\mathrm{V.s.m}^{-1})$
V_H	Hartree potential	$(\mathrm{J.c}^{-1})$
E_k	Kinetic energy	(J)
E_p	Potential energy	(J)
E_{cm}	Center of mass energy	(J)
E_{tot}	Total energy	(J)
V_{XC}	Exchange-correlation potential	(J)
$\boldsymbol{B}_{XC}$	Exchange-correlation magnetic field	(T)
E_{XC}	Exchange-correlation energy	(J)
ϵ_{XC}	Exchange-correlation functional	(J)
ϵ_X	Exchange functional	(J)
ϵ_C	Correlation functional	(J)
E_0	Laser field	$(\mathrm{V.m}^{-1})$
ω_l	Laser frequency	(s^{-1})

Δt	Laser pulse width	(s)
J	Exchange constant ion-ion	(J)
K	Exchange constant ion-electron	(J.nm^3)
J_{ref}	Reference exchange constant ion-ion	(J)
K_{ref}	Reference exchange constant ion-electron	(J.nm^3)
$\boldsymbol{B}_{sd}$	Magnetic exchange field ion-electron	(T)
$\boldsymbol{E}_{i-i}$	Exchange energy ion-ion	(J)
$\boldsymbol{E}_{i-e}$	Exchange energy ion-electron	(J)
ω_L	Spin precession frequency associated to an external magnetic field	(s^{-1})
ω_J	Ion spin frequency associated to the exchange constant J	(s^{-1})
ω_{i-K}	Ion spin frequency associated to the exchange constant K	(s^{-1})
ω_{e_K}	Electron spin frequency associated to the exchange constant K	(s^{-1})
Ψ	Electronic wave function	(m^{-3})
Ψ^{D}	Dirac wave function	(m^{-3})
Ψ^N	N-body wave function	(m^{-3})
$\boldsymbol{\sigma}, \sigma_0$	Pauli matrices	(No units)
$\boldsymbol{\alpha}, \beta$	Dirac matrices	(No units)
A	Wave function amplitude	(m^{-3})
S	Wave function phase	(J.s)
$\widehat{\mathcal{H}}$	Hamiltonian operator	(J)
$\mathcal{H}$	Classical Hamiltonian	(J)
$\hat{\boldsymbol{R}}$	Position operator	(m)
$\hat{\boldsymbol{V}}$	Velocity operator	(m.s^{-1})
$\hat{\boldsymbol{P}}$	Impulsion operator	(kg.m.s^{-1})
$\hat{\boldsymbol{\Pi}}$	Generalized impulsion operator	(kg.m.s^{-1})
$\hat{\mathcal{F}}$	Wigner distribution function	(s^3.m^{-6})
$\hat{\rho}$	Density matrix	(m^{-3})
S	Entropy	(J.K^{-1})
N_x	Number of points in x	(No units)
N_v	Number of points in v	(No units)
δt	Numerical time step	(s)
$\overline{\chi}$	Fourier transform of χ	(No units)
$\tilde{\chi}$	Laplace transform of $\overline{\chi}$	(No units)
$\boldsymbol{k}$	wave vector	(m^{-1})
p, ω	Complex frequency	(s^{-1})
ϵ	Dielectric function	(No units)
Res	Residue of a complex function	(No units)
Z	Plasma dispersion function	(No units)
$\mathscr{L}_D$	Lagrangian density	(J.m^{-3})
L	Lagrangian	(J)
Tr	Matrix trace	(No units)
$\star$	Star product	(No units)

$[\ ,\ ]$	Commutator	(No units)
$\{\ ,\ \}_\star$	Moyal bracket	(No units)
$\{\ ,\ \}$	Poisson bracket	(No units)
$\boldsymbol{\nabla}$	Gradient with respect to $\boldsymbol{r}$	(m^{-1})
$\boldsymbol{\nabla}_{\boldsymbol{v}}$	Gradient with respect to $\boldsymbol{v}$	$(\mathrm{s.m}^{-1})$
$\boldsymbol{\nabla}_{\boldsymbol{p}}$	Gradient with respect to $\boldsymbol{p}$	$(\mathrm{s.m}^{-1}\mathrm{.kg}^{-1})$
$\boldsymbol{\nabla}_{\boldsymbol{\pi}}$	Gradient with respect to $\boldsymbol{\pi}$	$(\mathrm{s.m}^{-1}\mathrm{.kg}^{-1})$
∂_i	Partial derivative with respect to position coordinates	(m^{-1})
∂_{v_i}	Partial derivative with respect to velocity coordinates	$(\mathrm{s.m}^{-1})$
∂_{p_i}	Partial derivative with respect to impulsion coordinates	$(\mathrm{s.m}^{-1}\mathrm{.kg}^{-1})$
∂_{π_i}	Partial derivative with respect to generalized impulsion coordinates	$(\mathrm{s.m}^{-1}\mathrm{.kg}^{-1})$

Introduction

The physics of metallic nano-structures has stimulated a huge amount of scientific interest in the last two decades, both for fundamental research and for potential technological applications that range from the recent fields of nanophotonics [1,2], physical chemistry [3] and even biology and medicine [4,5]. Metallic nano-structures are mesoscopic systems composed of a relatively small numbers of metallic atoms, typically between a few tens and several millions. The typical size of those systems are of few nanometres with properties that are intermediate between those of molecules and bulk solids. They can have different geometries, ranging from spherical nanoparticles, thin films or nanorods, see Fig. 12. Moreover metallic nano-structures present an intrinsic fundamental interest as large objects that still display quantum features [6–9]. Quantum effects arise because of the large density, which means that electrons are closely packed together. The typical size at which quantum effects dominate is given by the de Broglie wavelength $\lambda_B = \hbar/mv$, where m and v are, respectively, the mass and velocity of the electrons. In recent years, there has been tremendous progress in the manipulation of those objects. Many experimental studies focused on the charge dynamics of an electron gas confined in metallic nano-structures such as thin films [11, 12], nanotubes [13], metal clusters [14, 15] and nanoparticles [6,7,16]. On one hand, metallic nano-structures are small enough so that their magnetic and electric properties are strongly dependent on their geometries. On the other hand, they are large enough to exhibit collective effects. The latter are mediated by the conduction electrons and can be viewed as a mobile plasma neutralized by the ionic background. Collective effects are interesting because they can be measured experimentally and used for applications (nanoplasmonics). Experimentally, the electron dynamics in a metallic nano-structures can be

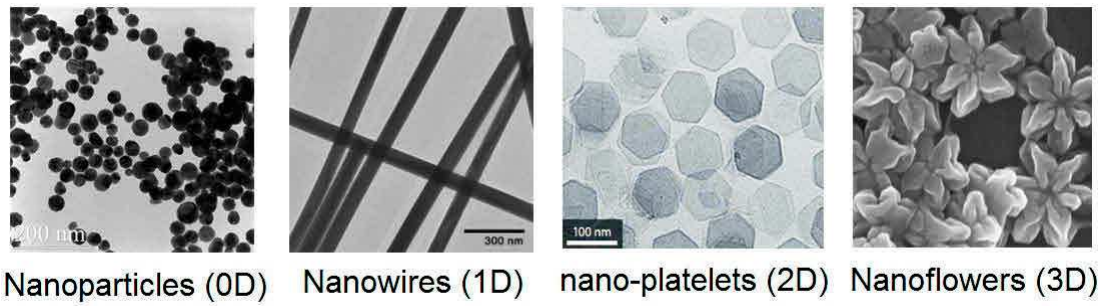

FIGURE 12: From [10], Sketch of different nano-structure geometries.

probed with great precision using ultrafast spectroscopy techniques in the femtosecond regime [12, 16]. For instance plasmon resonances, i.e. electron oscillations near the plasma frequency $\omega_p = \sqrt{n_0 e^2/m\epsilon_0}$, are routinely observed in metallic nanoparticles and their properties (resonance frequency, damping, ...) are studied experimentally and used for instance for medical applications [17, 18] or high harmonic generations [19, 20].
In this kind of experiment the electron dynamics is excited thanks to a femtosecond laser pulse and displays a broad range of physical regimes associated with various time scales. The following typical scenario is generally assumed, see Fig. 13. In the first tens of femtoseconds the interaction between the electrons (charges and spins) and the laser field (photons) is coherent, meaning that the electron dynamics is mainly driven by the laser and the self-consistent fields. This early stage leads to many physical effects. From the point of view of the charge dynamics it leads to the creation of a collective charge oscillation, the so-called surface plasmon. From the point of view of the spin dynamics, the laser pulse induced a demagnetization of the system. The latter was observed experimentally in many magnetic systems [21, 22]. In the coherent regime, there is no general agreement about the underlying mechanism of the ultrafast demagnetization. Some recent works [23, 24] pointed out that the spin-orbit interaction is responsible of the ultrafast demagnetization. Other works [25] attribute the ultrafast demagnetization to a superdiffusive

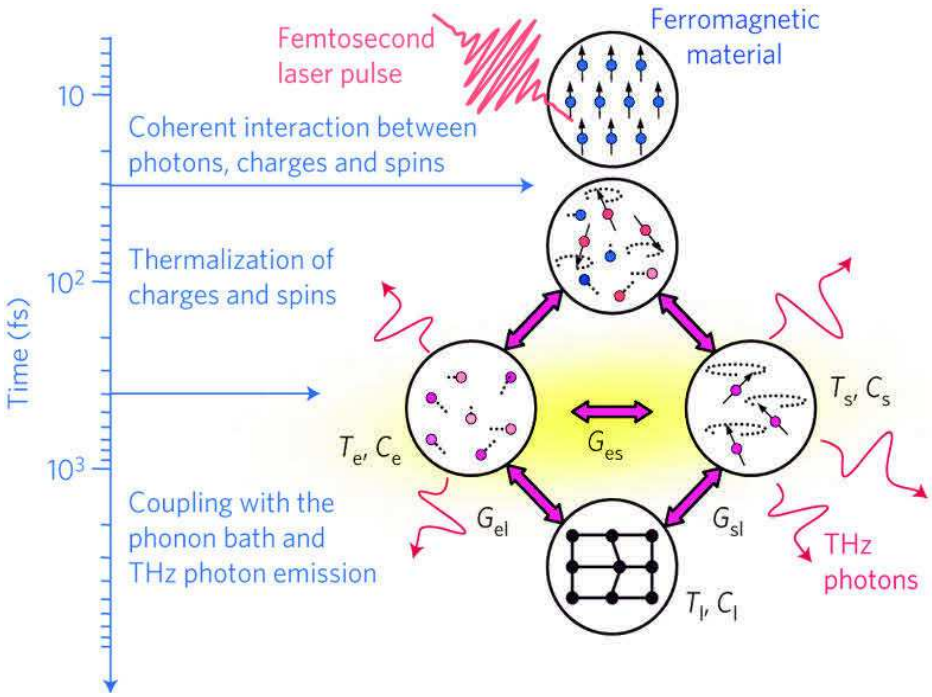

FIGURE 13: From [21], diagram of the different physical processes and the associated time scales induced by the interaction between a femtosecond laser pulse and a magnetic nano-structure.

transport of electrons induced by the laser field . During these fast processes, the ionic background remains frozen and the electron distribution is nonthermal. As a result, the electron temperature cannot be properly defined at this stage of the relaxation process. A few times after the coherent regime ($t > 50 - 100$ fs in Fig. 13), the laser energy injected in the system is redistributed between the electrons through electron–electron collisions and spin-flip processes, leading to the thermalization of the electron's charges and spins. Finally, in the picosecond regime, electron-phonon scattering lead to the relaxation of the electron's energy and to the thermalization of the full system.

From a theoretical point of view, the description of the electronic dynamics in metallic nano-structures is a very complex challenge. Exact approaches based on the N body Schrödinger equation are necessarily limited to a very small number of particles. Although such few- or even single-electron systems can nowadays be realized in laboratory, in most practical situations a great many electrons are involved [26,27]. In that case, self-consistent effects arising from the Coulomb interactions (between all the electrons) play a crucial role on the dynamics. Several theoretical and computational studies, which treat the many-body dynamics in an approximate way, focused on the linear and nonlinear electron response. Earlier works were based on phenomenological models [28–30] that employed Boltzmann-type equations within the framework of the Fermi-liquid theory [31]. Studies based on microscopic models (either classical or quantum) are more recent and limited to relatively small systems, due to their considerable computational cost. In the quantum regime, ultrafast electron dynamics in metallic clusters was studied by Calvayrac et al. [32] and more recently by Teperik et al. [33] using the time-dependent density functional theory (DFT). The many-particle quantum dynamics of the electron gas in a thin metal film was studied by Schwengelbeck et al. [34] within the framework of time-dependent Hartree-Fock (HF) approximation. Even the above-cited methods can be computationally too costly for very large systems.
A possible alternative relies on a semiclassical description of the electron dynamics. The semiclassical limit of the above quantum models (DFT and HF) is the self-consistent Vlasov-Poisson system. The Vlasov-Poisson model was used by many authors to model the electron dynamics in metal clusters [32, 35, 36] and in thin metallic films [37, 38]. For instance in Ref. [38], Manfredi and Hervieux identified, in addition to the the plasmon mode, a ballistic electron mode generated by bunches of electrons bouncing back and forth on the film surfaces. These works were later extended to the quantum regime using the Wigner phase-space description [39]. As it is based on the classical phase space, the Wigner formulation is often a more intuitive approach than the more standard Schrödinger approach, especially for problems where semiclassical considerations are important. For these reasons, it is used in many areas of quantum physics, including quantum optics [40], semiclassical analysis [41,42], electronic transport [43], nonlinear electron dynamics [39],

and quantum plasma theory [44]. It is also the starting point for the construction of quantum hydrodynamic equations, which are approximate models obtained by taking velocity moments of the Wigner function. Such models were used in the past to study the electron dynamics in molecular systems [45], metal clusters and nanoparticles [46–48], thin metal films [49], quantum plasmas [50,51], and semiconductors [52].

The above studies included the electron's charge, but not the electron's spin degrees of freedom. However, it is well known that spin effects (particularly the Zeeman interaction and the spin-orbit coupling) can play a decisive role in nanometric systems such as for instance semiconductor quantum dots [53,54] or diluted magnetic semiconductors [55,56]. The coupling between the spin degrees of freedom and the electron's orbital motion is of the utmost importance in many experimental studies involving magnetized nano-objects. A particularly interesting example is the ultrafast demagnetization induced by a femtosecond laser pulse in ferromagnetic thin films [21], an effect that is not yet completely elucidated from the theoretical viewpoint. Recent time-dependent density functional theory (TDDFT) simulations suggest that the spin-orbit coupling plays a central role in the demagnetization process [23].

Phase-space models based on the Boltzmann equation [57], and the corresponding fluid models [58], were derived in the past to describe the dynamics of a gas where the constituents possess internal degrees of freedom (internal angular momentum). However, in these models the spin is not treated ab-initio as a fundamental quantity, but is rather incorporated into the transport equations to ensure the correct conservation properties. More recently, a few theoretical models that include the spin in the Wigner formalism were also developed. One approach [59] consists in defining a scalar probability distribution that evolves in an extended phase space, where the spin is treated as a classical two-component variable (related to the two angles on a unit-radius sphere) on the same footing as the position or the momentum. This approach was used to derive a Wigner equation that incorporates spin effects through the Zeeman interaction [59]. Semiclassical [60] and hydrodynamic [61] spin equations were also derived from those models, including other relativistic effects such as the spin-orbit coupling, the Darwin term, and the relativistic mass correction.

An alternative approach keeps the 2×2 matrix character of the distribution function [62], so that the orbital and spin dynamics are represented by different Wigner functions. Using this approach, the corresponding Wigner equations were derived from the full Dirac theory [63]. However, their complexity makes them unsuitable for applications to condensed matter and nanophysics. Both approaches (extended phase space and matrix Wigner function) are equivalent from the mathematical point of view. However, the extended phase space approach leads to cumbersome hydrodynamic equations that are in practice very hard to solve, either analytically or numerically, even in the non-relativistic limit. The matrix technique separates clearly the orbital motion from the spin dynamics and leads to simpler and more

transparent hydrodynamic models. In this thesis we shall use the matrix technique to investigate the spin dynamics in metallic nano-structures.

This thesis is divided into two main parts. The first part is composed of the first four chapters and concerns the development of theoretical models and numerical simulations on the spin dynamics in ferromagnetic thin films (nickel). We shall derive a more tractable Wigner equation from the Pauli (instead of Dirac) theory, including both Zeeman and spin-orbit interactions. Then, from the Wigner formulation, we shall construct a four component Vlasov equation for a system composed of spin-1/2 electrons. The orbital part of the motion will be classical, whereas the spin degrees of freedom will be treated quantum-mechanically. This model will be applied to study the spin dynamics in ferromagnetic thin films of nickel. The second part corresponds to the chapter 5 and concerns the nonlinear charge dynamics of electrons (without spin) confined in metallic nanoparticles (Gold) or in anisotropic and nonparabolic wells. We shall use a variational approach based on the quantum hydrodynamic models to describe the electron dynamics.

The first chapter summarizes the different methods commonly used to describe the charge dynamics of an ensemble of interacting electrons. We first discuss the general many body problem in quantum mechanics. Then we present the general phase-space formulation of quantum mechanics as well as the way to perform semi-classical developments. Finally we discuss also the possibility to construct hydrodynamic models based on the Wigner phase-space distribution.

The second chapter concerns the extension of the phase-space methods to the spin. We will first use a gauge invariant formulation of the Weyl transformation to derive a set of Wigner equations for a system of spin-1/2 fermions. A self-consistent mean-field model will be further obtained by coupling these Wigner equations to the set of Maxwell equations for the electromagnetic fields, where the sources (charges and current densities) are related to velocity moments of the Wigner function. A related mean-field model was obtained recently by Dixit et al. [64] in the framework of the Schrödinger-Pauli equation. Subsequently, we will derive the corresponding semiclassical limit and obtain the Vlasov equations describing the evolution of an electron gas with spin and semi-relativistic effects. In this model, the orbital dynamics is treated classically, whereas the spin is represented as a fully quantum variable. Finally, the Vlasov equations will be used to derive a hierarchy of hydrodynamic equations by taking velocity moments of the probability distribution functions. This is an infinite hierarchy that needs to be closed using some additional physical hypotheses. Although this is relatively easy for spinless systems (where the closure can be obtained by a assuming a suitable equation of state), things are more subtle when the spin degrees of freedom are included. Here, we shall use a general method based on the maximization of the entropy (MEP) [65] to obtain a closed set of fluid equations with spin effects.

The third chapter deals with the linear analysis of the semiclassical phase-space models (with spin effects) developed in chapter 2. We essentially present the dispersion relation of a spin polarized electron gas and study the influence of spin effects on the plasma frequency.

The fourth chapter concerns the application of the phase-space methods developed in this thesis. We shall study the coherent spin dynamics in ferromagnetic thin film of nickel. The model is based on a distinction between local and itinerant magnetism, both interacting together through an Heisenberg exchange interaction. In the first part of the chapter, we will define a procedure to construct a self-consistent ground state which correctly describes the magnetic properties of nickel. Then we will present the numerical methods that we used to solve the phase-space equations. Finally the non linear electron dynamics will be investigated by means of numerical simulations, we will namely discover the possibility to create a spin current in a thin film of nickel with electric excitations (femtosecond laser pulses). We will analyse in details this process and propose a physical explanation for the underlying mechanisms.

Finally, in the last chapter we focus on the charge dynamics of electrons confined in metallic nanoparticles (Gold) and anisotropic and nonparabolic wells. The electron dynamics is investigated using a variational approach. The latter is based on the Lagrangian formulation of the quantum hydrodynamic equation. By postulating a reasonable ansatz for the electron density, it is possible to obtain a set of ordinary differential equations for some macroscopic quantities, such as the center of mass and the radial extension of the electron gas. Using this approach, we study the dynamics of collective modes (surface plasmons) excited with laser pulses in the visible range. One observes that using chirped pulses with a slowly varying frequency (so-called autoresonance phenomenon), it is possible to drive the plasmon mode far into the nonlinear regime, leading to the emission of an electromagnetic radiation with a power spectrum rich in high-order harmonics. This process is called autoresonance [66], meaning that the frequency of the system and the frequency of the excitation are phase locked. The autoresonant technique is very flexible and efficient, the required laser intensities are modest (10^{10} $\mathrm{W/cm^2}$) and no feedback mechanism is needed to match the driving frequency with the oscillator frequency.

Chapter 1

Theoretical methods to describe the electron dynamics in metallic nano-structures

In this chapter, we present the theoretical framework to describe the electronic dynamics in metallic nano-structures. In particular, we give a brief overview of the different existing methods to treat the case of spinless electrons. In the first part of this chapter, we shall highlight the physical quantities which characterize our system, as well as the different physical regimes (classical/quantum, collisionless/collisional). Then, in the second part, starting from the full Schrödinger formulation of the problem, we shall move into the phase-space representation of quantum mechanics, the so-called Wigner representation. Finally, we shall see how this formalism is helpful to construct reduced models, such as semiclassical and fluid models.

1.1 Basic concepts about electrons in metals

In this thesis, we focus on the theoretical description of electrons in metallic nano-structures. Metals are condensed matter systems with the specificity to have a half filled conduction band. The electrons that belong to the conduction band are not attached to a particle nucleus but are rather delocalized in the materials, leading to high transport properties. The latter could be understood by considering the conduction electrons as a non interacting system. Such model was used by Drude [67] in the beginning of the twentieth century to give approximative estimations of the electric and the thermal conductivity of metals. A more accurate understanding could be achieved by treating electrons as a plasma, globally neutralized by the surrounding ions. As it was pointed out in many papers [68, 69], conduction electrons in metals can be modelled as a quantum plasma. Quantum plasma systems were recently studied by several authors [44, 68, 70]. Before studying the general properties of a quantum plasma, we shall briefly remind basic elements of classical plasma physics.

1.1.1 Classical plasmas

A plasma is a state of the matter where all its constituents, atoms or molecules, has been partially or completely ionized. It is characterized by the fact that the average kinetic energy is larger than the interaction energy of next-nearest neighbors. This property is characterized by a small coupling parameter $\gamma \ll 1$. For a classical system of charged particles with density n, mass m, electric charge e and interacting via Coulomb forces (with an electric permittivity ϵ_0), the coupling parameter writes:

$$\gamma = \frac{E_{\text{pot}}}{E_{\text{kin}}} = \frac{e^2 n^{1/3}}{\epsilon_0 k_{\text{B}} T}, \tag{1.1}$$

where T is the temperature of the system that is related to the velocity of the particles

$$v_T = \left(2\frac{k_{\text{B}} T}{m}\right)^{1/2}. \tag{1.2}$$

In the case where the coupling parameter of the system is small, thermal effects are dominating, this regime is also known as the collisionless regime. In this regime the mean-field description of the system is feasible. This appears in a clearest way by introducing the Debye length:

$$\lambda_{\text{D}} = \sqrt{\frac{\epsilon_0 k_{\text{B}} T}{n e^2}}. \tag{1.3}$$

The Debye length represents the typical length on which the Coulomb interactions are screened by the charged medium. Using this quantity, the coupling parameter is rewritten as

$$\gamma = \left(\frac{1}{n^{1/3}\lambda_{\text{D}}}\right)^2. \tag{1.4}$$

Therefore, the plasma condition, $\gamma \ll 1$, implies that the Debye screening length is much larger than the interparticle distances, i.e. $\lambda_{\text{D}} \gg n^{-1/3}$, which is required to treat the system with a mean-field model. The latter condition implies also that collective effects would be dominant in the system compared to individual effects. In the opposite situation, i.e. $\gamma \geq 1$, the plasma is mainly governed by binary collisions. This regime is called the collisional or strongly coupled regime.
Moreover, the typical time scale for plasma particles is given by the inverse of the plasma frequency:

$$\omega_p = \sqrt{\frac{e^2 n}{m\epsilon_0}}. \tag{1.5}$$

If we consider the case of electrons in nano-structures, it corresponds to the typical oscillation frequency of the electrons with respect to the fixed ionic background.

1.1.2 Quantum plasmas

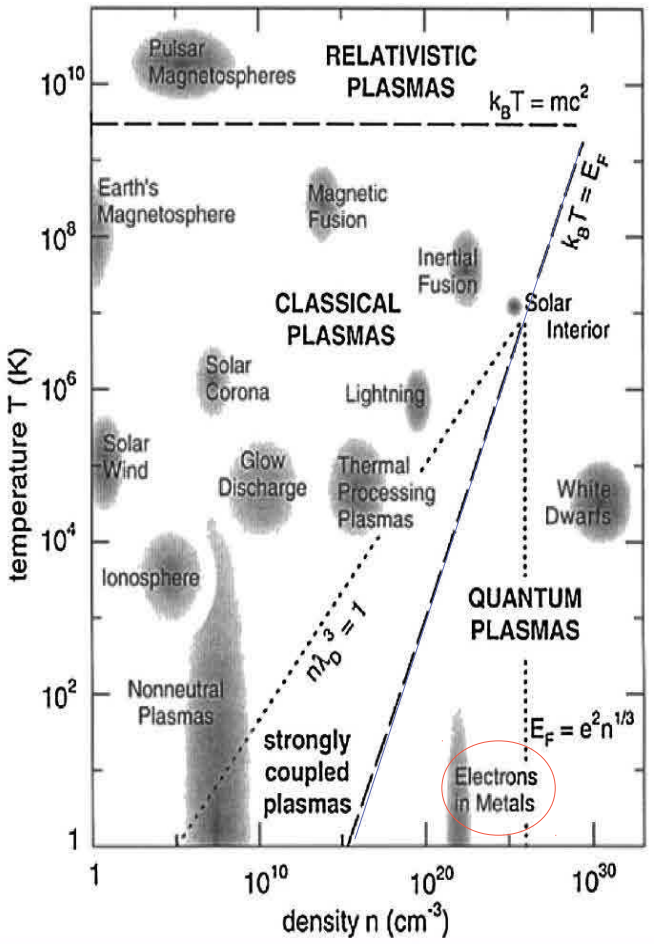

FIGURE 1.1: From Ref. [68], phase diagram of the different plasma regimes depending on the density and the temperature of the plasma. The blue line represents the transition between classical and quantum plasmas. The dot lines, inside both regions, represents the limit between collisional and collisionless plasmas. Finally, the dashed line represents the transition between relativistic and non-relativistic plasmas. Different physical systems are also represented in this diagram, such as electrons in metals (red circle).

Quantum effects can be measured with the thermal de Broglie wavelength of the particles composing the plasma:

$$\lambda_{\mathrm{DB}} = \frac{h}{p}, \tag{1.6}$$

where p is the typical impulsion of the particles and h the Planck constant.
The de Broglie wavelength roughly represents the spread of the particle's wave

function. For classical plasma this length is so small compare to the interparticle distances, such that the particles can be considered as pointlike and no overlaps of the wave function or quantum interferences happen. Therefore it is reasonable to say that quantum effects become important when the interparticle distance is smaller than the de Broglie wavelength, i.e $n^{1/3}\lambda_{\mathrm{DB}} \geq 1$. This condition can be expressed in another way. In the case of an electrons gas the Pauli exclusion principle, which is a purely quantum effect, imposes that all electrons should be in different quantum states. The consequence is that the statistical distribution of electrons follows the so-called Fermi-Dirac distribution. In this case, the characteristic temperature of the system is the Fermi temperature $T_{\mathrm{F}} = \hbar/(2mk_{\mathrm{B}})\left(3\pi^2 n\right)^{2/3}$. Indeed the Fermi-Dirac distribution deviates drastically from the classical Maxwell-Boltzmann distribution for temperatures much lower than the Fermi temperature. In the case where $T \ll T_{\mathrm{F}}$, the electron gas is said to be fully degenerate. Using the above expressions, one can write the ratio T_{F}/T as follows:

$$\frac{T_{\mathrm{F}}}{T} = \frac{(3\pi^2)^{2/3}}{(2\pi)^2}\left(n^{1/3}\lambda_{\mathrm{DB}}\right)^2. \tag{1.7}$$

Therefore quantum effects are also important when $T_{\mathrm{F}}/T \geq 1$.
All the quantities that characterize classical plasmas should be redefined for quantum plasmas. For a quantum plasma of electrons, the kinetic energy of the particles is not determined by thermal effects but rather by statistical effects. Indeed, as it is mentioned above, the Pauli exclusion principle implies that even at zero temperature the highest particle's velocity is not zero but is equal to the Fermi velocity:

$$v_{\mathrm{F}} = \sqrt{\frac{2E_{\mathrm{F}}}{m}} = \frac{\hbar}{m}\left(3\pi^2 n\right)^{1/3}. \tag{1.8}$$

In this case, the quantum coupling parameter writes:

$$\gamma_q = \frac{E_{\mathrm{pot}}}{E_{\mathrm{kin}}} = \frac{e^2 n^{1/3}}{\epsilon_0 m v_{\mathrm{F}}^2} = \left(\frac{1}{n^{1/3}\lambda_{\mathrm{F}}}\right)^2, \tag{1.9}$$

where $\lambda_{\mathrm{F}} = v_{\mathrm{F}}/\omega_p$ is the quantum analogue of the Debye length, also called the Thomas-Fermi screening length. Therefore in the quantum regime, the plasma condition is verified when the ratio between the interparticle distance and the the Thomas-Fermi screening length is much smaller than one : $n^{1/3} \ll \lambda_{\mathrm{F}}$.
Quantum plasma systems can be found in nature. For instance in the interior of neutrons stars and giant planets, white dwarfs and also (as we shall see below) electrons in metals.
Finally, if we consider an ensemble of interacting electrons, we notice from the discussion above that the different plasma regimes are characterized by the density and the temperature of the system. A phase diagram of the different plasma regimes is given in the Fig. 1.1.

r_s	$0.16\,\mathrm{nm}$
n	$5.9 \times 10^{28}\,\mathrm{m}^{-3}$
T	$300\,\mathrm{K}$
ω_p^{-1}	$0.5\,\mathrm{fs}$
T_F	$64000\,\mathrm{K}$
v_F	$1.4 \times 10^6\,\mathrm{m/s}$
λ_F	$0.11\,\mathrm{nm}$
γ_q	5.5

TABLE 1.1: Typical parameters for electrons in Gold at room temperature ($T = 300\,\mathrm{K}$)

1.1.3 Electrons in metals

In this section, we are going to evaluate the preceding plasma parameters in the case of electrons in metals. The typical electron density can be found using the Wigner-Seitz radius: $n = 3/(4\pi r_s^3)$. For numerical applications, we consider the case of Gold ($r_s = 3\ a_0$, a_0 being the Bohr radius), which corresponds to an electron density of $n = 6.0 \times 10^{28}\,\mathrm{m}^{-3}$. The typical time scale associated to this density is given by the inverse of the plasma frequency $T_p = 2\pi/\omega_p = 0.5\,\mathrm{fs}$. Using Eq. (1.8), one obtains the following Fermi velocity $v_\mathrm{F} = 1.4 \times 10^6\,\mathrm{m/s}$, which corresponds to a Fermi temperature of $T_\mathrm{F} = 65000\,\mathrm{K}$. Therefore at room temperature the ratio T_F/T is much larger than one, and hence the electrons should be treated as a quantum system. This is illustrated on the Fig. 1.1, where one clearly sees that electrons in metals are located in the quantum part of the phase diagram.
According to the formula (1.9), we found a quantum coupling parameter that is a bit larger than one: $\gamma_q \simeq 5.5$. That means that electron-electron collisions are as much important as collective effects and therefore the mean-field approximation is not valid any more and one should in principle go back to N body methods. However, and fortunately, collisions are decreased because of the Pauli blocking. This effect originates from the Pauli exclusion principle which forbids a large numbers of transitions at low temperature [71] and thus reduces the electron-electron collision rate ν_{ee}. A rough estimation of this reduction is given in Ref. [68]. It is found that, for temperature lower than T_F, the electron-electron collision rate reads:

$$\frac{\nu_{ee}}{\omega_p} \simeq \frac{E_\mathrm{F}}{\hbar\omega_p}\left(\frac{T}{T_F}\right)^2. \tag{1.10}$$

In the case of gold at room temperature ($T = 300\,\mathrm{K}$), one obtains the following value $\nu_{ee}^{-1} = 10^{-10}\,\mathrm{s}$. This collision time is valid for the equilibrium configuration. However during the dynamics, the electronic temperature increase leading to a smaller

collision time. However, for electronic temperatures lower than the Fermi temperature ($64000\,\mathrm{K}$ for Gold), the latter is estimated to be over a hundred of femtoseconds [72]. This is good news, since in this thesis, we want to study coherent electronic dynamics induced by femtosecond laser pulses and which typically occurs in the first hundred femtoseconds. Therefore, in a first approximation, we shall neglect the electron-electron collisions. In Tab. 1.1, we give the numerical values of several physical quantities that characterize the conduction electrons of Gold at room temperature.

1.2 The Schrödinger description of quantum mechanics

The N body quantum problem is a fascinating problem in physics. In quantum mechanics, particles are indistinguishable, this makes the problem more complicated to solve than in classical mechanics. Indeed, in classical mechanics particles are evolving separately, each of them obey a Newton equation, whereas in quantum mechanics they are described with the same object, the N body wave function

$$\Psi^N = \Psi\left(\boldsymbol{r}_1, \boldsymbol{r}_2, \cdots, \boldsymbol{r}_n, t\right), \tag{1.11}$$

where $\boldsymbol{r}_i$ is the position of the i-th particle. The non separability of the particles creates quantum correlations between them which have no classical counterpart. Therefore even solving a two-particle problem is quite challenging because of the high dimensionality of the wave function. Up to now exact methods are limitated to a small numbers of particles ($N < 10$), to treat larger systems one needs to make some approximations.

1.2.1 The mean-field approach

Let us consider a system of N interacting electrons, the most fundamental equation we have to describe such a system is the N body Schrödinger equation

$$i\hbar\frac{\partial\Psi^N}{\partial t} = -\frac{\hbar^2}{2m}\sum_{i=1}^{N}\left[\boldsymbol{\nabla}_i^2\Psi^N + \sum_{k=1,k\neq i}^{N}\frac{1}{2}\mathcal{V}\left(|\boldsymbol{r}_i - \boldsymbol{r}_k|\right)\Psi^N\right], \tag{1.12}$$

where $\mathcal{V}(\boldsymbol{r}) = \frac{e^2}{4\pi\epsilon_0}\frac{1}{|\boldsymbol{r}|}$ is the Coulomb potential.
This equation is supposed to be exact in non relativistic quantum mechanics. The usual approximation, which is often made, consists to factorize the N body wave function (1.11) into single-particle wave functions

$$\Psi^N = \Psi_1\left(\boldsymbol{r}_1, t\right)\Psi_2\left(\boldsymbol{r}_2, t\right)\cdots\Psi_N\left(\boldsymbol{r}_N, t\right). \tag{1.13}$$

This approximation consists to suppress all two-particle correlations (and hence higher-order particle correlations). Using Eqs. (1.12)-(1.13), the N body linear Schrödinger equation becomes the Hartree equations

$$i\hbar\frac{\partial\Psi_\alpha(\boldsymbol{r},t)}{\partial t} = -\frac{\hbar^2}{2m}\boldsymbol{\nabla}^2\Psi_\alpha(\boldsymbol{r},t) + \underbrace{\frac{e^2}{4\pi\epsilon_0}\left[\sum_{\alpha'=1}^{N}\int\frac{|\Psi_{\alpha'}(\boldsymbol{r'},t)|^2}{|\boldsymbol{r}-\boldsymbol{r'}|}d\boldsymbol{r'}\right]}_{V_{\mathrm{H}}}\Psi_\alpha(\boldsymbol{r},t)$$
$$-\underbrace{\frac{e^2}{4\pi\epsilon_0}\int\frac{|\Psi_\alpha(\boldsymbol{r'},t)|^2}{|\boldsymbol{r}-\boldsymbol{r'}|}d\boldsymbol{r'}}_{V_{sic}}\Psi_\alpha(\boldsymbol{r},t). \tag{1.14}$$

where the quantum states of each particle are labelled by the wave functions $\{\Psi_\alpha(\boldsymbol{r},t),\ \alpha=1,\cdots,N\}$. The term V_{H}, generally called the Hartree potential, can also be expressed in the form of the Poisson equation

$$\boldsymbol{\nabla}^2 V_{\mathrm{H}}(\boldsymbol{r},t) = \frac{e}{\epsilon_0}\sum_{\alpha=1}^{N}|\Psi_\alpha(\boldsymbol{r},t)|^2. \tag{1.15}$$

The potential V_{sic} is the self-interaction correction of the Hartree potential. It takes into account that an electron in orbital Ψ_α shall not interact with itself, but only with the $N-1$ remaining electrons of the system. The self interaction correction (SIC) is often neglected but in some case it has to be taken into account. For instance, the SIC correction is often important to describe long-range phenomena. Indeed in Ref. [73] the authors found that, in the case of Sodium clusters, the exchange-correlation potential did not have the correct asymptotic behaviour without considering the SIC correction (it decreases exponentially rather than $1/r$). In the rest of the thesis we shall neglect the SIC correction, in this case Eq. (1.14) can be rewritten in terms of the so-called Schrödinger-Poisson equation:

$$\begin{cases} i\hbar\dfrac{\partial\Psi_\alpha(\boldsymbol{r},t)}{\partial t} &= -\dfrac{\hbar^2}{2m}\boldsymbol{\nabla}^2\Psi_\alpha(\boldsymbol{r},t) - eV_{\mathrm{H}}(\boldsymbol{r},t)\Psi_\alpha(\boldsymbol{r},t), \\ \boldsymbol{\nabla}^2 V_{\mathrm{H}}(\boldsymbol{r},t) &= \dfrac{e}{\epsilon_0}\displaystyle\sum_{\alpha=1}^{N}|\Psi_\alpha(\boldsymbol{r},t)|^2. \end{cases} \tag{1.16}$$

We end up with a self-consistent set of N coupled single-particle Schrödinger equations. This type of model was first considered by Hartree in 1927 [74] in the context of atomic physics, to describe the self-consistent effect of atomic electrons on the Coulomb potential of the nucleus. The problem is considerably simplified because we passed from a $3N$ dimensional problem to N coupled three dimensional problems. This approximation in which correlations between particles are suppressed is called the mean-field approximation. In practice, it is impossible to solve the N body Schrödinger equation for more than few electrons. Therefore the factorization,

Eq. (1.13), seems to be the easiest way to treat many-particle systems.
However, the Hartree equations suffer from two problems. Firstly, they violate the Pauli exclusion principle which stipulates that two fermions can not be in the same quantum state. Therefore the total wave function has to be antisymmetric with respect to particles exchange. This kind of interaction creates some special correlations between particles known under the name of exchange interactions. In 1930 Slater and Fock proposed an exact method to describe the exchange interactions. They introduce the Slater determinant [75] to factorize the N body wave function as follows:

$$\Psi^N = \frac{1}{\sqrt{N!}} \begin{vmatrix} \Psi_1(\boldsymbol{r}_1,t) & \Psi_2(\boldsymbol{r}_1,t) & \cdots & \Psi_N(\boldsymbol{r}_1,t) \\ \Psi_1(\boldsymbol{r}_2,t) & \Psi_2(\boldsymbol{r}_2,t) & \cdots & \Psi_N(\boldsymbol{r}_2,t) \\ \vdots & \vdots & & \\ \Psi_1(\boldsymbol{r}_N,t) & \Psi_2(\boldsymbol{r}_N,t) & \cdots & \Psi_N(\boldsymbol{r}_N,t) \end{vmatrix}, \tag{1.17}$$

where $\left|\ddots\right|$ is the matrix determinant. In this case the Hartree equations become the Hartree-Fock equations [76]:

$$\begin{aligned} i\hbar\frac{\partial\Psi_\alpha(\boldsymbol{r},t)}{\partial t} = &-\frac{\hbar^2}{2m}\boldsymbol{\nabla}^2\Psi_\alpha(\boldsymbol{r},t) + \frac{e^2}{4\pi\epsilon_0}\left[\sum_{\alpha'=1}^{N}\int\frac{|\Psi_{\alpha'}(\boldsymbol{r'},t)|^2}{|\boldsymbol{r}-\boldsymbol{r'}|}d\boldsymbol{r'}\right]\Psi_\alpha(\boldsymbol{r},t) \\ &- \frac{e^2}{4\pi\epsilon_0}\left[\sum_{\alpha'=1}^{N}\int\frac{\Psi^*_{\alpha'}(\boldsymbol{r'},t)\Psi_\alpha(\boldsymbol{r'},t)}{|\boldsymbol{r}-\boldsymbol{r'}|}d\boldsymbol{r'}\right]\Psi_{\alpha'}(\boldsymbol{r},t). \end{aligned} \tag{1.18}$$

The Hartree-Fock equations differ from the Hartree equations by the last term in Eq. (1.18) that is related to the exchange interactions. Because of this term the Hartree-Fock equations belong to the class of non-local differential equations. This is why they are much complicated to solve numerically than the Hartree equations. For practical applications the Hartree-Fock equations are used for systems where exchange effects are important such as in nuclear physics [77] or in quantum chemistry [78]. Secondly, the other problem inherent to the the Hatree or Hartree-Fock methods comes from the fact that we do not take into account two-particle correlations. Indeed, in both models they are suppressed with the factorization of the N body wave function.
Another approach, based on the electron density, was developed in 1964 by Kohn and Sham [79] to treat many-body quantum systems. In this method, called density functional theory (DFT), the factorization of the total wave function is not needed anymore and the exchange-correlation effects are approximated by effective potentials. DFT is based on the two Hohenberg–Kohn theorems [80]. The first theorem states that the ground state properties of a many-electron system are uniquely determined by the electron density. Therefore the complicated N-body problem ($3N$ spatial coordinates) is reduced to find the correct electronic ground state density (3

spatial coordinates). The second theorem defines an energy functional for the system and proves that the correct ground state electron density minimizes this energy functional. However this functional cannot be formally written since the kinetic energy of an interacting electron gas is unknown. This problem is solved with the Kohn-Sham ansatz which states that the electron density of an interacting particle system can be written as the electron density of a non-interacting particle system. Therefore, the intractable many-body quantum problem of interacting electrons is reduced to a tractable problem of non-interacting electrons evolving in an effective potential. The effective potential includes the external potential, the Coulomb interactions between the electrons and the exchange and correlation interactions. The two latter are not known exactly and the art of DFT is to find the best way to approximate them. The simplest approximation is the so-called local density approximation [79], where the exchange and the correlation functionals depend locally on the electron density. DFT methods are very powerful and lead to considerable applications in materials science, chemistry, etc. [81]. A time dependent version of DFT, the time dependent density functional theory (TDDFT) [82] was also developed to treat dynamical systems.
Here, we are going to work in the spirit of density functional theories. It means that we will stay in the Hartree approximation and exchange-correlation effects will be taken into account by adding some suitable functionals of the density in our model. The Schrödinger approach was successfully used to treat a large numbers of quantum systems starting from the hydrogen atom to more complex structures such as bulk materials or molecules. The recent progress of computational science allows us to treat more and more complex systems. However all these studies are generally applied to determine the electronic ground state properties or in the framework of the linear response. To solve the nonlinear dynamics of many-body quantum systems is still an open problem.
The Schrödinger approach of quantum mechanics is not unavoidable, there exist other ways to deal with quantum mechanics. In this thesis we will work with the Wigner formulation of quantum mechanics. As we shall see, the advantage to use this formalism rather than the Schrödinger one, is that one can construct reduced models, either semiclassical or fluid, for which numerical simulations are easier to perform.

1.3 Quantum mechanics in phase space

In this section, we introduce the Wigner formulation of quantum mechanics. It is a formulation of quantum mechanics in the phase-space, it was first introduced by Eugene Wigner in 1932 to study quantum corrections to classical statistical mechanics [83]. The goal was to link the wave function that appears in the Schrödinger

equation to a pseudo-probability distribution function defined in the classical phase-space. This pseudo-probability distribution changes in time according to an evolution equation (Wigner equation) which is somewhat similar to the classical Liouville equation. Mathematically speaking, the Wigner formulation is based on the Weyl transformation [84,85], which is a general method to transform operators defined in the Hilbert space into phase-space functions.
In the first part of this section, we shall present a fast overview on the Weyl transformation, then we shall use this tool to derive the Wigner equation for spinless particles and its classical counterpart, the Vlasov equation. Finally we shall discuss the problem of gauge invariance when we consider particles evolving in magnetic fields.

1.3.1 The Weyl transformation

The basic idea of the phase-space formulation of quantum mechanics is to associate at each operator $\widehat{\mathcal{O}}\left(\widehat{\boldsymbol{R}},\widehat{\boldsymbol{P}}\right)$, depending on the position and momentum operators $\widehat{\boldsymbol{R}}$ and $\widehat{\boldsymbol{P}}$, a function $\mathcal{O}(\boldsymbol{r},\boldsymbol{p})$ of the classical phase-space variables $\boldsymbol{r}$ and $\boldsymbol{p}$. This correspondence is provided by the Weyl transformation [84,85], and is given by:

$$\widehat{\mathcal{O}}\left(\widehat{\boldsymbol{R}},\widehat{\boldsymbol{P}}\right)\equiv\int d\boldsymbol{r}\;d\boldsymbol{p}\;\mathcal{O}\left(\boldsymbol{r},\boldsymbol{p}\right)\widehat{\mathcal{F}}\left(\boldsymbol{r},\boldsymbol{p}\right), \tag{1.19}$$

where $\widehat{\mathcal{F}}\left(\boldsymbol{r},\boldsymbol{p}\right)$ is the Wigner operator defined as

$$\widehat{\mathcal{F}}\left(\boldsymbol{r},\boldsymbol{p}\right)\equiv\frac{1}{\left(2\pi\hbar\right)^{6}}\int d\boldsymbol{u}\;d\boldsymbol{v}\exp\left[\frac{i}{\hbar}\left(\boldsymbol{u}\cdot\left(\widehat{\boldsymbol{P}}-\boldsymbol{p}\right)+\boldsymbol{v}\cdot\left(\widehat{\boldsymbol{R}}-\boldsymbol{r}\right)\right)\right]. \tag{1.20}$$

The inverse of the Weyl transformation can be deduced[1] from the above definition:

$$\mathcal{O}\left(\boldsymbol{r},\boldsymbol{p}\right)=\left(2\pi\hbar\right)^{3}Tr\left[\widehat{\mathcal{F}}\left(\boldsymbol{r},\boldsymbol{p}\right)\widehat{\mathcal{O}}\left(\widehat{\boldsymbol{R}},\widehat{\boldsymbol{P}}\right)\right], \tag{1.21}$$

where Tr denotes the trace.
The Wigner phase-space distribution $\mathcal{F}\left(\boldsymbol{r},\boldsymbol{p}\right)$, or simply called the Wigner function, is related to the mean value of any arbitrary operator

$$\langle\widehat{\mathcal{O}}\left(\widehat{\boldsymbol{R}},\widehat{\boldsymbol{P}}\right)\rangle\equiv\int d\boldsymbol{r}\;d\boldsymbol{p}\;\mathcal{O}\left(\boldsymbol{r},\boldsymbol{p}\right)\mathcal{F}\left(\boldsymbol{r},\boldsymbol{p}\right). \tag{1.22}$$

The Wigner function plays a central role in the Wigner formulation because it is related to physical quantities which are always given in terms of operator's expected values.

[1] For the demonstration, we use the following properties of the Wigner operator: $Tr\left[\widehat{\mathcal{F}}\left(\boldsymbol{r},\boldsymbol{p}\right)\widehat{\mathcal{F}}\left(\boldsymbol{r'},\boldsymbol{p'}\right)\right]=\frac{1}{\left(2\pi\hbar\right)^{3}}\delta\left(\boldsymbol{p}-\boldsymbol{p'}\right)\delta\left(\boldsymbol{r}-\boldsymbol{r'}\right)$.

Considering a system in a statistical distribution of quantum state $\{p_i;|\phi_i\rangle\}$, we introduce the density operator $\widehat{\rho}=\sum_i p_i|\phi_i\rangle\langle\phi_i|$ and we use Eq. (1.19) to determine the mean value of an arbitrary operator

$$\langle\widehat{\mathcal{O}}\left(\widehat{\boldsymbol{R}},\widehat{\boldsymbol{P}}\right)\rangle=Tr\left[\widehat{\mathcal{O}}\left(\widehat{\boldsymbol{R}},\widehat{\boldsymbol{P}}\right)\widehat{\rho}\right]=\int d\boldsymbol{r}\;d\boldsymbol{p}\;\mathcal{O}\left(\boldsymbol{r},\boldsymbol{p}\right)Tr\left[\widehat{\mathcal{F}}\left(\boldsymbol{r},\boldsymbol{p}\right)\widehat{\rho}\right]. \tag{1.23}$$

The Wigner function is then defined as the phase-space function associated to the density operator

$$f\left(\boldsymbol{r},\boldsymbol{p}\right)=Tr\left[\widehat{\mathcal{F}}\left(\boldsymbol{r},\boldsymbol{p}\right)\widehat{\rho}\right]=\frac{1}{(2\pi\hbar)^3}\int d\boldsymbol{\lambda}\exp\left(\frac{i}{\hbar}\boldsymbol{\lambda}\cdot\boldsymbol{p}\right)\left\langle\boldsymbol{r}-\frac{1}{2}\boldsymbol{\lambda}|\widehat{\rho}|\boldsymbol{r}+\frac{1}{2}\boldsymbol{\lambda}\right\rangle. \tag{1.24}$$

The Wigner function obeys to the following equation of motion (Wigner equation):

$$i\hbar\frac{\partial f}{\partial t}=\{\mathcal{H},f\}_\star, \tag{1.25}$$

where the last term is referred to as the Moyal bracket [86] (here and in the following, we use Einstein's summation convention):

$$\begin{aligned}\{A(\boldsymbol{r},\boldsymbol{p}),B(\boldsymbol{r},\boldsymbol{p})\}_\star&=A(\boldsymbol{r},\boldsymbol{p})\star B(\boldsymbol{r},\boldsymbol{p})-B(\boldsymbol{r},\boldsymbol{p})\star A(\boldsymbol{r},\boldsymbol{p}),\\&=2i\sin\left[\frac{\hbar}{2}\left({}^L\partial_i{}^R\partial_{p_i}-{}^L\partial_{p_j}{}^R\partial_j\right)\right](A(\boldsymbol{r},\boldsymbol{p}),B(\boldsymbol{r},\boldsymbol{p})).\end{aligned} \tag{1.26}$$

The indices L and R mean that the derivative acts only on the left or on the right term in the parenthesis[2].

The Wigner equation is the analogue of the density matrix evolution equation in the operator's representation of quantum mechanics: $i\hbar\partial_t\widehat{\rho}=\left[\widehat{\mathcal{H}},\widehat{\rho}\right]$, sometimes called the Von Neumann equation. The Moyal brackets can be easily developed as a power series of $\hbar$, which makes the Wigner formulation particularly interesting to study the semiclassical limit. The lowest order term leads to the standard Poisson bracket and to the equations of classical mechanics. In Eq. (1.25), $\mathcal{H}$ is the phase-space function associated to the Hamiltonian operator $\widehat{\mathcal{H}}$ of the system, both are related by Eq. (1.19). In order to determine the phase-space function of any arbitrary operator $\widehat{\mathcal{O}}\left(\widehat{\boldsymbol{R}},\widehat{\boldsymbol{P}}\right)$, one should apply the Weyl correspondence rules [85, 87], defined as follows: (i) first symmetrize the operator $\widehat{\mathcal{O}}\left(\widehat{\boldsymbol{R}},\widehat{\boldsymbol{P}}\right)$ with respect to the position and the momentum operators $\widehat{\boldsymbol{R}}$ and $\widehat{\boldsymbol{P}}$; (ii) then replace $\widehat{\mathcal{O}}\left(\widehat{\boldsymbol{R}},\widehat{\boldsymbol{P}}\right)$ by their associated classical variables. For instance, for the operator $\widehat{P}_x\widehat{X}$ one finds

$$\widehat{P}_x\widehat{X}=\frac{1}{2}\left(\widehat{P}_x\widehat{X}+\widehat{X}\widehat{P}_x\right)-\frac{i\hbar}{2}\to xp_x-\frac{i\hbar}{2}, \tag{1.27}$$

[2] For instance: ${}^L\partial_i{}^R\partial_{p_j}\left(A(\boldsymbol{r},\boldsymbol{p}),B(\boldsymbol{r},\boldsymbol{p})\right)=\left(\partial_i A\right)\left(\partial_{p_j}B\right)$.

where use has been made of the commutator $[\widehat{P}_x, \widehat{X}] = \hbar/i$. We note that the Weyl correspondence defined above is not unique, and one could have defined other rules leading to different phase-space functions, such as the the Husimi representation [88]. This issue is discussed in more details in Ref. [85].

1.3.2 The Wigner-Poisson equation

The preceding methodology can be used to derive the Wigner equation for a system of N interacting electrons treated in a mean-field approach. The density matrix of such a system is given by:

$$\widehat{\rho} = \sum_{\alpha=1}^{N} p_\alpha \left|\Psi_\alpha\right\rangle\left\langle\Psi_\alpha\right|, \tag{1.28}$$

where p_α is the probability for one particle to be in the sate Ψ_α. Since we are in a mean-field approach, the state Ψ_α obeys to a Schrödinger-Poisson equation (1.16). Then using Eqs. (1.24) and (1.28), we obtain the following Wigner function of the system:

$$f\left(\boldsymbol{r},\boldsymbol{p},t\right) = \frac{1}{\left(2\pi\hbar\right)^3}\sum_{\alpha=1}^{N} p_\alpha \int d\lambda \exp\left(\frac{i\boldsymbol{p}\cdot\boldsymbol{\lambda}}{\hbar}\right)\Psi_\alpha^*\left(\boldsymbol{r}+\frac{\boldsymbol{\lambda}}{2},t\right)\Psi_\alpha\left(\boldsymbol{r}-\frac{\boldsymbol{\lambda}}{2},t\right). \tag{1.29}$$

The evolution equation for the Wigner function can be derived[3] using Eq. (1.25). We obtain the Wigner-Poisson equation for an interacting electron gas:

$$\begin{cases} \dfrac{\partial f}{\partial t} + \dfrac{1}{m}\boldsymbol{p}\cdot\boldsymbol{\nabla} f &= \dfrac{ie}{\hbar}\dfrac{1}{\left(2\pi\hbar\right)^3}\displaystyle\int d\boldsymbol{\lambda} d\boldsymbol{p'} \exp\left[\frac{i\left(\boldsymbol{p}-\boldsymbol{p'}\right)\cdot\boldsymbol{\lambda}}{\hbar}\right]\left[V_{\mathrm{H}}\left(\boldsymbol{r}_+\right)-V_{\mathrm{H}}\left(\boldsymbol{r}_-\right)\right] f(\boldsymbol{r},\boldsymbol{p'},t), \\ \boldsymbol{\nabla}^2 V_{\mathrm{H}} &= \dfrac{e}{\epsilon_0}\displaystyle\int f(\boldsymbol{r},\boldsymbol{p},t) d\boldsymbol{p}. \end{cases} \tag{1.30}$$

where the indices $\pm$ design shifted positions $\boldsymbol{r}_+ = \boldsymbol{r} \pm \boldsymbol{\lambda}/2$.
This equation is completely equivalent to the Schrödinger-Poisson equations (1.16). It is on the basis of all the different models that we shall develop in this work. It gives the evolution in time of the phase-space distribution function $f(\boldsymbol{r},\boldsymbol{p},t)$. We notice that the equation is non local in both position and velocity space. This property is clearly due to quantum effects. A numerical integration of such equation is not trivial, it as been done in Ref. [89] for a one dimensional system (film of sodium) to study the electron thermalization and the quantum decoherence. As it is mentioned in the previous section, the Wigner equation is useful to perform semiclassical analysis, this shall be illustrated in the next section.

[3] The derivation is given in details in the appendix A.

1.3.3 Classical limit and Vlasov equation

The Wigner formulation of quantum mechanics is really convenient to study the classical limit, i.e. $\hbar \to 0$. Indeed the Moyal product given by Eq. (1.26) can be expend as a power series of $\hbar$

$$\begin{aligned}\{A(\boldsymbol{r},\boldsymbol{p}),B(\boldsymbol{r},\boldsymbol{p})\}_\star = &\{A(\boldsymbol{r},\boldsymbol{p}),B(\boldsymbol{r},\boldsymbol{p})\}\\ &+2i\sum_{n=1}^{\infty}\left(\frac{\hbar}{2}\right)^{2n+1}\frac{(-1)^n}{(2n+1)!}\left({}^{L}\partial_i{}^{R}\partial_{p_i}-{}^{L}\partial_{p_j}{}^{R}\partial_j\right)^{2n+1}\left(A(\boldsymbol{r},\boldsymbol{p}),B(\boldsymbol{r},\boldsymbol{p})\right),\end{aligned} \tag{1.31}$$

where the zero order term is the Poisson bracket

$$\{A(\boldsymbol{r},\boldsymbol{p}),B(\boldsymbol{r},\boldsymbol{p})\}=\left(\partial_i A\right)\left(\partial_{p_i}B\right)-\left(\partial_{p_j}A\right)\left(\partial_j B\right), \tag{1.32}$$

which is often used in classical mechanics. If we set $\hbar = 0$ in the Eq. (1.31), then we recover the Liouville equation:

$$\partial_t f(\boldsymbol{r},\boldsymbol{p},t)=\{H,f(\boldsymbol{r},\boldsymbol{p},t)\}. \tag{1.33}$$

The Liouville equation is the classical equivalence of the density operator evolution equation in quantum mechanics:

$$i\hbar\partial_t\widehat{\rho}(\boldsymbol{r},t)=\left[\widehat{H},\widehat{\rho}(\boldsymbol{r},t)\right]. \tag{1.34}$$

It is well known that if we consider a system of N interacting particles in a mean-field approach, we found that the Liouville equation is equivalent to the Vlasov equation [90]

$$\frac{\partial f}{\partial t}+\frac{\boldsymbol{p}}{m}\cdot\boldsymbol{\nabla}f+e\boldsymbol{\nabla}V_{\mathrm{H}}\cdot\boldsymbol{\nabla}_{\boldsymbol{p}}f=0 \tag{1.35}$$

Therefore, the classical limit of the Wigner-Poisson equation (1.30) is the Vlasov-Poisson equation

$$\begin{cases}\dfrac{\partial f}{\partial t}+\dfrac{\boldsymbol{p}}{m}\cdot\boldsymbol{\nabla}f+e\boldsymbol{\nabla}V_{\mathrm{H}}\cdot\boldsymbol{\nabla}_{\boldsymbol{p}}f=0,\\[2ex] \boldsymbol{\nabla}^2V_{\mathrm{H}}=\dfrac{e}{\epsilon_0}\displaystyle\int f(\boldsymbol{r},\boldsymbol{p},t)d\boldsymbol{p}.\end{cases} \tag{1.36}$$

For simulation purposes, the Vlasov-Poisson system of equations (1.36) is much easier to solve numerically than the corresponding Wigner-Poisson equation (1.30), mainly because the former are local in space while the latter are not. The Vlasov approximation is valid when quantum effects in the orbital dynamics are small. From Eq. (1.26), it appears that the semiclassical expansion is valid when $\hbar/(mL_0v_0)\ll 1$, where L_0 and v_0 are typical length and velocity scales. For a degenerate electron

gas with density n, the typical velocity is the Fermi speed $v_F = \hbar(3\pi^2 n)^{1/3}/m$. Inserting into the previous inequality, we obtain the validity condition $L_0 n^{1/3} \gg 1$, which means that the typical length scale must be larger than the interparticle distance $d = n^{-1/3}$. For this reason, the semiclassical limit is also referred to as the long wavelength approximation. All in all, the above Vlasov equations constitute a valuable tool to simulate the charge dynamics in condensed matter systems, particularly semiconductor and metallic nano-objects.

1.3.4 Magnetic field and gauge invariance

For the moment we didn't include any magnetic effects. This approximation can be justified in some case, for instance if we are only interested in the plasmon excitations. However, magnetic interactions can not be avoid if we want to include spin degrees of freedom in our models. As we will see the introduction of magnetic field in the Wigner formalism is not trivial. It is well known that in presence of magnetic fields one should use the kinetic momentum operator $\widehat{\boldsymbol{\Pi}} = \widehat{\boldsymbol{P}} - q\widehat{\boldsymbol{A}}$ instead of $\widehat{\boldsymbol{P}}$ (with $q = -e$ for an electron). This situation cannot be addressed by simply replacing $\widehat{\boldsymbol{P}}$ with $\widehat{\boldsymbol{\Pi}}$ in the Weyl transformation. Indeed it can be easily proved that with such substitution the Wigner function, Eq. (1.24), is not gauge invariant. As spin effects, such as the Zemann interaction or the spin-orbit coupling, strongly depend on the magnetic field, it is of paramount importance to work with a gauge invariant formulation of the Weyl transformation. A gauge independent definition of the Wigner function was first introduced by Stratonovich [91]:

$$f(\boldsymbol{r},\boldsymbol{v},t) = \left(\frac{m}{2\pi\hbar}\right)^3 \int d\boldsymbol{\lambda} \exp\left[\frac{i\boldsymbol{\lambda}}{\hbar}\cdot\left(m\boldsymbol{v} - e\int_{-1/2}^{1/2} d\tau \boldsymbol{A}\left(\boldsymbol{r}+\tau\boldsymbol{\lambda}\right)\right)\right]\left\langle \boldsymbol{r} - \frac{\boldsymbol{\lambda}}{2}\middle|\widehat{\rho}\middle|\boldsymbol{r}+\frac{\boldsymbol{\lambda}}{2}\right\rangle, \tag{1.37}$$

where the impulsion $\boldsymbol{p}$ was replaced by $m\boldsymbol{v} - e\int_{-1/2}^{1/2} d\tau \boldsymbol{A}\left(\boldsymbol{r}+\tau\boldsymbol{\lambda}\right)$.
To be consistent with this new definition of the Wigner function, one should also modify the Weyl correspondence rules [87]. The procedure is almost identical to the no magnetic field case, except that one should use $\widehat{\boldsymbol{\Pi}}$ instead of $\widehat{\boldsymbol{P}}$. The only difference is that one must also symmetrize operators with respect to the different components of $\widehat{\boldsymbol{\Pi}}$, because they do not commute, i.e. $\left[\widehat{\Pi}_i, \widehat{\Pi}_j\right] = -i\hbar e\epsilon_{ijk}B_k(\widehat{\boldsymbol{R}})$, where ϵ_{ijk} is the Levi-Civita symbol. The classical phase-space variables associated to the kinetic momentum operator is the linear momentum $\widehat{\boldsymbol{\Pi}} \to \boldsymbol{\pi} = m\boldsymbol{v}$.
The Moyal product defined in Eq. (1.26) is also modified in the presence of magnetic fields. A gauge invariant Moyal product was derived by Müller [92], and reads

$$A(\boldsymbol{r},\boldsymbol{\pi}) \star C(\boldsymbol{r},\boldsymbol{\pi}) = \exp\left[i\hbar\mathcal{L} + ie\sum_{n=1}^{\infty}\hbar^n\mathcal{L}_n\right]\left(A(\boldsymbol{r},\boldsymbol{\pi}), C(\boldsymbol{r},\boldsymbol{\pi})\right), \tag{1.38}$$

where $\mathcal{L}$ is the operator corresponding to the free magnetic field case:

$$\mathcal{L}\left(A(\boldsymbol{r},\boldsymbol{\pi}),C(\boldsymbol{r},\boldsymbol{\pi})\right)=\frac{1}{2}\left({}^{L}\partial_{i}{}^{R}\partial_{\pi_i}-{}^{R}\partial_{j}{}^{L}\partial_{\pi_j}\right)\left(A(\boldsymbol{r},\boldsymbol{\pi}),C(\boldsymbol{r},\boldsymbol{\pi})\right), \tag{1.39}$$

and $\mathcal{L}_n$ is a new operator that depends on the magnetic field:

$$\mathcal{L}_n\left(A(\boldsymbol{r},\boldsymbol{\pi}),C(\boldsymbol{r},\boldsymbol{\pi})\right)=\left(\frac{i}{2}\right)^{n+1}\frac{\epsilon_{jlr}}{(n+1)^2\,n!}\sum_{i_1\ldots i_{n-1}=1}^{3}\left(\frac{\partial^{n-1}}{\partial r_{i_1}\ldots\partial r_{i_{n-1}}}B_r\right){}^{L}\partial_{\pi_j}{}^{R}\partial_{\pi_l}\sum_{p=1}^{n}$$
$$\binom{n+1}{p}g(n,p)\,\frac{\partial^{p-1}}{\partial\pi_{i_1}\ldots\partial\pi_{i_{p-1}}}\frac{\partial^{n-p}}{\partial\pi_{i_p}\ldots\partial\pi_{i_{n-1}}}\left(A(\boldsymbol{r},\boldsymbol{\pi}),C(\boldsymbol{r},\boldsymbol{\pi})\right). \tag{1.40}$$

with $g(n,p)=\left[\left(1-(-1)^{p}\right)(n+1)-\left(1-(-1)^{n+1}\right)p\right]$, $(r_1,r_2,r_3)=(x,y,z)$ and $(\pi_1,\pi_2,\pi_3)=(\pi_x,\pi_y,\pi_z)$. This new definition of the Moyal product makes the calculation of the evolution equation much more cumbersome than in the unmagnetized case. Its great advantage is that it ensures that the final equations of motion are gauge invariant.

A very complete description on the inclusion of electromagnetic fields in the Wigner formalism can be also found in Ref. [87]. In this reference, the author discuss also the case where the electromagnetic fields are quantized.

Using Eqs. (1.38) - (1.40) and Eq. (1.25), one is able to write the Wigner equation for a spinless particle interacting with electromagnetic fields as follows[4]:

$$\frac{\partial f}{\partial t}+\frac{1}{m}\left(\boldsymbol{\pi}+\boldsymbol{\Delta\widetilde{\pi}}\right)\cdot\boldsymbol{\nabla}f-\frac{e}{m}\left[m\widetilde{\boldsymbol{E}}+\left(\boldsymbol{\pi}+\boldsymbol{\Delta\widetilde{\pi}}\right)\times\widetilde{\boldsymbol{B}}\right]_i\partial_{\pi_i}f=0, \tag{1.41}$$

where $\boldsymbol{\Delta\widetilde{\pi}}$ depends on the magnetic field and corresponds to a quantum shift of the velocity

$$\boldsymbol{\Delta\widetilde{\pi}}=-i\hbar e\partial_{\boldsymbol{\pi}}\times\left[\int_{-1/2}^{1/2}d\tau\,\tau\boldsymbol{B}\left(\boldsymbol{r}+i\hbar\tau\partial_{\boldsymbol{\pi}}\right)\right] \tag{1.42}$$

and $\widetilde{\boldsymbol{E}}$, $\widetilde{\boldsymbol{B}}$ are written in terms of the electric and magnetic fields

$$\widetilde{\boldsymbol{E}}=\int_{-1/2}^{1/2}d\tau\boldsymbol{E}\left(\boldsymbol{r}+i\hbar\tau\partial_{\boldsymbol{\pi}}\right),\quad\widetilde{\boldsymbol{B}}=\int_{-1/2}^{1/2}d\tau\boldsymbol{B}\left(\boldsymbol{r}+i\hbar\tau\partial_{\boldsymbol{\pi}}\right). \tag{1.43}$$

This illuminating form of the Wigner equation was first proposed by Serimaa et al. [87]. In the classical limit, i.e. $\hbar=0$, it is straightforward to notice that we simply have $\widetilde{\boldsymbol{E}}=\boldsymbol{E}$, $\widetilde{\boldsymbol{B}}=\boldsymbol{B}$ and $\boldsymbol{\Delta\widetilde{\pi}}=0$. Thus, the Wigner equations writes :

$$\frac{\partial f}{\partial t}+\boldsymbol{v}\cdot\boldsymbol{\nabla}f-\frac{e}{m}\left(\boldsymbol{E}+\boldsymbol{v}\times\boldsymbol{B}\right)\cdot\boldsymbol{\nabla}_{\boldsymbol{v}}f=0 \tag{1.44}$$

[4]The demonstration is given in the appendix A.

We simply recover the Vlasov equation where the force term is just the Lorentz force according to classical mechanics.

1.4 Fluid models

Wigner and Vlasov equations belong to the class of kinetic models because they make evolve objects defined in the phase-space, namely the distribution function. These type of models contain the same amount of informations as the Newton equations (for the Vlasov equations) or the Schrödinger equations (for the Wigner equations). We have seen before that the Wigner approach is really useful to study semi-classical limits of the full quantum problem.
These approaches are also often used to construct fluid models (or hydrodynamic models). The construction of such models is based on the following consideration. First, we notice that by taking different velocity moments of the Wigner function, one is able to construct average quantities such as the electron density, the charge current, the pressure tensor, etc. Indeed, if we integrate the usual Wigner distribution function (1.29) over the impulsion space, then after some straightforward algebra, one obtains the zero order moment of the Wigner function

$$\int f d\boldsymbol{p} = \sum_{\alpha=1}^{N} \Psi_\alpha^* \left(\boldsymbol{r}, t\right) \Psi_\alpha \left(\boldsymbol{r}, t\right) \equiv n \left(\boldsymbol{r}, t\right), \tag{1.45}$$

which is the electronic density. With the same kind of calculation, one can prove that the first order moment gives the electronic current:

$$\int \boldsymbol{p} f d\boldsymbol{p} = \frac{i\hbar}{2} \sum_{\alpha=1}^{N} \left[\Psi_\alpha \left(\boldsymbol{r}, t\right) \boldsymbol{\nabla} \Psi_\alpha^* \left(\boldsymbol{r}, t\right) - \Psi_\alpha^* \left(\boldsymbol{r}, t\right) \boldsymbol{\nabla} \Psi_\alpha \left(\boldsymbol{r}, t\right)\right] \equiv \boldsymbol{j} \left(\boldsymbol{r}, t\right), \tag{1.46}$$

Fluid models are constructed by taking different moments of the Wigner equation. For instance, if we integrate the Wigner equation (1.30) over the impulsion, we obtain the well known continuity equation:

$$\frac{\partial n}{\partial t} + \boldsymbol{\nabla} \left(n \boldsymbol{u}\right) = 0, \tag{1.47}$$

which originates from the local conservation of the mass in the system.
We notice that in Eq. (1.47), we have used the average velocity $\boldsymbol{u}(\boldsymbol{r}, t) \equiv \boldsymbol{j}(\boldsymbol{r}, t)/n(\boldsymbol{r}, t)$ instead of the the current density. The continuity equation gives formally the time evolution of the electronic density as a function of the charge current. To obtain, the time evolution of the charge current, one simply has to multiply the Wigner equation by $\boldsymbol{p}$ and then integrate it over the impulsion. In this case one obtains an Euler

type of equation:

$$\frac{\partial u_i}{\partial t} + u_j(\partial_j u_i) = -\frac{1}{nm}\partial_j P_{ij} + \frac{1}{m}\partial_i V, \tag{1.48}$$

where V is an arbitrary potential.
The Euler equation gives the evolution of the mean velocity of the particles with respect to the force acting on them. One part of the forces is due to the potential V whereas the other part is related to a new fluid quantity P_{ij}. This new term corresponds to the pressure tensor of the system and is a second order moment of the distribution function defined as follows:

$$P_{ij} = \int w_i w_j f d\boldsymbol{p}, \tag{1.49}$$

where we separated the mean fluid velocity $\boldsymbol{u}$ from the velocity fluctuations $\boldsymbol{w} \equiv \boldsymbol{v} - \boldsymbol{u}$.
To obtain the evolution equation of the pressure term P_{ij} present in the fluid equation (1.48), one should take the second order moment of the Wigner equations. However this procedure has no end, each time that we derive an evolution equation for a certain fluid quantity then we will introduce a higher order moment of the Wigner function in the fluid equations. Such that the Wigner equation is equivalent to an infinite set of fluid equations. For practical use they need to be closed using some additional physical hypotheses.
A simple closure can be achieved by writing the pressure term as a function of the electronic density. This can be shown by writing the pressure tensor in terms of the electronic wave functions. For instance, using Eqs. (1.29) and (1.49) and after some algebra, one is able to write the pressure tensor as follows:

$$\begin{aligned} P_{ij} =& \frac{\hbar^2}{4m}\sum_\alpha p_\alpha \left[\left(\partial_i \Psi_\alpha^*\right)\left(\partial_j \Psi_\alpha\right) + \left(\partial_j \Psi_\alpha^*\right)\left(\partial_i \Psi_\alpha\right) - \Psi_\alpha^*\left[\partial_i\left(\partial_j \Psi_\alpha\right)\right] - \Psi_\alpha\left[\partial_i\left(\partial_j \Psi_\alpha^*\right)\right]\right] \\ &+ \frac{\hbar^2}{4mn}\left[\sum_\alpha p_\alpha \left[\Psi_\alpha^*\left(\partial_i \Psi_\alpha\right) - \Psi_\alpha\left(\partial_i \Psi_\alpha^*\right)\right]\left[\Psi_\alpha^*\left(\partial_j \Psi_\alpha\right) - \Psi_\alpha\left(\partial_j \Psi_\alpha^*\right)\right]\right]^2. \end{aligned} \tag{1.50}$$

In order to interpret this pressure tensor, we shall use the Madelung decomposition of the wave function [93]:

$$\Psi_\alpha(\boldsymbol{r}, t) = A_\alpha(\boldsymbol{r}, t)\exp\left(\frac{iS_\alpha(\boldsymbol{r}, t)}{\hbar}\right), \tag{1.51}$$

where $A_\alpha(\boldsymbol{r}, t)$ is the amplitude of the wave function and $S_\alpha(\boldsymbol{r}, t)$ its phase, both are real functions.
This transformation of the wave function is at the origin of the Bohm formulation of quantum mechanics [94], in which the Schrödinger equation writes as a fluid equation. The individual particle density and velocity of the quantum flow are defined

as follows:

$$n_\alpha(\boldsymbol{r},t) = A_\alpha^2(\boldsymbol{r},t), \quad \boldsymbol{u}_\alpha(\boldsymbol{r},t) = \frac{1}{m}\boldsymbol{\nabla} S_\alpha(\boldsymbol{r},t). \tag{1.52}$$

The connection with the fluid models, derived from the Wigner approach, are made by taking statistical average of Eq. (1.52) to construct the total electronic density and the mean velocity

$$n = \sum_{\alpha=1}^{N} p_\alpha n_\alpha \quad \text{and} \quad \langle u \rangle \equiv u = \frac{1}{n}\sum_{\alpha=1}^{N} p_\alpha n_\alpha u_\alpha. \tag{1.53}$$

Then using, Eqs. (1.51)-(1.53), one obtains a simple form for the pressure tensor, Eq. (1.50):

$$P_{ij} = mn\left(\langle u_i u_j\rangle - \langle u_i\rangle\langle u_j\rangle\right) + \frac{\hbar^2}{2m}\sum_\alpha p_\alpha\left[\left(\partial_i\sqrt{n_\alpha}\right)\left(\partial_j\sqrt{n_\alpha}\right) - \sqrt{n_\alpha}\left(\partial_i\left(\partial_j\sqrt{n_\alpha}\right)\right)\right]. \tag{1.54}$$

The first term of the right side is related to the dispersion of the velocity and thus corresponds to a classical pressure. For instance, in the case of a completely degenerated electron gas, the classical pressure writes as function of the density [71]:

$$P_C = \frac{\left(3\pi^2\right)^{2/3}\hbar^2}{5m} n_0^{5/3}. \tag{1.55}$$

Here, n_0 design the equilibrium electronic density.
The second term of the right side is proportional to $\hbar$. Therefore, it is a quantum pressure P_Q, with no classical counterpart. The latter depends on the individual electronic density. Under the assumption that the amplitude of all wave functions are equal, i.e. $A_\alpha(\boldsymbol{r},t) = A(\boldsymbol{r},t)$, Manfredi proposed in the Ref. [68] to rewrite simply the quantum pressure as follows:

$$\left(P_Q\right)_{ij} = \frac{\hbar^2}{2m}\left[\left(\partial_i\sqrt{n}\right)\left(\partial_j\sqrt{n}\right) - \sqrt{n}\left[\partial_i\left(\partial_j\sqrt{n}\right)\right]\right]. \tag{1.56}$$

Then using the equations for the classical pressure (1.55) and the quantum pressure (1.56), one is able to rewrite the fluid equations (1.47) and (1.48) in a closed form:

$$\begin{cases} \dfrac{\partial n}{\partial t} + \boldsymbol{\nabla}\cdot(n\boldsymbol{u}) = 0, \\ \dfrac{\partial u_i}{\partial t} + u_j(\partial_j u_i) = +\dfrac{\hbar^2}{2m^2}\partial_i\left[\dfrac{\boldsymbol{\nabla}^2\sqrt{n}}{\sqrt{n}}\right] - \dfrac{1}{nm}\partial_j\left(P_C\right)_{ij} + \dfrac{1}{m}\partial_i V. \end{cases} \tag{1.57}$$

In this fluid model, the quantum pressure appears as a force term $\nabla \mathcal{U}_{\mathrm{B}}$, where we have introduced the Bohm potential [94]:

$$\mathcal{U}_{\mathrm{B}} = -\frac{\hbar^2}{2m}\frac{\nabla^2\sqrt{n_\alpha}}{\sqrt{n_\alpha}}. \tag{1.58}$$

This type of closure was not obtained rigorously. In the section 2.3, we shall employ a general procedure based on the maximization of entropy to close the fluid equations. The above fluid model was constructed from the Wigner equation, the same work can be also done with the Vlasov equation. In this case, one should mention that the two first fluid equations (contnuity and Euler) are the same for the classical and the quantum case. The differences appear only for the evolution equation of the pressure tensor [95].
From the numerical point of view, the fluid equations are much simpler to solve than the full Wigner equations. They were recently used to study the electrons dynamics in metallic films [49]. The set of fluid equations (1.57) will be used in the chapter 5, to study the non linear electron dynamic in metallic nano-structures.

1.5 Dispersion relation and model comparisons

In this section, we shall analyse the domain of validity of the fluid models trough the calculation of the dispersion relation. The latter would be obtained by linearising the Wigner-Poisson equation (1.30) around a homogeneous equilibrium background. In this case, one obtains the longitudinal dielectric function [97, 98]

$$\epsilon(\omega, \boldsymbol{k}) = 1 + \frac{\omega_p^2 m}{\hbar \boldsymbol{k}^2 n_0}\int d\boldsymbol{v}\frac{f^{(0)}\left(\boldsymbol{v}+\hbar\boldsymbol{k}/2m\right) + f^{(0)}\left(\boldsymbol{v}-\hbar\boldsymbol{k}/2m\right)}{\omega - \boldsymbol{k}\cdot\boldsymbol{v}}, \tag{1.59}$$

where $f^{(0)}$ and n_0 are respectively the equilibrium distribution function and the associated density. To simplify the analysis we consider a one dimensional system, i.e. $f(x, v_x = v)$ and $k_x = k$.
The dispersion relation $\omega(k)$ is obtained by setting $\epsilon(\omega, k) = 0$, where ω and k are, respectively, the complex frequency and the wave vector of the excitation modes. Finding the complete dispersion relation is in general a challenging problem. The origin of the problem comes from the singularity at the denominator in Eq. (1.59). To avoid the singularity we have to apply the Landau contour method. This latter will be explained in more details in the chapter 3.
Here, we shall find the dispersion relation using different approximations. First we suppose that quantum effects are small. That means, according to the formula (1.6), that $\hbar k/(2m) << v$. In this case, we can perform a Taylor development on

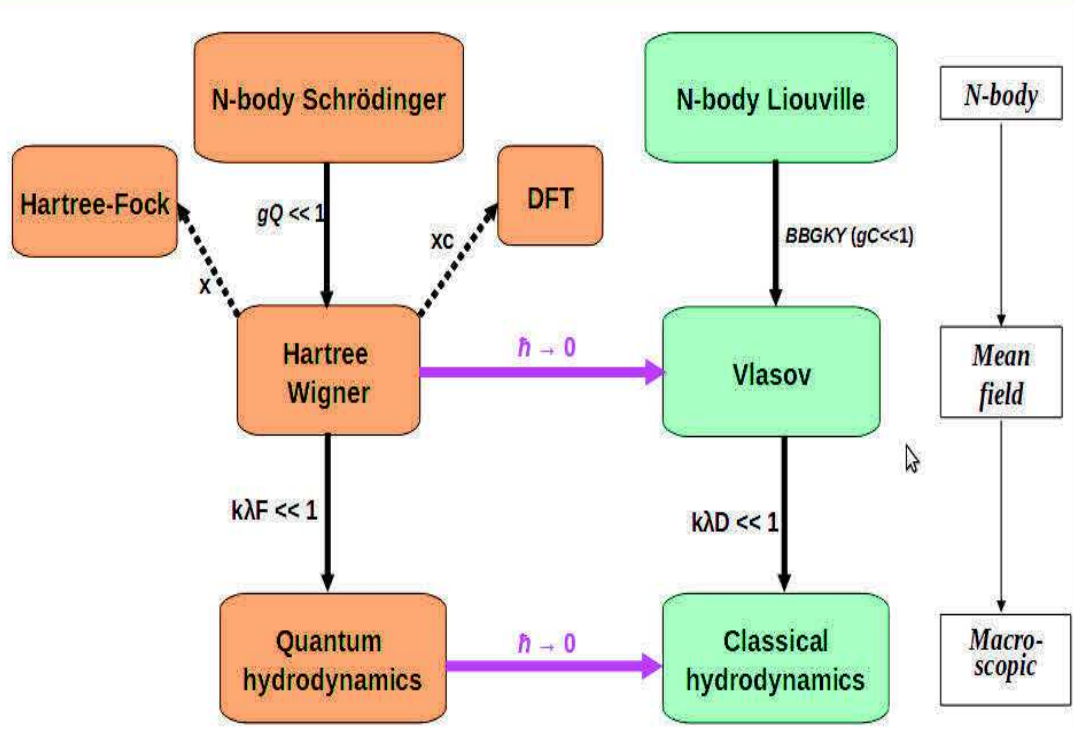

FIGURE 1.2: From Ref. [96], we represent the different models to describe the dynamic of an interacting system of electrons as well as the limit of validity of each model. The left part of the figure deals with quantum models whereas the right part deals with their classical counterpart. The parameters gC and gQ represent, respectively, the classical and the quantum coupling parameters γ and γ_q defined in Eqs. (1.1) and (1.9).

.

$f^{(0)}\left(v \pm \hbar k/2m\right)$:

$$f^{(0)}\left(v \pm \frac{\hbar k}{2m}\right) = f^{(0)}\left(v\right) \pm f^{(0)'}\left(v\right)\frac{\hbar k}{2m} + \frac{1}{2!}f^{(0)''}\left(v\right)\left(\frac{\hbar k}{2m}\right)^2 + \cdots . \tag{1.60}$$

Then, using this development, the dielectric function can be rewritten as follows:

$$\epsilon(\omega,k) = 1 + \frac{\omega_p^2}{kn_0}\int dv \frac{f^{(0)'}\left(v\right)}{\omega - kv} + \frac{\omega_p^2\hbar^2 k}{24m^2n_0}\int dv \frac{f^{(0)'''}\left(v\right)}{\omega - kv} + \cdots . \tag{1.61}$$

As expected, if we set $\hbar = 0$ in the previous equation, we recover the dielectric function corresponding to the Vlasov equation [99]. The problem of the singularity in the denominator is still present, even in the classical case.
If we search real solutions in the long-wave length limit, i.e. $k << \omega/v$ then we do not have any singularities at the denominator. Moreover, the latter can be expand

as follows:

$$\frac{1}{\omega - kv} = \frac{1}{\omega} + \frac{kv}{\omega^2} + \frac{k^2v^2}{\omega^3} + \cdots . \tag{1.62}$$

Then up to the third order in kv/ω, the dielectric function writes:

$$\epsilon(\omega, k) = 1 - \frac{\omega_p^2}{kn_0}\left[\frac{k}{\omega^2}\int dv f^{(0)}(v) + 3\frac{k^3}{\omega^4}\int dv\, v^2 f^{(0)}(v)\right] - \frac{\omega_p^2\hbar^2 k}{24m^2n_0}\frac{12k^3}{\omega^4}\int dv\, f^{(0)}(v) + \cdots . \tag{1.63}$$

In the case of a 1D Fermi-Dirac distribution function at zero temperature, i.e. $f^{(0)}(v) = n_0/(2v_F)$ for $v < v_F$ and $f^{(0)}(v) = 0$ otherwise, one obtains the following dispersion relation:

$$\omega^2 = \omega_p^2 + k^2v_F^2 + \frac{\hbar^2k^4}{4m^2} + \cdots . \tag{1.64}$$

This dispersion relation shows that in the long wavelength limit the resonant frequency of the system is mainly given by the plasma frequency. The second term in Eq. (1.64) (proportional to k^2) is a correction due to thermal effects. Whereas the third term (proportional to k^4) is a quantum correction that is related to the Bohm potential (1.58).
This dispersion relation was found by many authors [68,100]. Moreover we recover this dispersion relation if we consider the fluid model (1.57) with taking the pressure of a 1D degenerate electron gas [101]: $P_C = mv_F^2n_0/3$. Therefore the fluid equation and the Wigner equation give the same dispersion relation in the long wavelength limit, i.e. $\lambda k << 1$, where λ represents the characteristic length of the system (λ_F for a quantum system and λ_D for a classical system). In Fig. 1.2, we summarize all the models that were developed in this chapter, starting from the N body Schrödinger equation to the fluid models, as well as the domain of validity of each model.

Chapter 2

Phase-space description of the spin dynamics in metallic nano-structures

In this chapter, we are going to generalise the results presented in the previous chapter by including the spin degree of freedom in our models. The equations derived here constitute some of the original results that I obtained during my PhD work. First, we will use the gauge invariant formulation of the Weyl transformation and the Moyal product (see Sec. 1.3.4) to derive a set of Wigner equations describing a system of spin-1/2 fermions. A self-consistent mean-field model will be further obtained by coupling these Wigner equations to the set of Maxwell equations for the electromagnetic fields, where the sources (charges and current densities) are related to velocity moments of the Wigner function. Subsequently, we will derive the corresponding semiclassical limit and obtain the Vlasov equations describing the evolution of an electron gas with spin and semi-relativistic effects. In this model, the orbital dynamics is treated classically, whereas the spin is represented as a fully quantum variable. Finally, the Vlasov equations will be used to derive a hierarchy of hydrodynamic equations by taking velocity moments of the probability distribution function. This is an infinite hierarchy that needs to be closed using some additional physical hypotheses. Although this is relatively easy for spinless systems (where the closure can be obtained by assuming a suitable equation of state), things are subtler when the spin degrees of freedom are included. Here, we shall use an intuitive closure to obtain a closed set of fluid equations with spin effects.

2.1 The spin in quantum mechanics

In the previous chapter, we omit to discuss about the spin of the electrons. The spin is an intrinsic quantity of a particle as much as the mass or the charge. On the experimental point of view , the spin was first discovered in 1922 with the experiment of Stern and Gerlach [102] and it was interpreted as an internal kinetic moment of the electrons. On the theoretical point of view, the spin appears in the Dirac equation, which is the relativistic expansion of the Schrödinger equation for spin $1/2$ particles. For an electron interacting with an external electromagnetic field, the Dirac equation

writes

$$i\hbar\frac{\partial\Psi^{\mathrm{D}}(\boldsymbol{r},t)}{\partial t}=\left[c\boldsymbol{\alpha}\cdot(\boldsymbol{p}+e\boldsymbol{A}(\boldsymbol{r},t))+\beta mc^{2}-e\phi(\boldsymbol{r},t)\right]\Psi^{\mathrm{D}}(\boldsymbol{r},t)\,, \tag{2.1}$$

where $\phi(\boldsymbol{r},t)$ and $\boldsymbol{A}(\boldsymbol{r},t)$ are, respectively, the scalar and vector potentials associated to the electromagnetic field. The operators $\boldsymbol{\alpha}$ and β that appear in the Dirac equation (2.1) are 4×4 matrices

$$\boldsymbol{\alpha}=\begin{pmatrix}0 & \boldsymbol{\sigma}\\ \boldsymbol{\sigma} & 0\end{pmatrix},\quad \beta=\begin{pmatrix}\sigma_0 & 0\\ 0 & -\sigma_0\end{pmatrix}, \tag{2.2}$$

where $\boldsymbol{\sigma}$ is the vector of the 2×2 Pauli matrices and σ_0 is the 2×2 identity matrix. Therefore the wave functions $\Psi^{\mathrm{D}}(\boldsymbol{r},t)$ that obey to the Dirac equation (2.1) are four-component objects called bispinors.

The Dirac equation contains much more informations than just the spin, it describes at the same time the dynamics of particles and antiparticles. In the case of electrons the associated antiparticles are positrons. Basically the former are described by the two first components of the Dirac wave functions whereas the latter are described by the two last components. The Dirac equation can be used to describe phenomena such as particle pair creation or annihilation, which appear in high energy physics. In our case, since we want to describe electrons in metallic nano-structures (which are in the domain of low energy physics), these effects will be out of our interest.

There exists a unitary transformation, called the Foldy-Wouthuysen transformation [103], which allows us to separate the electron and the positron dynamics in the Dirac equation. This transformation is exact in the free particle case but in the case of a particle interacting with an external electromagnetic field, it leads to a semi-relativistic development in $\frac{1}{c}$. A very clear description of this transformation is given in the book of Paul Strange [104]. Up to the second order in $\frac{1}{c}$, the Dirac equation transforms into the extended Pauli equation

$$\begin{aligned}i\hbar\frac{\partial\Psi(\boldsymbol{r},t)}{\partial t}=\Bigg\{&\left[\frac{-\hbar^{2}}{2m}\nabla^{2}-\frac{i\hbar e}{m}\boldsymbol{A}(\boldsymbol{r},t)\cdot\nabla+\frac{e^{2}}{2m}\boldsymbol{A}^{2}(\boldsymbol{r},t)-e\phi(\boldsymbol{r},t)\right]\sigma_0\\&+\mu_{\mathrm{B}}\boldsymbol{\sigma}\cdot\boldsymbol{B}(\boldsymbol{r},t)+\frac{\mu_{\mathrm{B}}}{4mc^{2}}\boldsymbol{\sigma}\cdot[\boldsymbol{E}\times(\boldsymbol{p}+e\boldsymbol{A})-(\boldsymbol{p}+e\boldsymbol{A})\times\boldsymbol{E}]\Bigg\}\Psi(\boldsymbol{r},t)\,.\end{aligned} \tag{2.3}$$

The wave functions $\Psi={}^{t}\!\left(\Psi^{\uparrow},\Psi^{\downarrow}\right)$ are spinors, the upper components $\Psi^{\uparrow}$ describe the spin up electrons whereas the lower components $\Psi^{\downarrow}$ describe the spin down electrons. High order expansions of the Foldy-Wouthuysen transformation can be found in Ref. [105]. It is shown that the spin couples to the orbital motion through time and space derivatives of the electric and the magnetic fields.

In the Eq. (2.3), only two relativistic terms are retained, the Zeeman interaction which is proportional to μ_{B} and the spin-orbit interaction which is proportional to

$\mu_B/(4mc^2)$. We decide to take only these two terms into account since they are of fundamental importance to describe the magnetic properties of the system. The Zeeman interaction describes the alignment of the spin along the local magnetic field whereas the spin-orbit interaction describes the exchange of magnetic moments between the orbital and the spin angular momentums. The spin-orbit interaction plays a fundamental role in many experiments were the magnetisation is strongly excited with optical pulses. For instance, it was suggest in recent TDDFT simulations [23] that the spin-orbit coupling is responsible of the ultrafast demagnetization processes [22]. There are also other terms appearing at the same order of the Foldy-Wouthuysen expansion, the mass correction and the Darwin term. The first is related to the gamma factor in special relativity and the second is related to the Zitterbewegung phenomena [64]. Since they affect directly the orbital motion of the electrons and do not directly act on the magnetic properties[1], they will be neglected in a first approximation. However, with the methodology that shall be developed below, they can be incorporated in the model without too much difficulties.
The electromagnetic fields entering in the Pauli equation (2.3) have different origins:

$$\boldsymbol{E} = \boldsymbol{E}_{int} + \boldsymbol{E}_{ext} + \boldsymbol{E}_{XC}, \quad \boldsymbol{B} = \boldsymbol{B}_{int} + \boldsymbol{B}_{ext} + \boldsymbol{B}_{XC}. \tag{2.4}$$

An internal part $\boldsymbol{E}_{int}$ and $\boldsymbol{B}_{int}$, reflecting the interactions between the particles. In this case the electric and magnetic fields are self-consistent solutions of the Maxwell equations. An external part $\boldsymbol{E}_{ext}$ and $\boldsymbol{B}_{ext}$, which represents for instance the interaction with a laser field. And an other part $\boldsymbol{E}_{XC}$ and $\boldsymbol{B}_{XC}$ to model exchange-correlation effects that are not present in our model (more details are given in section 2.2.4).
In the extended Pauli equation (2.3), there are two types of magnetic fields which are fundamentally different. The magnetic field in the Maxwell equations that is related to a vector potential $\boldsymbol{A}$ through the following relation: $\boldsymbol{B} = \boldsymbol{\nabla} \times \boldsymbol{A}$. This magnetic field couples both to the orbital and to the spin dynamics and is created by the source terms in the Maxwell equations. The other magnetic field is the exchange-correlation magnetic field $\boldsymbol{B}_{XC}$ that only acts on the spin part and does not directly couple to the orbital part. Moreover it cannot be included as a vector potential in the Schrödinger equation. Contrary to the Maxwell's magnetic field, the exchange magnetic field does not have a zero divergence. In this work the exchange magnetic field is not included ab-initio but rather ad-hoc to have a local approximation of exchange-correlation effects and is only present in the Zeeman interaction. Recent papers [106, 107] propose to include other terms in the extended Pauli Hamiltonian that are proportional to $1/c^2$ and which depend on this exchange magnetic field. The latter provide corrections to the spin-orbit coupling or to the orbital dynamics. In this work, we will not take them into account.

[1] They will have indirect effects on the magnetic properties because they will contribute to the self-consistent electromagnetic fields generated by the particles and acting on them.

2.2 Phase-space spin dynamics

2.2.1 Introduction of the spin in the Wigner formalism

In the absence of the spin, the Wigner function is a scalar function related to the density matrix by the formula (1.37). This definition can be generalized to take into account spin degrees of freedom, then the Wigner function writes :

$$\mathcal{F}(\boldsymbol{r},\boldsymbol{v},t)=\left(\frac{1}{2\pi\hbar}\right)^3\int d\boldsymbol{\lambda}\exp\left[\frac{i\boldsymbol{\lambda}}{\hbar}\cdot\left(m\boldsymbol{v}-e\int_{-1/2}^{1/2}d\tau\boldsymbol{A}\left(\boldsymbol{r}+\tau\boldsymbol{\lambda}\right)\right)\right]\rho(\boldsymbol{r}-\boldsymbol{\lambda}/2,\boldsymbol{r}+\boldsymbol{\lambda}/2,t) \tag{2.5}$$

where, for particles with spin $1/2$, $\mathcal{F}$ is a 2×2 matrix and ρ is the density matrix of the system

$$\mathcal{F}=\begin{pmatrix}f^{\uparrow\uparrow} & f^{\uparrow\downarrow}\\ f^{\downarrow\uparrow} & f^{\downarrow\downarrow}\end{pmatrix}\quad\text{and}\quad\rho=\begin{pmatrix}\rho^{\uparrow\uparrow} & \rho^{\uparrow\downarrow}\\ \rho^{\downarrow\uparrow} & \rho^{\downarrow\downarrow}\end{pmatrix}. \tag{2.6}$$

The matrix components of the density matrix $\rho^{\eta\eta'}(\boldsymbol{r},\boldsymbol{r}',t)$, where $\eta=\uparrow,\downarrow$ design respectively the spin up and down components, are given by

$$\rho^{\eta\eta'}(\boldsymbol{r},\boldsymbol{r}')=\sum_{\mu}\Psi_{\mu}^{\eta}(\boldsymbol{r},t)\Psi_{\mu}^{\eta'*}(\boldsymbol{r}',t). \tag{2.7}$$

In order to study the macroscopic properties of the system, it is convenient to project $\mathcal{F}$ onto the Pauli basis set [108, 109]

$$\mathcal{F}=\frac{1}{2}\sigma_0 f_0+\frac{1}{2}\boldsymbol{f}\cdot\boldsymbol{\sigma}, \tag{2.8}$$

where

$$f_0=Tr\left\{\mathcal{F}\right\}=f^{\uparrow\uparrow}+f^{\downarrow\downarrow},\quad \boldsymbol{f}=Tr\left(\mathcal{F}\boldsymbol{\sigma}\right). \tag{2.9}$$

Here, Tr denotes the trace, $\boldsymbol{\sigma}$ is the vector of the 2×2 Pauli matrices and σ_0 is the 2×2 identity matrix. With this definition, the particle density n and the spin polarization $\boldsymbol{S}$ of the electron gas are easily expressed by the moments of the pseudo-distribution functions f_0 and $\boldsymbol{f}$:

$$n(\boldsymbol{r},t) = \sum_{\mu}\left|\Psi_{\mu}^{\dagger}(\boldsymbol{r},t)\right|^2=\int f_0(\boldsymbol{r},\boldsymbol{v},t)d\boldsymbol{v}, \tag{2.10}$$

$$\boldsymbol{S}(\boldsymbol{r},t) = \frac{\hbar}{2}\sum_{\mu}\Psi_{\mu}^{\dagger}(\boldsymbol{r},t)\boldsymbol{\sigma}\Psi_{\mu}(\boldsymbol{r},t)=\frac{\hbar}{2}\int\boldsymbol{f}(\boldsymbol{r},\boldsymbol{v},t)d\boldsymbol{v}. \tag{2.11}$$

In this representation, the Wigner functions have a clear physical interpretation: f_0 is related to the total electron density (in phase space), whereas f_i $(i=x,y,z)$ is related to the spin polarization in the direction i. In other words, f_0 represents the probability to find an electron at one point of the phase space at a given time, while

f_i represents the probability to have a spin-polarization probability in the direction i for this electron.
According to Eq. (2.10), the scalar distribution f_0 provides the particle density, whereas the vector distribution $\boldsymbol{f}$ yields the spin polarization as defined in Eq. (2.11). One can prove the following bound:

$$|\boldsymbol{S}(\boldsymbol{r},t)| \leq n(\boldsymbol{r},t)\frac{\hbar}{2}. \tag{2.12}$$

Equation (2.12) is a direct consequence of the following property of the density matrix: $Tr\,(\rho^2) \leq 1$. The equality holds true for a pure state or for a fluid where all the spins are aligned along the same direction (fully spin-polarized state).
There exist other way to include the spin in the Wigner formalism as the one described above. The solution, developed by Brodin et al. [59, 110], consists to defined an extended phase space depending on the position $\boldsymbol{r}$, the impulsion $\boldsymbol{p}$ and a unitary vector $\boldsymbol{s}$, which corresponds to the spin direction. Thus, the distribution function evolves in an extended phase space $(\boldsymbol{r},\boldsymbol{v},\boldsymbol{s})$. This is in contrast with our approach, where the spin is treated as a fully quantum variable (evolving in a two-dimensional Hilbert space). The correspondence relations between our distribution functions $f_0(\boldsymbol{r},\boldsymbol{v},t)$ and $f_i(\boldsymbol{r},\boldsymbol{v},t)$ and the scalar distribution used by Zamanian et al. $f(\boldsymbol{r},\boldsymbol{v},\boldsymbol{s},t)$ write:

$$f_0 = \int f d^2\boldsymbol{s}, \quad \boldsymbol{f} = 3\int \boldsymbol{s} f d^2\boldsymbol{s}. \tag{2.13}$$

Both approach are equivalent on the mathematical point of view. On the physical point of view our approach clearly separates the orbital motion from the spin dynamics. As we shall see below, this separation leads to simpler and more transparent hydrodynamic models, where the meaning of each term in the equations will be more intuitive. On the numerical point of view, in our approach, we have to work with four distribution functions and a six dimensional phase space whereas in the other approaches, one should work only with one distribution function but in a nine dimensional phase space. Therefore, it seems that our approach is more convenient for numerical applications. This is even more true if one think about parallel computing techniques.

2.2.2 The Wigner equation with the spin

In this section, we search the Wigner equation for an ensemble of spin-1/2 particles (electrons) in the presence of an electromagnetic field, $\boldsymbol{E}$ and $\boldsymbol{B}$. We denote the Schrödinger wave function of the $\mu-$th particle state by

$$\Psi_\mu(\boldsymbol{r},t) = \Psi_\mu^{\uparrow}(\boldsymbol{r},t)\,|\uparrow\rangle + \Psi_\mu^{\downarrow}(\boldsymbol{r},t)\,|\downarrow\rangle\,, \tag{2.14}$$

where $\Psi_\mu^\uparrow(\boldsymbol{r},t)$ and $\Psi_\mu^\downarrow(\boldsymbol{r},t)$ are respectively the spin-up and spin-down components of the wave function. As we have seen in section 2.1, the evolution of the system is governed by the Pauli-Schrödinger equation

$$i\hbar\frac{\partial\Psi_\mu(\boldsymbol{r},t)}{\partial t}=\widehat{\mathcal{H}}\Psi_\mu(\boldsymbol{r},t)\,,\quad \widehat{\mathcal{H}}=\left[\frac{\widehat{\boldsymbol{\Pi}}^2}{2m}+V\right]\sigma_0+\left[\mu_{\mathrm{B}}\widehat{\boldsymbol{B}}+\frac{\mu_{\mathrm{B}}}{4mc^2}\left(\widehat{\boldsymbol{E}}\times\widehat{\boldsymbol{\Pi}}-\widehat{\boldsymbol{\Pi}}\times\widehat{\boldsymbol{E}}\right)\right]\cdot\boldsymbol{\sigma}. \tag{2.15}$$

Here, $\mu_{\mathrm{B}}=e\hbar/2m$ is the Bohr magneton, V, $\boldsymbol{E}$ and $\boldsymbol{B}$ are, respectively, the electric potential, the electric field and the magnetic field. The operator $\boldsymbol{\Pi}$ corresponds to the generalized impulsion operator defined in section 1.3.4.
The equation (2.15) can be split in two coupled Schrödinger equations:

$$i\hbar\frac{\partial\Psi^\uparrow}{\partial t}=\widehat{\mathcal{H}}^{\uparrow\uparrow}\Psi^\uparrow+\widehat{\mathcal{H}}^{\uparrow\downarrow}\Psi^\downarrow\quad i\hbar\frac{\partial\Psi^\downarrow}{\partial t}=\widehat{\mathcal{H}}^{\downarrow\downarrow}\Psi^\downarrow+\widehat{\mathcal{H}}^{\downarrow\uparrow}\Psi^\uparrow. \tag{2.16}$$

with

$$\widehat{\mathcal{H}}^{\uparrow\uparrow}=\frac{\widehat{\boldsymbol{\Pi}}^2}{2m}+V(\widehat{\boldsymbol{R}})+\mu_{\mathrm{B}}B_z(\widehat{\boldsymbol{R}})+\frac{\mu_{\mathrm{B}}}{4mc^2}\left[E(\widehat{\boldsymbol{R}})\times\widehat{\boldsymbol{\Pi}}-\widehat{\boldsymbol{\Pi}}\times E(\widehat{\boldsymbol{R}})\right]_z, \tag{2.17}$$

$$\widehat{\mathcal{H}}^{\uparrow\downarrow}=\frac{\mu_{\mathrm{B}}}{4mc^2}\left\{\left[E(\widehat{\boldsymbol{R}})\times\widehat{\boldsymbol{\pi}}-\widehat{\boldsymbol{\Pi}}\times E(\widehat{\boldsymbol{R}})\right]_x-i\left[E(\widehat{\boldsymbol{R}})\times\widehat{\boldsymbol{\Pi}}-\widehat{\boldsymbol{\Pi}}\times E(\widehat{\boldsymbol{R}})\right]_y\right\}, \tag{2.18}$$

$$\widehat{\mathcal{H}}^{\downarrow\uparrow}=\frac{\mu_{\mathrm{B}}}{4mc^2}\left\{\left[E(\widehat{\boldsymbol{R}})\times\widehat{\boldsymbol{\Pi}}-\widehat{\boldsymbol{\Pi}}\times E(\widehat{\boldsymbol{R}})\right]_x+i\left[E(\widehat{\boldsymbol{R}})\times\widehat{\boldsymbol{\Pi}}-\widehat{\boldsymbol{\Pi}}\times E(\widehat{\boldsymbol{R}})\right]_y\right\}, \tag{2.19}$$

$$\widehat{\mathcal{H}}^{\downarrow\downarrow}=\frac{\widehat{\boldsymbol{\Pi}}^2}{2m}+V(\widehat{\boldsymbol{R}})-\mu_{\mathrm{B}}B_z(\widehat{\boldsymbol{R}})-\frac{\mu_{\mathrm{B}}}{4mc^2}\left[E(\widehat{\boldsymbol{R}})\times\widehat{\boldsymbol{\Pi}}-\widehat{\boldsymbol{\Pi}}\times E(\widehat{\boldsymbol{R}})\right]_z. \tag{2.20}$$

In order to derive the Wigner equation, we have to apply the procedure describe in section 1.3.4, namely finding the phase-space functions associated to each components of the Hamiltonian, Eqs. (2.17) - (2.20). Then the Wigner equation formally writes

$$i\hbar\frac{\partial\mathcal{F}}{\partial t}=[\mathcal{H},\mathcal{F}]_\star\,, \tag{2.21}$$

where one has to use the Moyal product, Eq. (1.38) to describe magnetic interactions. After some tedious calculations, developed in appendix A, Eq. (2.21) leads to the

following quantum evolution equations for the Wigner functions

$$\begin{aligned}
&\frac{\partial f_0}{\partial t} + \frac{1}{m}\left(\boldsymbol{\pi} + \boldsymbol{\Delta\widetilde{\pi}}\right)\cdot\boldsymbol{\nabla} f_0 - \frac{e}{m}\left[m\widetilde{\boldsymbol{E}} + \left(\boldsymbol{\pi} + \boldsymbol{\Delta\widetilde{\pi}}\right)\times\widetilde{\boldsymbol{B}}\right]_i \partial_{\pi_i} f_0 \\
&- \mu_{\mathrm{B}}\boldsymbol{\nabla}\left(\widetilde{\boldsymbol{B}} - \frac{1}{2mc^2}\boldsymbol{\pi}\times\widetilde{\boldsymbol{E}}\right)_i \cdot \boldsymbol{\nabla}_{\boldsymbol{\pi}} f_i + \frac{\mu_{\mathrm{B}}}{4mc^2}\left[\left(\boldsymbol{E}_+ + \boldsymbol{E}_-\right)\times\boldsymbol{\nabla}\right]\cdot\boldsymbol{f} \\
&- \frac{\mu_{\mathrm{B}} e}{2mc^2}\left[\widetilde{\boldsymbol{E}}\times\left[\widetilde{\boldsymbol{B}}\times\boldsymbol{\nabla}_{\pi}\right]\right]\cdot\boldsymbol{f} - \frac{\mu_{\mathrm{B}}}{2mc^2}\frac{i}{\hbar}\left[\boldsymbol{\Delta\widetilde{\pi}}\times\left(\boldsymbol{E}_+ - \boldsymbol{E}_-\right)\right]\cdot\boldsymbol{f} = 0,
\end{aligned} \tag{2.22}$$

$$\begin{aligned}
&\frac{\partial f_k}{\partial t} + \frac{1}{m}\left(\boldsymbol{\pi} + \boldsymbol{\Delta\widetilde{\pi}}\right)\cdot\boldsymbol{\nabla} f_k - \frac{e}{m}\left[m\widetilde{\boldsymbol{E}} + \left(\boldsymbol{\pi} + \boldsymbol{\Delta\widetilde{\pi}}\right)\times\widetilde{\boldsymbol{B}}\right]_i \partial_{\pi_i} f_k \\
&- \mu_{\mathrm{B}}\boldsymbol{\nabla}\left(\widetilde{\boldsymbol{B}} - \frac{1}{2mc^2}\boldsymbol{\pi}\times\widetilde{\boldsymbol{E}}\right)_k \cdot \boldsymbol{\nabla}_{\boldsymbol{\pi}} f_0 + \frac{\mu_{\mathrm{B}}}{4mc^2}\left[\left(\boldsymbol{E}_+ + \boldsymbol{E}_-\right)\times\boldsymbol{\nabla}\right]_k f_0 \\
&- \frac{\mu_{\mathrm{B}} e}{2mc^2}\left[\widetilde{\boldsymbol{E}}\times\left[\widetilde{\boldsymbol{B}}\times\boldsymbol{\nabla}_{\pi}\right]\right]_k f_0 - \frac{\mu_{\mathrm{B}}}{2mc^2}\frac{i}{\hbar}\left[\boldsymbol{\Delta\widetilde{\pi}}\times\left(\boldsymbol{E}_+ - \boldsymbol{E}_-\right)\right]_k f_0 \\
&- \frac{e}{2m}\left[\left(\boldsymbol{B}_+ + \boldsymbol{B}_- - \frac{1}{2mc^2}\left(\boldsymbol{\pi} + \boldsymbol{\Delta\widetilde{\pi}}\right)\times\left(\boldsymbol{E}_+ + \boldsymbol{E}_-\right)\right)\times\boldsymbol{f}\right]_k \\
&+ \frac{\mu_{\mathrm{B}}}{2mc^2}\frac{i}{2}\left[\left(\left(\boldsymbol{E}_+ - \boldsymbol{E}_-\right)\times\left(\boldsymbol{\nabla} - e\widetilde{\boldsymbol{B}}\times\boldsymbol{\nabla}_{\boldsymbol{\pi}}\right)\right)\times\boldsymbol{f}\right]_k = 0.
\end{aligned} \tag{2.23}$$

Where $\boldsymbol{\Delta\widetilde{\pi}}$ depends of the magnetic field and corresponds to a quantum shift of the velocity

$$\boldsymbol{\Delta\widetilde{\pi}} = -i\hbar e\boldsymbol{\nabla}_{\boldsymbol{\pi}}\times\left[\int_{-1/2}^{1/2} d\tau\tau\boldsymbol{B}\left(\boldsymbol{r} + i\hbar\tau\boldsymbol{\nabla}_{\boldsymbol{\pi}}\right)\right], \tag{2.24}$$

$\widetilde{\boldsymbol{E}}$ and $\widetilde{\boldsymbol{B}}$ are written in terms of the electric and the magnetic fields

$$\widetilde{\boldsymbol{E}} = \int_{-1/2}^{1/2} d\tau\boldsymbol{E}\left(\boldsymbol{r} + i\hbar\tau\boldsymbol{\nabla}_{\boldsymbol{\pi}}\right), \quad \widetilde{\boldsymbol{B}} = \int_{-1/2}^{1/2} d\tau\boldsymbol{B}\left(\boldsymbol{r} + i\hbar\tau\boldsymbol{\nabla}_{\boldsymbol{\pi}}\right). \tag{2.25}$$

The index $\pm$ means that the associated quantity is evaluated at a shifted position $\boldsymbol{r} \pm i\hbar\boldsymbol{\nabla}_{\boldsymbol{\pi}}/2$.
This particularly illuminating form was proposed by Serimaa et al. [87] in the case of a charged particle without spin evolving in an external electromagnetic field. These equations can be view as a generalization of those obtained in Ref. [111], were the authors only included the Zeeman interaction. In this case the Wigner equations writes:

$$\begin{aligned}
&\frac{\partial f_0}{\partial t} + \frac{1}{m}\left(\boldsymbol{\pi} + \boldsymbol{\Delta\widetilde{\pi}}\right)\cdot\boldsymbol{\nabla} f_0 - \frac{e}{m}\left[m\widetilde{\boldsymbol{E}} + \left(\boldsymbol{\pi} + \boldsymbol{\Delta\widetilde{\pi}}\right)\times\widetilde{\boldsymbol{B}}\right]_i \partial_{\pi_i} f_0 \\
&- \mu_{\mathrm{B}}\boldsymbol{\nabla}\widetilde{B}_i \cdot \boldsymbol{\nabla}_{\boldsymbol{\pi}} f_i = 0,
\end{aligned} \tag{2.26}$$

$$\frac{\partial f_k}{\partial t} + \frac{1}{m}\left(\boldsymbol{\pi} + \boldsymbol{\Delta}\widetilde{\boldsymbol{\pi}}\right)\cdot\boldsymbol{\nabla} f_k - \frac{e}{m}\left[m\widetilde{\boldsymbol{E}} + \left(\boldsymbol{\pi} + \boldsymbol{\Delta}\widetilde{\boldsymbol{\pi}}\right)\times\widetilde{\boldsymbol{B}}\right]_i \partial_{\pi_i} f_k$$
$$- \mu_{\mathrm{B}}\boldsymbol{\nabla}\widetilde{B}_k\cdot\boldsymbol{\nabla}_{\boldsymbol{\pi}} f_0 - \frac{e}{2m}\left[\left(\boldsymbol{B}_+ + \boldsymbol{B}_-\right)\times\boldsymbol{f}\right]_k = 0. \tag{2.27}$$

The zeman interaction has two effects, the first is to couple the spin to the orbital dynamics through the gradient of the magnetic field $\mu_{\mathrm{B}}\boldsymbol{\nabla}\widetilde{B}_k\cdot\boldsymbol{\nabla}_{\boldsymbol{\pi}}$. The other makes the spin precess around an effective magnetic field $\boldsymbol{B}_+ + \boldsymbol{B}_-$.
In Eqs. (2.22) - (2.23), plenty of new terms appear due to the spin-orbit interaction, they can be easily identified because they are proportional to $1/c^2$. Basically, as it is the case for the Zeeman interaction, some of them couple the spin to the orbital dynamics, whereas the other provide corrections to the spin precession. The physical origin of all of these terms will appear in a clearest fashion in the session 2.2.5, from the semiclassical expansion of the Wigner equations.

2.2.3 Self-consistent model

Eqs. (2.22) - (2.23) can be used, in a mean-field approach, to described the self-consistent spin dynamics of an ensemble of interacting charged particles. In this case the electric and the magnetic field present in these equations are solutions of the following Maxwell equations:

$$\begin{cases} \boldsymbol{\nabla}\cdot\boldsymbol{E} &= \dfrac{\rho}{\epsilon_0} - \dfrac{\boldsymbol{\nabla}\cdot\boldsymbol{P}}{\epsilon_0}, \\ \boldsymbol{\nabla}\cdot\boldsymbol{B} &= 0, \\ \boldsymbol{\nabla}\times\boldsymbol{E} &= -\dfrac{\partial\boldsymbol{B}}{\partial t}, \\ \boldsymbol{\nabla}\times\boldsymbol{B} &= \mu_0\boldsymbol{j} + \mu_0\epsilon_0\dfrac{\partial\boldsymbol{E}}{\partial t} + \mu_0\dfrac{\partial\boldsymbol{P}}{\partial t} + \mu_0\boldsymbol{\nabla}\times\boldsymbol{M}. \end{cases} \tag{2.28}$$

Where, we introduce new sources terms, namely a spin magnetization $\boldsymbol{M}$, a "spin" polarization $\boldsymbol{P}$ and a new contribution to the current density, Eq. (2.30). These modifications should be done because our Hamiltonian, Eq. (2.15), is obtained from a semi-relativistic development of the Dirac Hamiltonian. Therefore one should use the appropriate limit of the source term appearing in the Dirac theory. Such analysis was clearly made in [64, 112], where the authors used a Lagrangian approach to obtain a consistent expression of the source terms in the Schrödinger picture. Using Eq. (1.37), we can transpose their results to our formulation, in this case the source

terms write :

$$\rho = -e \int f_0 d\boldsymbol{v}, \tag{2.29}$$

$$\boldsymbol{j} = -e \left[\int \boldsymbol{v} f_0 d\boldsymbol{v} + \frac{\boldsymbol{E} \times \boldsymbol{M}}{2mc^2} \right], \tag{2.30}$$

$$\boldsymbol{M} = -\mu_{\mathrm{B}} \int \boldsymbol{f} d\boldsymbol{v}, \tag{2.31}$$

$$\boldsymbol{P} = -\frac{\mu_{\mathrm{B}}}{2c^2} \int \boldsymbol{v} \times \boldsymbol{f} d\boldsymbol{v}. \tag{2.32}$$

The mean-field approach can also be extended, in the spirit of density functional theory (DFT), to include exchange and correlation effects by adding suitable potentials and fields that are functionals of the electron density [96]. The resulting equations are potentially equivalent to the exact N-body treatment, although the exchange-correlations functionals are not known and need to be somehow approximated.
The Wigner equations (2.22) - (2.23) coupled to the Maxwell equations (2.28) constitute a self-consistent set of equations to describe the spin dynamics of an interacting electron gas. Up to our knowledge those equations were never solved numerically, even in the spinless case. The reason is that one has to solve numerically the propagation of the electromagnetic fields in matter as well as the particles dynamics. However in metallic nano-structures those two time scales are rather decoupled from each other. Indeed for such systems, the shortest particle time scale is given by the inverse plasma frequency, which is on the order of the femtosecond (see section 1.1.3). Whereas the propagation time of the electromagnetic waves is much lower, it takes approximatively $1/300\,\mathrm{fs}$ to travel through $1\,\mathrm{nm}$ of distance. Therefore we shall consider the electromagnetic interactions as instantaneous. In the Lorenz gauge, the Maxwell equations (2.28) writes:

$$\begin{cases} \dfrac{1}{c^2}\dfrac{\partial^2 \phi}{\partial t^2} - \boldsymbol{\nabla}^2 \phi = \dfrac{\rho}{\epsilon_0} - \dfrac{\boldsymbol{\nabla} \cdot \boldsymbol{P}}{\epsilon_0}, \\ \dfrac{1}{c^2}\dfrac{\partial^2 \boldsymbol{A}}{\partial t^2} - \boldsymbol{\nabla}^2 \boldsymbol{A} = \mu_0 \boldsymbol{j} + \mu_0 \dfrac{\partial \boldsymbol{P}}{\partial t} + \mu_0 \boldsymbol{\nabla} \times \boldsymbol{M}, \end{cases} \tag{2.33}$$

where the scalar and the vector potential ϕ and $\boldsymbol{A}$ are, respectively, related to the electromagnetic fields by the following relations:

$$\boldsymbol{E} = -\boldsymbol{\nabla}\phi - \partial_t \boldsymbol{A} \quad \text{and} \quad \boldsymbol{B} = \boldsymbol{\nabla} \times \boldsymbol{A}. \tag{2.34}$$

If we now suppose that the electromagnetic fields propagate instantaneously, then we have to suppress the time derivatives of the potentials that appear in the Maxwell equations (2.33). In this case, the Maxwell equations reduce to the Poisson and the

Ampere equations:

$$\begin{cases} \boldsymbol{\nabla}^2\phi = -\dfrac{\rho}{\epsilon_0} + \dfrac{\boldsymbol{\nabla}\cdot\boldsymbol{P}}{\epsilon_0} \\ \\ \boldsymbol{\nabla}^2\boldsymbol{A} = -\mu_0\boldsymbol{j} - \mu_0\dfrac{\partial\boldsymbol{P}}{\partial t} - \mu_0\boldsymbol{\nabla}\times\boldsymbol{M}. \end{cases} \tag{2.35}$$

The above approximation is called the quasi-static limit of the Maxwell equations. A more complete discussion about the validity of the static limits of the Maxwell equations can be found in Ref. [112].
In the rest of this work, one shall use the spin-Wigner equations (2.22) - (2.23) coupled to the Poisson and the Ampere equations (2.35) to describe the self-consistent dynamics of an interacting electron gas.

2.2.4 Exchange and correlation effects

Exchange and correlation effects are not present in our model because of the factoring of the N body wave function, Eq. (1.13). More precisely, correlation effects are not described in our model because we suppressed the two-particle correlations. Exchange effects are not present either because we do not take into account the antisymmetric character of the N body wave function.
Here, we present a way to include exchange-correlation effects for an ensemble of spin polarized electrons in the local spin density approximation (LSDA). In collinear magnetism, we have to deal with two spin-dependent electron densities $n^{\uparrow}$ (spin up) and $n^{\downarrow}$ (spin down), such that the electron density is given by $n = n^{\uparrow} + n^{\downarrow}$ and the magnetization by $m = n^{\uparrow} - n^{\downarrow}$.
In LSDA, the exchange-correlation energy is:

$$E_{XC}^{LSDA}\left[n^{\uparrow}, n^{\downarrow}\right] \equiv E_{XC}\left[n^{\uparrow}, n^{\downarrow}\right] = \int n(\boldsymbol{r})\epsilon_{XC}\left[n^{\uparrow}(\boldsymbol{r}), n^{\downarrow}(\boldsymbol{r})\right] d\boldsymbol{r}, \tag{2.36}$$

where $n^{\uparrow}$ and $n^{\downarrow}$ are respectively the spin up and the spin down densities and ϵ_{XC} is the exchange correlation potential[2]. In general this functional does not only depend on the local density. For instance one can add gradient density corrections in the exchange-correlation functional (2.36) to better describe the nonlocal character of the exchange-correlation interactions. For our purposes we shall stay in LSDA.
From the Eq. (2.36), one can obtain the exchange-correlation potential acting on the spin up and spin down components according to the following formulas:

$$V_{XC}^{\uparrow} = \frac{\delta E_{XC}}{\delta n^{\uparrow}(\boldsymbol{r})}, \quad V_{XC}^{\downarrow} = \frac{\delta E_{XC}}{\delta n^{\downarrow}(\boldsymbol{r})}. \tag{2.37}$$

[2]DFT assumes the existence of an exact form of this functional. However in practice such a functional is not known and all the art of DFT is to find the best form of this exchange-correlation functional.

A usual approximation consists to separate the exchange from the correlation contributions as follows: $\epsilon_{XC} = \epsilon_X + \epsilon_C$, were the exchange part ϵ_X is derived from the Hartree-Fock theory and is exact in the case of a homogeneous spin density

$$\epsilon_X\left[n^{\uparrow}, n^{\downarrow}\right] = -\frac{3}{2}\left(\frac{3}{4\pi}\right)^{1/3} \frac{(n^{\uparrow})^{4/3} + (n^{\downarrow})^{4/3}}{n}. \tag{2.38}$$

For the correlation part ϵ_C, we use the expression derived in Ref. [113]

$$\epsilon_C\left[n^{\uparrow}, n^{\downarrow}\right] = \epsilon_C^U(r_s) + \left[\epsilon_C^P(r_s) - \epsilon_C^U(r_s)\right] f(\xi), \tag{2.39}$$

with

$$\epsilon_C^U(r_s) = \frac{-0.1423}{1 + 1.0529\sqrt{r_s} + 0.3334 r_s}, \tag{2.40}$$

$$\epsilon_C^P(r_s) = \frac{-0.0843}{1 + 1.3981\sqrt{r_s} + 0.2611 r_s}, \tag{2.41}$$

$$f(\xi) = \frac{(1+\xi)^{4/3} + (1-\xi)^{4/3} - 2}{2^{4/3} - 2}, \tag{2.42}$$

where $r_s = (4\pi n/3)^{1/3}$ is the Wigner-Seitz radius and ξ is the local spin polarization $\xi = \left(n^{\uparrow} - n^{\downarrow}\right)/n$.
However in our case, we need to describe exchange-correlation effects for non-collinear magnetism. In this case the spin projection on a single axis is not a good quantum number. The wave function and the electronic density are 2×2 matrices, see Eq. (2.6), where $n^{\uparrow\downarrow}(\boldsymbol{r})$ and $n^{\downarrow\uparrow}(\boldsymbol{r})$ are responsible for the non-collinear magnetism. Therefore, we have four independent electronic quantities, the electronic density n and the magnetization $\boldsymbol{m}$:

$$n = n^{\uparrow\uparrow} + n^{\downarrow\downarrow}, \quad m_x = n^{\uparrow\downarrow} + n^{\downarrow\uparrow}, \quad m_y = -i\left(n^{\uparrow\downarrow} - n^{\downarrow\uparrow}\right), \quad m_z = n^{\uparrow\uparrow} - n^{\downarrow\downarrow}. \tag{2.43}$$

In order to calculate the exchange-correlation energy in the non-collinear case, we will use a method describe in Ref. [114]. First we have to align the spin moment along the quantization axis (here it is the z axis) at each point in space. Then, we define a rotation matrix $U(\boldsymbol{r})(\theta, \phi) \in \mathcal{SU}(2)$ depending on the position $\boldsymbol{r}$

$$U(\boldsymbol{r})(\theta,\phi) = R_z(\theta)R_y(\phi) = e^{i\frac{\theta}{2}\sigma_y} e^{i\frac{\phi}{2}\sigma_z} = \begin{pmatrix} e^{i\phi/2}\cos(\theta/2) & e^{-i\phi/2}\sin(\theta/2) \\ -e^{+i\phi/2}\sin(\theta/2) & e^{-i\phi/2}\cos(\theta/2) \end{pmatrix}, \tag{2.44}$$

where $\theta(\boldsymbol{r})$ and $\phi(\boldsymbol{r})$ are the usual Euler angles, defined as follows:

$$\cos(\theta) = \frac{m_z}{|\boldsymbol{m}|}, \quad \cos(\phi) = \frac{m_x}{\sqrt{m_x^2 + m_y^2}} \quad \text{and} \quad \sin(\phi) = \frac{m_y}{\sqrt{m_x^2 + m_y^2}}. \tag{2.45}$$

Then according to the previous transformation, the density matrix in the rotated frame is diagonal

$$\begin{pmatrix} n_{Loc}^{\uparrow} & 0 \\ 0 & n_{Loc}^{\downarrow} \end{pmatrix} = U(\boldsymbol{r}) \begin{pmatrix} n^{\uparrow\uparrow}(\boldsymbol{r}) & n^{\uparrow\downarrow}(\boldsymbol{r}) \\ n^{\downarrow\uparrow}(\boldsymbol{r}) & n^{\downarrow\downarrow}(\boldsymbol{r}) \end{pmatrix} U^{\dagger}(\boldsymbol{r}). \tag{2.46}$$

Then using Eqs. (2.44) - (2.46), we obtain $n_{Loc}^{\uparrow} = (n + |\boldsymbol{m}|)/2$ and $n_{Loc}^{\downarrow} = (n - |\boldsymbol{m}|)/2$. Using Eq. (2.37), the local exchange-correlation potential can be expressed as follows:

$$(\mathcal{V}_{XC})_{Loc} = \begin{pmatrix} V_{XC}^{\uparrow}(\boldsymbol{r}) & 0 \\ 0 & V_{XC}^{\downarrow}(\boldsymbol{r}) \end{pmatrix}, \tag{2.47}$$

with

$$V_{XC}^{\uparrow} = \epsilon_{XC} + \left(n_{loc}^{\uparrow} + n_{loc}^{\downarrow}\right) \frac{\partial \epsilon_{XC}}{\partial n_{loc}^{\uparrow}}, \quad V_{XC}^{\downarrow} = \epsilon_{XC} + \left(n_{loc}^{\uparrow} + n_{loc}^{\downarrow}\right) \frac{\partial \epsilon_{XC}}{\partial n_{loc}^{\downarrow}}. \tag{2.48}$$

Finally, we go back to the initial frame to obtain the general expression of the exchange correlation potential acting on our system

$$\mathcal{V}_{XC}(\boldsymbol{r}) = \begin{pmatrix} V_{XC}^{\uparrow\uparrow}(\boldsymbol{r}) & V_{XC}^{\uparrow\downarrow}(\boldsymbol{r}) \\ V_{XC}^{\downarrow\uparrow}(\boldsymbol{r}) & V_{XC}^{\downarrow\downarrow}(\boldsymbol{r}) \end{pmatrix} = U^{\dagger}(\boldsymbol{r}) \begin{pmatrix} V_{XC}^{\uparrow} & 0 \\ 0 & V_{XC}^{\downarrow} \end{pmatrix} U(\boldsymbol{r}). \tag{2.49}$$

Using the Pauli matrix basis, it is possible to write the exchange-correlation interactions as a scalar potential and a magnetic field : $\mathcal{V}_{XC}(\boldsymbol{r}) = V_{XC}\sigma_0 + \boldsymbol{\sigma} \cdot \boldsymbol{B}_{XC}$, where

$$V_{XC} = \frac{V_{XC}^{\uparrow\uparrow} + V_{XC}^{\downarrow\downarrow}}{2}, \quad (B_{XC})_x = \frac{V_{XC}^{\uparrow\downarrow} + V_{XC}^{\downarrow\uparrow}}{2}, \quad (B_{XC})_y = \frac{V_{XC}^{\downarrow\uparrow} - V_{XC}^{\uparrow\downarrow}}{2i} \quad \text{and}$$
$$(B_{XC})_z = \frac{V_{XC}^{\uparrow\uparrow} - V_{XC}^{\downarrow\downarrow}}{2}. \tag{2.50}$$

Exchange-correlation effects will thus simply enter in the phase-space equations by making the following substitution : $V \to V + V_{XC}$ and $\mu_{\mathrm{B}}\boldsymbol{\sigma} \cdot \boldsymbol{B} \to \mu_{\mathrm{B}}\boldsymbol{\sigma} \cdot (\boldsymbol{B} + \boldsymbol{B}_{XC})$. We insist on the fact that this procedure should be done for each point in the position space.

In this section we presented an approximate way to include exchange and correlation effects in our model. In the region where the physical quantities such as the density or the magnetization are homogeneous this approximation seems to be rather valid. At the border of the film, the situation is different since the electronic density is rapidly vanishing. There are different way to address this problem. A first

solution would be to add gradient corrections to the exchange-correlation potential but in this case the previous method should be modified, particularly because the rotation matrix (2.44) is not necessarily the same for the nearby space points. In Ref. [115] the author address this problem and propose a solution to add gradient correction terms in the exchange-correlation functionals for non-collinear spins. A second solution consists to use local density functionals adapted to the geometry of the systems; for instance in Ref. [116], the authors proposed to use an exchange-correlation functional that are designed for slab systems. Finally, one should also mentioned that the spin-Wigner equation could also be formulated within the antisymmetrization principle of the wave function. In this case the Wigner equations are equivalent to the Hartee-Fock equations. This work was also done with the spin degrees of freedom but in the framework of the extended phase space formulation [117]. The resulting equations are more complex to solve because of the nonlocal character of the exchange interactions. For our purposes, we shall stay with the local exchange-correlation functionals given by the Eqs. (2.38)-(2.39).

2.2.5 Semiclassical limit and spin-Vlasov model

The form of the equations (2.22)-(2.23) is particularly interesting to study the semiclasscial limit of the model. Indeed we can easy expand $\widetilde{\boldsymbol{E}}$, $\widetilde{\boldsymbol{B}}$ and $\boldsymbol{\Delta}\widetilde{\boldsymbol{\pi}}$ as a power series of $\hbar$

$$\begin{aligned}\widetilde{\boldsymbol{E}} &= \sum_{n=0}^{\infty}\left(\frac{\hbar}{2m}\right)^{2n}\frac{(-1)^n}{(2n+1)!}\sum_{i_1\ldots i_{2n}=1}^{3}\left(\frac{\partial^{2n}}{\partial r_{i_1}\ldots\partial r_{i_{2n}}}\boldsymbol{E}\right)\frac{\partial^{2n}}{\partial v_{i_1}\ldots\partial v_{i_{2n}}}\\ &= \boldsymbol{E}-\frac{\hbar^2}{12m^2}\sum_{i_1,i_2=1}^{3}\frac{\partial^2\boldsymbol{E}}{\partial r_{i_1}\partial r_{i_2}}\frac{\partial^2}{\partial v_{i_1}\partial v_{i_2}}+\mathcal{O}\left(\hbar^4\right), \qquad (2.51)\\ \widetilde{\boldsymbol{B}} &= \sum_{n=0}^{\infty}\left(\frac{\hbar}{2m}\right)^{2n}\frac{(-1)^n}{(2n+1)!}\sum_{i_1\ldots i_{2n}=1}^{3}\left(\frac{\partial^{2n}}{\partial r_{i_1}\ldots\partial r_{i_{2n}}}\boldsymbol{B}\right)\frac{\partial^{2n}}{\partial v_{i_1}\ldots\partial v_{i_{2n}}}\\ &= \boldsymbol{B}-\frac{\hbar^2}{12m^2}\sum_{i_1,i_2=1}^{3}\frac{\partial^2\boldsymbol{B}}{\partial r_{i_1}\partial r_{i_2}}\frac{\partial^2}{\partial v_{i_1}\partial v_{i_2}}+\mathcal{O}\left(\hbar^4\right), \qquad (2.52)\\ \boldsymbol{\Delta}\widetilde{\boldsymbol{\pi}} &= m\mu_{\mathrm{B}}\sum_{n=0}^{\infty}\left(\frac{\hbar}{2m}\right)^{2n+1}\frac{(-1)^n(2n+2)}{(2n+3)!}\sum_{i_1\ldots i_{2n}=1}^{3}\left(\frac{\partial^{2n+1}}{\partial r_{i_1}\ldots\partial r_{i_{2n+1}}}\boldsymbol{B}\right)\frac{\partial^{2n+1}}{\partial v_{i_1}\ldots\partial v_{i_{2n+1}}}\\ &= \sum_{i=1}^{3}\frac{\mu_{\mathrm{B}}\hbar}{6}\frac{\partial\boldsymbol{B}}{\partial r_i}\frac{\partial}{\partial v_i}+\mu_{\mathrm{B}}\mathcal{O}\left(\hbar^3\right). \qquad (2.53)\end{aligned}$$

From these semiclassical expansions, we notice that the velocity shift $\boldsymbol{\Delta}\widetilde{\boldsymbol{\pi}}$ has a purely quantum origin because the first term in the development is already in order one in $\hbar$. Therefore it has no classical counterpart. In the case of $\widetilde{\boldsymbol{E}}$ and $\widetilde{\boldsymbol{B}}$, the first term in the development corresponds just to the classical electric and magnetic fields.

At zero order, the equations for f_0 and f_i decouple, so that one can study the particle motion irrespectively from the spin degrees of freedom. The latter is simply transport by the particles. Keeping the first order term in $\hbar$ in the Eqs. (2.22) - (2.23), one obtains

$$\begin{aligned}&\frac{\partial f_0}{\partial t}+\boldsymbol{v}\cdot\boldsymbol{\nabla} f_0-\frac{e}{m}\left(\boldsymbol{E}+\boldsymbol{v}\times\boldsymbol{B}\right)\cdot\boldsymbol{\nabla}_{\boldsymbol{v}} f_0+\frac{\mu_{\mathrm{B}}}{2mc^2}\left(\boldsymbol{E}\times\boldsymbol{\nabla}\right)_i f_i\\&-\frac{\mu_{\mathrm{B}}}{m}\boldsymbol{\nabla}\left[B_i-\frac{1}{2c^2}\left(\boldsymbol{v}\times\boldsymbol{E}\right)_i\right]\cdot\boldsymbol{\nabla}_{\boldsymbol{v}} f_i-\frac{\mu_{\mathrm{B}}e}{2m^2c^2}\left[\boldsymbol{E}\times\left(\boldsymbol{B}\times\boldsymbol{\nabla}_{\boldsymbol{v}}\right)\right]_i f_i=0.\end{aligned}\tag{2.54}$$

$$\begin{aligned}&\frac{\partial f_i}{\partial t}+\boldsymbol{v}\cdot\boldsymbol{\nabla} f_i-\frac{e}{m}\left(\boldsymbol{E}+\boldsymbol{v}\times\boldsymbol{B}\right)\cdot\boldsymbol{\nabla}_{\boldsymbol{v}} f_i+\frac{\mu_{\mathrm{B}}}{2mc^2}\left(\boldsymbol{E}\times\boldsymbol{\nabla}\right)_i f_0\\&-\frac{\mu_{\mathrm{B}}}{m}\boldsymbol{\nabla}\left[B_i-\frac{1}{2c^2}\left(\boldsymbol{v}\times\boldsymbol{E}\right)_i\right]\cdot\boldsymbol{\nabla}_{\boldsymbol{v}} f_0-\frac{\mu_{\mathrm{B}}e}{2m^2c^2}\left[\boldsymbol{E}\times\left(\boldsymbol{B}\times\boldsymbol{\nabla}_{\boldsymbol{v}}\right)\right]_i f_0\\&-\frac{2\mu_{\mathrm{B}}}{\hbar}\left\{\left[\boldsymbol{B}-\frac{1}{2c^2}\left(\boldsymbol{v}\times\boldsymbol{E}\right)\right]\times\boldsymbol{f}\right\}_i=0.\end{aligned}\tag{2.55}$$

where the factor $\hbar$ is hidden in the definition of the Bohr magneton $\mu_{\mathrm{B}}=e\hbar/(2m)$. All the quantum corrections in Eqs (2.54)- (2.55), couple the orbital and the spin components together trough the Zeeman and the spin-orbit interactions. There is no quantum corrections to the orbital electronic dynamics because they appears only at the second order in $\hbar$. For instance the Darwin term would not appears in these equations because it would correspond to a $\hbar^2$ correction in the orbital motion of the electron. This is why, the Eqs. (2.54) and (2.55) have the same structure as classical Vlasov equations.

In Eqs (2.54) and (2.55), the Zeeman interaction gives two contributions. The term $\mu_{\mathrm{B}}\boldsymbol{\nabla}B_i\cdot\boldsymbol{\nabla}_{\boldsymbol{v}}$, which reflects the force exerted on a magnetic dipole by an inhomogeneous magnetic field, and which is at the basis of Stern-Gerlach-type experiments [102]. And the term $\boldsymbol{f}\times\boldsymbol{B}$ which represents the precession of the spin around the magnetic field. The latter corresponds to the classical precession of a magnetic dipole in a magnetic field described by the Landau-Lifshitz equation.

The spin-orbit interaction provides a correction to the magnetic field $\boldsymbol{B}\rightarrow\boldsymbol{B}-\left(\boldsymbol{v}\times\boldsymbol{E}\right)/2c^2$ which corresponds to the first order term in the non relativistic limit of the Thomas precession [118, 119]. The other terms are related to the spin-orbit correction of the velocity operator. Indeed in the Heisenberg pictures the velocity operators $\widehat{\boldsymbol{V}}$ is determined by the evolution equation of the position operator.

$$\widehat{\boldsymbol{V}}=\frac{1}{i\hbar}\left[\widehat{\boldsymbol{R}},\widehat{\mathcal{H}}\right]=\frac{\widehat{\boldsymbol{\Pi}}}{m}-\frac{\mu_{\mathrm{B}}}{2mc^2}\widehat{\boldsymbol{E}}\times\boldsymbol{\sigma},\tag{2.56}$$

where we used the Hamiltonian defined in Eq. (2.15). The associated phase-space function is determined with the Weyl correspondence principle

$$\boldsymbol{V}=\boldsymbol{v}-\frac{\mu_{\mathrm{B}}}{2mc^2}\boldsymbol{E}\times\boldsymbol{\sigma}.\tag{2.57}$$

This is the phase-space function which can be used to calculate the average velocity or the charge current. Therefore the particles are transport with a modified velocity. The term $(\boldsymbol{E} \times \boldsymbol{\nabla})_i f_i$ in Eqs. (2.54)-(2.55) is a direct consequence of this effect. Whereas the term $[\boldsymbol{E} \times (\boldsymbol{B} \times \boldsymbol{\nabla}_{\boldsymbol{v}})]_i f_i$ corresponds to the velocity correction in the Lorentz force $\boldsymbol{v} \times \boldsymbol{B}$.
One should also remains that the spin-Vlasov equations, Eqs. (2.54) and (2.55), are on the second order in $1/c$. An alternative form of these equations was obtained by Asenjo et al. [61] in the extended phase-space formalism.
The Maxwell equations, Eq. (2.28), combined with the spin-Vlasov equations, Eqs. (2.54)-(2.55), form a self-consistent model to study the charges and the spins dynamics of a system of interacting particles. Where the spin is treated on full a quantum fashion (two dimensional Hilbert space), whereas the orbital motion is treated classically, i.e. the particles follow classical phase-space trajectories. One can demonstrate that the following quantities are conserved during the time evolution

$$M_{tot} = m \int f_0 d\boldsymbol{v} d\boldsymbol{r}, \tag{2.58}$$

$$\boldsymbol{P}_{tot} = m \int \boldsymbol{v} f_0 d\boldsymbol{v} d\boldsymbol{r} + \int \boldsymbol{D} \times \boldsymbol{B} d\boldsymbol{r}, \tag{2.59}$$

$$E_{tot} = \frac{m}{2} \int \boldsymbol{v}^2 f_0 d\boldsymbol{v} d\boldsymbol{r} + \mu_{\mathrm{B}} \int \boldsymbol{f} \cdot \boldsymbol{B} d\boldsymbol{v} d\boldsymbol{r} + \frac{\epsilon_0}{2} \int \boldsymbol{E}^2 d\boldsymbol{r} + \frac{1}{2\mu_0} \int \boldsymbol{B}^2 d\boldsymbol{r}, \tag{2.60}$$

$$\boldsymbol{J}_{tot} = m \int (\boldsymbol{r} \times \boldsymbol{v}) f_0 d\boldsymbol{r} d\boldsymbol{v} + \frac{\hbar}{2} \int \boldsymbol{f} d\boldsymbol{r} d\boldsymbol{v} + \int \boldsymbol{r} \times (\boldsymbol{D} \times \boldsymbol{B}) d\boldsymbol{r}, \tag{2.61}$$

where we have introduced the electric and the magnetic field in the matter $\boldsymbol{D} = \epsilon_0 \boldsymbol{E} + \boldsymbol{P}$ and $\boldsymbol{H} = \boldsymbol{B} - \mu_0 \boldsymbol{M}$. The first term is the total mass of the system. The second terms is the total impulsion of the system, it writes as a sum of the particle impulsion and the field impulsion. The third term is the total energy of the system, it writes as a sum of the kinetic energy, the Zeeman energy and the electromagnetic field energy. The last term is the total angular momentum, it writes as a sum of the orbital momentum, the spin momentum and the electromagnetic field momentum.
In terms of numerical simulations the spin-Vlasov equations are more tractable than the full Wigner-spin model, namely because the Vlasov equation are local in phase space in contrast with the Wigner equations. For instance, they can be used to simulate the charge and the spin dynamics in metallic nano-structures. From Eq. (1.26), we notice that the quantity which should be small is $\hbar/(mL_0v_0)$, where L_0 and v_0 are, respectively, typical length and velocity scales. Introducing the DeBroglie wavelength $\lambda_{\mathrm{DB}} = \frac{\hbar}{mv}$, the spin-Vlasov equations may be considered as valid when the characteristic lengths of the system are much more larger than the DeBroglie wavelength : $L >> \lambda_{\mathrm{DB}}$. This is the reason why the semiclassical limit is also called the long wavelength approximation.

2.3 Fluid model with spin effects

The Wigner equation and the Vlasov equation belong to the class of kinetic equations because they give the evolution in time of the position and the velocity of the particles. In this section, we will derive fluid models (sometimes called also hydrodynamic models) with spin effects. Hydrodynamic equations including the spin degrees of freedom were derived by Brodin and Marklund [120] using the Madelung transformation of the wave function [93]. More recently, a relativistic hydrodynamic model was obtained by Asenjo et al. [121] from the Dirac equation. These approaches based on the Madelung transformation usually lead to cumbersome equations that are in practice very hard to solve, either analytically or numerically, even in the nonrelativistic limit.
Our technique, which separates clearly the (classical) orbital motion from the (quantum) spin dynamics, leads to a simpler and more transparent fluid model, where the meaning of each term in the equations is more intuitive. Starting from the spin-Vlasov Eqs. (2.54) - (2.55), we derive the hydrodynamic evolution equations for a spin system by taking velocity moments of the phase-space distribution functions. The fluid equations derived from the Vlasov model constitute an infinite hierarchy of equations that need to be closed using some additional physical hypotheses. Although this is relatively easy for spinless systems[3], things are far subtler when the spin degrees of freedom are included.
In a first time we will only consider the Zeeman interaction. we shall employ a general procedure based on the maximization of entropy. Using this approach, we obtain a closed set of fluid equations for both Maxwell-Boltzmann and the Fermi-Dirac statistics, keeping up to four fluid moments of the Vlasov distribution function. Fluid models with spin-orbit effects will be discussed in a second time.

2.3.1 Hydrodynamic model with the Zeeman interaction

In addition to the particle density and spin polarization, Eqs. (2.10) - (2.11), we define the following macroscopic quantities

$$\boldsymbol{u} = \frac{1}{n}\int \boldsymbol{v} f_0 d\boldsymbol{v}, \tag{2.62}$$

$$J^S_{i\alpha} = \frac{\hbar}{2}\int v_i f_\alpha d\boldsymbol{v}, \tag{2.63}$$

$$P_{ij} = m\int w_i w_j f_0 d\boldsymbol{v}, \tag{2.64}$$

$$\Pi_{ij\alpha} = \frac{\hbar}{2} m\int v_i v_j f_\alpha d\boldsymbol{v}, \tag{2.65}$$

$$Q_{ijk} = m\int w_i w_j w_k f_0 d\boldsymbol{v}, \tag{2.66}$$

[3] Fluid models for spinless systems were introduced in section 1.4.

where we separated the mean fluid velocity $\boldsymbol{u}$ from the velocity fluctuations $\boldsymbol{w} \equiv \boldsymbol{v} - \boldsymbol{u}$. Here, P_{ij} and Q_{ijk} are respectively the pressure and the generalized energy flux tensors. They coincide with the analogous definitions for spinless fluids with probability distribution function f_0. The spin-velocity tensor $J^S_{i\alpha}$ represents the mean fluid velocity along the $i-$th direction of the $\alpha-$th spin polarization vector, while $\Pi_{ij\alpha}$ represents the corresponding spin-pressure tensor[4]. The evolution equations for the above fluid quantities are easily obtained by the straightforward integration of Eqs. (2.54) - (2.55) with respect to the velocity variable. We obtain :

$$\frac{\partial n}{\partial t} + \boldsymbol{\nabla} \cdot (n\boldsymbol{u}) = 0, \tag{2.67}$$

$$\frac{\partial S_\alpha}{\partial t} + \partial_i J^S_{i\alpha} + \frac{e}{m} (\boldsymbol{S} \times \boldsymbol{B})_\alpha = 0, \tag{2.68}$$

$$\frac{\partial u_i}{\partial t} + u_j(\partial_j u_i) + \frac{1}{nm}\partial_j P_{ij} + \frac{e}{m}\left[E_i + (\boldsymbol{u} \times \boldsymbol{B})_i\right] + \frac{e}{nm^2} S_\alpha (\partial_i B_\alpha) = 0, \tag{2.69}$$

$$\frac{\partial J^S_{i\alpha}}{\partial t} + \partial_j \Pi_{ij\alpha} + \frac{eE_i}{m} S_\alpha + \frac{e}{m}\epsilon_{jki} B_k J^S_{j\alpha} + \frac{e}{m}\epsilon_{jk\alpha} B_k J^S_{ij} + \frac{\mu_B \hbar}{2m} (\partial_i B_\alpha)\, n = 0, \tag{2.70}$$

$$\frac{\partial P_{ij}}{\partial t} + u_k \partial_k P_{ij} + P_{jk}\partial_k u_i + P_{ik}\partial_k u_j + P_{ij}\partial_k u_k + \partial_k Q_{ijk} + \frac{e}{m}\left[\epsilon_{lki} B_k P_{jl} + \epsilon_{lkj} B_k P_{il}\right] + \frac{e}{m^2}\sum_\alpha \left[\partial_i B_\alpha \left(J^S_{j\alpha} - S_\alpha u_j\right) + \partial_j B_\alpha \left(J^S_{i\alpha} - S_\alpha u_i\right)\right] = 0. \tag{2.71}$$

Other sets of hydrodynamic equations for spin-1/2 particles were derived by Brodin and Marklund [120] using a Madelung transformation on the Pauli wave function. The resulting model is much more cumbersome than the above system (2.67)-(2.71), and it is hard to identify the physical meaning of each term in their equations. A different hydrodynamic theory was derived by Zamanian et al. [60] from a Vlasov equation that includes the spin as an independent variable [59]. Their equations are very similar to ours. The main difference is that, in the equations of Ref. [60], each quantity (including the spin polarization) is transported by a fluid element travelling with the mean fluid velocity $\mathbf{u}$. In other words, the convective derivative is always $D_t = \partial_t + \mathbf{u} \cdot \boldsymbol{\nabla}$. In contrast, in our equations (2.67)-(2.71), only the spinless quantities (velocity, pressure) are transported by the fluid velocity, whereas the spin quantities (S_α, $J^S_{i\alpha}$) are not. However, it can be shown that our fluid equations (2.67)-(2.71) are equivalent to those of Ref. [60]. The apparent discrepancy in the two sets of fluid equations arises mainly from the different definitions of the velocity moments in the two approaches.

As it is always the case for hydrodynamic models, some further hypothesis are needed to close the above set of equations (2.67)-(2.71). In the next Section, we will deal with the closure problem by resorting to a maximum entropy principle (MEP) – an approach that has been developed for spinless systems and that can be

[4]Strictly speaking a pressure tensor should be defined in terms of the velocity fluctuations $w_i w_j$, but this would unduly complicate the notation. Thus, we stick to the above definition of $\Pi_{ij\alpha}$ while still using the term "pressure" for this quantity.

straightforwardly generalized to our case of a fluid with spin. In order to fix the ideas before addressing the general framework of the MEP, we discuss an intuitive closure relation that arises naturally from the equations. In Sec. 2.3.3 , this intuitive approach will be justified rigorously on the basis of the MEP, and then overcome in Sec. 2.3.4. We first note that, by definition, the following equation is always satisfied: $\int w_i f_0 d\boldsymbol{v} = 0$. The same is not true, however, for the expression obtained by replacing f_0 with f_α in the preceding integral. If we assume that such a quantity indeed vanishes, i.e. $\int w_i f_\alpha d\boldsymbol{v} = 0$, we immediately obtain that

$$J^S_{i\alpha} = u_i S_\alpha. \tag{2.72}$$

The physical interpretation of the above equation is that the spin of a particle is simply transported along the mean fluid velocity. This is of course an approximation that amounts to neglecting some spin-velocity correlations [60].
With this assumption, Eq. (2.70) and the definition of the spin-pressure $\Pi_{ij\alpha}$ are no longer necessary. The system of fluid equations simplifies to

$$\frac{\partial n}{\partial t} + \boldsymbol{\nabla}\cdot(\boldsymbol{u}n) = 0, \tag{2.73}$$

$$\frac{\partial S_\alpha}{\partial t} + \partial_i\left(u_i S_\alpha\right) + \frac{e}{m}\left(\boldsymbol{S}\times\boldsymbol{B}\right)_\alpha = 0, \tag{2.74}$$

$$\frac{\partial u_i}{\partial t} + u_j(\partial_j u_i) + \frac{1}{nm}\partial_j P_{ij} + \frac{e}{m}\left[E_i + (\boldsymbol{u}\times\boldsymbol{B})_i\right] + \frac{e}{nm^2}S_\alpha\left(\partial_i B_\alpha\right) = 0, \tag{2.75}$$

$$\begin{aligned}\frac{\partial P_{ij}}{\partial t} &+ u_k\partial_k P_{ij} + P_{jk}\partial_k u_i + P_{ik}\partial_k u_j + P_{ij}\partial_k u_k + \partial_k Q_{ijk}\\ &+ \frac{e}{m}\left[\epsilon_{lki}B_k P_{jl} + \epsilon_{lkj}B_k P_{il}\right] = 0.\end{aligned} \tag{2.76}$$

Interestingly, in Eq. (2.74) the spin polarization is now transported by the fluid velocity $\mathbf{u}$, as in the model of Zamanian et al. [60].
We note that in Eqs. (2.73)–(2.76) we have already closed [thanks to Eq. (2.72)] the spin-dependent part of the equations. In order to complete the closure procedure, one can proceed in the same way as is usually done for spinless fluids, see section 1.4, for instance by supposing that the system is isotropic and adiabatic. The isotropy condition imposes that $P_{ij} = (P/3)\delta_{ij}$ where δ_{ij} is the Kronecker delta, while the adiabatic condition requires that the heat flux $Q^{th}_i = m\int \boldsymbol{w}^2 w_i f_0 d\boldsymbol{v}$ vanish. In this case, one can prove that the pressure takes the usual form for the equation of state of an adiabatic system, i.e. $P = \text{const.}\times n^{\frac{D+2}{D}}$ (D is the dimensionality of the system), which replaces Eq. (2.76). In summary, Eqs. (2.73)-(2.75), together with the preceding expression for the pressure, constitute a closed system of hydrodynamic equations with spin.

2.3.2 Fluid closure: Maximum entropy principle

The maximum entropy principle is a well-developed theory that has been successfully applied to various areas of gas, fluid, and solid-state physics [65,122–124]. The underlying assumption of the MEP is that, at equilibrium, the probability distribution function is given by the most probable microscopic distribution (i.e., the one that maximizes the entropy) compatible with some macroscopic constraints. The constraints are generally given by the various velocity moments, i.e., the local density, mean velocity, and temperature. From a mathematical point of view, this procedure leads to a constrained maximization problem.
In order to illustrate the application of the MEP theory to a spin system, we write the Hamiltonian in a more general way

$$\mathcal{H} = h_0(\boldsymbol{r},\boldsymbol{v})\sigma_0 + \boldsymbol{h}(\boldsymbol{r},\boldsymbol{v})\cdot\boldsymbol{\sigma}, \tag{2.77}$$

where h_0 and $\boldsymbol{h}$ are functions of the particle position $\boldsymbol{r}$ and velocity $\boldsymbol{v} \equiv (\boldsymbol{p}+e\boldsymbol{A})/m$. In our case

$$h_0 = m\frac{|\boldsymbol{v}|^2}{2} + V, \tag{2.78}$$

$$\boldsymbol{h} = \mu_B \boldsymbol{B}. \tag{2.79}$$

In order to simplify the notation, we denote the fluid moments by

$$\boldsymbol{m}_i(\boldsymbol{r}) = Tr\int \boldsymbol{\chi}_i \mathcal{F} d\boldsymbol{v}, \tag{2.80}$$

where $\mathcal{F}$ is the 2×2 distribution functions defined in Eq. (2.6) and χ_i is the function associated with the $i-$th fluid moment. Thus, the definitions (2.10)–(2.11) and (2.62)–(2.66) correspond to

$$\boldsymbol{m} = \begin{pmatrix} n \\ \boldsymbol{S} \\ \boldsymbol{u} \\ J^S_{i\alpha} \\ \vdots \end{pmatrix}; \qquad \boldsymbol{\chi} = \begin{pmatrix} 1 \\ \frac{\hbar}{2}\boldsymbol{\sigma} \\ \boldsymbol{v} \\ \frac{\hbar}{2}v_i\sigma_\alpha \\ \vdots \end{pmatrix}. \tag{2.81}$$

The relevant entropy density is

$$s(\mathcal{F}) = \begin{cases} k_B\, Tr\left\{\mathcal{F}\log\mathcal{F} - \mathcal{F}\right\} & \text{(M–B)} \\ k_B\, Tr\left\{\mathcal{F}\log\mathcal{F} + (1-\mathcal{F})\log(1-\mathcal{F})\right\} & \text{(F–D),} \end{cases} \tag{2.82}$$

where we distinguished between Maxwell-Boltzmann (M–B) and Fermi-Dirac (F–D) statistics. The MEP assumes that the equilibrium phase-space distribution function

$\mathcal{F}$ is the extrema of the free-energy functional

$$\mathcal{E} \;=\; Tr \int \left[Ts(\mathcal{F}) + \mathcal{H}'\mathcal{F}\right] d\boldsymbol{v}d\boldsymbol{r} - \int \lambda_i(\boldsymbol{r}) m_i(\boldsymbol{r}) d\boldsymbol{r}, \tag{2.83}$$

where we defined $\mathcal{H}' = \mathcal{H} + \lambda_i(\boldsymbol{r})\boldsymbol{\chi}_i$, T is the temperature and the functions λ_i are the Lagrange multipliers. The λ_i constitute a set of independent functions that are used to parameterize the equilibrium distribution $\mathcal{F}^{eq}$. A major technical difficulty of the MEP method is to express the λ_i set in terms of $\boldsymbol{m}$ in a closed form. This point will be illustrated in details in the following paragraphs. The total variation (Lie derivative) of $\mathcal{E}$ gives

$$\delta\mathcal{E} \;=\; \delta\lambda_i \frac{\delta}{\delta\lambda_i}\mathcal{E} + \delta\mathcal{F}\frac{\delta}{\delta\mathcal{F}}\mathcal{E}. \tag{2.84}$$

The local equilibrium distribution $\mathcal{F}^{eq}$ corresponds to the extremum $\delta\mathcal{E}(\mathcal{F}^{eq}) = 0$. It is easy to verify that the variation with respect the Lagrange multipliers [the first term of the right hand side of Eq. (2.84)] gives Eq. (2.80).

The equilibrium distribution is formally obtained by taking the variation of $\mathcal{E}$ with respect to $\mathcal{F}$

$$\delta\mathcal{F}\frac{\delta\mathcal{E}}{\delta\mathcal{F}} = Tr \int \left[T\frac{\delta s}{\delta\mathcal{F}} + \mathcal{H}'\right] \delta\mathcal{F} d\boldsymbol{v}d\boldsymbol{r}. \tag{2.85}$$

Setting $\delta\mathcal{E}/\delta\mathcal{F} = 0$, yields

$$\mathcal{F}^{eq} = \begin{cases} a\exp\left(-\beta\mathcal{H}'\right) & \text{(M–B)} \\ a\left[\exp\left(\beta\mathcal{H}'\right) + 1\right]^{-1} & \text{(F–D),} \end{cases} \tag{2.86}$$

where a is a constant and $\beta = 1/(k_B T)$. Equation (2.86) is a very general result that holds irrespectively of the number and the type of moments that are being considered. For every specific choice of the moments to be preserved, the explicit form of the local equilibrium function $\mathcal{F}^{eq}$ can be constructed from Eq. (2.86). In order to illustrate the results for a fluid with spin, in the next sections we shall consider various models characterized by a different number of fluid moments (three or four) and by the use of the M–B or F–D statistics.

2.3.3 Three-moment closure

To begin with, we consider a simplified situation where only three fluid moments (density n, mean velocity $\boldsymbol{u}$, and spin polarization $\boldsymbol{S}$) are kept, that is:

$$\boldsymbol{m} = \begin{pmatrix} n \\ \boldsymbol{S} \\ \boldsymbol{u} \end{pmatrix}. \tag{2.87}$$

It is convenient to write the hamiltonian $\mathcal{H}'$ in the following way

$$\mathcal{H}' = h'_0 + \boldsymbol{h'} \cdot \boldsymbol{\sigma} = \frac{m}{2} \left(\boldsymbol{v} - \boldsymbol{v_0}\right)^2 + \lambda_0 + \boldsymbol{\lambda_S} \cdot \boldsymbol{\sigma}, \tag{2.88}$$

where the Lagrange multipliers λ_0, $\boldsymbol{\lambda_S}$ and $\boldsymbol{v_0}$ (seven scalar quantities in total) are associated respectively to the density, the spin polarization vector, and the mean velocity. We then evaluate the equilibrium distribution for the M–B and F–D statistics.

A. Maxwell-Boltzmann statistics

We fix the normalization constant $a_0 = \left(\frac{m}{2\pi\hbar}\right)^3$. Equation (2.86) (for M–B statistics) gives

$$\begin{aligned} \mathcal{F}^{eq} &= a_0 \, \sigma_0 e^{-\beta h'_0} \exp\left(-\beta \boldsymbol{h'} \cdot \boldsymbol{\sigma}\right) \\ &= a_0 \left[\sigma_0 \cosh\left(-\beta |\mathbf{h}'|\right) + \frac{\boldsymbol{h'} \cdot \boldsymbol{\sigma}}{|\boldsymbol{h'}|} \sinh\left(-\beta |\boldsymbol{h'}|\right) \right] e^{-\beta h'_0}. \end{aligned} \tag{2.89}$$

By calculating the moments of $\mathcal{F}^{eq}$, we can express the fluid moments in terms of the Lagrangian multipliers. We find

$$\begin{aligned} n &= 2a_0 \Gamma(T) \exp\left(-\beta\lambda_0\right) \cosh\left(-\beta |\boldsymbol{\lambda_S}|\right), \\ \boldsymbol{S} &= \hbar \, a_0 \, \frac{\boldsymbol{\lambda_S}}{|\boldsymbol{\lambda_S}|} \, \Gamma(T) \exp\left(-\beta\lambda_0\right) \sinh\left(-\beta |\boldsymbol{\lambda_S}|\right), \\ \boldsymbol{u} &= \boldsymbol{v_0}, \end{aligned}$$

where $\Gamma(T) = \left(2\pi k_{\mathrm{B}} T/m\right)^{3/2}$. The previous equations can be inverted:

$$\exp\left(-\beta\lambda_0\right) = a_0 \frac{1}{2\Gamma(T)} \sqrt{\left(n^2 - \frac{4|\boldsymbol{S}|^2}{\hbar^2}\right)}, \tag{2.90}$$

$$\boldsymbol{\lambda}_S = \frac{\boldsymbol{S}}{|\boldsymbol{S}|} \frac{k_{\mathrm{B}} T}{2} \ln\left(\frac{n - \frac{2|\boldsymbol{S}|}{\hbar}}{n + \frac{2|\boldsymbol{S}|}{\hbar}}\right). \tag{2.91}$$

Note that the quantities on the right-hand side of the above expressions are real, thanks to Eq. (2.12). Finally, the equilibrium distribution can be expressed in terms of the fluid moments in a simple form

$$\mathcal{F}^{eq} = \left(\sigma_0 n + \boldsymbol{\sigma} \cdot \boldsymbol{S}\right) \frac{1}{\Gamma(T)} \exp\left(-\beta \frac{m \left(\boldsymbol{v} - \boldsymbol{u}\right)^2}{2}\right). \tag{2.92}$$

The pressure and the spin current at equilibrium are thus given by

$$P_{ij} = m \, Tr\left(\int v_i v_j \mathcal{F}^{eq} d\boldsymbol{v}\right) - mnu^2 = n k_{\mathrm{B}} T \delta_{ij} \tag{2.93}$$

$$J^S_{i\alpha} = S_\alpha u_i. \tag{2.94}$$

Thus, considering three fluid moments and M–B statistics, leads to the standard expression for the isotropic pressure of an ideal gas, together with the "intuitive" closure condition (2.72) for the spin current tensor.

B. Fermi-Dirac statistics

We now consider the F–D case. After some tedious but straightforward calculations (details can be found in Appendix B.1), Eq. (2.86) gives

$$\mathcal{F}^{eq} = \frac{a_0}{2}\frac{\left(\cosh\left(\beta|\boldsymbol{h'}|\right) + \exp^{-\beta h'_0}\right)\sigma_0 - \sinh\left(\beta h'_0\right)\frac{\boldsymbol{h'}\cdot\boldsymbol{\sigma}}{|\boldsymbol{h'}|}}{\left[\cosh\left(\beta h'_0\right) + \cosh\left(\beta|\boldsymbol{h'}|\right)\right]}. \tag{2.95}$$

In the case of the F–D statistics, it is no longer possible to obtain a closed expression of $\mathcal{F}^{eq}$ when $T > 0$. However, for many applications of the hydrodynamic model, the assumption that the particle have zero temperature is not too restrictive. Indeed, for solid-state metallic densities, the Fermi temperature is of the order $T_F \approx 5 \times 10^4$ K, so that in the vast majority of conceivable situations $T \ll T_F$, and the zero-temperature approximation is sufficiently accurate. We have evaluated the macroscopic moment of $\mathcal{F}^{eq}$ in the case $T = 0$. We obtain (details of the calculations are given in Appendix B.1):

$$n = \frac{4\pi}{3}a_0\left(\left[\frac{2}{m}\left(|\boldsymbol{\lambda_S}| + |\lambda_0|\right)\right]^{3/2} + \left[\frac{2}{m}\left(|\lambda_0| - |\boldsymbol{\lambda_S}|\right)\right]^{3/2}\right), \tag{2.96}$$

$$\boldsymbol{S} = -\frac{\hbar}{2}a_0\frac{\boldsymbol{\lambda^S}}{|\boldsymbol{\lambda^s}|}\frac{4\pi}{3}\left(\left[\frac{2}{m}\left(|\boldsymbol{\lambda^S}| + |\lambda_0|\right)\right]^{3/2} - \left[\frac{2}{m}\left(|\lambda_0| - |\boldsymbol{\lambda^S}|\right)\right]^{3/2}\right), \tag{2.97}$$

$$\boldsymbol{u} = \boldsymbol{v_0}. \tag{2.98}$$

Note that, in the above expressions, the quantities under square root are nonnegative for all physically admissible states, as is shown in Appendix B.1.
As in the case of M–B statistics, we find that $J^S_{i\alpha} = u_i S_\alpha$. For the pressure, we obtain

$$P = \frac{\hbar^2}{5m}\frac{\left(6\pi^2\right)^{2/3}}{2^{5/3}}\left[\left(n - \frac{2}{\hbar}|\boldsymbol{S}|\right)^{5/3} + \left(n + \frac{2}{\hbar}|\boldsymbol{S}|\right)^{5/3}\right]. \tag{2.99}$$

When the spin polarization vanishes, Eq. (2.99) reduces to the usual expression of the zero-temperature pressure of a spinless Fermi gas: $P = \frac{\hbar^2}{5m}\left(3\pi^2\right)^{2/3} n^{5/3}$. The modification of the spin pressure induced by the spin has a simple physical interpretation. Equation (2.99) can be interpreted as the total pressure of a plasma composed by two populations, the spin-up and the spin-down particles. Due to the Zeeman splitting, the density of the particles whose spin is parallel to the magnetic field is lower than the energy of the particles whose spin is antiparallel. Equation (2.99) shows that the two populations provide a separate contribution to the total fluid pressure.

2.3.4 Four-moment closure

As a final example, we consider the complete four-moment model:

$$\boldsymbol{m} = \begin{pmatrix} n \\ \boldsymbol{S} \\ \boldsymbol{u} \\ J^S_{i\alpha} \end{pmatrix} \quad \text{and} \quad \chi = \begin{pmatrix} \lambda_0 \\ \boldsymbol{\lambda_S} \\ \boldsymbol{v_0} \\ \lambda^J_{i\alpha} \end{pmatrix}. \tag{2.100}$$

In this case, the hamiltonian $\mathcal{H}'$ becomes

$$\mathcal{H}' = \frac{m\left(\boldsymbol{v}-\boldsymbol{v_0}\right)^2}{2} + \lambda^0 + \left(\lambda^S_\alpha + \lambda^J_{i\alpha} v_i\right)\sigma_\alpha. \tag{2.101}$$

Here, we consider a particular situation where the evaluation of the closure expressions can be obtained analytically, namely the collinear case with Maxwell-Boltzmann statistics. With the term "collinear" we denote a fluid whose spin polarization is parallel to a fixed direction (here, the z direction). In the collinear case, the Hamiltonian reduces to $\mathcal{H}_{\text{col}} = \frac{m}{2}v^2 + \mu_B B_z \sigma_z$. The equilibrium distribution $\mathcal{F}^{eq}$ is given by Eq. (2.89) with

$$h'_0 = m\left(\boldsymbol{v}-\boldsymbol{v_0}\right)^2/2 + \lambda_0 \tag{2.102}$$
$$h'_z = \lambda^S_z + \lambda^J_{xz} v_x + \lambda^J_{yz} v_y + \lambda^J_{zz} v_z \tag{2.103}$$
$$h'_x = h'_y = 0. \tag{2.104}$$

Proceeding as before, we obtain the relations between the moments and the Lagrange multipliers. The details of the calculations are given in Appendix B.2. We obtain

$$\boldsymbol{\gamma} = \frac{2n\hbar m}{\hbar^2 n^2 + 4S_z^2}\left(S_z \boldsymbol{u} - \boldsymbol{J}^S\right), \tag{2.105}$$
$$\boldsymbol{v_0} = \frac{1}{\hbar^2 n^2 + 4S_z^2}\left(\hbar^2 n^2 \boldsymbol{u} + 4S_z \boldsymbol{J}^S\right), \tag{2.106}$$
$$e^{-\beta\lambda_0} = \frac{e^{\beta\gamma^2/2m}}{\Gamma(T)}\sqrt{\left(\frac{n}{2}\right)^2 - \left(\frac{S_z}{\hbar}\right)^2}, \tag{2.107}$$
$$\lambda^S_z = \frac{k_B T}{2}\ln\left(\frac{n - \frac{2|\boldsymbol{S}|}{\hbar}}{n + \frac{2|\boldsymbol{S}|}{\hbar}}\right) - \boldsymbol{\gamma}\cdot\boldsymbol{v_0}. \tag{2.108}$$

In order to simplify the notation, we defined $\gamma_i = \lambda^J_{iz}$ and $J^S_{iz} = J^S_i$. We can now calculate the equilibrium distribution function:

$$\mathcal{F}^{eq} = \frac{e^{\beta\boldsymbol{\gamma}^2/2m}}{\Gamma(T)} e^{-\beta m(\boldsymbol{v}-\boldsymbol{v_0})^2/2} \Big\{ \sigma_0 \left[n\cosh\left(\beta\boldsymbol{\gamma}\cdot(\boldsymbol{v}-\boldsymbol{v_0})\right) - \frac{2S_z}{\hbar}\sinh\left(\beta\boldsymbol{\gamma}\cdot(\boldsymbol{v}-\boldsymbol{v_0})\right)\right] + \sigma_z\left[\frac{\hbar}{2}n\sinh\left(-\beta\boldsymbol{\gamma}\cdot(\boldsymbol{v}-\boldsymbol{v_0})\right) + S_z\cosh\left(\beta\boldsymbol{\gamma}\cdot(\boldsymbol{v}-\boldsymbol{v_0})\right)\right]\Big\}. \tag{2.109}$$

Finally, we calculate the pressure tensor P_{ij} and the spin pressure tensor Π_{ijz} (details are given in the Appendix B.2). We obtain

$$\begin{aligned} P_{ij} &= e^{\beta\boldsymbol{\gamma}^2/m}\Big\{ nk_{\mathrm{B}}T\delta_{i,j} + mn\left(\frac{\hbar^2n^2u_iu_j + 4J^s_iJ^s_j}{\hbar^2n^2+4S_z^2}\right) \\ &\quad + 8mnS_z\left[\frac{\left(J^S_i - S_zu_i\right)\left(\hbar^2n^2u_j + 4S_zJ^s_j\right) + \left(J^S_j - S_zu_j\right)\left(\hbar^2n^2u_i + 4S_zJ^s_i\right)}{\left(\hbar^2n^2+4S_z^2\right)^2}\right]\Big\} \\ &\quad - mnu_iu_j, \end{aligned} \tag{2.110}$$

$$\begin{aligned} \Pi_{ijz} &= e^{\beta\boldsymbol{\gamma}^2/m}\Big\{ S_zk_{\mathrm{B}}T\delta_{i,j} + mS_z\left(\frac{\hbar^2n^2u_iu_j + 4J^s_iJ^s_j}{\hbar^2n^2+4S_z^2}\right) \\ &\quad + 2mn^2\hbar^2\left[\frac{\left(J^S_i - S_zu_i\right)\left(\hbar^2n^2u_j + 4S_zJ^s_j\right) + \left(J^S_j - S_zu_j\right)\left(\hbar^2n^2u_i + 4S_zJ^s_i\right)}{\left(\hbar^2n^2+4S_z^2\right)^2}\right]\Big\}. \end{aligned} \tag{2.111}$$

It is easy to verify that Eq. (2.110) is consistent with Eq. (2.94) in the limit $\boldsymbol{\gamma} \to 0$. Finally, we can write a four-moment model with collinear spin and Maxwell-Boltzmannn statistics at zero temperature:

$$\begin{aligned} \frac{\partial n}{\partial t} &+ \boldsymbol{\nabla}\cdot(n\boldsymbol{u}) = 0, \\ \frac{\partial S_z}{\partial t} &+ \partial_i J^S_{iz} = 0, \\ \frac{\partial u_i}{\partial t} &+ u_j\partial_j u_i + \frac{1}{nm}\partial_j P_{ij} + \frac{e}{m}\left(E_i + \epsilon_{jki}u_jB_k\right) + \frac{e}{nm^2}S_z\left(\partial_iB_z\right) = 0, \\ \frac{\partial J^S_{iz}}{\partial t} &+ \partial_j\Pi_{ijz} + \frac{eE_i}{m}S_z + \frac{e\hbar^2}{4m^2}\left(\partial_iB_z\right)n = 0. \end{aligned} \tag{2.112}$$

The above fluid equations, together with Eqs. (2.110) and (2.111), constitute a closed system.

2.3.5 Fluid models with spin-orbit effects

In the latter calculations, we constructed fluids models with spin effects by only considering the zeeman interaction. The same work can be done by adding also the spin-orbit interaction. A straightforward integration of Eqs. (2.54) - (2.55), with

respect to the velocity variable, leads to the following fluid equations :

$$\frac{\partial n}{\partial t}+\boldsymbol{\nabla}\cdot(n\overline{\boldsymbol{u}})=0, \tag{2.113}$$

$$\frac{\partial S_\alpha}{\partial t}+\partial_i\overline{J}^S_{i\alpha}+\frac{e}{m}\left(\boldsymbol{S}\times\boldsymbol{B}\right)_\alpha+\frac{e}{2mc^2}\epsilon_{jk\alpha}\epsilon_{rlj}E_lJ^S_{rk}=0, \tag{2.114}$$

$$\begin{aligned}&\frac{\partial u_i}{\partial t}+u_j(\partial_ju_i)+\frac{1}{nm}\partial_jP_{ij}+\frac{e}{m}\left[E_i+(\widetilde{\boldsymbol{u}}\times\boldsymbol{B})_i\right]+\frac{e}{nm^2}S_\alpha\left(\partial_iB_\alpha\right)\\&+\frac{\mu_{\mathrm{B}}}{2mc^2n}\epsilon_{jkl}\left[u_i\partial_j\left(E_kS_l\right)+E_j\left(\partial_kJ^S_{il}\right)-\left(\partial_iE_k\right)J^S_{jl}-\left(\partial_jE_k\right)J^S_{il}\right]=0,\end{aligned} \tag{2.115}$$

$$\begin{aligned}&\frac{\partial J^S_{i\alpha}}{\partial t}+\partial_j\Pi_{ij\alpha}+\frac{eE_i}{m}S_\alpha+\frac{e}{m}\epsilon_{jki}B_k\widetilde{J}^S_{j\alpha}+\frac{e}{m}\epsilon_{jk\alpha}B_kJ^S_{ij}+\frac{\mu_{\mathrm{B}}\hbar}{2m}\left(\partial_iB_\alpha\right)n\\&+\frac{\mu_{\mathrm{B}}}{2mc^2}\epsilon_{kl\alpha}\partial_l\left(E_knu_i\right)-\frac{\mu_{\mathrm{B}}}{2mc^2}\epsilon_{kl\alpha}\left(\partial_iE_l\right)nu_k+\frac{\mu_{\mathrm{B}}}{\hbar c^2}\epsilon_{kl\alpha}\epsilon_{rsk}E_s\Pi^S_{irl}=0,\end{aligned} \tag{2.116}$$

$$\begin{aligned}&\frac{\partial P_{ij}}{\partial t}+u_k\partial_kP_{ij}+P_{jk}\partial_ku_i+P_{ik}\partial_ku_j+P_{ij}\partial_ku_k+\partial_kQ_{ijk}+\frac{e}{m}\left[\epsilon_{kli}P_{jk}+\epsilon_{klj}P_{ik}\right]B_l\\&+\frac{\mu_{\mathrm{B}}}{m}\left[\partial_iB_k\left(J^S_{jk}-u_jS_k\right)+\partial_jB_k\left(J^S_{ik}-U_iS_k\right)\right]+\frac{\mu_{\mathrm{B}}}{2mc^2}\epsilon_{rsl}\partial_s\left[E_r\left(\Pi^S_{ijl}-u_iu_jS_l\right)\right]\\&+\frac{\mu_{\mathrm{B}}}{2mc^2}\epsilon_{rkp}E_r\left[\epsilon_{kli}\left(J^S_{jp}-u_jS_p\right)+\epsilon_{klj}\left(J^S_{ip}-u_iS_p\right)\right]B_l\\&-\frac{\mu_{\mathrm{B}}}{2mc^2}\epsilon_{rsl}\left[\partial_iE_s\left(\Pi^S_{jrl}-u_jJ^S_{rl}\right)+\partial_jE_s\left(\Pi^S_{irl}-u_iJ^S_{rl}\right)\right]\\&-\frac{\mu_{\mathrm{B}}}{2mc^2}u_i\epsilon_{rsl}\partial_s\left[E_r\left(J^S_{jl}-u_jS_l\right)\right]-\frac{\mu_{\mathrm{B}}}{2mc^2}u_j\epsilon_{rsl}\partial_s\left[E_r\left(J^S_{il}-u_iS_l\right)\right]=0,\end{aligned} \tag{2.117}$$

where we introduced a new average velocity and a new spin current

$$\overline{\boldsymbol{u}}=\boldsymbol{u}-\frac{\mu_{\mathrm{B}}}{2mc^2n}\boldsymbol{E}\times\boldsymbol{S},\quad\overline{J}^S_{ij}=J^S_{ij}+\frac{\mu_{\mathrm{B}}}{2mc^2}\epsilon_{ijk}E_kn. \tag{2.118}$$

The above corrections reflect the modification of the velocity due to the spin-orbit coupling. Indeed the average velocity can be immediately obtained from the velocity phase-space function, Eq. (2.57), yielding

$$\overline{\boldsymbol{u}}=\frac{1}{nm}Tr\left[\int\boldsymbol{V}(\boldsymbol{r},\boldsymbol{\pi})\mathcal{F}d\boldsymbol{\pi}\right]=\boldsymbol{u}-\frac{\mu_{\mathrm{B}}}{2mc^2n}\boldsymbol{E}\times\boldsymbol{S}, \tag{2.119}$$

where $\mathcal{F}$ is the 2×2 distribution function defined in Eq. (2.8). The same holds for the spin current operator, which is defined as follows:

$$\widehat{J}^S_{ij}=\frac{\hbar}{2}\widehat{v}_i\sigma_j=\frac{\hbar}{2}\frac{\widehat{\Pi}_i}{m}\sigma_j-\frac{\hbar\mu_{\mathrm{B}}}{8mc^2}\left[\left(\widehat{\boldsymbol{E}}\times\boldsymbol{\sigma}\right)_i\sigma_j+\sigma_j\left(\widehat{\boldsymbol{E}}\times\boldsymbol{\sigma}\right)_i\right], \tag{2.120}$$

where we symmetrized the operator so that it is Hermitian. Then the associated phase-space function

$$J^S_{ij}\left(\boldsymbol{r},\boldsymbol{\pi}\right)=\frac{\hbar}{2}\frac{\pi_i}{m}\sigma_j-\frac{\hbar\mu_{\mathrm{B}}}{8mc^2}\left[\left(\boldsymbol{E}\times\boldsymbol{\sigma}\right)_i\sigma_j+\sigma_j\left(\boldsymbol{E}\times\boldsymbol{\sigma}\right)_i\right] \tag{2.121}$$

can be used to determine the spin current

$$\overline{J}^S_{ij} = \frac{1}{m} Tr\left[\int J^s_{ij}(\boldsymbol{r},\boldsymbol{\pi})\mathcal{F}d\boldsymbol{\pi}\right] = J^S_{ij} + \frac{\mu_{\mathrm{B}}}{2mc^2}\epsilon_{ijk}E_k n. \tag{2.122}$$

As is always the case for hydrodynamic models, some further hypotheses are needed to close the above set of equations (2.113)-(2.117). Unfortunately the MEP does not provide any conclusive analytical results when one adds the spin-orbit interaction. The difficulty arises from the fact that the spin-orbit interaction couples all the components of the velocity. However an intuitive closure can be found by inspecting the evolution equation (2.117) for the pressure tensor. There, most spin-dependent terms cancel if we set

$$J^S_{i\alpha} = u_i S_\alpha \quad \text{and} \quad \Pi^S_{ij\alpha} = u_i J^S_{j\alpha}. \tag{2.123}$$

The physical interpretation of the above equations is that the spin of a particle is simply transported along the mean fluid velocity. This is the same kind of approximation as used in the Sec. 2.3.3, which neglects spin-velocity correlations. With this assumption, Eq. (2.116) and the definition of the spin-pressure $\Pi_{ij\alpha}$ are no longer necessary. The system of fluid equations simplifies to

$$\frac{\partial n}{\partial t} + \boldsymbol{\nabla}\cdot(n\overline{\boldsymbol{u}}) = 0, \tag{2.124}$$

$$\frac{\partial S_\alpha}{\partial t} + \partial_i\left(u_i S_\alpha\right) - \frac{\mu_{\mathrm{B}}}{2mc^2}\left(\boldsymbol{\nabla}\times n\boldsymbol{E}\right)_\alpha + \frac{e}{m}\left[\boldsymbol{S}\times\left(\boldsymbol{B} - \frac{1}{2c^2}\boldsymbol{u}\times\boldsymbol{E}\right)\right]_\alpha = 0, \tag{2.125}$$

$$\frac{\partial u_i}{\partial t} + u_j(\partial_j u_i) + \frac{1}{nm}\partial_j P_{ij} + \frac{e}{m}\left[E_i + (\overline{\boldsymbol{u}}\times\boldsymbol{B})_i\right] + \frac{e}{nm^2}S_\alpha\left(\partial_i B_\alpha\right) + \frac{\mu_{\mathrm{B}}}{2mc^2 n}\epsilon_{jkl}\left[E_j\left(\partial_k u_i\right) - u_k\left(\partial_i E_j\right)\right]S_l = 0, \tag{2.126}$$

$$\frac{\partial P_{ij}}{\partial t} + u_k\partial_k P_{ij} + P_{jk}\partial_k u_i + P_{ik}\partial_k u_j + P_{ij}\partial_k u_k + \partial_k Q_{ijk} + \frac{e}{m}\left[\epsilon_{kli}P_{jk} + \epsilon_{klj}P_{ik}\right]B_l = 0. \tag{2.127}$$

Then by supposing that the system is isotropic and adiabatic, i.e. $P_{ij} = n^{\frac{D+2}{D}}\delta_{ij}$ (where D is the dimensionality of the system) and $Q_{ijk} = 0$, one is able to close the system of fluid equation. In summary, Eqs. (2.124)-(2.126), together with an adapted expression of the pressure, constitute a closed system of hydrodynamic equations including spin-orbit effects.

2.4 Conclusions and perspectives

In this chapter we developed new phase-space models to study the spin and charge dynamics for an ensemble of interacting electrons. Phase-space methods can be applied in nanophysics to model the quantum or the classical dynamics of electrons.

Spinless studies have been done in the past to study the electron dynamics in metallic nano-structures [32, 89, 96] both with the Wigner and the Vlasov equations. Here we addressed the situation, where the spin of the electrons cannot be neglected. We focused particularly one two spin effects, the Zeeman interaction and the spin-orbit coupling which are of most importance in many areas of physics. For instance in ultrafast spectroscopy the electron spin is strongly involved in the dynamics of the system, as it interacts with the incident laser field and with the self-consistent field generated by the electrons themselves. The methodology used to derive the different models can be easily generalized to describe other relativistic effects such as the Darwin term or the relativistic mass correction.
We first derived a four-component Wigner equation to describe the quantum dynamics of a system of spin-1/2 fermions including the Zeeman and the spin-orbit interaction. These equations coupled with the appropriate Maxwell equations form a self-consistent model to study the spin and the charge dynamics in the mean-field approximation. Exchange and correlation effects can be easily add to our model, as they can be expressed, by means of some approximations, as an electric potential and a magnetic field. Further, this model should not be limited to the linear response, as nonlinear effects are often important, especially for large incident laser powers. From a semiclassical expansion at the order one in $\hbar$, we obtained a four-component Vlasov equation. The orbital part of the motion is classical, i.e. the particles follow classical phase-space trajectories. Whereas the spin degree of freedom is treated in a fully quantum fashion (two dimensional Hilbert space). On the numerical point of view, these spin-Vlasov equations are more tractable than the Wigner equations. Namely because they are local in phase space in contrast to the Wigner equations which are typically non local. They constitute a relatively good approximation of the quantum version when the characteristic lengths are much larger than the de Broglie wavelength.
The corresponding hydrodynamic equations were derived by taking velocity moments of the phase-space distribution functions. The spin-orbit interaction introduce some considerable changes in the hydrodynamic equation, we have namely seen that the charge and the spin current are modified in the presence of the spin-orbit coupling. As always the hydrodynamic equations need to be closed on the basis of some physical hypothesis. A set of closed hydrodynamic equations with spin effects is proposed and can be used for applications. For instance to study the electron dynamics in metallic nanoparticles excited with intense laser pulses, where spin and charge effects are closely intertwined.

All the phase-space methods were developed to study coherent effects and are valid to describe the early stages of the electronic dynamics. As it was demonstrated in the Sec. 2.2.5, the resulting equations conserve several physical quantities as the mass, the impulsion, the total angular momentum and the energy. However for

longer time scales the electrodynamic dynamics start to be dissipative namely because phenomena such as spin flips, electron-electron collisions or electron-phonon scattering take place. The latter are not included in our models. The modelling of dissipation in quantum mechanic is rather difficult and there is not yet a general consensus on how to deal with many body dissipative quantum systems. In the recent years some author [30, 89] proposed methods based on the Boltzman equation to include such dissipation effects. The latter study has been done for spinless electrons. Those approaches could be used to add dissipation effects in our spin-Wigner or spin-Vlasov equations.

All the fluid models developed in this chapter were constructed from the spin-Vlasov equations. Therefore only the first order quantum effects (proportional to $\hbar$) are taken into account. The latter couple the spin dynamics to the orbital dynamics. As it is explained in section 1.4, quantum effects on the orbital dynamics appear only at the second order in $\hbar$ in the semiclassical developments. The consequences of such quantum effects is the presence of the quantum Bohm potential in the Euler equation (1.58). Therefore, a simple way to include quantum effects in the above fluid models would be to add the Bohm potential in the spin-fluid models. However this procedure is not consistent, one of the correct way to derive quantum fluid models with spin effects is to start from the spin-Wigner equations and then use the MEP to close the set of hydrodynamic equations. An extension of this work should use this procedure to construct quantum fluid models with spin effects. However this issue is complex and even the definition of the entropy from the Wigner function (2.82) should be modified in the quantum case [125]. Some complex developments on quantum fluids models using the MEP can be found in Ref. [126] in the case of spinless particles. Alternative methods using the Madelung transformation, generalized to spinors, were also developed to construct quantum fluid models with spin effects [127, 128]. The resulting fluid equations exhibit the complexity of the problem. Namely new terms with a purely quantum origin and that couple the spin to the charge dynamics appear.

Chapter 3

Spin effects on the plasmon oscillations - Linear response

This chapter is devoted to the linear analysis of the spin-Vlasov model. This method is used to study the propagation of a small perturbation around the equilibrium state, i.e. $f_0 = f_0^{(0)} + \delta f_0$ and $f_i = f_i^{(0)} + \delta f_i$, where the perturbed distribution functions δf_0 and δf_i are supposed to be small compare to the equilibrium distribution functions $f_0^{(0)}$ and $f_i^{(0)}$. We consider that the perturbation is applied at $t = 0$ and is periodic in space:

$$\delta f_\mu = \delta_\mu \cos(\boldsymbol{k} \cdot \boldsymbol{r}). \tag{3.1}$$

Here the index $\mu = \{0, x, y, z\}$ corresponds to the different distribution functions. The above perturbation represents a periodic fluctuation, with a wave vector $\boldsymbol{k}$, of the electron density and magnetization. In that case the linear response is characterized by the dielectric function $\epsilon(\omega, \boldsymbol{k})$ [129]. The zeros of this function correspond to the different eigenmodes of the system. Moreover the excitation amplitudes of each mode depends on the initial perturbation.
The spinless linear response, corresponding to the Vlasov-Poisson equation (1.36), has been discovered long-time ago [130]. The principal oscillation mode is the plasmon, the latter oscillates at the plasma frequency $\omega_p = e^2 n_0 / m\epsilon_0$. Physically, the plasma frequency corresponds to a collective oscillation of the electrons immersed in a neutralizing background of positive ions, which are supposed to be fixed because of the huge difference of mass between the electrons and the ions. The plasmon oscillations originate from a displacement of the electron gas that creates a net Coulomb force between ions and electrons. Then the electrons are pulled back inside the system but due to their inertia, they will travel further away, thus recreating a new Coulomb force in the opposite direction. After few cycles, the plasma oscillations are usually damped through the well known Landau damping [131] process. The latter is not a dissipative process, in the sense that the total energy of the system is conserved, but is rather due to self-consistent effects. Plasmons were observed in several systems, for instance in gold nano-particles [132]. An illustration of plasmon oscillations is given in Fig. 3.1.

The principal aim of this chapter is to answer the following question : Is there a

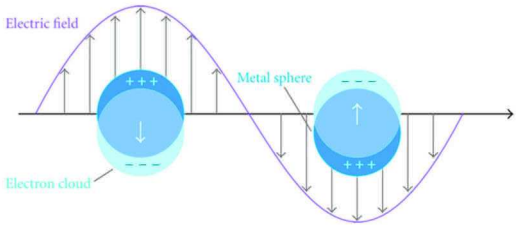

FIGURE 3.1: From [133], illustration of a surface plasmon resonance resulting from the collective oscillations of delocalized electrons in response to an external electric field.

visible trace of the spin polarization on the plasma frequency?
To answer that question, we shall derive the dielectric function of the spin-Vlasov model and then find the associated dispersion relation. In general, this is a complicated task to solve. Here, we simplify the problem by considering that the equilibrium ground state is homogeneous and isotropic leading to an electronic and ionic spin dynamics that is along the z direction (collinear approximation). Therefore the equilibrium distribution functions read:

$$f_0^{(0)} = f_0^{(0)}(|\boldsymbol{v}|) = \mathcal{G}\left(m\boldsymbol{v}^2/2 + \mu_B B\right) + \mathcal{G}\left(T, m\boldsymbol{v}^2/2 - \mu_B B\right),$$
$$f_z^{(0)} = f_z^{(0)}(|\boldsymbol{v}|) = \mathcal{G}\left(m\boldsymbol{v}^2/2 + \mu_B B\right) - \mathcal{G}\left(T, m\boldsymbol{v}^2/2 - \mu_B B\right).$$

where $\mathcal{G}$ is either a Maxwell-Boltzmann or a Fermi-Dirac function. The magnetic field $B \equiv B_z$ is a homogeneous magnetic field in the z direction that allows us to have a spin polarized ground state. The distribution functions verify also the following properties : $\int f_0 d\boldsymbol{v} = n_0$ and $\int f_z d\boldsymbol{v} = m_0$, where n_0 and m_0 are, respectively, the equilibrium density and magnetization.
The initial perturbation (3.1) is chosen in order to excite an electrostatic mode, in that case we must have $\delta_0 = \delta_z$[1]. Moreover we also consider that the magnetic field has no effect on the orbital electronic dynamics. In other words, it means that there is no magnetic Lorentz force in the Vlasov equation. In this case the electrostatic waves created in the electron gas must be purely longitudinal, i.e. along the direction of the wave vector $\boldsymbol{k}$. Here we choose the x direction for the wave vector: $\boldsymbol{k} = k\boldsymbol{u_x}$. Therefore the electric field, created by the initial perturbation (3.1), writes:

$$\boldsymbol{E} = -\boldsymbol{\nabla}\phi(x) = -\partial_x\phi(x)\boldsymbol{u_x} = E(x)\boldsymbol{u_x} \tag{3.2}$$

and all the physical quantities shall only depend on the position variable x, in particular the distribution functions. This situation is sketched in the Fig. 3.2 , where we represent a longitudinal electrostatic wave that propagates in a spin polarized electron gas. The spin is polarized in the z direction and the electrostatic wave oscillates in the x direction with a wave vector k. We represent also the electron and the

[1]We could also excite a magnetic mode, in this case we have $\delta_0 = -\delta_z$. This case corresponds to the situation where the spin up and down are excited in an opposite way.

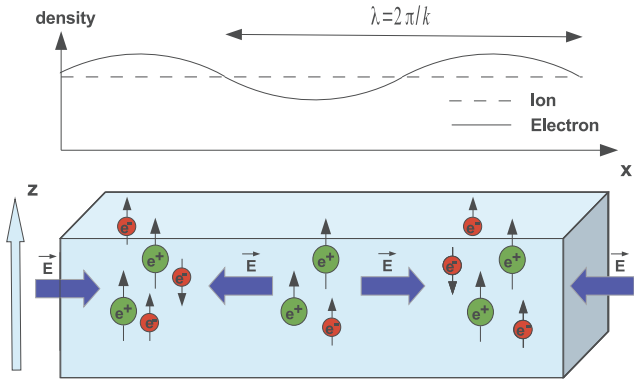

FIGURE 3.2: Picture of a longitudinal electrostatic wave in the x direction and the associated electron and ion densities. The spins are polarized in the z direction.

ion densities associated to this longitudinal electrostatic wave. Using the approximations mentioned above, the spin-Vlasov model (2.54) - (2.55) reads:

$$\frac{\partial f_0}{\partial t} + v\,\partial_x f_0 - \frac{1}{m}\partial_x\left(-e\phi + V_{XC}\right)\partial_v f_0 - \frac{\mu_B}{m}\partial_x\left(B_{XC} + B_z\right)\partial_v f_z = 0, \tag{3.3}$$

$$\frac{\partial f_z}{\partial t} + v\,\partial_x f_z - \frac{1}{m}\partial_x\left(-e\phi + V_{XC}\right)\partial_v f_z - \frac{\mu_B}{m}\partial_x\left(B_{XC} + B_z\right)\partial_v f_0 = 0, \tag{3.4}$$

$$\frac{\partial^2\phi}{\partial x^2} = \frac{e}{\epsilon_0}\left(\int f_0 dv - n_0\right), \qquad \frac{\partial B_z}{\partial x} = -\mu_B\mu_0\frac{\partial}{\partial x}\left(\int f_z dv\right), \tag{3.5}$$

where the velocity variable $v \equiv v_x$ stands for the x-component of the velocity vector. We use the tools of the Fourier-Laplace transforms to determine the linear response of the above spin-Vlasov model (3.3)-(3.5). Such methods are well adapted for homogeneous systems and were successfully used to determine the collective response for systems described by the Vlasov-Poisson model [134]. In the first section, we apply the Fourier Laplace method to determine the linear response of the spin-Vlasov model (3.3)-(3.5). The second and third sections concern the use of the linear response associated to different ground state distribution functions (Maxwell-Boltzmann and Fermi-Dirac).

3.1 General theory about the linear analysis of the spin-Vlasov model

In order to perform a linear analysis, we study the propagation of a weak perturbation around the equilibrium configuration

$$f_0(x,v,t) = f_0^{(0)}(v^2) + \delta f_0(x,v,t) \quad \text{and} \quad f_z(x,v,t) = f_z^{(0)}(v^2) + \delta f_z(x,v,t). \tag{3.6}$$

Then using the spin-Vlasov model (3.3)-(3.5) and the previous expressions (3.6), one obtains the following equations:

$$\frac{\partial \delta f_0}{\partial t} + v\,\partial_x \delta f_0 - \frac{1}{m}\partial_x\left(-e\delta\phi + \delta V_{XC}\right)\,\partial_v f_0^{(0)} - \frac{\mu_B}{m}\partial_x\left(\delta B_{XC} + \delta B_z\right)\partial_v f_z^{(0)} = 0, \quad (3.7)$$

$$\frac{\partial \delta f_z}{\partial t} + v\,\partial_x \delta f_z - \frac{1}{m}\partial_x\left(-e\delta\phi + \delta V_{XC}\right)\,\partial_v f_z^{(0)} - \frac{\mu_B}{m}\partial_x\left(\delta B_{XC} + \delta B_z\right)\partial_v f_0^{(0)} = 0, \quad (3.8)$$

$$\frac{\partial^2 \delta\phi}{\partial x^2} = \frac{e}{\epsilon_0}\int \delta f_0 dv, \qquad \frac{\partial B_z}{\partial x} = -\mu_B\mu_0\frac{\partial}{\partial x}\int \delta f_z dv, \quad (3.9)$$

where all the second order terms have been suppressed and where the exchange-correlation potentials have been developed as follows:

$$V_{XC} = V_{XC}^{(0)} + \partial_n V_{XC}(n_0, m_0)\int \delta f_0 dv + \partial_m V_{XC}(n_0, m_0)\int \delta f_z dv = V_{XC}^{(0)} + \delta V_{XC}, \quad (3.10)$$

$$B_{XC} = B_{XC}^{(0)} + \partial_n B_{XC}(n_0, m_0)\int \delta f_0 dv + \partial_m B_{XC}(n_0, m_0)\int \delta f_z dv = B_{XC}^{(0)} + \delta B_{XC}. \quad (3.11)$$

We use the Fourier-Laplace transformations to solve the linearized spin-Vlasov model. The Fourier transform and its inverse are defined as follows:

$$\mathcal{F}\left(A\left(x,t\right)\right) = \overline{A}(k,t) = \frac{1}{2\pi}\int_{-\infty}^{\infty}\exp\left(-ikx\right)A\left(x,t\right)dx, \quad (3.12)$$

$$\mathcal{F}^{-1}\left(\overline{A}\left(k,t\right)\right) = A(x,t) = \int_{-\infty}^{\infty}\exp\left(ikx\right)\overline{A}\left(k,t\right)dk. \quad (3.13)$$

Similarly, the Laplace transform and its inverse are defined as follows:

$$\mathcal{L}\left(\overline{A}\left(k,t\right)\right) = \tilde{A}(k,p) = \int_{0}^{\infty}\exp\left(-pt\right)\overline{A}\left(k,t\right)dt, \quad (3.14)$$

$$\mathcal{L}^{-1}\left(\tilde{A}(k,p)\right) = \overline{A}\left(k,t\right) = \frac{1}{2\pi i}\int_{p_0-i\infty}^{p_0+i\infty}\exp\left(pt\right)\tilde{A}\left(k,t\right)dp. \quad (3.15)$$

We remind that the Laplace transform is only valid in the upper complex plane bounded by the following relation : $\Re(p) > p_0$, where p_0 is chosen such that $\exp\left(-p_0 t\right)\overline{A}\left(k,t\right) \to 0$ when $t \to \infty$.
After some straightforward algebra, one obtains the following set of equations for

the Fourier-Laplace components of the perturbed self-consistent fields:

$$-e\tilde{\delta\phi}+\delta\tilde{V_{XC}}=\frac{1}{\epsilon\left(p,k\right)}\Bigg\{\left(\frac{e^2}{\epsilon_0k^2}+\partial_nV_{XC}\right)J_0+\partial_mV_{XC}\,J_z \\ +\frac{\mu_{\mathrm{B}}k}{m}\left[\left(\frac{e^2}{\epsilon_0k^2}+\partial_nV_{XC}\right)\left(\partial_mB_{XC}-\mu_{\mathrm{B}}\mu_0\right)-\partial_mV_{XC}\,\partial_nB_{XC}\right]\left(J_0I_0-J_zI_z\right)\Bigg\}, \tag{3.16}$$

$$\delta\tilde{B}_z+\delta\tilde{B_{XC}}=\frac{1}{\epsilon\left(p,k\right)}\Bigg\{\partial_nB_{XC}\,J_0+\left(\partial_mB_{XC}-\mu_{\mathrm{B}}\mu_0\right)J_z \\ +\frac{\mu_{\mathrm{B}}k}{m}\left[\left(\frac{e^2}{\epsilon_0k^2}+\partial_nV_{XC}\right)\left(\partial_mB_{XC}-\mu_{\mathrm{B}}\mu_0\right)-\partial_mV_{XC}\,\partial_nB_{XC}\right]\left(J_zI_0-J_0I_z\right)\Bigg\}, \tag{3.17}$$

where, the integral quantities J_0, J_z, I_0 and I_z are defined as follows:

$$J_{0,z}=\int\frac{\overline{\delta f_{0,z}}(t=0)}{p+ikv}dv\quad\text{and}\quad I_{0,z}=-i\int\frac{\partial_vf_{0,z}^{(0)}}{p+ikv}dv. \tag{3.18}$$

The quantity $\overline{\delta f_{0,z}}(t=0)$ represents the Fourier transform of the initial perturbation (3.1) that is applied at $t=0$. The quantity $\epsilon\left(p,k\right)$ is the so-called dielectric function of the system

$$\epsilon\left(p,k\right)=1+\frac{\omega_p^2}{kn_0}\mathcal{I}_0-\frac{k\mu_{\mathrm{B}}^2\mu_0}{m}\mathcal{I}_0+\frac{k}{m}\left[\left(\partial_nV_{XC}+\mu_{\mathrm{B}}\partial_mB_{XC}\right)\mathcal{I}_0+\left(\partial_mV_{XC}+\mu_{\mathrm{B}}\partial_nB_{XC}\right)\mathcal{I}_z\right] \\ +\frac{\mu_{\mathrm{B}}k^2}{m^2}\left[\left(\partial_nV_{XC}\right)\left(\partial_mB_{XC}\right)-\left(\partial_nB_{XC}\right)\left(\partial_mV_{XC}\right)\right]\left[\mathcal{I}_0^2-\mathcal{I}_z^2\right] \\ +\left[-\frac{\omega_p^2\mu_{\mathrm{B}}^2\mu_0}{n_0m}+\frac{\mu_{\mathrm{B}}\omega_p^2}{n_0m}\partial_mB_{XC}-\frac{k^2\mu_{\mathrm{B}}^2\mu_0}{m^2}\partial_nV_{XC}\right]\left(\mathcal{I}_0^2-\mathcal{I}_z^2\right). \tag{3.19}$$

The integral quantities I_0, I_z depend only on the ground state properties, whereas the integral quantities J_0, J_z depend on the initial perturbation.
The dielectric function is an important object in linear analysis, since its zeros give the linear excitation modes of the system. It can be divided in two parts, the first part is linear in $\mathcal{I}_0$ or $\mathcal{I}_z$ and the second part is quadratic in those quantities. Each term in Eq. (3.19) corresponds to a special kind of interaction or to a mixing between two different interactions. All the terms that contained the plasma frequency ω_p are related to electrostatic interactions (Poisson equation), the terms proportional to μ_0 are related to magnetostatic interactions (Ampère equation) and the terms that depend on V_{XC} or B_{XC} are related to exchange-correlation interactions.
Usually the dielectric function has several zeros, each of them corresponds to a different mode of oscillations. Moreover the zeros are complex numbers with a real part and an imaginary part that correspond, respectively, to the oscillation frequency

and the damping or the expansion of the modes. The dielectric function, Eq. (3.19), depends only on the initial equilibrium state, through the quantities I_0 and I_z. However, as we shall see below, each mode is weighted by a factor that depends on the initial perturbation.
Let us perform an inverse Laplace transform on the expressions (3.16) - (3.17), in order to find the temporal profile of the Fourrier components of the self-consistent potentials. Using Eq. (3.15), one obtains:

$$-e\overline{\delta\phi} + \overline{\delta V_{XC}} = \int_{p_0-i\infty}^{p_0+i\infty} \left[-e\tilde{\delta\phi} + \delta\tilde{V}_{XC}\right] \exp(pt)\, dp, \tag{3.20}$$

$$-e\overline{\delta B_z} + \overline{\delta B_{XC}} = \int_{p_0-i\infty}^{p_0+i\infty} \left[-e\tilde{\delta B}_z + \delta\tilde{B}_{XC}\right] \exp(pt)\, dp. \tag{3.21}$$

The expressions above contain some integrals of the following type:

$$\overline{\chi}(k,t) = \int_{p_0-i\infty}^{p_0+i\infty} \tilde{\chi}(p,k) \exp(pt)\, dp = \int_{p_0-i\infty}^{p_0+i\infty} \left[\frac{\exp(pt)}{\epsilon(p,k)} \int_{-\infty}^{\infty} \frac{g(v)}{p+ikv} dv\right] dp. \tag{3.22}$$

To calculate the integral over the variable p, we shall deform the integration path from $p_0 - i\infty ... p_0 + i\infty$ to $-\infty - i\infty ... -\infty + i\infty$, in such a way that the factor $\exp(pt)$ makes the integrand vanishing, see Fig. 3.3 (a and b). However the function $\tilde{\chi}(p,k)$ is not an holomorphic function, it has some poles at points p_j where the dielectric function cancels: $\epsilon(p_j,k) = 0$. Therefore one has to circumvent those poles when we deform the integration path. This is sketched in Fig. 3.3, where we draw the initial integration path on the left part (a) and the new integration path on the right part (b). Then using the residue theorem, one obtains:

$$\begin{aligned}\overline{\chi}(k,t) &= \int_{\infty-i\infty}^{\infty+i\infty} \left[\frac{\exp(pt)}{\epsilon(p,k)} \int_{-\infty}^{\infty} \frac{g(v)}{p+ikv} dv\right] dp + \sum_j Res_{p=p_j}\left(\tilde{\chi}(p,k)\right) \exp(p_j t), \\ &= \sum_j Res_{p=p_j}\left(\tilde{\chi}(p,k)\right) \exp(p_j t).\end{aligned} \tag{3.23}$$

where p_j are the zeros of the dielectric function and $Res_{p=p_j}\left(\tilde{\chi}(p,k)\right)$ are the residues of $\tilde{\chi}(p,k)$ in its poles.
However, one should be careful when we carry out this deformation. Indeed, the function $\tilde{\chi}(p,k)$ contains some integrals over the velocity space of the following type (see Eq. (3.22)):

$$\mathcal{I}(p,k) = \int_{-\infty}^{\infty} \frac{g(v)}{v - ip/k} dv. \tag{3.24}$$

The latter are always well defined once one integrates over the initial path because in this case $\Re(p) = p_0$ and the poles of the integrand are above the real axis of v.

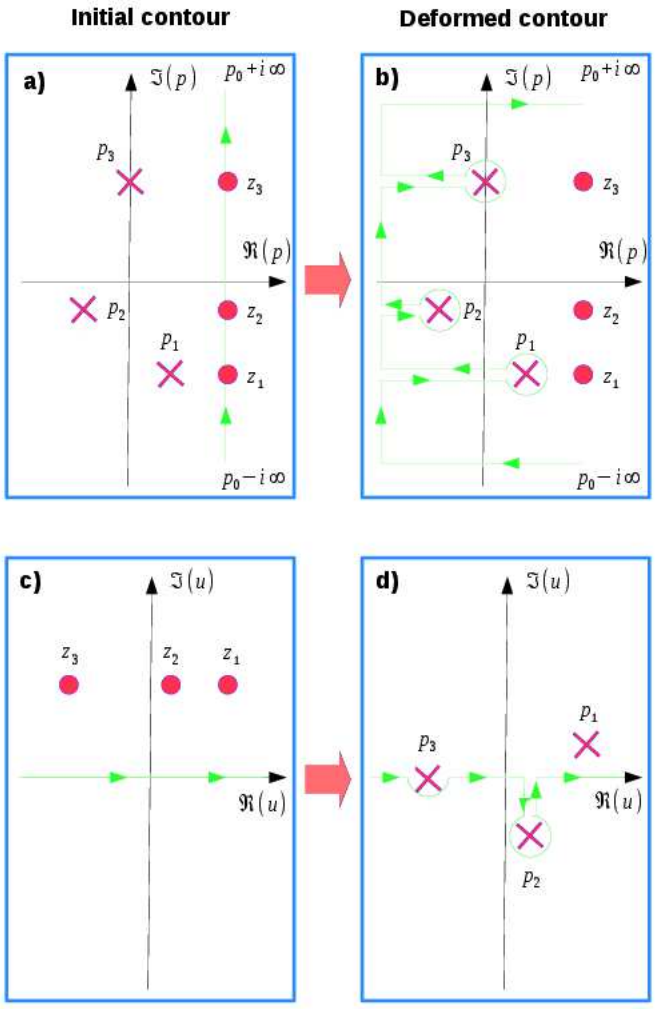

FIGURE 3.3: (a), initial integration path (green line) in the p-plane. The red cross are the zeros of the dielectric function and the red dots are some complex numbers (z_1, z_2, z_3). (b), integration path in the p-plane after the deformation. (c), initial integration path in the v-plane. (d), integration path in the v-plane after having applied the Landau prescription.

However, since we deform the integration path in the p-plane, a singularity will appear in the integrand of Eq. (3.24) each time that we cross the imaginary axis. In the literature [99, 134], this problem is solved by using a method developped by Landau. The latter consists to deform the integration path in the v-plane by by-passing the poles from below when they cross the real axis. This situation is sketched on the Fig. 3.3 (c and d). The Landau prescription ensures the analytical prolongation of

the integral (3.24) in the lower part of the complex plane. It is defined as follows:

$$\mathcal{I}(p,k)=\int_{\mathcal{L}}\frac{g(v)}{v-ip/k}dv=\begin{cases}\displaystyle\int_{-\infty}^{\infty}\frac{g(v)}{v-ip/k}dv, & \text{if } \Re\left(p\right)>0\\ \\ \mathcal{V}_P\displaystyle\int_{-\infty}^{\infty}\frac{g(v)}{v-ip/k}dv+\pi ig(ip/k), & \text{if } \Re\left(p\right)=0\\ \\ \displaystyle\int_{-\infty}^{\infty}\frac{g(v)}{v-ip/k}dv+2\pi ig(ip/k), & \text{if } \Re\left(p\right)<0\end{cases} \tag{3.25}$$

where $\mathcal{V}_P$ denotes the Cauchy principal value and $\int_{\mathcal{L}}$ the Landau contour, see Fig. 3.3 (d). It is more convenient to work with the complex variable $\omega=ip$ instead of p. In this case, Eq. (3.23) becomes:

$$\overline{\chi}\left(k,t\right)=\sum_j Res_{\omega=\omega_j}\left(\tilde{\chi}(\omega,k)\right)\exp(-i\omega_j t) \tag{3.26}$$

and one obtains the following expression for the integral (3.25)

$$\mathcal{I}(\omega,k)=\int_{\mathcal{L}}\frac{g(v)}{v-\omega/k}dv=\begin{cases}\displaystyle\int_{-\infty}^{\infty}\frac{g(v)}{v-\omega/k}dv, & \text{if } \Im\left(\omega\right)>0\\ \\ \mathcal{V}_P\displaystyle\int_{-\infty}^{\infty}\frac{g(v)}{v-\omega/k}dv+\pi ig(\omega/k), & \text{if } \Im\left(\omega\right)=0\\ \\ \displaystyle\int_{-\infty}^{\infty}\frac{g(v)}{v-\omega/k}dv+2\pi ig(\omega/k), & \text{if } \Im\left(\omega\right)<0\end{cases} \tag{3.27}$$

According to the expression (3.26), the zeros of the dielectric function ($\{\omega_j\}$) govern the linear response of the system. In particular, one notices that if $\Im(w)>0$, than the modes are unstable (they grow exponentially) whereas if $\Im(w)<0$ the modes are stable (they are exponentially damped).
The above reasoning is only valid if $g(v)$ is a entire function of the complex variable v. We shall see in the next section that it is not always the case, specially if one considers Fermi-Dirac equilibrium distribution functions.
In all the cases that we shall study $\tilde{\chi}(\omega,k)$ can always be written as follows:

$$\tilde{\chi}(\omega,k)=\frac{N\left(\omega,k\right)}{\epsilon\left(\omega,k\right)}. \tag{3.28}$$

Then, one can perform a Taylor development of the denominator around the zeros of the dielectric function:

$$\epsilon\left(\omega,k\right)=\epsilon\left(\omega_j,k\right)+\left(\omega-\omega_j\right)\left(\frac{\partial\epsilon\left(\omega,k\right)}{\partial\omega}\right)_{\omega=\omega_j}+\mathcal{O}\left(\left(\omega-\omega_j\right)^2\right), \tag{3.29}$$

where the zero order terms cancel by definition of ω_j. Then if one supposes that all the zeros of the dielectric function have a multiplicity of one, then the following relation holds:

$$\begin{aligned}\overline{\chi}\left(k,t\right)&=\sum_j Res_{\omega=\omega_j}\left(\tilde{\chi}(\omega,k)\right)\exp(-i\omega_j t) \quad=\sum_j\lim_{\omega\to\omega_j}\left[\left(\omega-\omega_j\right)\frac{N\left(\omega,k\right)}{\epsilon\left(\omega,k\right)}\right]\exp(-i\omega_j t),\\&=\sum_j\left[\frac{N\left(\omega,k\right)}{\frac{\partial\epsilon(\omega,k)}{\partial\omega}}\right]_{\omega=\omega_j}\exp(-i\omega_j t).\end{aligned} \tag{3.30}$$

The physical quantities capable to be compared with the simulations are the Fourier transform of the self-consistent fields. The latter can be written as follows:

$$e\overline{E}+\nabla\overline{V_{XC}}=ik\left(-e\overline{\delta\phi}+\overline{\delta V_{XC}}\right)=\sum_j\left[\frac{N_1\left(\omega,k\right)}{\frac{\partial\epsilon(\omega,k)}{\partial\omega}}\right]_{\omega=\omega_j}\exp(-i\omega_j t), \tag{3.31}$$

$$\nabla\overline{B_z}+\nabla\overline{B_{XC}}=ik\left(\overline{B_z}+\overline{\delta B_{XC}}\right)=\sum_j\left[\frac{N_2\left(\omega,k\right)}{\frac{\partial\epsilon(\omega,k)}{\partial\omega}}\right]_{\omega=\omega_j}\exp(-i\omega_j t), \tag{3.32}$$

where, using Eqs. (3.16) and (3.17), the functions N_1 and N_2 are defined as follows:

$$\begin{aligned}N_1\left(\omega,k\right)=&\left(\frac{e^2}{\epsilon_0k^2}+\partial_nV_{XC}\right)ikJ_0+\partial_mV_{XC}\,ikJ_z\\&+\frac{\mu_{\mathrm{B}}k}{m}\left[\left(\frac{e^2}{\epsilon_0k^2}+\partial_nV_{XC}\right)\left(\partial_mB_{XC}-\mu_{\mathrm{B}}\mu_0\right)-\partial_mV_{XC}\,\partial_nB_{XC}\right]ik\left(J_0I_0-J_zI_z\right),\end{aligned} \tag{3.33}$$

$$\begin{aligned}N_2\left(\omega,k\right)=&\frac{1}{\epsilon\left(p,k\right)}\partial_nB_{XC}\,ikJ_0+\left(\partial_mB_{XC}-\mu_{\mathrm{B}}\mu_0\right)ikJ_z\\&+\frac{\mu_{\mathrm{B}}k}{m}\left[\left(\frac{e^2}{\epsilon_0k^2}+\partial_nV_{XC}\right)\left(\partial_mB_{XC}-\mu_{\mathrm{B}}\mu_0\right)-\partial_mV_{XC}\,\partial_nB_{XC}\right]ik\left(J_zI_0-J_0I_z\right).\end{aligned} \tag{3.34}$$

According to the Eqs. (3.31) and (3.32), the functions N_1 and N_2 are weighting the different modes of the system. They depend not only on the ground state properties but also on the form of the initial excitation through the integrals J_0 and J_z. The expressions (3.31)-(3.34) constitute a general result of the spin-Vlasov's linear theory. To go further, one has to specify the ground state distribution functions. This issue will be treated in the two next sections.

3.2 The dispersion relation with a Fermi-Dirac ground state

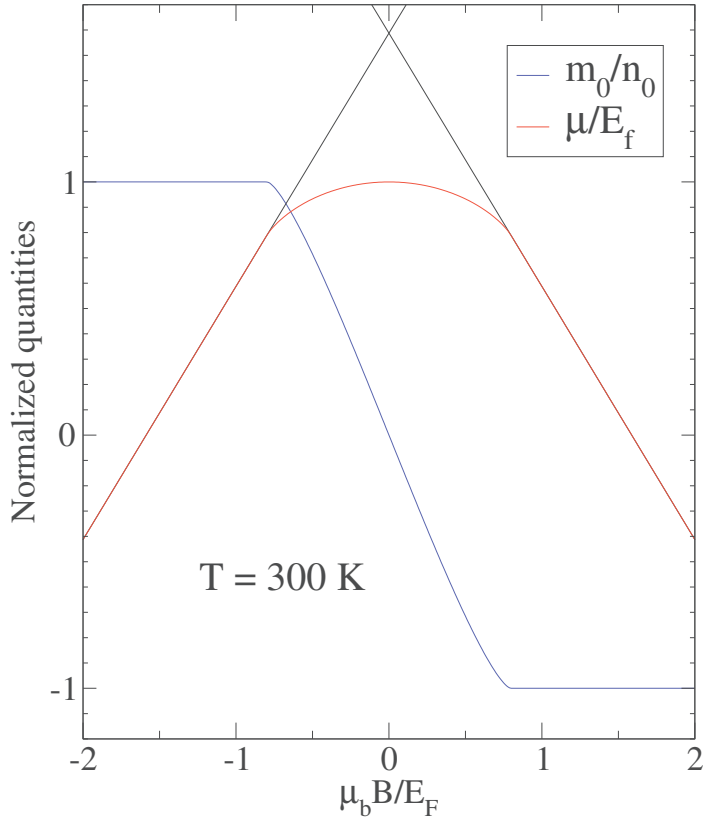

FIGURE 3.4: Chemical potential (red line) and electron magnetization (blue line) as a function of the external magnetic field in the case of a Fermi-Dirac equilibrium state. These calculations were performed with a density $n_0 = 5.9 \times 10^{28}\,\mathrm{m}^{-3}$ (Gold) and for a temperature of $300\,\mathrm{K}$. The dashed lines represent analytical solutions for $\mu < |\mu_B B|$.

The dispersion relation $\omega(k)$ is obtained by finding the roots of the dielectric function $\epsilon(\omega, k)$, see Eq. (3.19). As it was mentioned previously, the dielectric function depends on the equilibrium state trough the integral terms $\mathcal{I}_0$ or $\mathcal{I}_z$. Therefore we have to specify the equilibrium distribution functions $f_0^{(0)}$ and $f_z^{(0)}$. In the case of metallic electrons, the spin up and spin down electrons follow a Fermi-Dirac distribution[2]

$$f^{\uparrow(0)}(v) = \frac{2\pi k_b T}{m}\left(\frac{m}{2\pi\hbar}\right)^3 \ln\left[1+\exp\left(-\frac{1}{k_b T}\left(\frac{m}{2}v^2+\mu_B B-\mu\right)\right)\right], \tag{3.35}$$

$$f^{\downarrow(0)}(v) = \frac{2\pi k_b T}{m}\left(\frac{m}{2\pi\hbar}\right)^3 \ln\left[1+\exp\left(-\frac{1}{k_b T}\left(\frac{m}{2}v^2-\mu_B B+\mu\right)\right)\right], \tag{3.36}$$

[2]Here it is the Fermi-Dirac in one dimension obtained after integrating the three dimensional Fermi-Dirac function over the transversal velocities (v_y, v_z) : $f^{1d} = \int f^{3d} dv_\perp$.

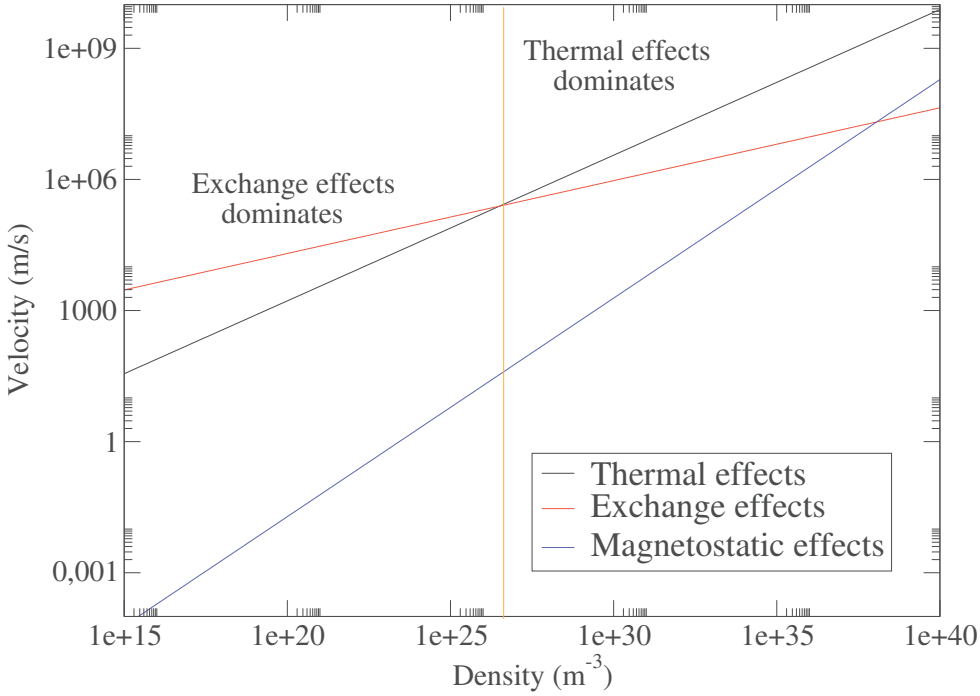

FIGURE 3.5: In this figure, we represent the different quantities that appear in the dispersion relation (3.44) as a function of the electronic density. The black curve represents v_{F} (thermal effects) , the red curve represents v_X (exchange effects) and the blue curve represents v_{ms} (magnetostatic effects). We took the following parameters: $m = 1\,\mathrm{a.u}$, $\epsilon_0 = 1/(4\pi)\,\mathrm{a.u}$ and $\alpha = 1/2$ (Spin polarization).

where the magnetic field B is present to have a spin polarized ground state. The chemical potential is then obtained to ensure that we have the correct number of electrons, i.e. $\int \left(f^{\uparrow(0)} + f^{\downarrow(0)}\right) dx\, dv = \int n_0 dx = N_0$.
In the Fig. 3.4, we plot the chemical potential as a function of the applied magnetic field in the case of Fermi-Dirac distribution functions, the temperature is set to $300\,\mathrm{K}$ and the density to metallic densities. In the case of a zero magnetic field we correctly found that the chemical potential is equal to the Fermi energy. In the same figure we draw also the magnetization as a function of the magnetic field, for a magnetic field larger than the Fermi magnetic field $B_{\mathrm{F}} = E_{\mathrm{F}}/\mu_{\mathrm{B}}$, we found that electron gas is completely spin-polarized.
In order to find the dispersion relation, one should also specify the form of the exchange-correlation functionals. The minimal requirement is to take an exchange functional which is local and spin dependent [135]

$$V_{XC} = V_X = -\frac{e^2}{4\pi\epsilon_0}\left(\frac{3}{4\pi}\right)^{\frac{1}{3}}\left[\left(\frac{n_0+m_0}{2}\right)^{\frac{1}{3}} + \left(\frac{n_0-m_0}{2}\right)^{\frac{1}{3}}\right], \tag{3.37}$$

$$\mu_{\mathrm{B}} B_{XC} = \mu_{\mathrm{B}} B_X = -\frac{e^2}{4\pi\epsilon_0}\left(\frac{3}{4\pi}\right)^{\frac{1}{3}}\left[\left(\frac{n_0+m_0}{2}\right)^{\frac{1}{3}} - \left(\frac{n_0-m_0}{2}\right)^{\frac{1}{3}}\right], \tag{3.38}$$

where n_0 and m_0 are the local density and magnetization of the ground state. The functionals (3.37) and (3.38) are the exact solutions of the Hartree-Fock equations in the case of homogeneous electronic densities. In our case, we are not so far from this situation, since we study perturbations around homogeneous ground states. The first order derivative of those exchange functionals write:

$$\partial_n V_X = \mu_B \partial_m B_X = -\frac{e^2}{4\pi\epsilon_0}\frac{1}{6}\left(\frac{3}{4\pi}\right)^{1/3}\left[\left(\frac{n_0+m_0}{2}\right)^{-2/3}+\left(\frac{n_0-m_0}{2}\right)^{-2/3}\right], \quad (3.39)$$

$$\partial_m V_X = \mu_B \partial_n B_X = -\frac{e^2}{4\pi\epsilon_0}\frac{1}{6}\left(\frac{3}{4\pi}\right)^{1/3}\left[\left(\frac{n_0+m_0}{2}\right)^{-2/3}-\left(\frac{n_0-m_0}{2}\right)^{-2/3}\right]. \quad (3.40)$$

Before addressing the complete determination of the dispersion relation, we are going to study the zero temperature case. In this regime the distribution functions can be written as follows:

$$f_0^{(0)}(T=0) = \frac{n_0}{2V_F}\left[1-\Theta\left(|v-v_F|\right)\right], \quad f_z^{(0)}(T=0) = \alpha f_0^{(0)}(T=0), \quad (3.41)$$

where $\alpha \in [-1;1]$ represents the spin polarization of the system and Θ is the Heaviside function. In this case the integrals $\mathcal{I}_0$ and $\mathcal{I}_z$ write:

$$\mathcal{I}_0 = \frac{n_0}{2v_F}\int \frac{\partial_v\left[1-\Theta\left(|v-v_F|\right)\right]}{w-kv}dv, \quad \mathcal{I}_z = \alpha\mathcal{I}_0. \quad (3.42)$$

Let us consider the case of long wavelength solutions, i.e. $\omega \gg kv$, in this case one can use the development (1.62) to by pass the singularity problem, one obtains:

$$\mathcal{I}_0 = -n_0 k\left[\frac{1}{\omega^2}-\frac{6k^2}{\omega^4}\right], \quad \mathcal{I}_z = \alpha\mathcal{I}_0. \quad (3.43)$$

In this particular limit, the dispersion relation associated to the dielectric function, Eq. (3.19), can be easily solved

$$\omega^2 = \omega_p^2 + k^2\left[v_F^2 - \underbrace{\frac{1}{6m}\frac{e^2}{4\pi\epsilon_0}\left(\frac{3n_0}{\pi}\right)^{1/3}\left[(1+\alpha)^{4/3}+(1-\alpha)^{4/3}\right]}_{v_X} - \underbrace{\frac{n_0\mu_B^2\mu_0\alpha^2}{m}}_{v_{ms}}\right]. \quad (3.44)$$

From this result, we see that the effect of the exchange and the magnetostatic interactions are proportional to k^2 such as temperature effects represented by $v_F = \hbar(3\pi^2 n_0)^{2/3}/m$, except that they appears with an opposite size. Therefore temperature effects tend to increase the plasmon frequency whereas exchange and magnetostatic interactions tend to decrease the plamson frequency. All the three terms in the parenthesis, on the right side of Eq. (3.44), depend only on the electron density

n_0 and the spin polarization α. In Fig. 3.5, we analyse the absolute value (in velocity units) of each of these terms as a function of the electron density. We clearly notice that there is a critical density for which the temperature effects are smaller than the exchange effects, i.e.

$$v_{\mathrm{F}}^2 < \frac{1}{6m}\frac{e^2}{4\pi\epsilon_0}\left(\frac{3n_0}{\pi}\right)^{1/3}\left[(1+\alpha)^{4/3}+(1-\alpha)^{4/3}\right]. \tag{3.45}$$

A simple calculation shows that this conditions is full-field when $n_0 < n_0^\star = 2.7 \times 10^{26}\,\mathrm{m}^{-3}$. We also notice that the magnetostatic interactions have a week influence on the dispersion relation. Therefore there are two different regimes, one for small densities $(n_0 < n_0^\star)$ where the system is mainly dominated by exchange interactions and and other one for large densities $(n_0 > n_0^\star)$ where thermal effects dominates. Electrons in metallic nano-structure have a density around $10^{28} - 10^{29}\,\mathrm{m}^{-3}$. Therefore in this kind of systems one should not observe a strong influence of exchange interaction on the plasmon mode. However for electrons in semi-conductor the density are even lower than $n_0^\star$, then the influence of the exchange interaction would be much stronger.

These results should not be considered as exact but rather as a basis for the future discussions. They are several approximations behind these results. First they are derived from the local density approximation of the exchange interaction and hence are correct only in the case of homogeneous densities. Secondly, this analysis is only valid for a system of electrons with a temperature much smaller than the Fermi temperature and for plasmon modes which are not damped ($\omega \gg kv$). Moreover, as it is showed in Fig. 1.1, for small electronic densities and temperatures the electron-electron correlation should start to play a significant role. This is particularly true in the regime dominated by the exchange effects.

One should also mentioned that the dispersion relation, Eq. (3.44) can be also obtained from a fluid model with spin effects. Indeed if one took the fluid model (2.73)-(2.75) and (2.99), closed with the maximum entropy method and with a Fermi-Dirac distribution function (see Sec. 2.3.3), then one obtains exactly the same dispersion relation.

Exchange interactions have two effects, one which is similar to an electric field and an other one which acts as a magnetic field. The latter acts differently on the spin up and spin down populations and could be in principle responsible of a trace of the spin polarization in the plasmon frequency. In the dispersion relation (3.44), it appears with the parameter α. However the difference between a full and a none polarized electron gas is small. Indeed in the first case, one has a corrective factor of 2 whereas in the other case it is equal to $2^{4/3}$. Of course this difference increases with the value of k, but in the same time one expects that the oscillation modes with a large value of k are rapidly damped. This could be verified by solving the full dispersion relation where ω is a complex quantity. This issue is in practice not easy to realize, particularly when one consider a Fermi-Dirac distribution function [70].

Indeed, in this case, it is more convenient to work with $\mathcal{I}_+$ and $\mathcal{I}_-$ instead of $\mathcal{I}_0$ and $\mathcal{I}_z$, which are defined as follows:

$$\mathcal{I}^+ = \int \frac{\partial v f^{\uparrow(0)}}{\omega - kv} dv = -2\pi \left(\frac{m}{2\pi\hbar}\right)^3 \frac{v_\mathrm{F}}{k} \int_{-\infty}^{\infty} \frac{v}{\frac{v_p}{v_\mathrm{F}} - v} \frac{dv}{1 + \exp\left(\frac{E_\mathrm{F}}{k_b T}\left(v^2 - \frac{\tilde{\mu}_-}{E_\mathrm{F}}\right)\right)}, \tag{3.46}$$

$$\mathcal{I}^- = \int \frac{\partial v f^{\downarrow(0)}}{\omega - kv} dv = -2\pi \left(\frac{m}{2\pi\hbar}\right)^3 \frac{v_\mathrm{F}}{k} \int_{-\infty}^{\infty} \frac{v}{\frac{v_p}{v_\mathrm{F}} - v} \frac{dv}{1 + \exp\left(\frac{E_\mathrm{F}}{k_b T}\left(v^2 - \frac{\tilde{\mu}_+}{E_\mathrm{F}}\right)\right)}, \tag{3.47}$$

where we have introduced a renormalized chemical potential : $\tilde{\mu}_\pm = \mu + \mu_\mathrm{B} B$ and the velocity $v_p = \omega/k$.

Comparing the expression (3.46) - (3.47) with the integral (3.24) , we found that in the case of Fermi-Dirac distribution functions, the function $g(v)$ is equal to

$$g(v) = \frac{v}{1 + \exp\left(\frac{E_\mathrm{F}}{k_b T}\left(v^2 - \frac{\tilde{\mu}_\pm}{E_\mathrm{F}}\right)\right)}. \tag{3.48}$$

However, the Landau method, developed in the previous section, is valid only if $g(v)$ is an analytical function of v. This is obviously not the case for a Fermi-Dirac distribution function because the denominator of Eq. (3.48) cancels for several particular values of v, i.e. when the following identity holds: $E_\mathrm{F}/(k_b T)\,(v^2 - \tilde{\mu}_\pm/E_\mathrm{F}) = \pi + 2n\pi,\ n \in \mathbb{Z}$.

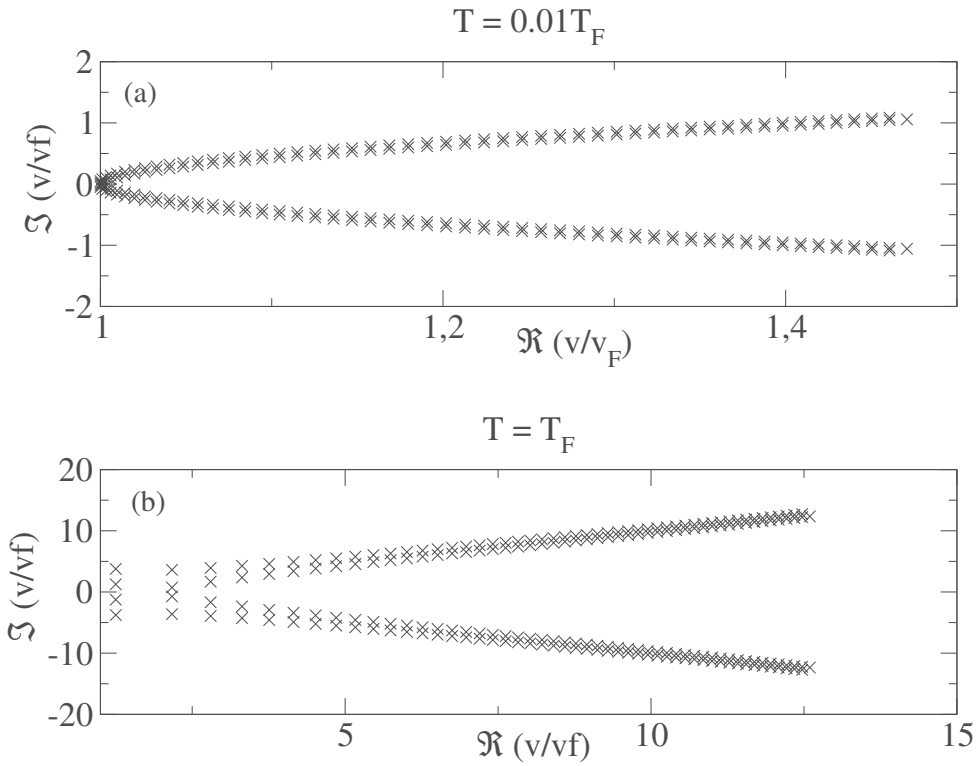

FIGURE 3.6: Poles of the function $g(v)$, Eq. (3.48), in the case of a metallic density $n_0 = 5.9 \times 10^{28}\,\mathrm{m}^{-3}$ and for different temperatures: $T = 0.01\ T_\mathrm{F}$ (a) and $T = T_\mathrm{F}$ (b).

In the Fig. 3.6, we represent the poles of the function $g(v)$ for different temperatures $T = 0.01\ T_{\mathrm{F}}$, $T = T_{\mathrm{F}}$ and in the case of metallic densities (Gold). We notice that one has a infinite numbers of poles and that for low temperatures they are more and more close from each other. In the limit $T = 0$, one can show that they are continuously connected. For practical applications in metallic nano-structures, one should consider temperatures close to $T = 0.01\ T_{\mathrm{F}}$ which correspond more or less to the room temperature.
Therefore the fact that the function $g(v)$ is not analytical make the analytical prolongation of the integrals $\mathcal{I}^{\pm}$ difficult to realize. One can not simply use the Landau method without considering those new singularities. We didn't find a method to solve this problem. In the next section we shall use a Maxwell-Boltzmann distribution function, for which the function $g(v)$ is analytical, to be able to find a plamson dispersion relation with spin effects.

3.3 The dispersion relation with a Maxwell-Boltzmann ground state

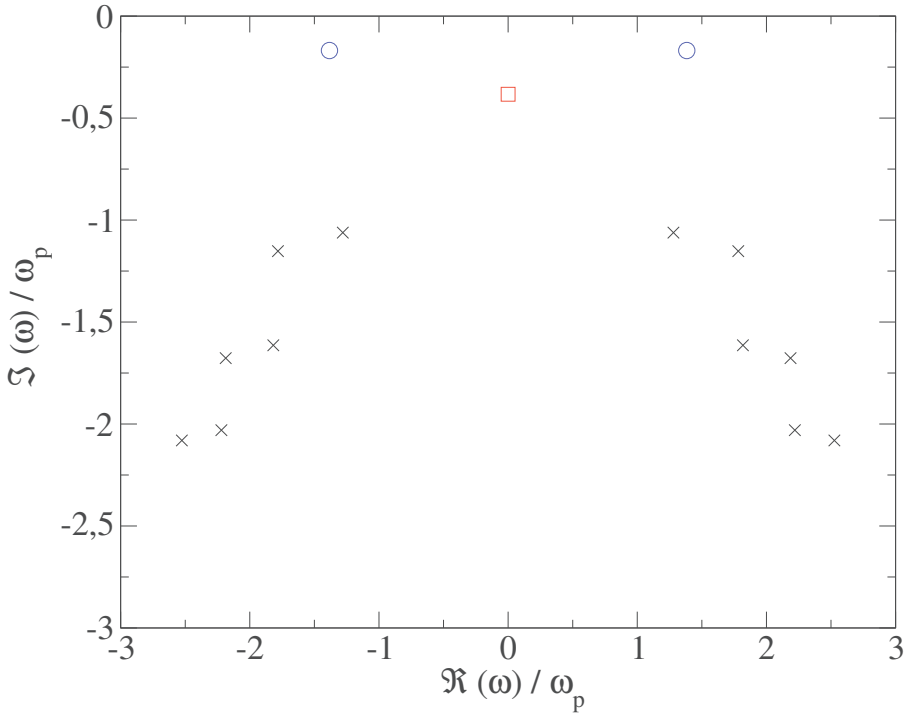

FIGURE 3.7: Zeros of the dielectric function, Eq. (3.56). The different symbols correspond to different type of modes: plasmon modes (blue circles), paramagnon mode (red square) and other modes that are strongly damped (black crosses). The following parameters are used : $n_0 = 5.9 \times 10^{28}\,\mathrm{m}^{-3}$, $T = 64000\,\mathrm{K}$ and $k = 0.4\ k_{\mathrm{D}}$.

The plasma dispersion relation for spinless systems, corresponding to a Vlasov-Poisson model with a Maxwell-Boltzmann equilibrium distribution function, was

intensively studied in the literature [134]. In that case the dispersion relation can be fully evaluated even in the strong damping regime. As we will see, for a Maxwell-Boltzmann distribution, the problem of the analytical prolongation of the function $g(v)$ is solved by introducing the plasma dispersion function.
For a system of electrons, the Maxwell-Boltzmann distribution functions read:

$$f_0^{(0)}(v) = \frac{n_0}{v_T\sqrt{\pi}} \exp\left[-\frac{m}{2k_B T}v^2\right], \tag{3.49}$$

$$f_z^{(0)}(v) = \frac{n_0}{v_T\sqrt{\pi}} \tanh\left(\frac{\mu_B B}{k_B T}\right) \exp\left[-\frac{m}{2k_B T}v^2\right], \tag{3.50}$$

where $v_T = \sqrt{2k_B T/m}$ represents the thermal speed of the electrons.
In this case the integrals $\mathcal{I}_0$ and $\mathcal{I}_z$ write:

$$\mathcal{I}_0 = -\frac{2n_0}{v_T^3\sqrt{\pi}} \int \frac{v \exp\left(-\frac{m}{2k_b T}v^2\right)}{\omega - kv}, \quad \mathcal{I}_z = \alpha\mathcal{I}_0. \tag{3.51}$$

To use the Landau method (3.27) we introduce the plasma dispersion function, which is defined as follows:

$$Z(\varrho) = \frac{1}{\sqrt{\pi}} \int_\gamma \frac{\exp(-z^2)}{z - \varrho} dz, \tag{3.52}$$

where γ is a contour in the complex plane following the real axis at infinity and passing under the singularities $z = \varrho$. This function was originally introduced by Fried et Conte [136], it is well defined for $\Im(\omega) > 0$ and it is analytically prolonged in the lower part of the complex plane, i.e. for $\Im(\omega) < 0$. The plasma dispersion function can be written in terms of the complementary error function $erfi(z) = 2/\sqrt{\pi}\int_0^z \exp(z^2)\, dz$:

$$Z(\varrho) = \sqrt{\pi}\exp\left(-\varrho^2\right)\left[i - erfi(\varrho)\right]. \tag{3.53}$$

The latter is a standard function and hence can be easily computed using a numerical library. Then, one can express the integrals $\mathcal{I}_0$ and $\mathcal{I}_z$ as a function of the plasma dispersion function. We have

$$\mathcal{I}_0 = \frac{2n_0}{kv_T^2}\left[1 + \frac{\omega}{kv_T} Z\left(\frac{\omega}{kv_T}\right)\right] = -\frac{n_0}{kv_T^2} Z'\left(\frac{\omega}{kv_T}\right), \quad \mathcal{I}_z = \alpha\mathcal{I}_0, \tag{3.54}$$

where the following property has been used:

$$Z'(\varrho) = -2\varrho Z(\varrho) - 2. \tag{3.55}$$

According to the expressions (3.54) for $\mathcal{I}_0$ and $\mathcal{I}_z$ and to the equation (3.19), one obtains the following dielectric function for a Maxwell-Boltzmann distribution

$$\begin{aligned}\epsilon(\omega,k) = 1 &- \frac{1}{v_T^2}\left[\frac{\omega_p^2}{k^2} - \frac{\mu_B^2\mu_0 n_0}{m} + 2\frac{n_0}{m}\left(\partial_n V_X + \alpha\partial_m V_X\right)\right] Z'\left(\frac{\omega}{kv_T}\right) \\ &+ \left(\frac{n_0}{mv_T^2}\right)^2 \left[(\partial_n V_X)^2 - (\partial_m V_X)^2\right]\left[1-\alpha^2\right] Z'\left(\frac{\omega}{kv_T}\right)^2 \\ &+ \left(\frac{n_0}{kv_T^2}\right)^2 \left[\frac{\mu_B\omega_p^2}{n_0 m}\partial_n V_X - \frac{\omega_p^2\mu_B^2\mu_0}{n_0 m} - \frac{k^2\mu_B^2\mu_0}{m^2}\partial_n V_X\right]\left[1-\alpha^2\right] Z'\left(\frac{\omega}{kv_T}\right)^2 .\end{aligned} \tag{3.56}$$

In order to find the zeros of this complex function, we use ZEAL [137], which is a mathematical software package for computing zeros of analytic complex functions. This algorithm is based on the following idea. We first define a rectangle region in the complex plane and instead of considering the function f, for which we want to determine the zeros, we consider the inverse of this function $g = 1/f$. Then using the residue theorem the program ZEAL is able to find the poles of g corresponding to the zeros of the function f.

The dispersion relation depends on the electron density (n_0) and the temperature (T). We first consider an electron gas having a metallic density $n_0 = 5.9 \times 10^{28}\,\mathrm{m}^{-3}$ (Gold). A first complication arrives when one wants to define the temperature of the system. Indeed, we use a Maxwell-Boltzmann distribution function instead of a Fermi-Dirac and therefore the temperature that we use should not be necessarily related to the physical temperature of the system. The Temperature has to be set in order to have electrons at the Fermi energy. Therefore we choose a thermal velocity equal to the Fermi velocity : $v_T = v_F$. In the case of Gold this leads to a temperature of $T = 64000\,\mathrm{K}$.

In Fig. 3.7, we represent the zeros of the dielectric function (Eq. (3.56)) using the previous values of density and temperature. We first notice that the zeros are symmetrically located with respect to the vertical axis. This is due to the symmetric properties of the plasma dispersion function. We also note the presence of an infinite number of zeros (black crosses), but several of them have no impact on the dynamical response. Indeed they have a large imaginary part compared to the real part and are therefore rapidly damped. Then, there are also three other zeros which have different origins. Two of them represented by the blue circles are responsible of the plasma frequency. For small value of k they have a real part larger than the imaginary part. Therefore they govern the dynamics of the system. The last zero represented by a red square has the specificity to have a zero real part. This means that the associated mode is not present in the dynamics. By removing the exchange interactions, we notice that this zero disappears. The latter corresponds to the paramagnon that is an oscillation in phase opposition of two spin populations (up and down). The paramagnon modes are purely magnetic modes in the sense that there

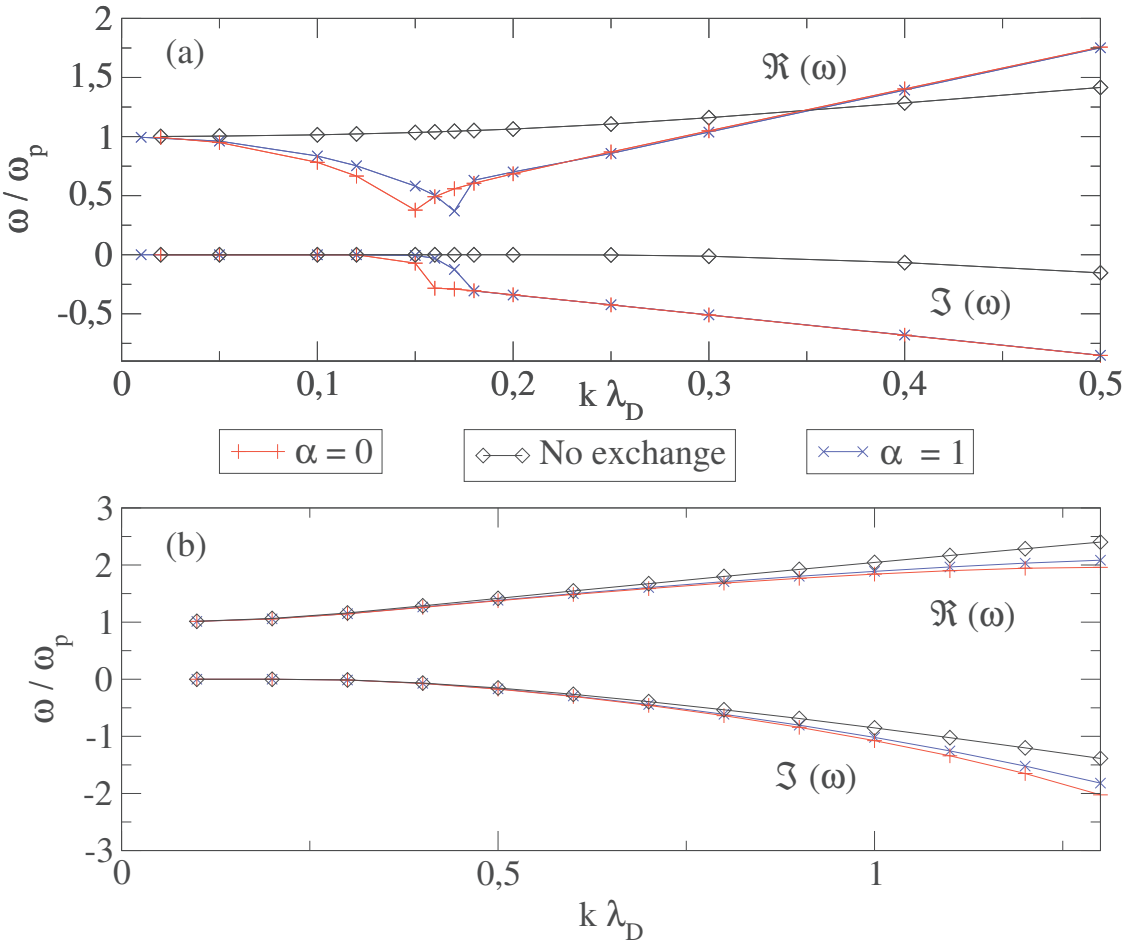

FIGURE 3.8: Plasmon dispersion relation $\omega(k)$ (nomalized to ω_p) for two different physical systems. The upper lines correspond to the real part of ω whereas the lower lines correspond to the imaginary part. The black lines and the color ones correspond, respectively, to the abscence and presence of exchange interactions. The blue lines correspond to a full polarized system, i.e. $m_0 = n_0$, whereas the red lines correspond to a non polarized system, i.e. $m_0 = 0$. In (a), we consider electrons with a density of: $n_0 = 10^{22}\,\mathrm{m}^{-3}$ and $T = 300\,\mathrm{K}$. In (b), we consider electrons in Gold with the following parameters: $n_0 = 5.9 \times 10^{28}\,\mathrm{m}^{-3}$ and $T = 64000\,\mathrm{K}$ ($v_T = v_\mathrm{F}$). In both case: $m = 1\,\mathrm{a.u}$, $\epsilon_0 = 1/4\pi\,\mathrm{a.u}$.

is no charge excitations but only spin excitations. In order to have paramagnon oscillations we need to have a magnetic coupling in the system. In our system, it is the exchange interaction that is responsible of the paramagnon oscillations. In the literature [138] it is found that the paramagnon has a zero real part for infinite system. This result was demonstrated in the quantum regime and that explains why the paramagnon have a zero real part in our semi-classical model. Paramagnon have been also studied in Ref. [139], The authors found that the real part of the paramagnon mode is non zero for finite-size systems. The exchange interaction does not only appear through this zero but it also modifies the zeros corresponding to the plasma frequency. This will be discussed below.

In Fig. 3.8, the plasma dispersion relation is depicted for two different physical systems. The first system corresponds to the case of electrons in metal with the density of Gold $n_0 = 5.9 \times 10^{28}\,\mathrm{m}^{-3}$ and a temperature $T = 64000\,\mathrm{K}$. As already mentioned, the temperature has to be set very high, because one uses a Maxwell-Boltzmann distribution instead of a Fermi-Dirac. The second system corresponds to an ideal case, where the electron density is about $n_0 = 10^{22}\,\mathrm{m}^{-3}$. For such a system, the Fermi temperature is close to $2\,\mathrm{K}$ ($v_T = v_\mathrm{F}$). Therefore, at room temperature ($T = 300\,\mathrm{K}$), it is justified to use a Maxwell-Boltzmann distribution function instead of a Fermi-Dirac. Indeed, for temperatures much larger than the Fermi temperature, the Fermi-Dirac distribution converges towards a Maxwell-Boltzmann distribution.
In the metallic case (Fig. 3.8 (b)), we note that the plasma frequency is dominated by the electrostatic interactions. Indeed the exchange interactions do not change significantly the dispersion relation, they may decrease a bit the value of the plasma frequency. This difference increase with the value of k but in the same times the plasma oscillations are more and more damped. These results are not so surprising because they are in agreement with the qualitative analysis that we made in the Sec. 3.2 in the long wavelength limit, see Eq. (3.44).
The same equation showed us that for smaller densities the effect of exchange interactions could be more important even for low value of k. In the Fig. 3.8 (a), we plot the plasma dispersion relation with an electronic density $n_0 = 10^{22}\,\mathrm{m}^{-3}$. With this kind of density, we are in a regime where the exchange interactions dominate over the electrostatic interactions (see Fig. 3.5). Indeed the effect of exchange interactions are clearly visible. For small value of k the plasma frequency first decrease instead of growing. Then for a special value of k it reaches a minimum before growing for larger value of k. The trace of the spin polarization is more visible in that system, we specially notice a shift in k for the minimum of the plasma frequency. However, it is difficult to find such systems in the nature. On can think about semiconductors, indeed the typical electronic densities are around $10^{22}\,\mathrm{m}^{-3}$. However in such systems, we should also take into account the effective mass and dielectric constant $m^\star = 0.07\,\mathrm{m}$ and $\epsilon_0^\star = 12\epsilon_0$ [96]. Such that the dimensionless physical quantities are similar for electrons in metallic nano-structures and electrons (or holes) in semi-conductors [140]. Therefore, if we compute the dispersion relation with the semi-conductors parameters, we would obtain the same behaviour as in the metallic case (Fig. 3.8 (b)).

3.4 Conclusions and perspectives

In this chapter we used the Fourier and the Laplace transforms to study the linear response of a spin polarized electron gas that is subject to a weak periodic perturbation. We have seen that the linear regime is characterized by the dielectric function $\epsilon(\omega, k)$ and that the zeros of this function give the eigenmodes of the system. The latter constitute the dispersion relation of the system $\omega(k)$ and depend on the ground

state distribution functions. In the first part we have seen how to include the spin in the dielectric function, through the Zeeman interaction, the exchange potential (LDA) and self-consistent effects. Then we studied the plasma dispersion relation for an electron gas with a Fermi-Dirac ground state. We encountered some mathematical difficulties that we have not been able to solve. We thus solved the problem with a Maxwell-Boltzmann ground state, for which we obtained the full dispersion relation. We have seen that the main influence of the spin on the plasma frequency originates from the spin dependent exchange interaction. However, at the usual electron density and temperature of metallic nano-structures, exchange effects are not enough strong to have an appreciable change of the plasma frequency.
The study that we have done here is not complete and should be extended to the following cases:

- The electrons in metallic nano-structures should be modelled using a Fermi-Dirac distribution instead of a Maxwell-Boltzmann. However to do so one has to deal with the natural singularities of the Fermi-Dirac distribution function. Such analysis was recently performed in Ref. [141], the author obtained the full semi-classical dispersion relation with a Fermi-Dirac ground state. However they did not include the spin in their analysis. It should be interesting to use their method to evaluate the dispersion relation with spin effects and with a Fermi-Dirac ground state.

- Quantum corrections to the plasma dispersion relation were recently study by several authors [141–143], in the case of spinless electrons. In those works, the authors studied the dispersion relation of the Wigner equation (1.30) for spinless particles. They solved numerically the plasma dispersion relation with a Fermi-Dirac ground state. In the quantum regime the dispersion relation of an electron gas is given by the so-called Lindhard function. In that case the analytical prolongation works well, but one has to deal with complex logarithms and with branch cuts in the complex plane. A possible extension of our work consists to include quantum effects in the dielectric function (3.19). In this case, one has to perform the linear analysis on the spin-Wigner model instead of the spin-Vlasov model. We should then obtain a generalized Lindhard dielectric function with spin effects.

- The spin-orbit interaction should be also included in the linear analysis. To correctly describe it, one has to consider also the electron dynamics in the transversal directions of the perturbation. In that case, the dielectric function becomes a tensor and the problem is more complicated to solve. It should be particularly interesting to see, how the plasmon modes are modified due to the spin-orbit interaction and also if there are some unstable magnetic modes that appears. One might even want to consider the possibility to study, in the linear regime, transfers between spin and orbital angular momentums.

Chapter 4

Nonlinear electron and spin dynamics in Nickel thin films

In the chapter 2, we derived a self-consistent semiclassical model, based on the spin-Vlasov equations (2.54)-(2.55), to study the spin dynamics in metallic nanostructures. In this chapter we shall apply this model to study the spin dynamics in nickel thin films. This type of system was chosen for the following reasons. Firstly, we restrict the problem to a four dimensional problem in the phase space instead of a six dimensional problem. Indeed, the longitudinal direction of the film, which will be denoted x in the rest of the chapter, is much smaller than the two other directions, see Fig. 4.1. Therefore we consider that the distribution functions are invariant in the transverse directions y-z, i.e. $f_\mu = f_\mu\left(x, v_x, v_y, v_z\right)$, with $\mu = \{0, x, y, z\}$. Secondly, there exist experimental results on the magnetization dynamics in nickel thin films.

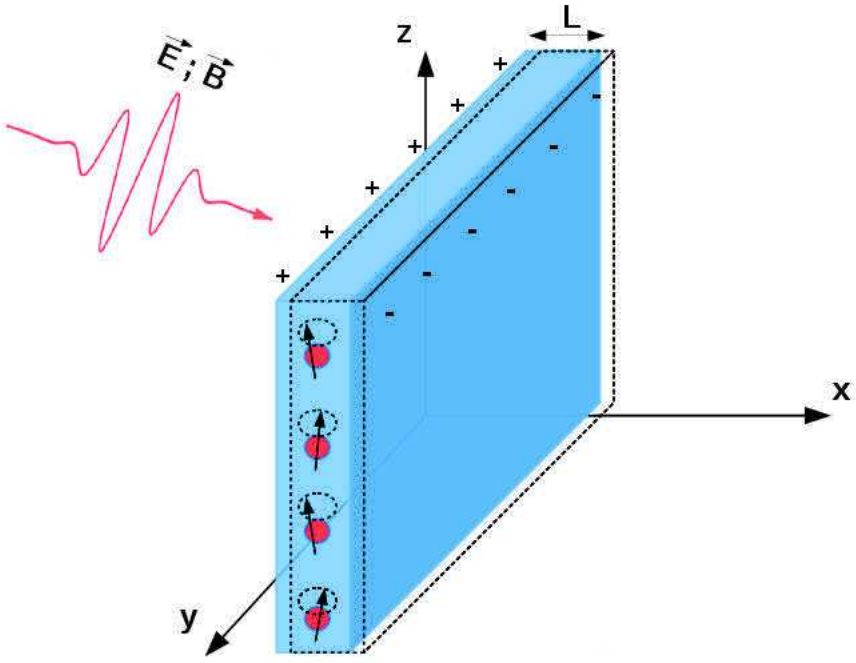

FIGURE 4.1: nickel thin film excited by a laser pulse.

For instance an ultrafast demagnetization induced by femtosecond laser pulses was first observed in 1996 in such systems [22]. Finally, the electron dynamics was recently investigated using a Vlasov-Poisson model [38, 144] and a Wigner-Poisson model [39, 89]. In those papers, the authors modelled the classical and quantum electron dynamics in thin films of Sodium without considering the spin degrees of freedom. This chapter concerns the extension of their analysis by including spin effects. However only the Zeeman interaction will be considered here. We shall not include the spin-orbit interaction in our simulations, essentially because of computational reasons.

4.1 Description of the system

nickel films are characterized by the following parameters: (L, σ, n_0^i, T). L is the thickness of the film and σ is a diffuseness parameter. The latter represents the typical length scale on which the density falls to zero on the border of the film. T is the temperature of the system and n_0^i is the ion density of the bulk metal. The ions are supposed to be fixed during the electron motion. This assumption is justified by the fact that there is a time scale separation between the ions and the electrons motion, which is given by the plasma frequency ω_p (1.5). We assume the following shape for the ion film density:

$$n^i(x) = \frac{n_0^i}{1 + \exp\left(\frac{|x|-L/2}{\sigma}\right)}. \tag{4.1}$$

This assumption holds if the film size in the directions parallel to its surfaces is large compared to L. In this case, it is appropriate to use a 1D model, where only the normal coordinate x plays a role. We have chosen the form (4.1) in reference to [144], basically σ will be around $0.5-1$ Å. However this is an assumption, one could imagine other functions, the point is that the ion density must be steep on the border of the film and practical to use for numerical applications. The density profile corresponding to the Eq. (4.1) is sketched in Fig. 4.2.
Afterwards, we are going to use adapted units to our system. Energies will be normalized to the Fermi energy E_{F}, time to the inverse of the plasma frequency $\omega_p = \sqrt{e^2 n_0^i/(m\epsilon_0)}$, velocities to the Fermi velocity $v_{\mathrm{F}} = \sqrt{2E_{\mathrm{F}}/m}$ and lengths to $L_{\mathrm{F}} = v_{\mathrm{F}}/\omega_p$. Electron and ion densities will be normalized to $n_0^i = 3/(4\pi r_s^3)$, where r_s is the Wigner-Seitz radius. In the case of nickel films one has : ($r_s = 2.6$ a.u.), $n_0^i = 0.0136$ a.u. $= 91.8$ nm^{-3}, $T_p = 2\pi\omega_p^{-1} = 15.32$ a.u. $= 0.37$ fs, $v_{\mathrm{F}} = 0.93$ a.u. $= 1.12\ 10^6$ m.s^{-1}, $L_{\mathrm{F}} = 2.27$ a.u. $= 0.120$ nm and $E_{\mathrm{F}} = 0.43$ a.u. $= 11.76$ eV. The electron structure of nickel is Ni = [Ar] $3d^8\ 4s^2$. So, there are ten valence electrons of which eight are in the $3d$ shell and the others two are in the $4s$ shell. The question being asked is actually, first of all, should we treat all the ten valence electrons with our spin-Vlasov model (2.54)-(2.55)?

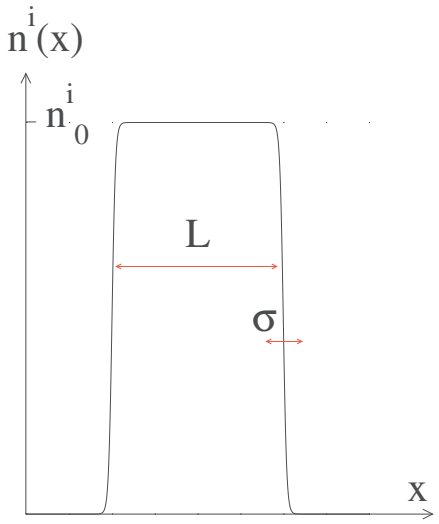

FIGURE 4.2: Ionic density defined by the Eq. (4.1).

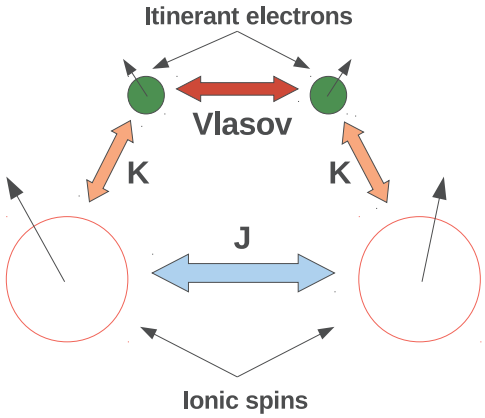

FIGURE 4.3: Exchange interactions between the different spin moments (K and J are exchange constants).

The answer is that we should, because the magnetic properties are carried by the valence electrons [145]. However, it is well known [146], that the $3d$ electrons in nickel are more localized around the ions than the $4s$ electrons. This effect is a purely quantum effect due the electron structure of nickel and cannot be obtained with our semi-classical model. For instance, it can be obtained with ab-initio techniques such as DFT calculations, where quantum effects are taken into consideration. So, we have to make a distinction between the two electron populations. The $4s^2$ electrons will be described with our set of Vlasov equations, thus they will have an orbital and a spin dynamics. Whereas the $3d^8$ electrons will be described with the Landau-Lifshitz equations [147], so they will form a localized ion spin which will not move in the position space but only precess in the spin space. In such a model, we make a distinction between two different types of magnetism, an itinerant magnetism carried by the $4s$ electrons and a localized magnetism carried by the spin of the ions (including the $3d$ electrons).
The total magnetic moment of nickel is $0.606\ \mu_{\mathrm{B}}$ per atom [148]. This magnetic moment comes from all the valence electrons, so one has to specify the proportion of magnetic moment carried by each type of electrons. In the book of Kittel [145], we found that the magnetic moment of the $3d$ electrons at 0 Kelvin is about $0.54\ \mu_{\mathrm{B}}$ per atom. Then we deduce that the magnetic moment of the $4s$ electrons is equal to $0.066\ \mu_{\mathrm{B}}$ per atom.
In our phase-space models, the spin magnetic moment of the electrons is defined as follows:

$$\boldsymbol{M}(x) = -\mu_{\mathrm{B}} \int \boldsymbol{f}(x, \boldsymbol{v})\, d\boldsymbol{v}, \tag{4.2}$$

and the spin magnetic moment of the ions as follows:

$$\boldsymbol{M}^i = -g\mu_{\mathrm{B}}\boldsymbol{S}^i, \tag{4.3}$$

where $g = 2$ is the Landé g-factor for an electron and $\boldsymbol{S}^i$ denotes the ion spins. The absolute value of the ion spins is equal to $|\boldsymbol{S}^i| \equiv S_0^i = 0.54/g = 0.270$ (No units), in such a way that one has $|\boldsymbol{M}^i| = 0.54\ \mu_{\mathrm{B}}$.
From the point of view of the magnetic interactions, we shall consider all the possible exchange interactions between the different spins. The exchange interaction between ion spins will be modelled using a Heisenberg exchange interaction [149] with a coupling constant J. Between the electron and ion spins, we will also use an Heisenberg exchange interaction but with a coupling constant K. The latter interaction, between local and itinerant magnets, is known as the RKKY (Rundermann-Kittel-Kasuya-Yosida) interaction [150]. This type of interaction was originally developed in the Zener model [151] to describe the magnetism of transition metals. It was also used in more recent works, for instance in Ref. [55] the authors studied the ultrafast magnetization dynamics in diluted magnetic semiconductors using an exchange interaction between localized and itinerant spins. Finally, exchange interactions between electron spins will be treated with exchange functionals of the electron density as in ab-initio calculations. All the different exchange interactions mentioned above are sketched in Fig. 4.3.
In this model, the ion spin is a discrete quantity (defined per atom) whereas the electron spin moment is a continuous quantity (defined per unit of volume). However the ion density (4.1) is a continuous function. Therefore to be consistent, the ion spins should be also treated in a continuous fashion. Moreover the exchange interaction between ions and electrons should be added in the model in a self-consistent way. This will be the issue of the two next sections.

4.1.1 Electron spin dynamics

To describe the exchange interaction between the ion and the electron spins we need to add a new term in the spin-Vlasov equations (2.54)-(2.55). So, we introduce the following exchange interaction in the Hamiltonian of the electrons:

$$\mathcal{H}_{el} = \mathcal{H}_0 + \mathcal{H}_{sd}, \tag{4.4}$$

where $\mathcal{H}_0$ is defined in Eq. (2.15) and $\mathcal{H}_{sd}$ corresponds to the Heisenberg exchange Hamiltonian between electron and ion spins

$$\mathcal{H}_{sd} = -\sum_j K\left(|x - X_j|\right) \boldsymbol{S}_j^i \cdot \boldsymbol{s}, \tag{4.5}$$

where X_j and x refers, respectively, to the ion and the electron position along the transversal direction of the film. The variable $\boldsymbol{s} = \frac{\boldsymbol{\sigma}}{2}$ refers to the spin of the electrons. This exchange interaction describes the interaction between localized ion spins on a lattice and delocalized electron spins in the material. This is the reason why the coupling constant K depends on the distance $|x - X_j|$. Moreover, one requires that K takes positive values to align the electron and the ion spins. In order to simplify the model, we will describe the ion spins in a continuous fashion. According to the following relations $X_j \to X$ and $\sum_j \to \int n_i(X)\, dX$, where $n_i(X)$ is the ion density, the Hamiltonian (4.5) becomes:

$$\mathcal{H}_{sd} = -\frac{\boldsymbol{\sigma}}{2} \cdot \int K(|x - X|)\, n_i(X) \boldsymbol{S}^i(X) dX, \tag{4.6}$$

where the exchange constant K is not any more given in $\mathrm{eV/link}$[1] but rather in $\mathrm{eV/nm^3}$. We also suppose that the exchange interaction is localized in space, i.e. $K(|x - X|) = K\delta(x - X)$. So the Hamiltonian (4.6) reads:

$$\mathcal{H}_{sd} = -\frac{K}{2} n_i(x) \boldsymbol{\sigma} \cdot \boldsymbol{S}^i(x). \tag{4.7}$$

We notice that the exchange interaction between ions and electrons can be written as a magnetic field $\boldsymbol{B}_{sd} = -\frac{K}{2\mu_B} n_i(x) \boldsymbol{S}^i(x)$. Therefore we simply have to substitute the magnetic field entering in the Zeeman interaction by: $\boldsymbol{B} \to \boldsymbol{B} + \boldsymbol{B}_{sd}$.
As it was mentioned at the beginning of the chapter, the spin-orbit interaction will not be taken into account. The reason is that, in order to describe the spin-orbit interaction we would need the three components of the velocity (v_x, v_y, v_z). Indeed the spin-orbit interaction couples all the velocity components of the distribution functions together as well as the spin and the orbital dynamics. In terms of numerical applications, the distribution functions, will evolve in a four dimensional phase space (x, v_x, v_y, v_z). Such numerical problems cannot be solved without using parallelization techniques[2]. This is the reason why we neglect the spin-orbit coupling. In this case, we can restrict our problem to a reduced phase space $(x, v_x \equiv v)$, where the electrons are only allowed to move in the direction normal to the surfaces of the film (x), see Fig. 4.1. Therefore, in the absence of the spin-orbit interaction, one obtains a new set of spin-Vlasov equations to describe the electron dynamics in nickel thin

[1] Usually the exchange constants are defined between two atoms, that is why we express them in $\mathrm{eV/link}$.

[2] To give an idea of the size of the problem, let us assume that we need 100 points per dimension to correctly characterize the distribution functions (as we shall see later, we need more than 100 points per dimension to obtain accurate results). We thus need 10^8 numbers, which roughly represent 1 Giga-bytes of memory (in double precision).

films:

$$\frac{\partial f_0}{\partial t} + v \cdot \partial_x f_0 - \frac{e}{m}\left[\boldsymbol{E} + \boldsymbol{v} \times \boldsymbol{B}\right]_x \partial_v f_0 - \frac{\mu_{\mathrm{B}}}{m}\left(\partial_x B_i\right)\left(\partial_v f_i\right) + \frac{K n_i\left(x\right)}{2m}\left[\left(\partial_x S_i^i\right)\left(\partial_v f_i\right)\right] = 0, \tag{4.8}$$

$$\frac{\partial f_k}{\partial t} + v \cdot \partial_x f_k - \frac{e}{m}\left[\boldsymbol{E} + \boldsymbol{v} \times \boldsymbol{B}\right]_x \partial_v f_k - \frac{\mu_{\mathrm{B}}}{m}\left(\partial_x B_k\right)\left(\partial_v f_0\right) + \frac{K n_i\left(x\right)}{2m}\left[\left(\partial_x S_k^i\right)\left(\partial_v f_0\right)\right] - \frac{e}{m}\left[\boldsymbol{B} \times \boldsymbol{f}\right]_k - \frac{K n_i\left(x\right)}{\hbar}\left(\boldsymbol{f} \times \boldsymbol{S}^i\right)_k = 0. \tag{4.9}$$

4.1.2 Ion spin dynamics

The next step is to find the evolution equation for the ion spins $\boldsymbol{S}^i(\boldsymbol{r})$. The latter are described by a classical Heisenberg Hamiltonian

$$\mathcal{H}_{ions} = -\sum_i \sum_{j \in v(i)} \frac{J_{ij}}{2} \boldsymbol{S}_i^i \cdot \boldsymbol{S}_j^i - \frac{K}{2} \sum_i \boldsymbol{S}_i^i \cdot \int \boldsymbol{f} d\boldsymbol{v} + g\mu_{\mathrm{B}} \sum_i \boldsymbol{S}_i^i \cdot \boldsymbol{B}_{ext}, \tag{4.10}$$

where $\boldsymbol{S}_i^i$ refers to the ions spin at the position $x = X_i$ and v_i denotes the nearest neighbours of the $i-th$ ion. The first term represents the exchange interaction between the ion spins. Because we only have one type of atom, we set $J_{ij} = J$. nickel is a ferromagnetic material, so the exchange constant J should only takes positive values, i.e. $J > 0$. The second term corresponds to the exchange interaction between ion and electron spins. The last term corresponds to the Zeeman interaction between ion spins and an external magnetic field.
The Hamiltonian (4.10) is equivalent to the Hamiltonian of an ensemble of N interacting spins evolving in an effective magnetic field

$$\mathcal{H}_{ions} = -\frac{J}{2} \sum_i \sum_{j \in v(i)} \boldsymbol{S}_i^i \cdot \boldsymbol{S}_j^i + g\mu_{\mathrm{B}} \sum_i \boldsymbol{S}_i^i \cdot \boldsymbol{B}_{eff}, \tag{4.11}$$

where $\boldsymbol{B}_{eff}$ is an effective magnetic field

$$\boldsymbol{B}_{eff} = \frac{K}{2g\mu_{\mathrm{B}}^2} \boldsymbol{M}(x) + \boldsymbol{B}_{ext}. \tag{4.12}$$

and $\boldsymbol{M}$ is the electron magnetic moment defined in Eq. (4.2). According to classical mechanics, the time-derivative of an angular moment is equal to the torque which acts on it

$$\hbar \frac{d\boldsymbol{S}_i^i}{dt} = -\boldsymbol{S}_i^i \times \frac{\partial \mathcal{H}_{ions}}{\partial \boldsymbol{S}_i^i}. \tag{4.13}$$

Equations (4.11) - (4.13) lead to the so-called Landau-Lifshitz equation for the ion spins :

$$\frac{d\boldsymbol{S}_i^i}{dt} = \frac{J}{\hbar}\boldsymbol{S}_i^i \times \sum_{j\in v(i)} \boldsymbol{S}_j^i - \gamma_g \boldsymbol{S}_i^i \times \boldsymbol{B}_{eff}, \tag{4.14}$$

where $\gamma_g = g\mu_B/\hbar$ is the gyromagnetic ratio of an electron.
Since the ion spin is a continuous quantity in the spin-Vlasov equation (4.8)-(4.9), it should also be the case in the Eq. (4.14). In the paper of Lakshmanan [152], a continuous version of the equation (4.14) is derived. In this case, $\boldsymbol{S}_i^i$ becomes a function of the position variable, i.e. $\boldsymbol{S}_i^i = \boldsymbol{S}^i(x_i)$.
In order to go from the discrete to the continuous case one should perform a Taylor development of the spin $\boldsymbol{S}_i(x)$ around the small parameter a, which represents the distance between nearest neighbours:

$$\boldsymbol{S}^i(x_{i+1}) = \boldsymbol{S}^i(x_i) + a\,\frac{\partial}{\partial x_i}\boldsymbol{S}^i(x_i) + \frac{a^2}{2}\,\frac{\partial^2}{\partial x_i^2}\boldsymbol{S}^i(x_i). \tag{4.15}$$

Injecting the expression (4.15) in (4.14), one obtains the continuous Landau-Lifshitz equation:

$$\frac{\partial \boldsymbol{S}^i(x)}{\partial t} = \frac{a^2 N_v J}{2\hbar}\left[\boldsymbol{S}^i(x) \times \frac{\partial^2}{\partial x^2}\boldsymbol{S}^i(x)\right] - \gamma_g \boldsymbol{S}^i(x) \times \boldsymbol{B}_{eff}. \tag{4.16}$$

This continuous spin description is only valid if the variation of the spin field $\boldsymbol{S}^i(x)$ is much larger than the inter-particle distance a. This can be easily shown by considering the linear response of both the discrete and continuous models.
In the continuous case, one obtains:

$$\frac{\partial S_x^i}{\partial t} = -\frac{a^2 J}{\hbar} S_0^i \frac{\partial^2}{\partial x^2} S_y^i, \qquad \frac{\partial S_y^i}{\partial t} = \frac{a^2 J}{\hbar} S_0^i \frac{\partial^2}{\partial x^2} S_x^i \quad \text{and} \quad \frac{\partial S_z^i}{\partial t} = 0, \tag{4.17}$$

where we have linearised the equation (4.16) around an homogeneous equilibrium state $\boldsymbol{S}^i(x) = S_0^i\,\widehat{e}_z$. Then, we write the solutions as plane waves

$$S_x^i(x,t) = \delta S_x^i \exp\left[i\left(kx - \omega t\right)\right] \quad \text{and} \quad S_y^i(x,t) = \delta S_y^i \exp\left[i\left(kx - \omega t\right)\right]. \tag{4.18}$$

We thus obtain the following system of algebraic equations

$$-i\omega\delta S_x^i = \frac{a^2 J}{\hbar} S_0^i k^2 \delta S_y^i, \qquad -i\omega\delta S_y^i = -\frac{a^2 J}{\hbar} S_0^i k^2 \delta S_x^i. \tag{4.19}$$

The latter have solutions only if the determinant is zero, i.e.

$$\omega = \frac{S_0^i J}{\hbar}\left(ak\right)^2. \tag{4.20}$$

In the case of a discrete system of spins, the dispersion relation is [145]:

$$\omega = \frac{2S_0^i J}{\hbar}\left[1-\cos\left(ka\right)\right]. \tag{4.21}$$

According to the equations (4.20 - 4.21), we clearly see that the continuous spin model is only valid if the typical excitation length k^{-1} is much larger than the inter-particle distance, i.e. $ka \ll 1$ such that $1-\cos\left(ka\right) \simeq (ak)^2$.
Finally by normalizing the continuous Landau-Lifshitz equation (4.16) to the absolute value of the spin S_0^i , one obtains

$$\frac{\partial \boldsymbol{S}^i(x)}{\partial t} = \frac{a^2 J S_0^i}{\hbar}\left[\boldsymbol{S}^i(x)\times\frac{\partial^2}{\partial x^2}\boldsymbol{S}^i(x)\right] - \gamma_g \boldsymbol{S}^i(x)\times\boldsymbol{B}_{eff}, \tag{4.22}$$

where $\boldsymbol{S}^i(x)$ is a unitary vector, J is the exchange constant (the number of nearest neighbours n_v is absorbed in the definition of J), a is the inter-particle distance ($a = 2r_s$) and $S_0^i = 0.270$ is the absolute value of the ion spins per atom. In the rest of this work, we shall use the Eq. (4.22) to model the ion spin dynamics.

4.1.3 Coupled electron and ion spin dynamics

In summary, Eqs. (4.8)-(4.9) and (4.22) constitute a self-consistent model that we will be used to describe the magnetization dynamics in ferromagnetic nickel films

$$\begin{cases}
\dfrac{\partial f_0}{\partial t} + v\cdot\partial_x f_0 - \dfrac{e}{m}\left[\boldsymbol{E}+\boldsymbol{v}\times\boldsymbol{B}\right]_x\partial_v f_0 - \dfrac{\mu_B}{m}\left(\partial_x B_i\right)\left(\partial_v f_i\right) + \dfrac{K S_0^i n_i(x)}{2m}\left[\left(\partial_x S_i^i\right)\left(\partial_v f_i\right)\right] = 0, \\
\dfrac{\partial f_k}{\partial t} + v\cdot\partial_x f_k - \dfrac{e}{m}\left[\boldsymbol{E}+\boldsymbol{v}\times\boldsymbol{B}\right]_x\partial_v f_k - \dfrac{\mu_B}{m}\left(\partial_x B_k\right)\left(\partial_v f_0\right) + \dfrac{K S_0^i n_i(x)}{2m}\left[\left(\partial_x S_k^i\right)\left(\partial_v f_0\right)\right] \\
\quad -\dfrac{e}{m}\left[\boldsymbol{B}\times\boldsymbol{f}\right]_k - \dfrac{K S_0^i n_i(x)}{\hbar}\left(\boldsymbol{f}\times\boldsymbol{S}^i\right)_k = 0, \\
\dfrac{\partial \boldsymbol{S}^i(x)}{\partial t} = \dfrac{a^2 J S_0^i}{\hbar}\left[\boldsymbol{S}^i(x)\times\dfrac{\partial^2}{\partial x^2}\boldsymbol{S}^i(x)\right] - \dfrac{\gamma_g K}{2g\mu_B^2}\boldsymbol{S}^i(x)\times\boldsymbol{M}, \\
\boldsymbol{E} = -\boldsymbol{\nabla}\phi \;;\; \boldsymbol{\nabla}^2\phi = \dfrac{e}{\epsilon_0}\left(\displaystyle\int f_0(x,v)dv - n_i\right), \\
\boldsymbol{B} = \boldsymbol{\nabla}\times\boldsymbol{A} \;;\; \boldsymbol{\nabla}^2\boldsymbol{A} = \dfrac{e}{\epsilon_0 c^2}\left(\displaystyle\int f_0(x,v)v dv - \dfrac{\hbar}{2m}\boldsymbol{\nabla}\times\int \boldsymbol{f}(x,v)dv\right).
\end{cases} \tag{4.23}$$

Here we did not include exchange-correlation effects and external fields. The latter can be easily incorporated by adding additional potentials and magnetic fields. The conservation properties of the Vlasov equation were discussed in the Sec. 2.2.5

but without being coupled to ion spins. The introduction of an exchange interaction between the electron and ion spins leads to an exchange of energy and angular momentum between the two spin populations. Therefore, the expression of the total energy and angular momentum, in the case of the fully coupled system (4.23), should be modified.
First, one has to define the ion energy. In the case of a one dimensional discrete system of spins, the ion energy is simply given by the Hamiltonian (4.11). However, in our case we consider a continuous system of spins. It is shown in Ref. [153] that in this case the energy is:

$$E = \frac{a^2 J (S_0^i)^2}{2} \int n_i(x) \frac{\partial \boldsymbol{S}^i}{\partial x} \cdot \frac{\partial \boldsymbol{S}^i}{\partial x} dx + \frac{K S_0^i}{2\mu_{\mathrm{B}}} \int n_i(x) \boldsymbol{S}^i \cdot \boldsymbol{M} dx + g\mu_{\mathrm{B}} \int n_i(x) \boldsymbol{S}^i \cdot \boldsymbol{B} dx, \tag{4.24}$$

where $\boldsymbol{B}$ is either an external or internal (created by the particles) magnetic field.
The first term corresponds to the exchange energy between the ion spins

$$E_{i-i} = \frac{a^2 J (S_0^i)^2}{2} \int n_i(x) \frac{\partial \boldsymbol{S}^i}{\partial x} \cdot \frac{\partial \boldsymbol{S}^i}{\partial x} dx. \tag{4.25}$$

The second term corresponds to the exchange energy between the electron spins and the ion spins

$$E_{i-e} = \frac{K S_0^i}{2\mu_{\mathrm{B}}} \int n_i(x) \boldsymbol{S}^i \cdot \boldsymbol{M} dx. \tag{4.26}$$

Finally the last term corresponds to the Zeeman interaction between the ion spins and an external magnetic field.
Thus, the total energy of the system (ions + electrons) is given by the sum of the electron energy (2.60) and the ion energy (4.24):

$$\begin{aligned} E_{tot} = {} & \frac{m}{2} \int \boldsymbol{v}^2 f_0 d\boldsymbol{v} d\boldsymbol{r} + \mu_{\mathrm{B}} \int \boldsymbol{f} \cdot \boldsymbol{B} d\boldsymbol{v} d\boldsymbol{r} + \frac{\epsilon_0}{2} \int \boldsymbol{E}^2 d\boldsymbol{r} + \frac{1}{2\mu_0} \int \boldsymbol{B}^2 d\boldsymbol{r} \\ & + \frac{a^2 J (S_0^i)^2}{2} \int n_i(x) \frac{\partial \boldsymbol{S}^i}{\partial x} \cdot \frac{\partial \boldsymbol{S}^i}{\partial x} dx + \frac{K S_0^i}{2\mu_{\mathrm{B}}} \int n_i(x) \boldsymbol{S}^i \cdot \boldsymbol{M} dx + g\mu_{\mathrm{B}} \int n_i(x) \boldsymbol{S}^i \cdot \boldsymbol{B} dx. \end{aligned} \tag{4.27}$$

It can be proven, using the Eqs. (4.23), that the total energy (4.27) is a conserved quantity, i.e. $dE_{tot}/dt = 0$.
The conservation law for the angular momentum should also be redefined. Let us write the total angular momentum as a sum of the ion and the electron angular momenta:

$$M_i^{tot} = -g\mu_{\mathrm{B}} \left[S_0^i \int n_i(x) S_i^i(x) dx + \frac{1}{g} \int f_i dx dv \right]. \tag{4.28}$$

	Electron time scales	Ion time scales
Electrostatic interaction Plasmon frequency	$\omega_p = e^2 n_e / (m\epsilon_0)$ $T_p = 0.25$ fs	-
Zeeman Interaction Precession frequency	$\omega_L = g\mu_B B/\hbar$ $\omega_L^{-1} = 35.4$ ps ($B = 1$ Tesla)	$\omega_L = g\mu_B B/\hbar$ $\omega_L^{-1} = 35.4$ ps ($B = 1$ Tesla)
Exchange interaction between the same particles	$\omega_x = \frac{e}{m}(3/8\pi)^{1/3}\left[(n_0+m_0)^{1/3} - (n_0-m_0)^{1/3}\right]$ $\omega_x^{-1} = 92$ fs	$\omega_J = a^2 k^2 J S_0^i/\hbar$ $\omega_J^{-1} = 3.8$ ps
Exchange interaction between different particles	$\omega_{e-K} = K n_0^i S_0^i/\hbar$ $\omega_{e-K}^{-1} = 22.2$ fs	$\omega_{i-K} = K\lvert\boldsymbol{M}\rvert/(2\mu_B\hbar)$ $\omega_{i-K}^{-1} = 89.9$ fs

TABLE 4.1: Different time scales present in the system (nickel film of thickness $L = 10$ nm).

It can be proven that the latter quantity is conserved, i.e. $d\mathcal{M}_i^{tot}/dt = 0$. However this relation is not true if we consider the spin-orbit interaction. Indeed, the latter can transfer orbital angular momentum into spin angular momentum and *vice versa*, see Eq. (2.61). Moreover, our model conserves separately the total amount of ion and electron spins[3]. For the ions, the form of the Landau-Lifshitz equation provides a local conservation of the norm of the spin

$$\frac{d}{dt}\left[\boldsymbol{S}^i(x)\cdot\boldsymbol{S}^i(x)\right] = 0. \tag{4.29}$$

For the electrons, since they are moving in the system, we do not have such a local conservation of the norm. We only have a global conservation

$$\frac{d}{dt}\left|\left(\int \boldsymbol{f}\,dvdx\right)\right|^2 = 0. \tag{4.30}$$

All those conservation properties will be used to validate our Vlasov simulations. Before going further, let us analyse the different time scales that are present in our model (4.23), see Table (4.1). The shortest time scale is given by the inverse of the plasma frequency (~ 1 fs). It corresponds to the electron motion due to electrostatic forces. For the ions such time scale does not exist, since they are supposed to be fixed during the motion of the electrons. The other time scales originate from magnetic interactions, such as the Zeeman interaction the exchange interactions. The ion and electron spin precession times are the same when one considers the action of an external magnetic field and are given by: $\omega_L = eB/m$. For reasonable magnetic fields (1 Tesla), this time is of few picoseconds. As we shall see in the next section, exchange interactions between the different spins can be viewed as a strong internal magnetic field ($10^3 - 10^4$ Tesla). Therefore one expects to have smaller time scales compare to the interaction with an external magnetic field. For the ions, the time scale corresponding to the exchange interaction between ions (with a coupling constant J) is given by $\omega_J = a^2 k^2 J S_0^i/\hbar$. Whereas the time scale

[3]This problem is intrinsically related to the fact that we work with a semiclassical approach.

corresponding to the exchange interaction between ions and electrons (with a coupling constant K) is given by $\omega_{i-K} = K|\boldsymbol{M}|/(2\mu_B\hbar)$. For the electrons, a first time scale corresponds to the exchange interactions between electron spins and is given by $\omega_x = \frac{e}{m}(3/8\pi)^{1/3}\left[(n_e+m_e)^{1/3} - (n_e-m_e)^{1/3}\right]$. A second time scale corresponds to the interaction of the electron spins with the local magnetic field created by the ion spins and is given by $\omega_{e-K} = Kn_0^iS_0^i/\hbar$.
Of course, all the previous time scales depend on the value of the exchange constants K and J. The latter will be determined in the next section. In the Tab. 4.1, we give the corresponding values of the different frequencies. We notice that the electron spin precession time that is due to the exchange interaction between the electron and the local ion spins is relatively small (~ 10 fs). Hence, it can have an influence on the ultra-fast magnetization dynamics. The other time scales are much larger, especially the ion time scales.

4.2 Ground state properties

In this section, we develop a method to construct the ground state of nickel thin films. In the first part we shall describe the self-consistent procedure to obtain the ground state of the spin-Vlasov model. Such methods were used in the past to obtain the electron ground state of non-magnetic metallic films [38, 144] and were compared to DFT results [49]. In a second part, we shall apply this method to find the electron and ion ground states of our films of nickel. Finally, this self-consistent method will be also applied to find the ground state of DMS (diluted magnetic semiconductors) in order to compare our results with Schrödinger-Poisson simulations [154].

4.2.1 Stationary state of the spin-Vlasov model

In the spinless case, the classical evolution equation for the electron distribution function f is given by:

$$\frac{\partial f}{\partial t} + \boldsymbol{v}\cdot\boldsymbol{\nabla} f - \frac{e}{m}(\boldsymbol{E}+\boldsymbol{v}\times\boldsymbol{B})\cdot\boldsymbol{\nabla}_{\boldsymbol{v}} f = 0, \tag{4.31}$$

which can be written as follows:

$$\frac{\partial f}{\partial t} = \{H, f\} + \frac{e}{m}\epsilon_{ijk}v_iB_j\frac{\partial f}{\partial v_k}, \quad \text{with} \quad H = \frac{m}{2}\boldsymbol{v}^2 - e\phi, \tag{4.32}$$

where ϵ_{ijk} is the Levi-civita tensor and where we introduced the Poisson bracket:

$$\{A(\boldsymbol{r},\boldsymbol{p}), B(\boldsymbol{r},\boldsymbol{p})\} = \frac{\partial A}{\partial x_i}\frac{\partial B}{\partial p_i} - \frac{\partial A}{\partial p_i}\frac{\partial B}{\partial x_i}. \tag{4.33}$$

By definition a stationary state is characterized by the following identity: $\partial_t f^{stat} = 0$. The first term on the right part of the Eq. (4.32) is zero if f^{stat} is a function of H. Indeed, one has:

$$\{H, g(H)\} = \sum_i \frac{\partial H}{\partial x_i}\frac{\partial g(H)}{\partial p_i} - \frac{\partial H}{\partial p_i}\frac{\partial g(H)}{\partial x_i} = \sum_i \frac{\partial H}{\partial x_i}\frac{\partial H}{\partial p_i}\frac{\partial g(H)}{\partial H} - \frac{\partial H}{\partial p_i}\frac{\partial H}{\partial x_i}\frac{\partial g(H)}{\partial H} = 0 \tag{4.34}$$

The second term in Eq. (4.32) is zero if f^{stat} is isotropic in the velocity space, i.e. $f^{stat}(x, v_x, v_y, v_z) = f^{stat}(x, |\boldsymbol{v}|)$. The second condition is automatically satisfied if the first condition holds. Thus we conclude that $f^{stat} = f^{stat}(H)$ is a stationary state. To satisfied the Pauli exclusion principle we write ${}^{stat}f$ as a Fermi-Dirac distribution function:

$$f^{stat} = n_0^i \mathcal{F}_{\mathcal{D}}(H) = n_0^i \mathcal{F}_{\mathcal{D}}\left(\frac{m}{2}\boldsymbol{v}^2 - e\phi\right), \tag{4.35}$$

where the electrostatic potential ϕ is derived self consistently from the Poisson equation:

$$\boldsymbol{\nabla}^2\phi = \frac{e}{\epsilon_0}\left(\int f^{stat} d\boldsymbol{v} - n_i\right) \tag{4.36}$$

and $\mathcal{F}_{\mathcal{D}}$ is the Fermi-Dirac distribution function

$$\mathcal{F}_{\mathcal{D}}(x) = \left[1 + \exp\left(\frac{x-\mu}{k_{\mathrm{B}}T}\right)\right]^{-1}, \tag{4.37}$$

with μ the chemical potential.
In presence of the spin, the situation is a bit different and we have to find the ground state of the spin-Vlasov equations:

$$\frac{\partial f_0}{\partial t} + \boldsymbol{v}\cdot\boldsymbol{\nabla}_{\boldsymbol{r}} f_0 - \frac{e}{m}(\boldsymbol{E} + \boldsymbol{v}\times\boldsymbol{B})\cdot\boldsymbol{\nabla}_{\boldsymbol{v}} f_0 - \frac{\mu_{\mathrm{B}}}{m}\sum_i \boldsymbol{\nabla}_{\boldsymbol{r}} B_i \cdot \boldsymbol{\nabla}_{\boldsymbol{v}} f_i = 0, \tag{4.38}$$

$$\frac{\partial f_i}{\partial t} + \boldsymbol{v}\cdot\boldsymbol{\nabla}_{\boldsymbol{r}} f_i - \frac{e}{m}\left[(\boldsymbol{E} + \boldsymbol{v}\times\boldsymbol{B})\cdot\boldsymbol{\nabla}_{\boldsymbol{v}} f_i - (\boldsymbol{f}\times\boldsymbol{B})_i\right] - \frac{\mu_{\mathrm{B}}}{m}\boldsymbol{\nabla}_{\boldsymbol{r}} B_i \cdot \boldsymbol{\nabla}_{\boldsymbol{v}} f_0 = 0, \tag{4.39}$$

where the electric and the magnetic fields are, respectively, given by the Poisson and the Ampere equations

$$\boldsymbol{E} = -\boldsymbol{\nabla}\phi \;\; ; \;\; \boldsymbol{\nabla}^2\phi = \frac{e}{\epsilon_0}\left(\int f_0 d\boldsymbol{v} - n_i\right), \tag{4.40}$$

$$\boldsymbol{B} = \boldsymbol{\nabla}\times\boldsymbol{A} \;\; ; \;\; \boldsymbol{\nabla}^2\boldsymbol{A} = \frac{e}{\epsilon_0 c^2}\left(\int f_0 \boldsymbol{v} d\boldsymbol{v} - \frac{\hbar}{2m}\boldsymbol{\nabla}\times\int \boldsymbol{f} d\boldsymbol{v}\right). \tag{4.41}$$

On the basis of the Eq. (4.32), it is straightforward to see that if we search stationary states for which the spins are polarized in the same direction (here and in the following it will be the z direction) and which are isotropic in the velocity space, then

the above spin-Vlasov equations can be written

$$\frac{\partial f_0}{\partial t} = \left\{H^{\uparrow\uparrow}, f^{\uparrow\uparrow}\right\} + \left\{H^{\downarrow\downarrow}, f^{\downarrow\downarrow}\right\} \quad \text{and} \qquad \frac{\partial f_z}{\partial t} = \left\{H^{\uparrow\uparrow}, f^{\uparrow\uparrow}\right\} - \left\{H^{\downarrow\downarrow}, f^{\downarrow\downarrow}\right\}, \tag{4.42}$$

with $H^{\uparrow\uparrow}$ and $H^{\downarrow\downarrow}$ are defined as follows:

$$H^{\uparrow\uparrow} = \frac{m}{2}\boldsymbol{v}^2 - e\phi + \mu_{\mathrm{B}} B_z, \quad H^{\downarrow\downarrow} = \frac{m}{2}\boldsymbol{v}^2 - e\phi - \mu_{\mathrm{B}} B_z. \tag{4.43}$$

Eq. (4.42) implies that $f^{\uparrow\uparrow}$ should be a function of $H^{\uparrow\uparrow}$ and $f^{\downarrow\downarrow}$ a function of $H^{\downarrow\downarrow}$. Therefore the stationary solutions are given by

$$f_0^{stat} = \alpha^{\uparrow}\left[\mathcal{F}_{\mathcal{D}}(H^{\uparrow\uparrow}) + \mathcal{F}_{\mathcal{D}}(H^{\downarrow\downarrow})\right] \quad \text{and} \quad f_z^{stat} = \alpha^{\downarrow}\left[\mathcal{F}_{\mathcal{D}}(H^{\uparrow\uparrow}) - \mathcal{F}_{\mathcal{D}}(H^{\downarrow\downarrow})\right]. \tag{4.44}$$

The coefficients $\alpha^{\uparrow}$ and $\alpha^{\downarrow}$ are determined by imposing the good normalization at $T = 0$ and in the case of a non interacting system. The free electron gas model predicts the following value for the spin-up and spin-down densities in presence of an external and constant magnetic field [155]:

$$n^{\uparrow}(T=0) = \frac{1}{6\pi^2}\left(E_{\mathrm{F}} - \mu_{\mathrm{B}} B\right)^{3/2}, \quad n^{\downarrow}(T=0) = \frac{1}{6\pi^2}\left(E_{\mathrm{F}} + \mu_{\mathrm{B}} B\right)^{3/2}. \tag{4.45}$$

with E_{F} the Fermi energy of the system, $E_{\mathrm{F}} = \hbar^2(3\pi n_0^i)^{2/3}/(2m)$.
In our case, the spin-up and the spin-down densities are:

$$n^{\uparrow} = \alpha^{\uparrow}\int \mathcal{F}_{\mathcal{D}}\left(\frac{m}{2}\boldsymbol{v}^2 + \mu_{\mathrm{B}} B\right) d\boldsymbol{v} = 4\pi\alpha^{\uparrow}\int_0^{\infty} \frac{v^2 dv}{1 + \exp\left[\left(\frac{m}{2}v^2 + \mu_{\mathrm{B}} B - \mu\right)/k_{\mathrm{B}}T\right]}, \tag{4.46}$$

$$n^{\downarrow} = \alpha^{\downarrow}\int \mathcal{F}_{\mathcal{D}}\left(\frac{m}{2}\boldsymbol{v}^2 - \mu_{\mathrm{B}} B\right) d\boldsymbol{v} = 4\pi\alpha^{\downarrow}\int_0^{\infty} \frac{v^2 dv}{1 + \exp\left[\left(\frac{m}{2}v^2 - \mu_{\mathrm{B}} B - \mu\right)/k_{\mathrm{B}}T\right]}. \tag{4.47}$$

In the limit $T \to 0$, one obtains

$$n^{\uparrow}(T=0) = \frac{4\pi}{3}\left(\frac{2}{3}\right)^{3/2}\alpha^{\uparrow}\left(E_{\mathrm{F}} - \mu_{\mathrm{B}} B\right)^{3/2}, \quad n^{\downarrow}(T=0) = \frac{4\pi}{3}\left(\frac{2}{3}\right)^{3/2}\alpha^{\uparrow}\left(E_{\mathrm{F}} + \mu_{\mathrm{B}} B\right)^{3/2}. \tag{4.48}$$

Comparing Eqs. (4.45) and (4.48), we deduce that

$$\alpha^{\uparrow} = \alpha^{\downarrow} = \left(\frac{m}{2\pi\hbar}\right)^3. \tag{4.49}$$

We can also include exchange and correlations in the stationary state. For a collinear system (in the z direction) we have to make the following transformation (see Sec.

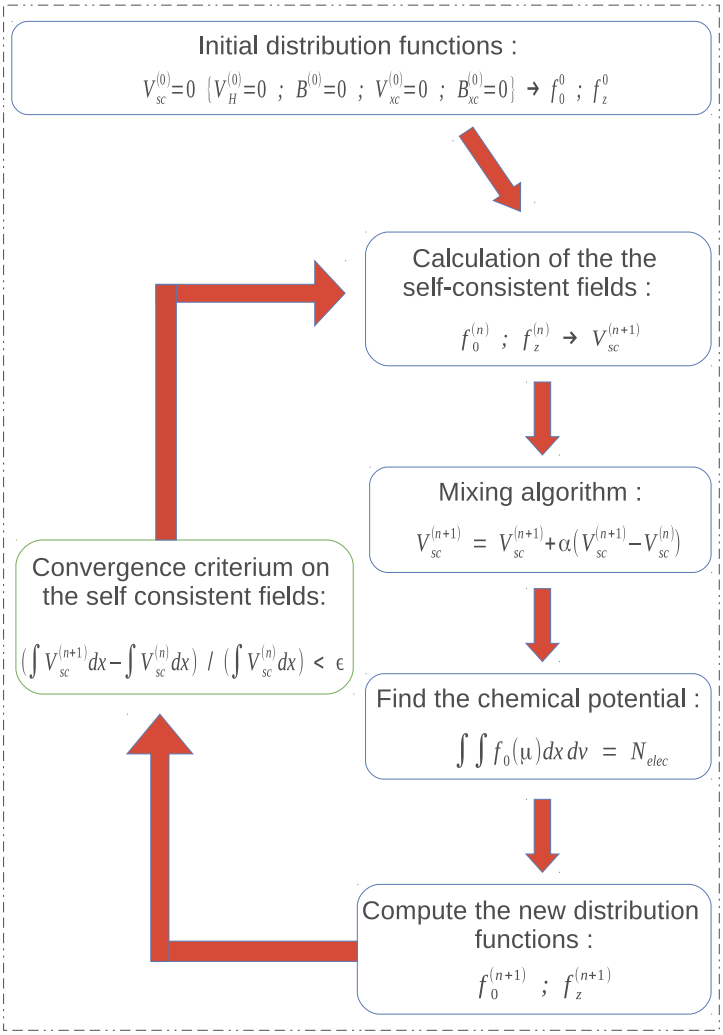

FIGURE 4.4: Description of the procedure to find the self consistent stationary states of the spin-Vlasov equations (2.54)-(2.55) combined with the Poisson and Ampere equations (4.40)-(4.41). The index $^{(n)}$ refers to the quantities at the $n-th$ step. The parameter α is a mixing parameter and the parameter ϵ is a convergence parameter.

2.2.4 with $\mathcal{U} = \mathbb{1}$) :

$$V \mapsto V + V_{XC} \quad \text{and} \quad B_z \mapsto B_z + \frac{(B_{XC})_z}{\mu_B}, \tag{4.50}$$

where the expression of V_{XC} and B_{XC} are given in Eq. (2.50).
Finally, the stationary states f_0^{stat} and f_z^{stat} read as:

$$f_0^{stat} = \left(\frac{m}{2\pi\hbar}\right)^3 \Big[\mathcal{F}_{\mathcal{D}}\left(\frac{m}{2}\boldsymbol{v}^2 - e\phi + V_{XC} + \mu_{\mathrm{B}}\left(B + B_{XC}\right)_z\right) + \mathcal{F}_{\mathcal{D}}\left(\frac{m}{2}\boldsymbol{v}^2 - e\phi + V_{XC} - \mu_{\mathrm{B}}\left(B + B_{XC}\right)_z\right)\Big], \tag{4.51}$$

$$f_z^{stat} = \left(\frac{m}{2\pi\hbar}\right)^3 \Big[\mathcal{F}_{\mathcal{D}}\left(\frac{m}{2}\boldsymbol{v}^2 - e\phi + V_{XC} + \mu_{\mathrm{B}}\left(B + B_{XC}\right)_z\right) - \mathcal{F}_{\mathcal{D}}\left(\frac{m}{2}\boldsymbol{v}^2 - e\phi + V_{XC} - \mu_{\mathrm{B}}\left(B + B_{XC}\right)_z\right)\Big]. \tag{4.52}$$

This is the general form of the electron ground states. In practice, since in the dynamics we will only work with a $2D$ distribution function, the Fermi-Dirac function reads:

$$\mathcal{F}_{\mathcal{D}}{}^{\pm} = \frac{2\pi k_{\mathrm{B}}T}{m}\left(\frac{m}{2\pi\hbar}\right)^3 \ln\left[1 + \exp\left(-\frac{1}{k_{\mathrm{B}}T}\left(\frac{m}{2}v^2 - e\phi + V_{XC} \pm \mu_{\mathrm{B}}\left(B + B_{XC}\right)_z - \mu(T)\right)\right)\right], \tag{4.53}$$

where $v \equiv v_x$ is the longitudinal velocity. Eq. (4.53) was obtained by integrating the $3D$ Fermi-Dirac function (4.37) over the transversal velocities (v_y, v_z). To find the ground state of the spin-Vlasov model is a self-consistent problem that we need to solve iteratively. Indeed in order to determine f_0 and f_z, we need to find the Hartree potential ϕ and the magnetic field B which both depend on f_0 and f_z via the source terms in the Poisson (4.40) an Ampere (4.41) equations. The same situation holds with the exchange-correlation functions V_{XC} and B_{XC} which both depend on the electron density and magnetization, see Eqs. (2.38)-(2.39).
Then, to determine the electron ground state of the system we will use the following strategy. First we start with an initial guess of the distribution functions f_0 and f_z. We chose to start with constant distribution functions which correspond homogeneous ion densities. Then we calculate the self-consistent fields with the Poisson equation, the Ampere equation and the exchange-correlation potentials. The Poisson and the Ampere equations are solved with Dirichlet boundary conditions by imposing that ϕ and $\boldsymbol{A}$ vanish at the border of the simulation box. The algorithm is based on a finite difference scheme and can be found in Ref. [156]. Then, in order to provide the convergence of the procedure, we have to use a mixing algorithm. We have to mix the old self-consistent field with the new one as follows:

$$V_{sc}^{(n+1)} = V_{sc}^{(n)} + \alpha\left(V_{sc}^{(n+1)} - V_{sc}^{(n)}\right), \tag{4.54}$$

where $V_{sc}^{(n)} = V_{\mathrm{H}}^{(n)} + V_{XC}^{(n)} \pm \mu_{\mathrm{B}}\left(B^{(n)} + B_{XC}^{(n)}\right)$ and $\alpha = 0.01 - 0.001$ is a mixing parameter. This procedure does not conserve the total number of particles. Therefore, at each step, one has to fix the chemical potential in such a way that the total number of electrons in our system is preserved. This problem is implicit because μ is the

fixed point of the following equation: $\int f_0(\mu)\, dxdv = N_{elec}$. Then we obtain our new distribution functions. At this step we defined a global criterion of convergence for the self-consistent potentials

$$\frac{\int V_{sc}^{(n+1)} dx - \int V_{sc}^{(n)} dx}{\int V_{sc}^{(n)} dx} < \epsilon, \tag{4.55}$$

where ϵ is the convergence parameter (usually we took $\epsilon = 10^{-10}$). If the identity (4.55) is not satisfied, we repeat the procedure again until it is satisfied. All the procedure described above is summarized in Fig. 4.4.

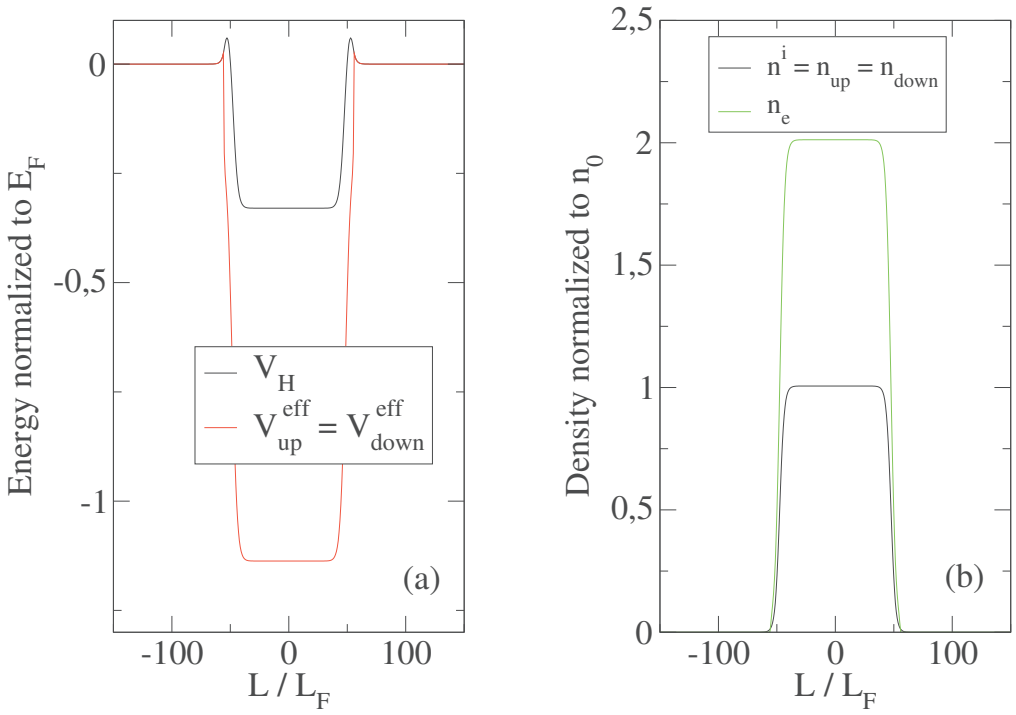

FIGURE 4.5: Ground state of an electron gas ($4s^2$) confined in a metallic films (nickel), with $L = 100$ L_F, $\sigma = 1$ L_F, and $T = 300$ K. In figure (a), we plot the Hartree potential (black curve), the effective potential acting on spin-up and spin-down (red curve). In figure (b), we plot the electron density (green curve), the ion density and the spin-up and spin-down electron densities (black curve).

Before studying the case of nickel films, for which one should introduce ion spins, let us study the self-consistent ground state of a confined electron gas. For the ion density, we took the density of nickel, i.e. $r_s = 2.6$ a.u., and for the electron density we took the double of the ion density. This corresponds to the situation where we only treat the $4s^2$ electrons and consider the $3d$ electrons as core electrons. We apply the procedure defined above, with one exception, we start with an initial spin polarized state. This allows us to see if exchange-correlation effects are strong enough to create a spin-polarized ground state.

In Fig. 4.5, we plot the ground state obtained with the following parameters: $L = 100$ L_F, $\sigma = 1$ L_F and a temperature of $T = 300$ K. We notice that the ground state

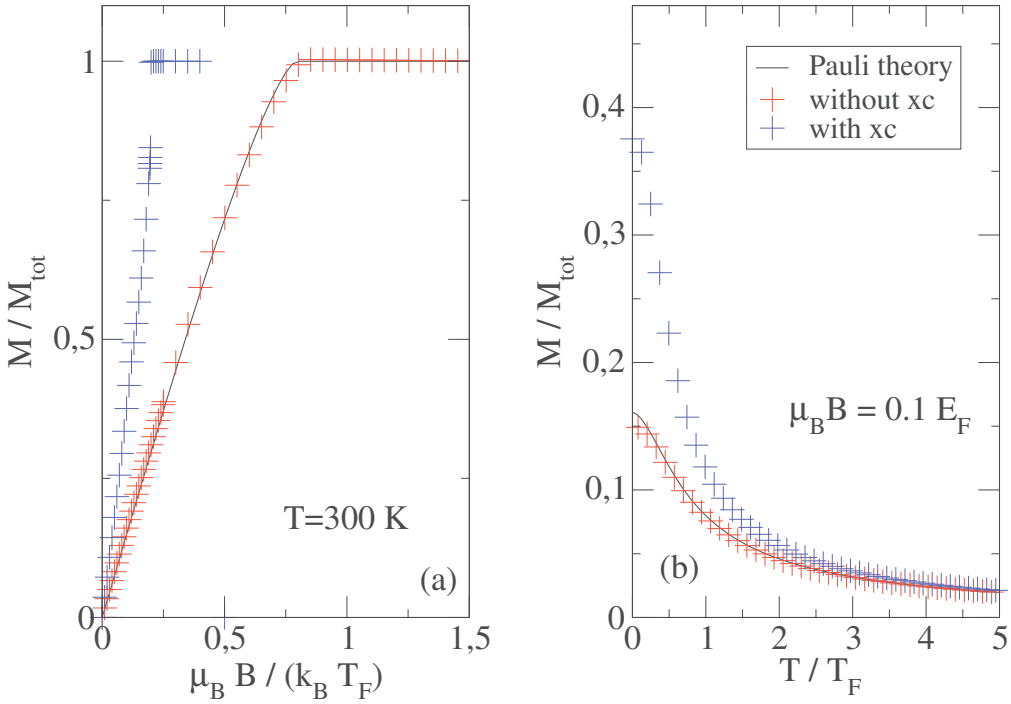

FIGURE 4.6: Magnetic properties of the ground state of a confined electron gas ($4s^2$) in metallic film (nickel) with $L = 100$ L_F and $\sigma = 1$ L_F. In figure (a), we plot the normalized spin magnetization at $T = 300$ K as a function of the applied magnetic field. We sketch three cases, the Pauli paramgnetism theory (black curve), the case without exchange-correlation effects (red cross) and the case with exchange-correlation effects (blue cross). In the right part, the same three cases are sketched but with a fixed magnetic field ($B = 0.1$ E_F/μ_B) and as a function of the temperature.

of the system is not magnetized because the density of spin-up and spin-down electrons are equal. They are actually not exactly equal but the difference is too small to create an appreciable magnetic state. We also notice that the Hartree potential is much smaller than the exchange-correlation potential, this was also observed for Sodium films [49]. Therefore we conclude that in these conditions of density and temperature, the only presence of the exchange-correlation effects is too weak to create a spin polarized ground state. However, if we apply a sufficiently strong external magnetic field , it is possible to create a magnetic ground state. This situation is sketched in Fig. 4.6, where we plot the magnetization (normalized to the maximum magnetization $M_{tot} = -\mu_B N_{el}$) as a function of the external magnetic field with and without exchange-correlation effects and at constant temperature $T = 300$ K. We notice that at this temperature, we need an extremely strong magnetic field (of the order of $10^3 - 10^4$ Tesla) to have a complete spin polarized electron gas. These results are well known, since in the Pauli theory of paramagnetism [155] the spin

magnetization can be written as follows:

$$\begin{aligned} M_z &= -\mu_{\mathrm{B}}\left(n^{\uparrow}-n^{\downarrow}\right), \\ &= -\frac{\mu_{\mathrm{B}}}{2\pi^2}\left(\frac{2m}{\hbar^2}\right)^{3/2}\left[\int d\epsilon \frac{\sqrt{\epsilon-\mu_{\mathrm{B}}B}}{1+\exp\left[\left(\epsilon-\mu\right)/k_{\mathrm{B}}T\right]} - \int d\epsilon \frac{\sqrt{\epsilon+\mu_{\mathrm{B}}B}}{1+\exp\left[\left(\epsilon-\mu\right)/k_{\mathrm{B}}T\right]}\right]. \end{aligned} \tag{4.56}$$

The Pauli theory holds for an homogeneous ensemble of non-interacting electrons subjected to an external constant magnetic field. The formula (4.56) is plotted on the figure 4.6. Electrostatic and magneto-static interactions or finite size effects do not modify the magnetic properties of the free electron gas. However, we notice that the exchange-correlation has an effect. This can be explained by the fact that a part of the exchange-correlation interactions can be written as a magnetic field, see Eq. (2.50). The latter is added to the external magnetic field to increase the spin polarization. In the right panel of the figure 4.6, we plot the normalized magnetization as a function of the temperature and with a constant external magnetic field $B_{ext} = 0.1\ \mathrm{E_F}$. Again, the case without exchange-correlation effects is in perfect agreement with the Pauli theory of paramagnetism and the effects of exchange and correlations are to increase the spin polarization of the system.
Thus we conclude that in the absence of strong external magnetic fields, we cannot have a significant magnetization of the nickel films. We clearly see that it is impossible with our Vlasov model to treat all the electrons on the same footing. Of course, nickel is a ferromagnetic material, so it possesses a magnetic moment at room temperature. There is only one type of interaction which is capable of producing such a large internal magnetic field, it is the exchange interaction [149]. This answer clearly the question that we asked at the beginning of this chapter, namely if we should make a distinction between the $4s$ and the $3d$ electrons. The answer is that we should, because in order to have an initial magnetic state, one needs to introduce ion spins and also exchange interactions between ion and electron spins. The corresponding ground state will be constructed in the next section.

4.2.2 Ferromagnetic nickel films

As it was explained in the previous sections, we should use the set of Eqs. (4.23) to study the magnetization dynamics in nickel films. The way to determine the ground state of the Vlasov model was detailed in Sec. 4.2.1. Now we are going to explain how to determine the magnetic ground state of the ions. We expect that this ground state depends on the temperature because, since nickel is a ferromagnetic material, the total magnetization should vanish at the Curie temperature ($T_c = 631\ \mathrm{K}$ for

nickel). The Hamiltonian for the ions is given by Eq. (4.11):

$$\mathcal{H}_{ions} = -\sum_i \boldsymbol{S}_i^i \cdot \left[\frac{J}{2} \sum_{j \in v(i)} \boldsymbol{S}_j^i - g\mu_{\mathrm{B}} \boldsymbol{B}_{eff} \right]. \tag{4.57}$$

We will use the tools of statistical physics to find the ground state of the above Hamiltonian. For interacting systems the problem is generally difficult to solve, but in our case we will work in the mean field approximation. The usual way to perform a mean field calculation is to rewrite the spin vector as follows:

$$\boldsymbol{S}_i^i \equiv \langle \boldsymbol{S}_i^i \rangle + \left(\boldsymbol{S}_i^i - \langle \boldsymbol{S}_i^i \rangle \right), \tag{4.58}$$

where the last term represents the deviation from the equilibrium, that is supposed to be small.
Neglecting second order terms we obtain:

$$\begin{aligned} \mathcal{H}_{ions} &= -\frac{J}{2} \sum_i \sum_{j \in v(i)} \Big(- \langle \boldsymbol{S}_i^i \rangle \cdot \langle \boldsymbol{S}_j^i \rangle + 2 \boldsymbol{S}_i^i \cdot \langle \boldsymbol{S}_j^i \rangle \Big) + \sum_i g\mu_{\mathrm{B}} \boldsymbol{S}_i^i \cdot \boldsymbol{B}_{eff}, \\ &= \frac{J}{2} \sum_i \sum_{j \in v(i)} \langle \boldsymbol{S}_i^i \rangle \cdot \langle \boldsymbol{S}_j^i \rangle - \sum_i \boldsymbol{S}_i^i \cdot \Big(J \sum_{j \in v(i)} \langle \boldsymbol{S}_j^i \rangle - g\mu_{\mathrm{B}} \boldsymbol{B}_{eff} \Big), \end{aligned} \tag{4.59}$$

where the second term in (4.59) (inside the parenthesis) is the molecular field. A second approximation consists to neglect the fluctuations of the molecular field, i.e. if j is near i then $\langle \boldsymbol{S}_j^i \rangle = \langle \boldsymbol{S}_i^i \rangle$. Within the framework of this approximation, the Hamiltonian of the ions becomes :

$$\mathcal{H}_{ions} = \frac{JN_v}{2} \sum_i \langle \boldsymbol{S}_i^i \rangle^2 - \sum_i \boldsymbol{S}_i^i \cdot \left(JN_v \langle \boldsymbol{S}_i^i \rangle - g\mu_{\mathrm{B}} \boldsymbol{B}_{eff} \right), \tag{4.60}$$

where we took the sum only between the N_v nearest neighbours. Then we can use the tools of statistical physics to determine $\langle \boldsymbol{S}_i^i \rangle \equiv \langle \boldsymbol{S}^i \rangle$. Since the stationary state is collinear, we adopt a collinear approach for which the spins are only along the z direction, i.e. $\boldsymbol{S}^i = S_0^i \, \widehat{e}_z$. Here the spins are not interacting directly together but rather with an effective magnetic field. Then the partition function factors out as a product on N single partition functions:

$$\mathcal{Z} = z^N = \left[\exp\left(-\frac{N_v J}{2 k_{\mathrm{B}} T} \langle S_z^i \rangle^2 \right) \sum_{S_z^i = -S_0^i}^{S_0^i} \exp\left(\frac{S_z^i}{k_{\mathrm{B}} T} \left(JN_v \langle S_z^i \rangle - g\mu_{\mathrm{B}} B_{eff} \right) \right) \right]^N. \tag{4.61}$$

Using geometrical sums, we are able to demonstrate the following identity:

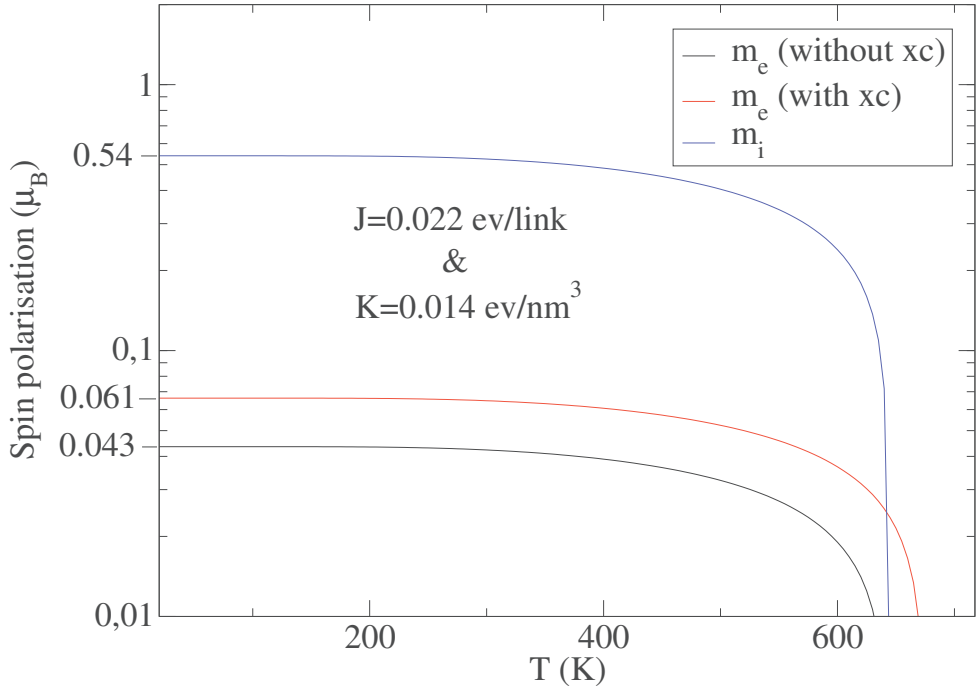

FIGURE 4.7: Magnetization of nickel films with $L = 100$ L_F and $\sigma = 1$ L_F as a function of the temperature. We used $J = 0.022$ eV/link and $K = 0.014$ eV.nm^3 for the exchange constants. We plot the magnetic moment of ions (blue curve), the magnetic moment of electrons without (black curve) and with (red curve) exchange-correlation effects as a function of the temperature.

$$\sum_{S_z=-S}^{S} \exp\left(AS_z\right) = \frac{\sinh\left(A(S+1/2)\right)}{\sinh\left(A/2\right)}. \tag{4.62}$$

Therefore, the one particle partition function writes:

$$z = \exp\left(-\frac{N_v J}{2k_B T}\langle S_z^i\rangle^2\right) \frac{\sinh\left(\frac{2S_0^i+1}{2k_B T}\left(JN_v\langle S_z^i\rangle - g\mu_B B_{eff}\right)\right)}{\sinh\left(\frac{1}{2k_B T}\left(JN_v\langle S_z^i\rangle - g\mu_B B_{eff}\right)\right)} \tag{4.63}$$

and the associated free energy is simply given by:

$$\mathcal{F} = -k_B T \ln z = \frac{N_v J}{2}\langle S_z^i\rangle^2 - k_B T \ln\left[\frac{\sinh\left(\frac{2S_0^i+1}{2k_B T}\left(JN_v\langle S_z^i\rangle - g\mu_B B_{eff}\right)\right)}{\sinh\left(\frac{1}{2k_B T}\left(JN_v\langle S_z^i\rangle - g\mu_B B_{eff}\right)\right)}\right]. \tag{4.64}$$

At equilibrium the value of $\langle S_z^i\rangle$ should minimize the free energy, i.e. $\frac{\partial \mathcal{F}}{\partial \langle S_z^i\rangle} = 0$. After some calculations, the solutions is given by:

$$\langle S_z^i\rangle = S_0^i \mathcal{B}_S\left(\beta S h_{eff}\right). \tag{4.65}$$

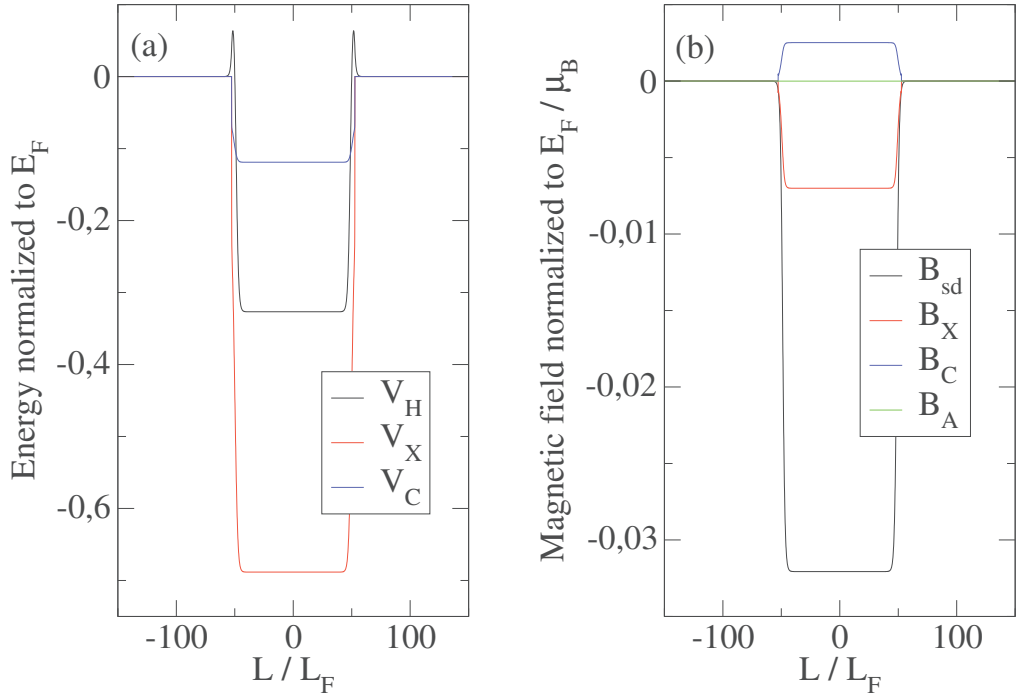

FIGURE 4.8: Self-consistent potentials and magnetic fields of nickel films with $L = 100$ $\mathrm{L_F}$, $\sigma = 1$ $\mathrm{L_F}$ and $T = 300$ K. In figure (a), we plot the Hartree potential (black curve), the exchange potential (red curve) and the correlation potential (blue curve). In figure (b), we plot the ion magnetic field (black curve), the exchange magnetic field (red curve), the correlation magnetic field (blue curve) and the Ampere magnetic field (green curve).

where $\mathcal{B}_S$ is the $S-th$ Brillouin function and $h_{eff} = -\frac{K}{2\mu_B} M_z\,(x) + JN_v\langle S_z^i\rangle$.
Eq. (4.65) will be used to determine the magnetic ground state of the ions. One notices that this ground state depends on the electron spin polarization through the quantity $M_z(x)$. The inverse is also true since both spins are interacting together with an exchange interaction. Therefore the electron and the ion ground state should be found together in a self-consistent fashion. Moreover we should also find a way to adjust the two exchange constants K and J. The latter are the two external parameters of our model. We will use the following procedure. First we set the spin of the ions to $S_0^i = 0.270$ then for low temperatures (compared to T_c) and for reasonable values of J the localized magnetization is always maximal, i.e. $\langle S_z^i\rangle = S_0^i\,\widehat{e}_z$. So the magnetization of the electron gas can be adjust to $M_z/n_0^i = 0.066\ \mu_B$ by playing with the coupling constant K. When this is done, we can increase the temperature and adapt the parameter J to obtain the correct Curie temperature.
In Fig. 4.7, we sketch the magnetization of the ions and the electrons in nickel films as a function of temperature. We used the following parameters: $L = 100$ $\mathrm{L_F}$ and $\sigma = 1$ $\mathrm{L_F}$ and we noticed by performing several simulations with different L and σ, that the results do not depend on the size of the film. This is expected since the magnetic properties of nickel originate from the bulk. We took the following values for the exchange constants: $\boldsymbol{J \equiv J_{ref} = 0.022\ \mathrm{eV}}$ and $\boldsymbol{K \equiv K_{ref} = 0.014\ \mathrm{eV.nm^3}}$

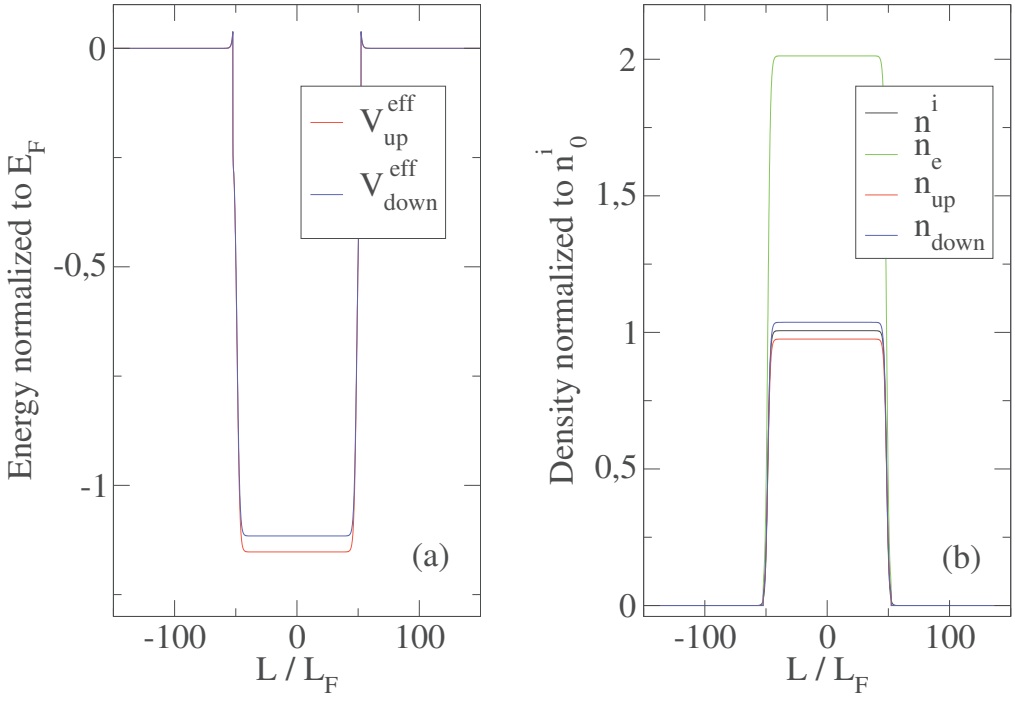

FIGURE 4.9: In figure (a), we plot the effective potentials for the spin-up (blue curve) and for the spin-down (red curve) corresponding to the self consistent fields given in Fig. 4.8. In figure (b), we plot the associated densities, the ion density (black curve), the electron density (green curve) the spin-up density (blue curve) and spin-down (red curve) densities.

to recover the correct spin magnetic moments at zero temperature, i.e. $M_z^i = 0.54\ \mu_B$ and $M_z/n_0^i = 0.066\ \mu_B$, and the correct Curie temperature $T_c = 631$ K. Those values of J and K will be set up as our reference values for both exchange constants in the rest of this work.

In Figs. 4.8 and 4.9, we plot the details of the electron ground states at 300 K. As in the previous section we notice that the exchange potential is the strongest one. The strongest magnetic field is also the magnetic field corresponding to the exchange interaction between ions and electrons, it is about 6×10^3 Tesla. The exchange and the correlation magnetic fields are slightly smaller but still strong. We notice that the correlation magnetic field is positive compared to the two other magnetic fields, which means that the correlations act as anti-ferromagnetic interactions between the electron spins compare to the exchange which act as a ferromagnetic interaction.

In the presence of ion spins, the exchange-correlation potentials are much larger than without ion spins. This is due to the local magnetic field created by the exchange interaction between ions and electrons. Its impact is to enhance the spin polarization of the electrons and thus the self-consistent exchange-correlation fields.

The ground state can also be analysed with the distribution functions $f_\uparrow$ and $f_\downarrow$ instead of f_0 and f_z. They are defined as follows:

$$f_\uparrow^{stat} = \left(\frac{m}{2\pi\hbar}\right)^3 \mathcal{F}_{\mathcal{D}}(H^{\uparrow\uparrow}) \quad \text{and} \quad f_\downarrow^{stat} = \left(\frac{m}{2\pi\hbar}\right)^3 \mathcal{F}_{\mathcal{D}}(H^{\downarrow\downarrow}). \tag{4.66}$$

Therefore the the spin-up and spin-down electron evolves, respectively, in the effective potentials V_{up}^{eff} and V_{down}^{eff}. Both of them are sketched in Fig. 4.9, where we notice a difference of 0.05 eV between them. This difference is exactly due to the Zeeman effect and the magnetic exchange interactions, which act with a positive sign on the spin "up" and with a negative sign on the spin "down". In the same figure, we have also plotted the corresponding spin densities. The latter exhibit clearly the magnetic properties of the electron ground state.

4.2.3 DMS and RKKY model

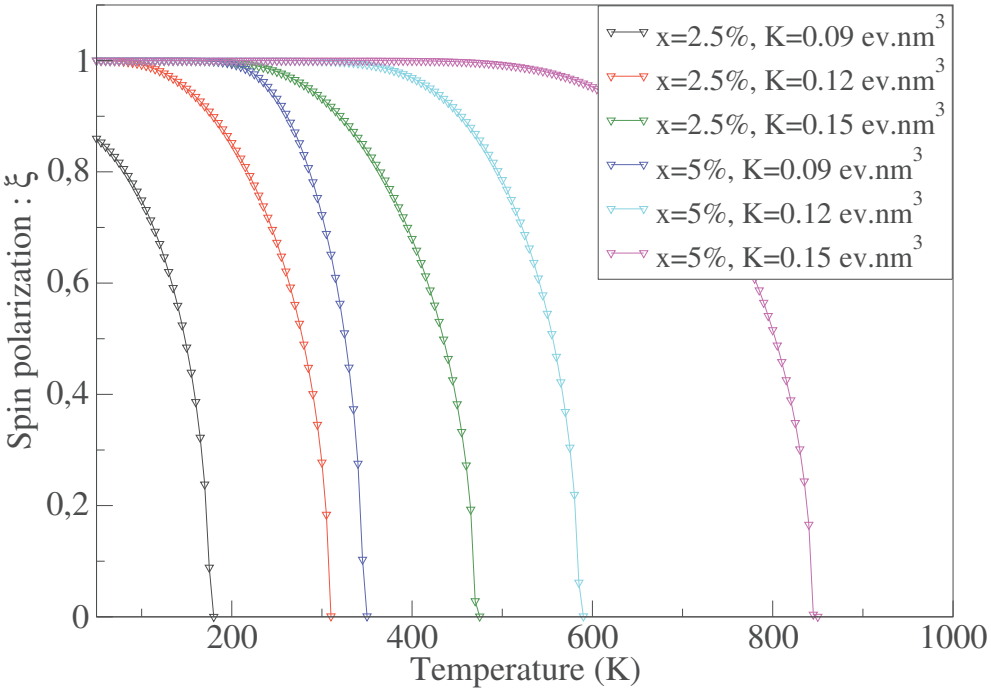

FIGURE 4.10: Spin polarization as a function of temperature for ZMnO. Different parameters are used, x is the proportion of impurities ($x = 2.5\%$ or 5%) and K is the exchange constant between impurities and holes ($K = 0.09$ eV.nm^3, $K = 0.12$ eV.nm^3 or $K = 0.15$ eV.nm^3).

Before studying the magnetization dynamics in nickel films, we will apply the previous methodology on a case studied in the literature: ZnMnO. The latter belongs to the class of diluted magnetic semi-conductors (DMS) and its magnetic properties were studied in the paper of Kim [154], using a fully quantum approach. In this paper, the authors used a Schrödinger-Poisson equation to characterize the ground state properties of charge careers, which are here holes positively charged.

The latter are confined in a quantum well and are subjected to electrostatic interactions between each other and negative acceptors. The holes have a spin $1/2$ and interact with the magnetic impurities of Manganese of spin $S_0^i = 3/2$ with an exchange constant K. Therefore an analogy can be made between their system and our nickel films, where the electrons become holes and the ion spins become Manganese impurities. The only difference is that there are no exchange interactions between the Manganese impurities because they are far enough from each other. The authors solved a self consistent problem, first finding the eigenvalues ϵ_n^σ and the eigenvectors ϕ_n^σ of the following Hamiltonian

$$H_{DMS} = \frac{P_\parallel^2}{2m} + \frac{P_\perp^2}{2m} + V_{conf}(x) + V_{\mathrm{H}}(x) + V_{XC}^\sigma(x) - H_{pd}, \tag{4.67}$$

where the index $\sigma = \{\uparrow;\downarrow\}$ denotes the spin-up or the spin-down populations. V_{conf} is a confinement potential equal to zero if $|x| < L/2$ and infinite everywhere else, so it is a infinite well. V_{XC}^σ is an exchange correlation potential different for the spin-up and the spin-down. V_{H} is the Hartree potential, which obeys the following Poisson equation

$$\nabla^2 V_{\mathrm{H}} = \frac{e^2}{\epsilon_0}\left[N - \left(n^\uparrow(x) + n^\downarrow(x)\right)\right], \tag{4.68}$$

where $N = 1/L \int_{-L/2}^{L/2} \left(n^\uparrow(x) + n^\downarrow(x)\right) dx$ satisfies the charge neutrality condition. Finally H_{pd} is the exchange Hamiltonian between holes and Manganese impurities

$$H_{pd} = -\frac{KxN_0\langle S\rangle\sigma_z}{2}, \tag{4.69}$$

where xN_0 indicates the average Mn concentration. The mean value of the Manganese's spin $\langle S\rangle$ is given by a thermal average

$$\langle S\rangle = SB_S\left(\frac{KSm_e}{2k_{\mathrm{B}}T}\right), \tag{4.70}$$

where $m_e = n^\uparrow - n^\downarrow$ is the magnetization of holes. Then the spin densities are obtained with the following formula

$$n^\sigma = \frac{m_\parallel k_{\mathrm{B}}T}{\pi\hbar^2}\sum_n |\phi_n^\sigma| \ln\left[1 + \exp\left(\frac{\mu - \epsilon_n^\sigma}{k_{\mathrm{B}}T}\right)\right]. \tag{4.71}$$

In our case we do not solve any Schrödinger equation, but we compute directly the spin-up and spin-down densities with the one dimensional Fermi-Dirac distribution

(4.53)

$$n^{\uparrow} = \frac{2\pi k_B T}{m_{\parallel}} \frac{m_{\parallel}^2 m_{\perp}}{(2\pi\hbar)^3} \int_{-\infty}^{\infty} \ln\left[1 + \exp\left(-\frac{1}{k_B T}\left(\frac{m_{\perp}}{2}v^2 + V_H + V_{XC}^{\uparrow} + \mu_B B_{pd} - \mu(T)\right)\right)\right] dv, \tag{4.72}$$

$$n^{\downarrow} = \frac{2\pi k_B T}{m_{\parallel}} \frac{m_{\parallel}^2 m_{\perp}}{(2\pi\hbar)^3} \int_{-\infty}^{\infty} \ln\left[1 + \exp\left(-\frac{1}{k_B T}\left(\frac{m_{\perp}}{2}v^2 + V_H + V_{XC}^{\downarrow} - \mu_B B_{pd} - \mu(T)\right)\right)\right] dv, \tag{4.73}$$

where $B_{pd} = KxN_0\langle S\rangle/2$ is the magnetic field associated to the exchange Hamiltonian H_{pd} (4.69). The parameters $m_{\parallel}$ and $m_{\perp}$ are, respectively, the effective electron masses in the $y-z$ plane and along the x direction.
The authors have simulated the spin polarization of the charge careers as a function of the temperature for different values of the exchange constant K and of the percentage of magnetic impurities x. In their simulations, the hole density is set to $n = n^{\uparrow} + n^{\downarrow} = 3\ 10^{20}\ \mathrm{cm}^{-3}$ and the density of cation sites (Manganese) is set to $N_0 = 41.99\ \mathrm{nm}^{-3}$.
We have performed simulations with our semi-classical model, (Eq. 4.72 - 4.73), using the same conditions as those used by the authors. The results are given in Fig. 4.10, where we sketch the spin polarization of charge careers (holes) $\xi = \int m_e dx / \int n dx$ as a function of temperature for different values of K and x. Our simulations shows the correct behaviour, indeed we have a magnetization which is maximal at low temperature and which decreases exponentially to zero at the Curie temperatures. Moreover the Curie temperature, for different values of K and x, appear in the right order with respect to the results obtained in the reference paper [154]. However the Curie temperatures are systematically 20% - 30% lower than those obtained with the full quantum model.
Therefore we conclude that it is possible to create a self-consistent ground state which is spin polarized with our semi-classical model. Moreover the results for global quantities, such as the total magnetization are a bit different from those predicted with the quantum model. However, it is always possible to correct this difference by changing the coupling constant K. In this case the general behaviour of the magnetization will be the same and the Curie temperature will be exactly the one predicted by the quantum simulations.

4.3 Spin-wave dispersion relation

In this section, we study the linear response of the self-consistent model, Eqs. (4.23). The study of the linear regime is interesting because one can solve the problem analytically under some specific conditions. This allows us to have a better understanding of the physics contained in our model. It can be also useful to have analytical results to verify if the code we developed provides correct results. Here, we will

focus on non-collinear spin effects by considering the following problem. We know that for localized spins, described with the Landau-Lifshitz equation (4.22), there is no spin-wave damping. Then we may ask the following question: Is it possible to have a damping of the spin waves, if one considers an exchange interaction between itinerant magnets and localized spins?
In order to answer this question we will use the tools of the linear analysis, more details are given in Sec. 3.1. Then we will use the analytical results to validate our numerical spin-Vlasov simulations.
We start from an homogeneous and collinear stationary state, i.e. $f_x^{(0)} = f_y^{(0)} = (S^i)_x^{(0)} = (S^i)_y^{(0)} = 0$, $(S^i)_z^{(0)} = S_0^i$, $f_0^{(0)} = f_0^{(0)}(v_x \equiv v)$ and $f_z^{(0)} = f_z^{(0)}(v_x \equiv v)$. Then we will perturb the system with the following type of excitations : $\delta S_x^i = \delta\, cos\,(kx)$ and $\delta S_y^i = \delta\, sin\,(kx)$. The model that we are going to use is a reduction of the full self-consistent model (4.23). Indeed, in the electron dynamics, we only keep the exchange interaction between the electron and the ion spins.

$$\frac{\partial f_0}{\partial t} + v \cdot \partial_x f_0 + \frac{K n_0^i}{2m}\left[\left(\partial_x S_i^i\right)\left(\partial_v f_i\right)\right] = 0, \tag{4.74}$$

$$\frac{\partial f_k}{\partial t} + v \cdot \partial_x f_k + \frac{K n_0^i}{2m}\left[\left(\partial_x S_k^i\right)\left(\partial_v f_0\right)\right] - \frac{K n_0^i}{\hbar}\left(\boldsymbol{f} \times \boldsymbol{S}^i\right)_k = 0, \tag{4.75}$$

$$\frac{\partial \boldsymbol{S}^i(x)}{\partial t} = \frac{a^2 J S_0^i}{\hbar}\left[\boldsymbol{S}^i(x) \times \frac{\partial^2}{\partial x^2}\boldsymbol{S}^i(x)\right] - \frac{K}{2\hbar}\boldsymbol{S}^i(x) \times \boldsymbol{f}. \tag{4.76}$$

We do not take into account the Hartree potential because we are not going to excite the electrostatic modes but only the magnetic ones. We suppress also the exchange-correlation effects as well as the self-consistent magnetic interaction (Ampere). The reason is that they are much smaller than the ion magnetic field. This was shown in Fig. 4.8 and is supposed to be valid in the linear regime.
As we have seen in the Sec. 4.1.2, the above excitation of the ion spins creates spin waves. If we do not consider any exchange interactions between the ion and the electron spins, i.e. $K = 0$, then the spin waves are not modulated in amplitude and oscillate at the following frequencies $\omega = \frac{S_0^i J}{\hbar}(ak)^2$, see Eq. (4.20). When K is different from zero the situation is more complicated and one has to find the dispersion relation of the Eqs (4.74)-(4.76). So, we will study the propagation of a perturbation around the following ground state: $f_\mu = f_\mu^{(0)} + \delta f_\mu$ and $S_i = (S^i)_z^{(0)} + \delta S_z^i$, where the δ quantities are weak compared to those of the ground state. Up to first order, the

linear model reads:

$$\frac{\partial \delta f_0}{\partial t} + v\partial_x \delta f_0 + \frac{K n_0^i S_0^i}{2m}\left[\left(\partial_x \delta S_z^i\right)\left(\partial_v f_z^0\right)\right] = 0, \tag{4.77}$$

$$\frac{\partial \delta f_x}{\partial t} + v\partial_x \delta f_x - \frac{K n_0^i S_0^i}{\hbar}\left[\delta f_y - f_z^{(0)}\delta S_y^i\right] + \frac{K n_0^i S_0^i}{2m}\left[\left(\partial_x \delta S_x^i\right)\left(\partial_v f_0^{(0)}\right)\right] = 0, \tag{4.78}$$

$$\frac{\partial \delta f_y}{\partial t} + v\partial_x \delta f_y + \frac{K n_0^i S_0^i}{\hbar}\left[\delta f_x - f_z^{(0)}\delta S_x^i\right] + \frac{K n_0^i S_0^i}{2m}\left[\left(\partial_x \delta S_y^i\right)\left(\partial_v f_0^{(0)}\right)\right] = 0, \tag{4.79}$$

$$\frac{\partial \delta f_z}{\partial t} + v\partial_x \delta f_z + \frac{K n_0^i S_0^i}{2m}\left[\left(\partial_x \delta S_z^i\right)\left(\partial_v f_0^{(0)}\right)\right] = 0, \tag{4.80}$$

$$\frac{\partial \delta S_x^i}{\partial t} = -\frac{a^2 J S_0^i}{\hbar}\frac{\partial^2}{\partial x^2}\delta S_y^i + \frac{K}{2\hbar}\left[\delta S_y^i \int f_z^0 dv - \int \delta f_y dv\right], \tag{4.81}$$

$$\frac{\partial \delta S_y^i}{\partial t} = \frac{a^2 J S_0^i}{\hbar}\frac{\partial^2}{\partial x^2}\delta S_x^i - \frac{K}{2\hbar}\left[\delta S_x^i \int f_z^0 dv - \int \delta f_x dv\right], \tag{4.82}$$

$$\frac{\partial \delta S_z^i}{\partial t} = 0. \tag{4.83}$$

Next step consists by performing a Fourier and a Laplace transform of the previous equations in order to obtain a set of algebraic equations that are easier to solve. According to Eqs. (3.12) and (3.14) and after some tedious calculations[4], one obtains the Fourier-Laplace transform of the ion spins in the $x-y$ directions:

$$\delta\tilde{S}_x^i(p,k) = \frac{1}{\epsilon(p,k)}\frac{1}{(kv_T)^2}\left[\left(\overline{\delta S_x^i} + E\int \frac{A_y}{Z_e}dv\right)\left(p + E\int \frac{C}{Z_e}dv\right) - \left(\overline{\delta S_y^i} - E\int \frac{A_x}{Z_e}dv\right)\left(D + E\int \frac{B}{Z_e}dv\right)\right], \tag{4.84}$$

$$\delta\tilde{S}_y^i(p,k) = \frac{1}{\epsilon(p,k)}\frac{1}{(kv_T)^2}\left[\left(\overline{\delta S_x^i} + E\int \frac{A_y}{Z_e}dv\right)\left(D + E\int \frac{B}{Z_e}dv\right) + \left(\overline{\delta S_y^i} - E\int \frac{A_x}{Z_e}dv\right)\left(p + E\int \frac{C}{Z_e}dv\right)\right], \tag{4.85}$$

where A_x and A_y depend only on the initial excitations

$$A_x = \frac{1}{p+ikv}\left[\overline{\delta f_x} + \frac{K n_0^i S_0^i}{\hbar}\frac{\overline{\delta f_y}}{p+ikv}\right], \quad A_y = \frac{1}{p+ikv}\left[\overline{\delta f_y} - \frac{K n_0^i S_0^i}{\hbar}\frac{\overline{\delta f_x}}{p+ikv}\right] \tag{4.86}$$

and $\epsilon(p,k)$ is the dielectric function of the system

$$\epsilon(p,k) = \frac{1}{(kv_T)^2}\left[\left(p + E\int \frac{C}{Z_e}dv\right)^2 + \left(D + E\int \frac{B}{Z_e}dv\right)^2\right], \tag{4.87}$$

[4]The calculations are similar to those performed in Sec. 3.1.

with the following definitions:

$$E = -\frac{K}{2\hbar}, \tag{4.88}$$

$$D = \frac{k^2 a^2 J}{\hbar} S_0^i - \frac{K}{2\hbar\mu_{\mathrm{B}}} m_0, \tag{4.89}$$

$$Z_e = 1 + \left(\frac{K n_0^i S_0^i}{\hbar}\right)^2 \frac{1}{(p+ikv)^2}, \tag{4.90}$$

$$B = \left(\frac{K n_0^i S_0^i}{\hbar}\right)^2 \frac{f_z^{(0)}}{(p+ikv)^2} - ik\frac{K n_0^i S_0^i}{2m}\frac{\left(\partial_v f_0^{(0)}\right)}{p+ikv}, \tag{4.91}$$

$$C = -\frac{K n_0^i S_0^i}{\hbar}\frac{f_z^{(0)}}{p+ikv} - \frac{ik}{2m\hbar}\left(K n_0^i S_0^i\right)^2 \frac{\left(\partial_v f_0^{(0)}\right)}{(p+ikv)^2}. \tag{4.92}$$

The latter quantities depend only on the ground state properties of the system and do not depend on the form of the initial excitation. As it is explained in Sec. 3.1, the zeros of the dielectric function give the eigenmodes of the system. For the sake of simplification, we shall use a Maxwell-Boltzmann function for the equilibrium distributions. This assumption is not correct since the physical distribution functions should be Fermi-Dirac's ones. Unfortunately, the dispersion relation is more complicated to obtain for a Fermi-Dirac distribution than for a Maxwell-Boltzmann distribution (for more details see Sec. 3.2). Therefore the electron ground state distribution functions read:

$$f_{\uparrow}^{(0)}(v) = \frac{n_0^i}{2v_T\sqrt{\pi}} \cosh\left(\frac{\mu_{\mathrm{B}} B_{sd}}{k_{\mathrm{B}} T}\right)^{-1} \exp\left[-\frac{1}{k_{\mathrm{B}} T}\left(\frac{m}{2}v^2 + \mu_{\mathrm{B}} B_{sd}\right)\right], \tag{4.93}$$

$$f_{\downarrow}^{(0)}(v) = \frac{n_0^i}{2v_T\sqrt{\pi}} \cosh\left(\frac{\mu_{\mathrm{B}} B_{sd}}{k_{\mathrm{B}} T}\right)^{-1} \exp\left[-\frac{1}{k_{\mathrm{B}} T}\left(\frac{m}{2}v^2 - \mu_{\mathrm{B}} B_{sd}\right)\right]. \tag{4.94}$$

The magnetic field B_{sd} corresponds to the local exchange magnetic field created by the ions, $B_{sd} = -\frac{K}{2\mu_{\mathrm{B}}} n_0^i S_0^i$. In terms of f_0 and f_z, the previous equations read:

$$f_0^{(0)}(v) = \frac{n_0^i}{v_T\sqrt{\pi}} \exp\left[-\frac{v^2}{v_T^2}\right] = F_0 \exp\left[-\frac{v^2}{v_T^2}\right], \tag{4.95}$$

$$f_z^{(0)}(v) = \frac{n_0^i}{v_T\sqrt{\pi}} \tanh\left(\frac{\mu_{\mathrm{B}} B_{sd}}{k_{\mathrm{B}} T}\right) \exp\left[-\frac{v^2}{v_T^2}\right] = F_z \exp\left[-\frac{v^2}{v_T^2}\right]. \tag{4.96}$$

Using Eqs. (4.95)-(4.96) and the plasma dispersion function (3.52), the dielectric function (4.87) may be written as:

$$\begin{aligned}\epsilon(\omega,k) = -\frac{1}{(kv_T)^2}\Bigg[\omega + \frac{Kn_0^iS_0^iE\sqrt{\pi}}{2\hbar k}\Bigg(- F_z\left[Z\left(\omega_k+\omega_K\right)+Z\left(\omega_k-\omega_K\right)\right] \\ + \frac{\hbar k}{2mv_T}F_0\left[Z'\left(\omega_k-\omega_K\right)-Z'\left(\omega_k+\omega_K\right)\right]\Bigg)\Bigg]^2 \\ + \frac{1}{(kv_T)^2}\Bigg[D - \frac{Kn_0^iS_0^iE\sqrt{\pi}}{2\hbar k}\Bigg(F_z\left[Z\left(\omega_k+\omega_K\right)-Z\left(\omega_k-\omega_K\right)\right] \\ + \frac{\hbar k}{2mv_T}F_0\left[Z'\left(\omega_k-\omega_K\right)+Z'\left(\omega_k+\omega_K\right)\right]\Bigg)\Bigg]^2, \end{aligned} \tag{4.97}$$

with the following definitions:

$$\omega = ip, \quad \omega_k = \frac{\omega}{kv_T} \quad \text{and} \quad \omega_K = \frac{Kn_0^iS_0^i}{\hbar k v_T}. \tag{4.98}$$

The temporal response of the Fourier components of the ion spins can be obtained by taking the inverse Laplace transform of Eqs. (4.84) and (4.85)

$$\overline{\delta S_x^i}(t,k) = \sum_j \left[\frac{N_x\left(\omega,k\right)}{\frac{\partial\epsilon(\omega,k)}{\partial\omega}}\right]_{\omega=\omega_j}\exp(-i\omega_j t), \quad \overline{\delta S_y^i}(t,k) = \sum_j \left[\frac{N_y\left(\omega,k\right)}{\frac{\partial\epsilon(\omega,k)}{\partial\omega}}\right]_{\omega=\omega_j}\exp(-i\omega_j t). \tag{4.99}$$

where w_j are the zeros of the dielectric function (4.97) and N_x and N_y are defined as:

$$\begin{aligned} N_x &= \frac{1}{(kv_T)^2}\left[\left(\overline{\delta S_x^i} + E\int\frac{A_y}{Z_e}dv\right)\left(\frac{\omega}{i}+E\int\frac{C}{Z_e}dv\right) - \left(\overline{\delta S_y^i} - E\int\frac{A_x}{Z_e}dv\right)\left(D+E\int\frac{B}{Z_e}dv\right)\right], \\ N_y &= \frac{1}{(kv_T)^2}\left[\left(\overline{\delta S_x^i} + E\int\frac{A_y}{Z_e}dv\right)\left(D+E\int\frac{B}{Z_e}dv\right) + \left(\overline{\delta S_y^i} - E\int\frac{A_x}{Z_e}dv\right)\left(\frac{\omega}{i}+E\int\frac{C}{Z_e}dv\right)\right]. \end{aligned} \tag{4.100}$$

The quantities $\overline{\delta S_x^i}(t)$ and $\overline{\delta S_y^i}(t)$ are the Fourier components of the ion spin components. They can be directly compared to the ion spin components obtained by numerical simulations, using the following relations:

$$\left(S^i\right)_x^k(t) \equiv \Re\left(\overline{S_x^i}(t)\right) = \int S_x^i(x,t)\,cos\left(kx\right)dx, \tag{4.101}$$

$$\left(S^i\right)_y^k(t) \equiv \Re\left(\overline{S_y^i}(t)\right) = \int S_y^i(x,t)\,sin\left(kx\right)dx, \tag{4.102}$$

which are meaningful only in the linear regime. Thus they can be used to have a direct comparison between the Vlasov simulations and the analytical solutions given

by the linear analysis. We are going to use them later to validate the Vlasov simulations.

To compute $\overline{\delta S_x^i}(t)$ and $\overline{\delta S_y^i}(t)$, we need to find the roots of the dielectric function (4.97). Mathematically speaking, one has to find the zeros of a complex function, this can be achieved using the program ZEAL [137]. It is a mathematical software package for computing zeros of analytic functions. The fact that we chose a Maxwell-Boltzmann function for the ground-state strongly simplify the problem, because the dispersion relation may be written in terms of the plasma dispersion function $\mathcal{Z}$.

The exchange constants K and J were defined in the Sec. for nickel to obtain

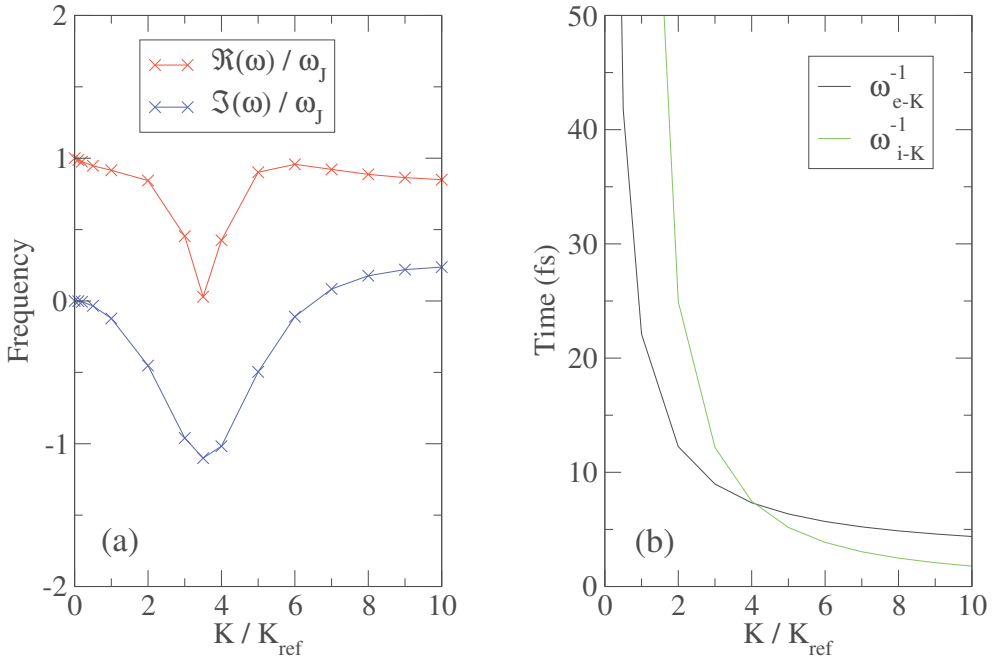

FIGURE 4.11: (a), dispersion relation corresponding to the dielectric function (4.97) as a function of the coupling constant K (normalized to $K_{ref} = 0.014$ eV.nm^3). The equilibrium state is given by a Maxwell-Boltzmann distribution with a temperature $T = 65000$ K. The excitation length is given by $k = 2\pi/10$ nm^{-1}. (b), typical electron ($\omega_{e-K} = Kn_0^i S_0^i/\hbar$) and ion ($\omega_{i-K} = Km_e/(2g\mu_B\hbar)$) time scales corresponding to the spin precession induced by the exchange interaction between both spins (K).

the correct proportion of localized/itinerant magnetic moments. Those values were founded using a Fermi-Dirac distribution function at 300 K for the electrons (itinerant magnetism). However if one takes a Maxwell-Boltzmann distribution function at a given temperature instead of a Fermi-Dirac, the proportion of localized/itinerant magnetic moments is going to change. To recover the correct proportion, i.e. $M_z^i = 0.54$ μ_B/atom and $M_z/n_0^i = 0.066$ μ_B/atom, one has to set the temperature of the Maxwell-Boltzmann function to 65000 K. This temperature has no physical meaning, since the ground state distribution functions of the electrons should be given by a Fermi-Dirac function at 300 K and not a Maxwell-Boltzmann function. The main difference between both distribution functions is that the Fermi-Dirac function is

steeper near the Fermi velocity than the Maxwell-Boltzmann. However, we expect to have a better understanding on the effects of the exchange interaction between electron and ion spins on the spin waves.
In order to study the influence of the electrons on the ion spin waves, we calculate the dispersion relation for different values of the exchange constant K. If we set $K = 0$, then the spin wave propagates without gaining or loosing any energy. In this case there is no coupling between the electron spins and the ion spins and the frequency of the spin wave is simply given by $\omega_J = k^2 a^2 J S_0^i/\hbar$. This result can be easily demonstrated using the Landau-Lifshitz equation (4.76), see Sec. 4.1.2. The situation is more complex if there is an exchange interaction between the ion and the electron spins. In this case the frequency of the spin wave is determined by founding the zeros of the dielectric function (4.97). This complex function posses a infinite numbers of zeros, but most of them have a strong negative imaginary part and then are directly damped on short time scales. The zeros that are dominating the dynamics on long time scales are those with an imaginary part much smaller than the real part or with a positive imaginary part[5]. There are two zeros of this kind, which are complex conjugated. We call them the principal zeros. The latter form the spin-wave dispersion relation. In Fig. 4.11(a), the spin-wave frequency (real and imaginary part) is depicted as a function of the exchange constant K. For $K = 0$, we recover the correct spin-wave frequency, i.e. $\omega = \omega_J$, as expected. Then, when the value of K increases, the imaginary part of the spin-wave frequency is negative and progressively decreases meaning that the spin waves are more and more damped, until reaching a minimum around $K = 4K_{ref}$). For this value of K, the spin-wave frequency is strongly affected by the presence of the electrons. This behaviour can be understood by investigating the typical exchange interaction time scales for the ion ($\omega_{i-K} = K m_e/2g\mu_B\hbar$) and the electron ($\omega_{e-K} = K n_0^i S_i/\hbar$) spins. The latter are represented in Fig. 4.11(b) as a function of the exchange constant K. We notice that the two time scales are equal near $K = 4K_{ref}$. It seems that we have a maximum of energy exchanged between the two spin populations for this special value of K. For larger values of K the imaginary part increases and becomes even positive, meaning that the spin wave undergoes an unstable dynamics. One should understand that when the value of K is changing the proportion of ion and electron spins is also modified in such a way that the total magnetic moment is preserved. For large value of K, the magnetism is essentially carried by the electrons and not by the ions. So the unstable case corresponds to a case for which the magnetism is essentially itinerant. This is not the case in our system (nickel thin films).

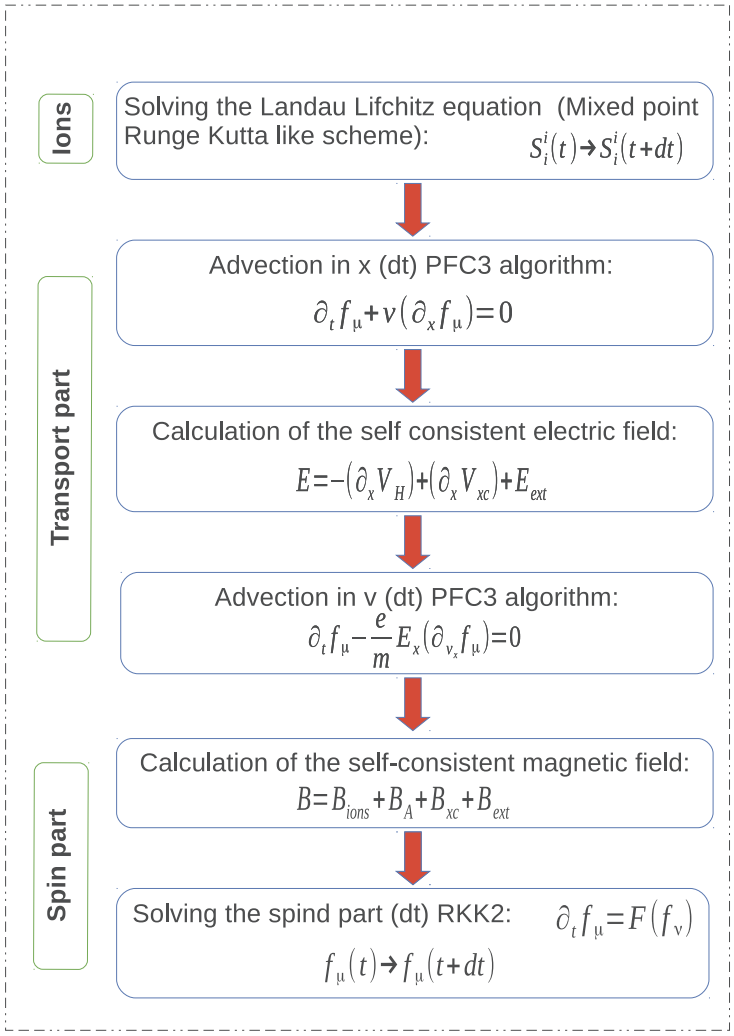

FIGURE 4.12: Description of the procedure applied to solve the spin-vlasov model, Eqs. (4.23). The subscript $\mu = \{0, x, y, z\}$ refers to distribution function components whereas the subscript $i = \{x, y, z\}$ refers to space coordinates.

4.4 Numerical methods and Vlasov simulations

In this section we will present the numerical methods to solve the full spin-Vlasov equations coupled to the Landau-Lifshitz equations, Eqs. (4.23). The Vlasov equation is used for long time in physics, many different numerical algorithms were developed to solve the Vlasov equation. However the form of the spin-Vlasov equations are a bit different from the usual Vlasov equations. Indeed they are composed of a transport part and a spin part (new part). A general form of the spin-Vlasov

[5] A positive imaginary part means that the associated mode is unstable.

equations reads as:

$$\partial_t f_\mu + v\partial_x f_\mu - \frac{e}{m} E_x \partial_{v_x} f_\mu = F\left(f_\nu\right). \tag{4.103}$$

The terms on the left-hand side of the equation (4.103) correspond to the transport part whereas the term on the right couples the different distribution functions. The usual strategy to solve numerically the Vlasov equation is to use a splitting algorithm [157]. That means instead of solving Eq.(4.103) on one time step, we decompose the problem in several steps. Let us introduce the splitting methods on the following differential problem:

$$\frac{dU}{dt} = (A + B)\, U(t), \tag{4.104}$$

where A and B are constant differential operators. Then the formal solution writes :

$$U(t + \Delta t) = \exp\left[(A + B)\, \Delta t\right] U(t). \tag{4.105}$$

The splitting algorithm is based on the following decomposition

$$U(t + \Delta t) = \exp\left(A\Delta t\right) \exp\left(B\Delta t\right) U(t). \tag{4.106}$$

That is equivalent to solve successively the two following differential problems

$$\frac{dU}{dt} = BU(t), \quad \text{then} \quad \frac{dU}{dt} = AU(t). \tag{4.107}$$

We notice that if the operators A and B commute then the splitting method is exact, but in general this is not the case. Indeed if we consider the basic case of particles accelerated in an electric field, then $A = \boldsymbol{v}\cdot\boldsymbol{\nabla}$ and $B = -e/m\boldsymbol{E}\cdot\boldsymbol{\nabla}_{\boldsymbol{v}}$ do not commute. Different orders (in time) of the splitting scheme can be constructed by splitting the complete differential problem (4.104) on sub-time steps. The first order method corresponds to the Eq. (4.106); a second order method would be written as follows:

$$U(t + \Delta t) = \exp\left(\frac{\Delta t}{2} A\right) \exp\left(\Delta t B\right) \exp\left(\frac{\Delta t}{2} A\right) U(t). \tag{4.108}$$

In our case we have to do three different splitting. One advection in the position space $\partial_t f + v\partial_x f = 0$, one advection in velocity space $\partial_t f - e/mE\partial_v f = 0$ and the spin part $\partial_t f = F\left(f_\nu\right)$. Several complex splitting scheme could be proposed to solve this problem, however in this work we choose a simple first order method. We first perform an advection in x with a time step Δt, then we do an advection in v_x with a time step Δt and finally we solve the spin part with a time step Δt. Between each splitting, we have to calculate the self consistent fields (Hartree, exchange-correlation and Ampere) that are involved in the next equation. This methodology is used to evolve in time the electron distribution functions f_0, f_i. But at the same time we also

have to evolve the spin of the ions with the Landau Lifshitz equation (4.22). Both are coupled together by an exchange interaction. Again, we use a simple algorithm, we first solve the ion spin dynamics with a time step Δt. The method used is a mixed point method combined with a Runge-Kutta integration scheme developed in Ref. [158]. This method ensure automatically the conservation of the norm of the magnetic moment. Then we solve the electron dynamics with the method described above. A summary of the algorithm used to solve the complete spin dynamics is presented in Fig. 4.12. More technical details will be given below. In the first and second part of this section we will, respectively, focus on the numerical method to solve the transport and the spin part of the spin-Vlasov equations.

4.4.1 The transport part

Here we focus on the numerical methods to solve the transport part of the spin-Vlasov equations. The latter reads:

$$\partial_t f_\mu + v\partial_x f_\mu - \frac{e}{m} E_x \left(\partial_{v_x} f_\mu\right) = 0. \tag{4.109}$$

where the electric field E_x is given by the Poisson equation.
Basically, there are two different strategies to address the problem. One can either use particle in cell method (PIC) or a phase-space-grid based method.
The idea of the first method is to represent the distribution function as a sum of delta functions:

$$f(x,v,t) = \sum_i w_i \delta\left(x - x_i(t)\right) \delta\left(v - v_i(t)\right) \tag{4.110}$$

where the w_i are constant weights, and the positions x_i and velocities v_i of the N test-particles obey the following equations of motion (characteristics of the Vlasov equation) : $\dot{x}_i = v_i$ and $\dot{v}_i = -eE(x_i)/m$. The electric field is computed by projecting the particle density on a spatial mesh and then solving Poisson's equation. With this method we never work with the distribution function, we use directly the particles position and velocity to construct fluid quantities and then calculate the self consistent fields. This method was for instance used to study the electron dynamics in metallic clusters [35]. However, it suffers from two problems. First, to construct the initial state particles are lunched randomly in the phase space. Therefore we introduce a statistical noise which can pollute our simulations, mainly in the region with low electron density. Secondly, the PIC simulations violate the Pauli exclusion principle. Therefore, after some times, the Fermi Dirac distribution relaxes naturally to a Maxwell Boltzmann distribution.
The other methods are called Eulerian methods, they are based on the resolution of the Vlasov equation on a regular mesh covering the entire phase-space (both position and velocity coordinates), which makes them somewhat more costly than PIC

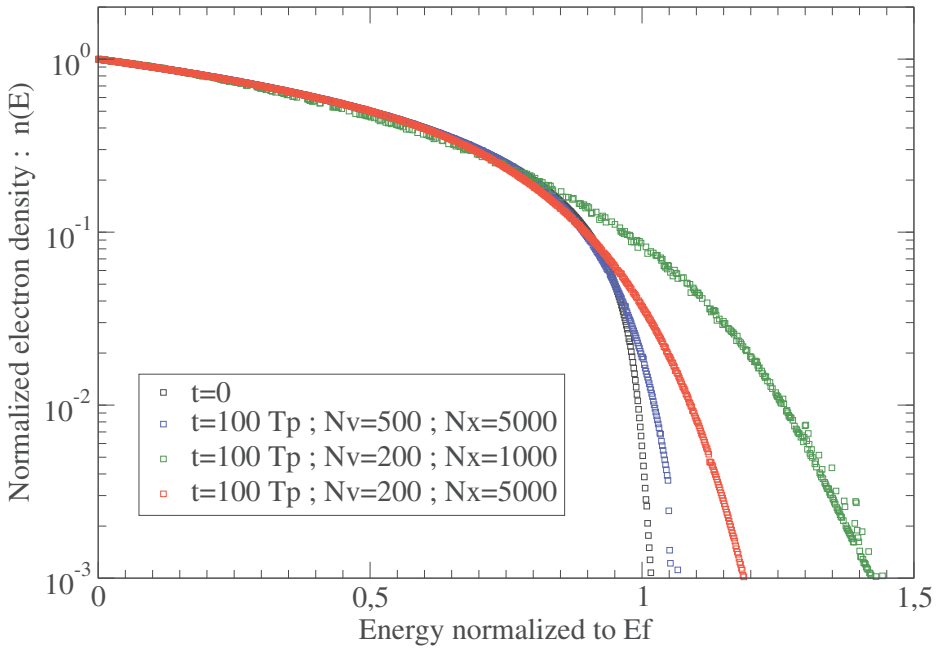

FIGURE 4.13: Energy densities of the electrons for the equilibrium distribution function of nickel films with $L = 100L_{\mathrm{F}}$ and $\sigma = 1L_{\mathrm{F}}$ ($L_{\mathrm{F}} \simeq 0.1\ nm$). The equilibrium case correspond to the black squares. The other cases correspond to the energy densities after $100\ Tp$ (without exciting the system) with different phase space grids.

codes in terms of memory storage and computing time. Eulerian methods were developed in the recent years [159, 160] and used to describe the electron charge dynamics in thin films [38]. The advantages of these methods is that good accuracy is guaranteed even in regions of feeble electron density, where the statistical noise of a PIC code would be most prominent. Moreover, the Fermi Dirac statistic is preserved during the simulations. However, the conservation properties can be lost. As we have seen in Sec. 2.2.3, the Vlasov equation has strong conservation properties, for instance for the mass, the momentum , the energy and the angular momentum. One should check during the simulations that all the previous quantities are conserved.

To solve our spin-Vlasov equations, we choose to use Eulerian methods. In particular we choose the so-called "flux balance method". The latter was first proposed by Fijalkow [159] and is based on the conservation of the flux of particles. This method has the advantage to conserve automatically the mass of the system, but it allows spurious oscillations of the distribution functions. In ref [160], the authors proposed a different technique to control these oscillations and to preserve the positivity of the distribution function. We use in our simulations the so called "PFC3" method. More technical details of this method can be found in Ref. [160].

In the simulations, we work with a numerical box of the following size : $-2L < x < 2L$ and $-2v_{\mathrm{F}} < v < 2v_{\mathrm{F}}$, where L is the thickness of the film and v_{F} is the Fermi velocity. At equilibrium, the electron gas is completely degenerate, therefore the maximal speed of the particles is very closed to the Fermi velocity. N_x and N_v represent the

number of points we used to sample the phase space (x, v_x). The smallest physical time scale is given by the inverse plasma frequency $T_p = \omega_p^{-1}$, therefore we chose a time step $\delta t = T_p/50$. We shall see later which numerical effects bound this choice.
The first step is to verify that the ground state distribution functions, constructed with the self-consistent procedure described in Sec. 4.2.1, does not change if we do not apply any perturbation. In Fig. 4.13 , we plot the energy densities at equilibrium (black curve) and after one hundred plasmon frequency (coloured curves). The latter are obtained by taking different values for N_x and N_v. We insist on the fact that in these simulations the initial distribution functions correspond to stationary solutions and are not excited at all. Therefore the distribution functions should not evolve in time. We notice that a large number of points $N_x = 5000$ and $N_v = 500$ are required to preserve the stationary solution on long time scales ($100\ T_p \simeq 36$ fs). These are numerical errors which come from the fact that the numerical method is sensitive to abrupt variation of the distribution function[6]. This occurs at the border of the film, where the electron density falls rapidly down to zero. In the velocity space the same situation holds since we deal with a quasi degenerate electron gas. Unless indicated otherwise we are going to use $N_x = 5000$ and $N_v = 500$ in the rest of this work. In order to validate the code, we shall compare our Vlasov simulations with previous works done on Sodium thin films without spin [38, 144]. The authors have used a Vlasov-Poisson model to study the plasmon created in a thin film of Sodium after exciting the electrons. They identified low frequency oscillations in the kinetic and potential energy of the electrons corresponding to a ballistic motion. We performed numerical simulations on Sodium films ($r_s = 4.0\ a_0$) with a thickness of $L = 100 L_{\mathrm{F}}$. In order to excite the electrons, we proceed in the same way as in [38, 144], i.e. we introduce an initial velocity shift $\Delta v = 0.1\ v_{\mathrm{F}}$ in the distribution functions. Such an excitation would correspond to the application of an instantaneous electric field.
In Fig. 4.14, we sketch the time evolution of the center of mass of the electrons. The latter is defined as follows : $\langle X \rangle = \int x f_0 dx dv$. Such quantity represents the electric dipole created in the system. As one can see, the electric dipole oscillates at a frequency close to the plasmon frequency (ω_p) and is exponentially damped after several oscillations because of the Landau damping. The fact that the electric dipole oscillates at a lower frequency than ω_p is due to the finite size of the system. This property was also observed in Ref. [38].
In Fig. 4.15, we plot the time evolution of different electron energies. The kinetic energy E_k, the potential energy E_p, the center of mass energy E_{cm} and the total energy

[6]The exact reason is that, at some step in the algorithm (PFC3), we have to reconstruct the distribution function at points in the phase space which are not on the grid. So we perform an interpolation using the nearest neighbour values of the distribution function. This interpolation is not exact and is at the origin of numerical errors. The latter can be reduced by increasing the sampling of the phase space.

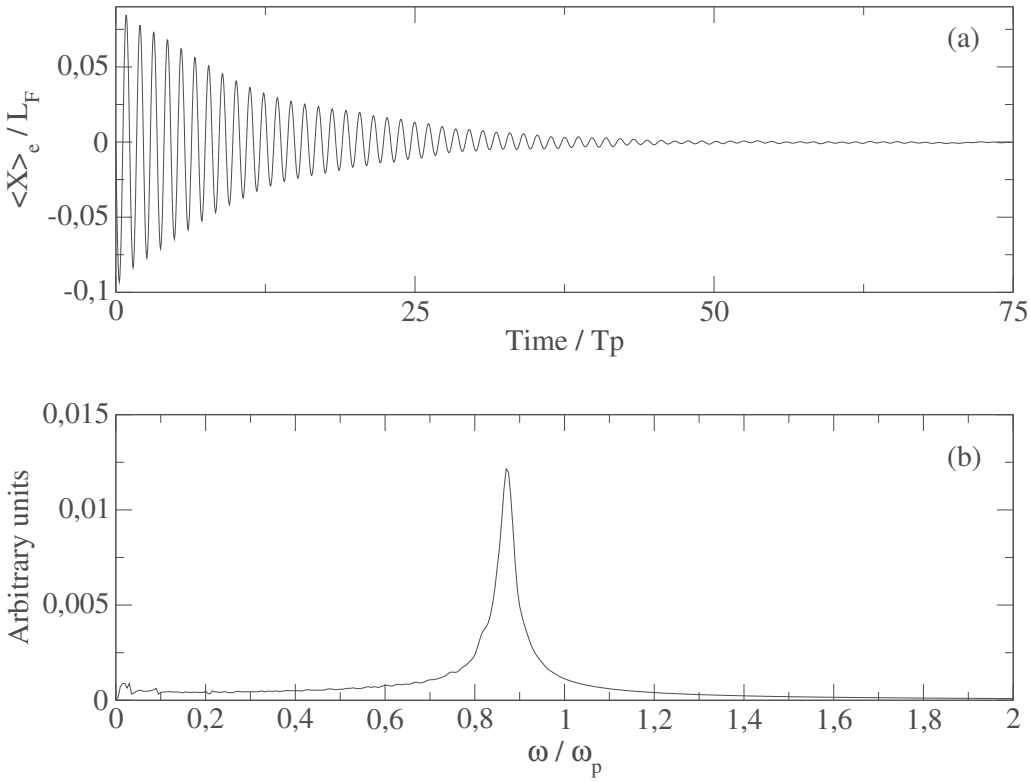

FIGURE 4.14: Simulations done on a film of Sodium of size $L = 100\ L_{\mathrm{F}}$ and $\sigma = 1\ L_{\mathrm{F}}$ with the following numerical parameters : $N_x = 5000$, $N_v = 500$, $\delta t = T_p/50$. The initial velocity kick is about $\Delta v = 0.1\ v_{\mathrm{F}}$. In the plot (a), we sketeched the electric dipole ($\langle X \rangle_e$) as a function of time (normalized to the inverse plasmon frequency : T_p). In the plot (b), we sketch the Fourier transform of the electric dipole.

$E_{tot} = E_k + E_p$. The latter are defined as follows:

$$E_k = \int \frac{m}{2} f_0 dx dv, \quad E_p = \int \boldsymbol{E}^2 dx, \quad E_{cm} = \int \left(\int v f_0 dv \right)^2 dx/n. \tag{4.111}$$

At the beginning of the simulations, the electrons are driven out of equilibrium. This leads to a net increase of the kinetic energy and a net decrease of the potential energy until $t = 30 - 40\ T_p$. At the same time the total energy is not well conserved, due to numerical errors, but its net variation is $10 - 100$ times lower than the other energy variations. After $50\ T_p$ the electrons have relaxed to a new quasi-stationary state characterized by a larger thermal energy (and therefore a larger temperature). At this time the plasmon is completely damped, this is confirmed by the fact that the center of mass energy is close to zero. In this new state the total energy is well conserved but there are still some periodic effects which occur in the electron dynamics and which lead to oscillations in the kinetic and potential energies. In [38], the author suggest that these oscillations are due to non-equilibrium electrons bouncing back and forth against the surfaces of the film. Indeed the oscillation period is

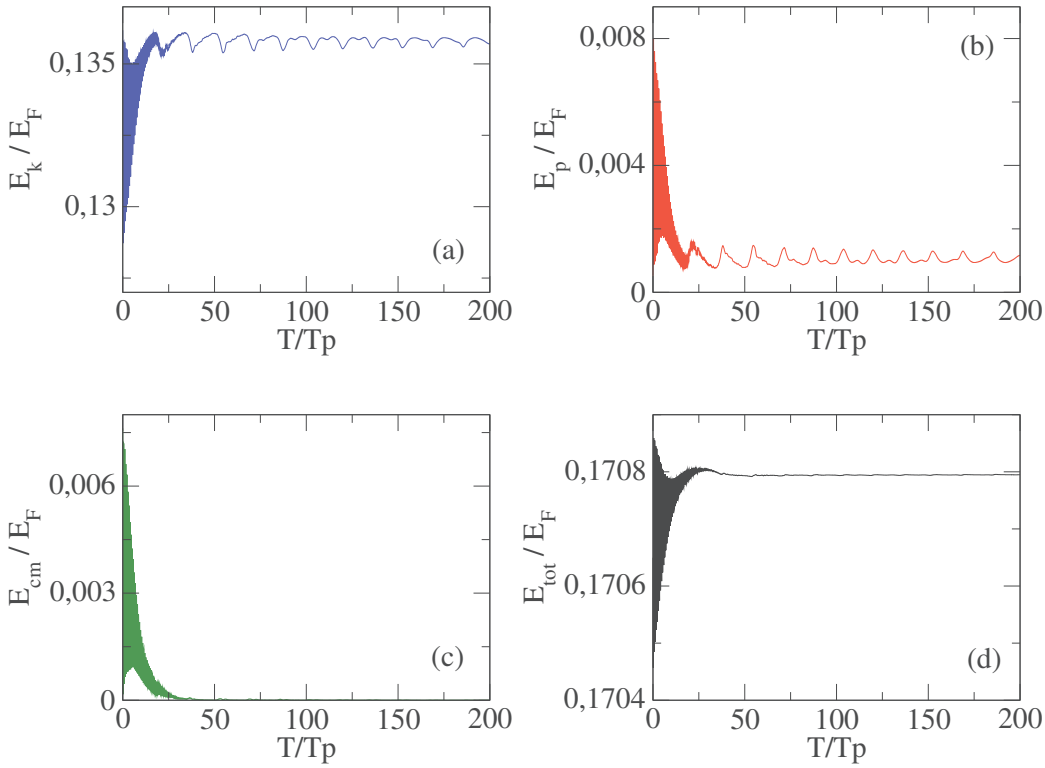

FIGURE 4.15: Simulations done on a film of Sodium of size $L = 100\ L_{\mathrm{F}}$ and $\sigma = 1\ L_{\mathrm{F}}$ with the following numerical parameters : $N_x = 5000$, $N_v = 500$, $\delta t = T_p/50$. The initial velocity kick is about $\Delta v = 0.1\ v_{\mathrm{F}}$. We sketch the time evolution of the different electron energies, the kinetic energy (plot a), the potential energy (plot b), the center of mass energy (plot c) and the total energy (plot d).

roughly equal to the time of flight of electrons travelling through the film at a velocity close to the Fermi velocity of the metal $T_b = 2L/v_{\mathrm{F}} \simeq 32\ T_p$. This is also in agreement with our numerical simulations.
All these simulations were done without taking the spin distribution functions into account. Therefore we were able to validate only the transport part of the spin-Vlasov code and not the spin part.

4.4.2 The spin part

The spin part of the Vlasov equation do not has the form of an advection because it couples different distribution functions

$$\partial_t f_\mu = F\left(f_\nu\right). \tag{4.112}$$

Therefore we cannot use the method developed in Sec. 4.4.1. To solve numerically the differential equation (4.112), we simply propose to use a Runge-Kutta method of the second order.
The method will be validated by comparing analytical solutions obtained in the previous section (on the spin-wave dynamics) with numerical simulations done with

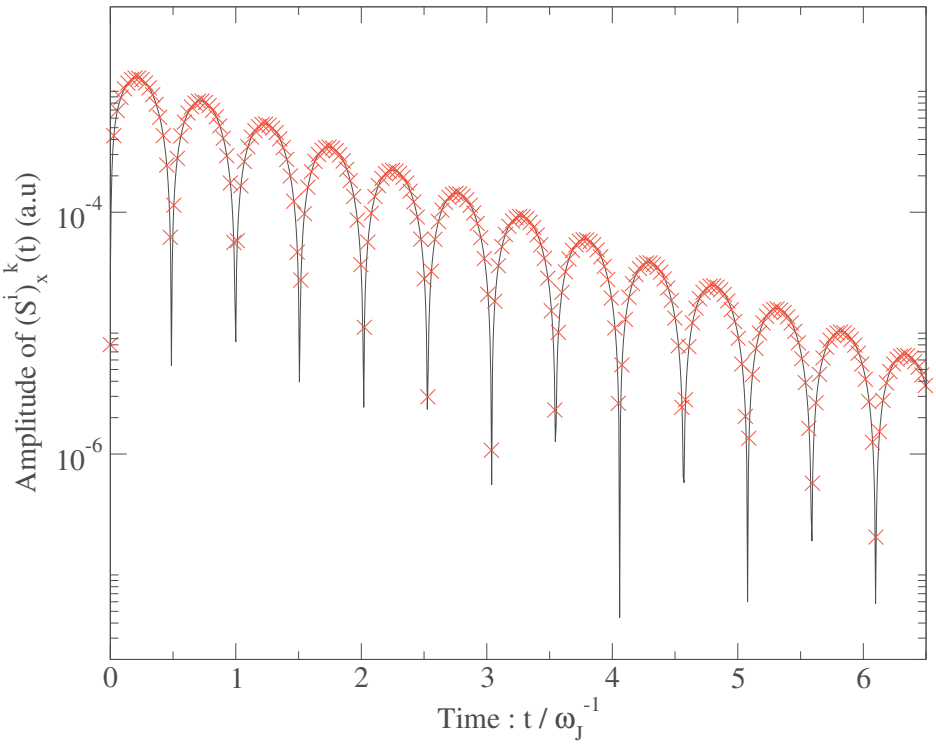

FIGURE 4.16: Simulations done on a film of nickel of size $L = 100\ L_{\mathrm{F}}$ and $\sigma = 1\ L_{\mathrm{F}}$ with the following numerical parameters : $N_x = 5000$, $N_v = 500$, $\delta t = T_p/10$. The initial perturbation on the ion spins reads: $S^i_x(t) = \epsilon\cos(kx)$ and $S^i_y(t) = \epsilon\cos(kx)$ with $\epsilon = 0.001$ and $k = 2\pi/10\ \mathrm{nm}^{-1}$. The black curve corresponds to the analytical solution given by Eq. (4.99), the red crosses correspond to the Fourier component of $S^i_x(t)$ (4.102) obtained with the Vlasov simulations.

the Spin-Vlasov code. Indeed, as it is shown by the Eq. (4.99), it is possible to have access (in the linear regime) to the exact time evolution of the Fourier components of the ion spins. The spin waves are excited by introducing the following perturbation with respect to the equilibrium state: $S^i_x(t) = \epsilon\cos(kx)$ and $S^i_y(t) = \epsilon\cos(kx)$ with $\epsilon = 0.001$ and $k = 2\pi/10\ \mathrm{nm}^{-1}$. ϵ is chosen to be small to ensure that we are in the linear regime. With such an excitation the electrons will not be transported in space. Indeed we can check that the electric field is always zero. However the electron spins will start to precess and interact with the ion spins. Therefore only the spin part of the Vlasov equation will play a part in the spin dynamics. One should also remember that one has to start with a ground state which is given by a Maxwell-Boltzmann distribution in order to compare our result with analytical solutions.
In Fig. 4.16, we compare the time evolution of the ion spins predicted by the linear theory and the results obtained with the numerical simulations. We found an excellent agreement between both curves, meaning that the numerical methods we used to integrate the spin part is correct at least in the linear regime. In Fig. 4.17, we represent numerical simulations done with our Vlasov code. As in the previous case, we do not excite the charge degrees of freedom but only the spins. In the left part, we plot the time evolution of the $x - y$ components of the ion spins. In the

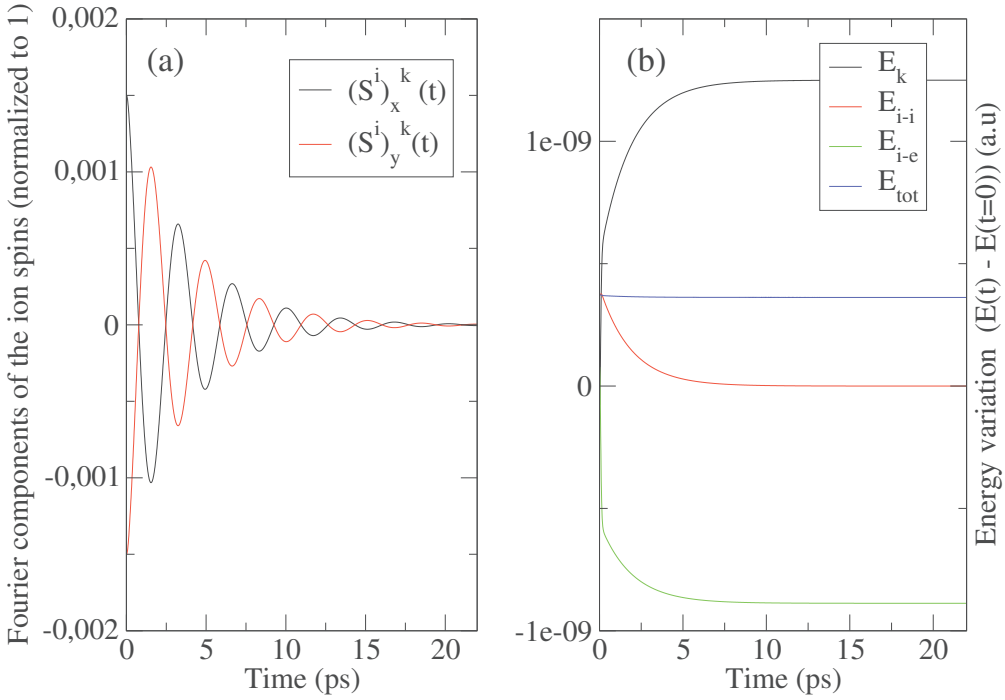

FIGURE 4.17: Simulations done on a film of nickel of size $L = 100\ L_{\mathrm{F}}$ and $\sigma = 1\ L_{\mathrm{F}}$ with the following numerical parameters : $N_x = 5000$, $N_v = 500$, $\delta t = T_p/10$. The initial perturbation is applied on the ion spins $S_x(t) = \epsilon\cos(kx)$ and $S_y(t) = \epsilon\cos(kx)$ with $\epsilon = 0.001$ and $k = 2\pi/10\ \mathrm{nm}^{-1}$. On the left part (a), we draw the time evolution of the Fourier component of the ion spins defined in Eq. (4.102). On the right part (b), we plot the associated energies: E_k is the kinetic energy of the electrons, see Eq. (2.60), E_{i-i} and E_{i-e} are respectively exchange energies due the interactions between ion spins Eq. (4.25) and between electron and ion spins Eq. (4.26). The total energy E_{tot} is the sum of the three energies.

right part, we plot the time evolution of different energies: the kinetic energy of the electrons and the exchange energies between the ion spins and between the ion and the electron spins.

We notice that the spin waves are damped, this is not so surprising since it was predicted by the linear analysis, see Sec. 4.3. According to the Eq. (4.25), the energy associated to the spin waves should decrease. This is also observed in Fig. 4.17(b) where we clearly see a net diminution of the spin-wave energy (E_{i-i}). Moreover we notice that the spin-wave energy is convert into electron kinetic energy. Physically speaking, that means that the ion spin waves are losing energy during their precession and that this energy is transferred to the electrons. Thus, we prove that our model is able to convert magnetic exchange energy into kinetic electron energy. As it is expected the total energy is constant. Of course there are weak variations due to numerical errors, but compared to the other energy variations it is completely negligible. The situation, we described above is ideal, a realistic excitation would excite the charge and spin dynamics and thus creates variations of the potential energy. This will be analysed in the next section, when we will consider laser pulse

excitations.
There is also another point to discuss before addressing the nonlinear dynamics. The fact that we use a Runge-Kutta method to solve one part of the Vlasov equation gives rise to the so-called CFL (Courant–Friedrichs–Lewy) condition [161]. The latter stipulates that the spatial and time mesh should be bounded by the following relation $v_{max}\Delta t \leq \Delta x$ in order to not propagate errors (this condition is necessary but not sufficient). Here v_{max} is the maximal speed of the particles ($v_{max} \simeq v_{\mathrm{F}}$). This was not observed for the transport part because the flux balance method is not restricted by the CFL condition [160]. However, the spin part is subjected to the CFL condition. In Practice, we always have to verify that the CFL condition are satisfied.[7]

4.5 Spin current generation with an electrical excitation

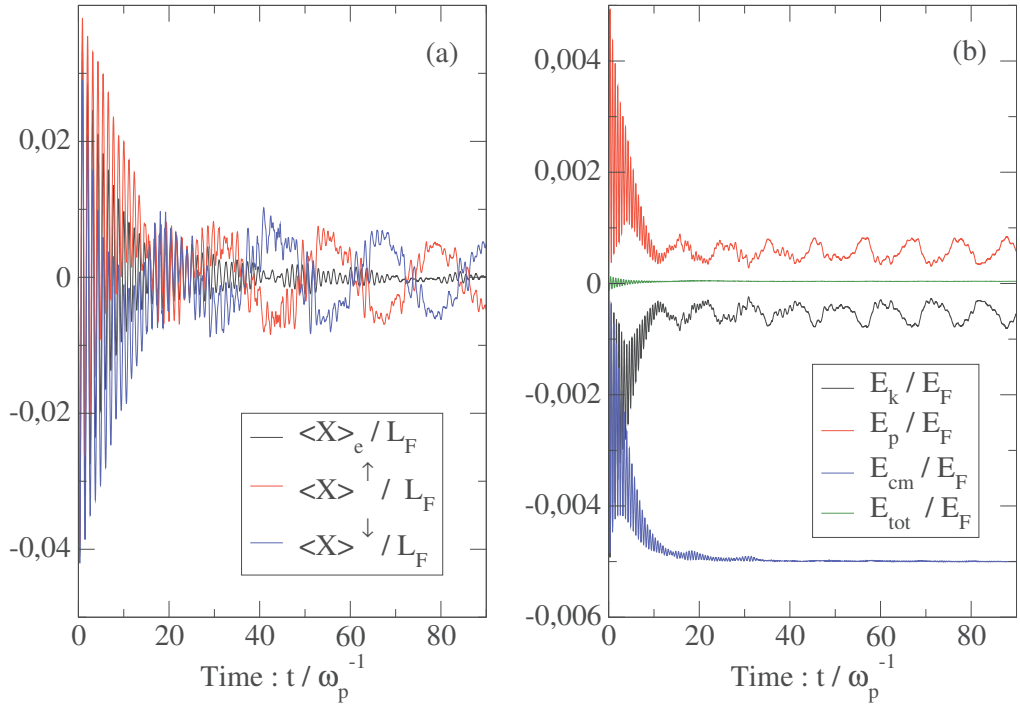

FIGURE 4.18: Simulations done on nickel films of size $L = 50\ L_{\mathrm{F}}$ and $\sigma = 1\ L_{\mathrm{F}}$ with the following numerical parameters : $N_x = 5000$, $N_v = 500$, $\delta t = T_p/20$. The electrons are excited with a velocity shift $\Delta v = 0.05\ v_{\mathrm{F}}$ on f_0. In th the plot (a), we draw the electric dipole (black curve), the spin-up dipole (red curve) and the spin-down dipole (blue curve) as a function of time. In the plot (b), we draw the corresponding energies, the kinetic energy (black curve), the potential energy (red curve), the center of mass energy (blue curve) and the total energy (green curve). The different energies are shifted by their initial values at $t = 0$.

[7] In most of the case, since we have to integrate the spin-Vlasov equation on a time step lower than the plasma period, the CFL conditions will be automatically satisfied.

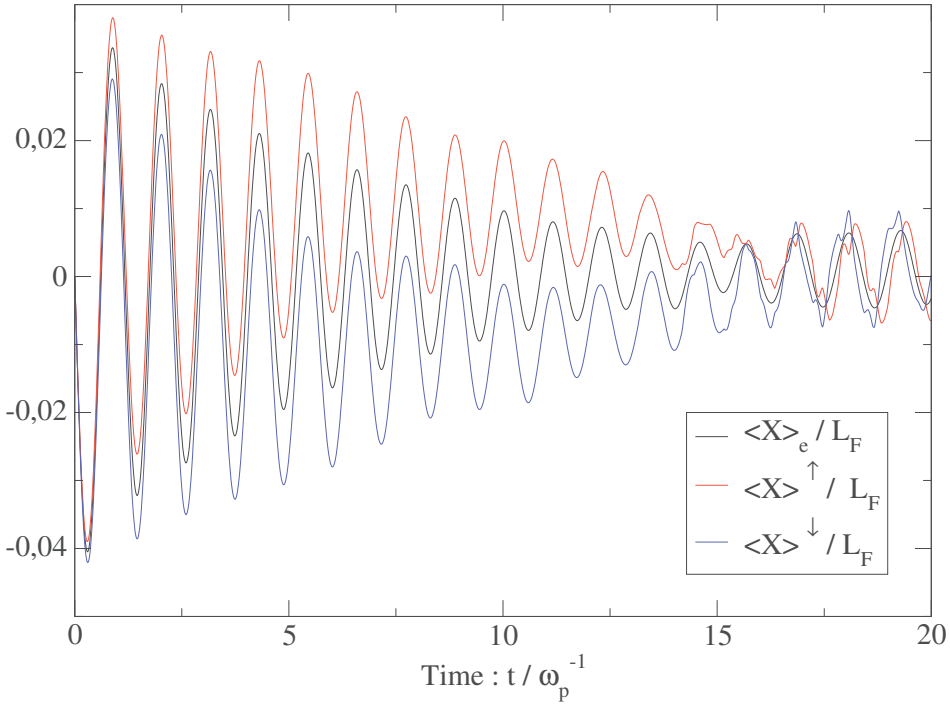

FIGURE 4.19: Zoom of the Fig.4.18 (a) during the first 20 plasmon oscillations.

In the above simulations, we have either excited a plasmon in a non magnetic medium or excited a spin wave but without the creation of a plasmon. In this section, we are going to study plasmon excitations in a magnetic and finite system. Our study shall consist to solve numerically the spin-Vlasov equations (4.23) in nickel thin films. We shall use the algorithm described in the previous section 4.4. These equations deal with the distribution functions f_0 and f_i, but to calculate average quantities or to analyse the data, we are also going to work with the spin-up and spin-down distribution functions $f^{\uparrow}$ and $f^{\downarrow}$. Both are related by linear combinations (2.8).

Starting from the electron ground state, calculated in the Sec. 4.2.2 we introduce a velocity shift Δv in the spin-up and spin-down distribution functions, $f^{\uparrow}$ and $f^{\downarrow}$, in order to excite a plasmon in the system[8]. With such an excitation we stay in the collinear magnetism regime, meaning that all the spins stay parallel to the z direction. Moreover the ion spins are not excited. This is due to the simple fact that no internal magnetic fields are created in the $x-y$ directions. Therefore all the dynamics is contained in the distribution functions f_0 and f_z (or equivalently in $f^{\uparrow}$ and $f^{\downarrow}$). For the moment, we also do not include exchange and correlation effects to simplify the study.

In Fig. 4.18, we represent a simulation done on films of nickel of size $L = 50 L_{\mathrm{F}}$ with an initial excitation $\Delta v = 0.05\ v_{\mathrm{F}}$. In the plot (a), we represent the following macroscopic observables, the electric dipole: $\langle X \rangle_e = \int x f_0\ dxdv$, the spin-up dipole:

[8]This is equivalent to introduce a velocity shift in the distribution functions f_0 and f_z

$\langle X\rangle_\uparrow = \int x f^\uparrow \, dxdv$ and the spin-down dipole: $\langle X\rangle_\downarrow = \int x f^\downarrow \, dxdv$. All of them are equal to zero in the ground state because the ground state distribution functions are symmetric with respect to $x = 0$. In the plot (b), we represent the corresponding time evolution of different energies: the kinetic energy, the potential energy, the center of mass energy and the total energy, which are defined in Eq. (4.111). Just after the excitation all the dipoles are excited with the same amplitude. This amplitude is about $1/1000$ of the size of the film, such that we surely are in the linear regime. For the electric dipole, during the first twenty plasmon oscillations the same situation holds as in the case of a non magnetic system, see Fig. 4.14. Indeed the system undergoes fast oscillations at the plasmon frequency, leading progressively to a heating of the electrons by a conversion of potential energy into kinetic energy. At the same time the Landau damping occurs and the electric dipole is exponentially damped. For the spin-up and spin-down dipoles, the situation is different. First, they are less damped than the electric dipole. Moreover, we notice that their centers of mass are well separated. This separation starts at the very beginning of the electron dynamics. This is confirmed in Fig. 4.19, where we represent a zoom of the different dipoles during the first twenty plasmon oscillations. We clearly see a progressive shift between both spin-up and spin-down mass centers. At longer time scale ($t > 40T_p$), when the electric dipole is relatively week, the spin-up and spin-down dipole are oscillating at lower frequency and in phase opposition. This situation was not expected. We were rather expecting that with such a simple excitation, both spin-up and spin-down dipoles would stay in phase and decay as the electric dipole. Physically, it means that we have created a magnetic dipole $\langle X\rangle_m \equiv \int x f_z \, dxdv$ or equivalently a spin current in the system, according to the following identity:

$$\frac{d}{dt}\langle X\rangle_m = \int v_x f_z \, dxdv \equiv J^S_{xz}. \tag{4.113}$$

The above relation above can be demonstrated by using the time evolution equation of the electron distribution functions, Eqs. (4.23).

This magnetic dipole or spin current is oscillating at a much lower frequency than the plasmon (about $0.043\ \omega_p$). This is sketched in Fig. 4.20, where we plot the different dipoles and their corresponding Fourier spectrums. Low frequency oscillations were also observed in non magnetic systems, such as in Sodium films, after exiting the plasmon mode [38]. However they appear only in the energy curves, see Fig. 4.15, and never in the electric dipole moment. These oscillations were interpreted as ballistic oscillations due to electrons travelling back and forth in the film. Therefore the frequency of these oscillations were directly related to the size of the film according to the following formula: $\omega_b = (2L/v_\mathrm{F})^{-1}$, where ω_b is the ballistic frequency. For nickel films ($v_\mathrm{F} = 0.93$ a.u. and $L = 50\ L_\mathrm{F}$), it is about $\omega_b = 0.063\ \omega_p$. Ballistic oscillations are also present in our energies curves, see Fig. 4.18(b), but they appear with twice the ballistic frequency. The reason is that energies are second order moments of the distribution functions. The new features of the spin-Vlasov simulations are

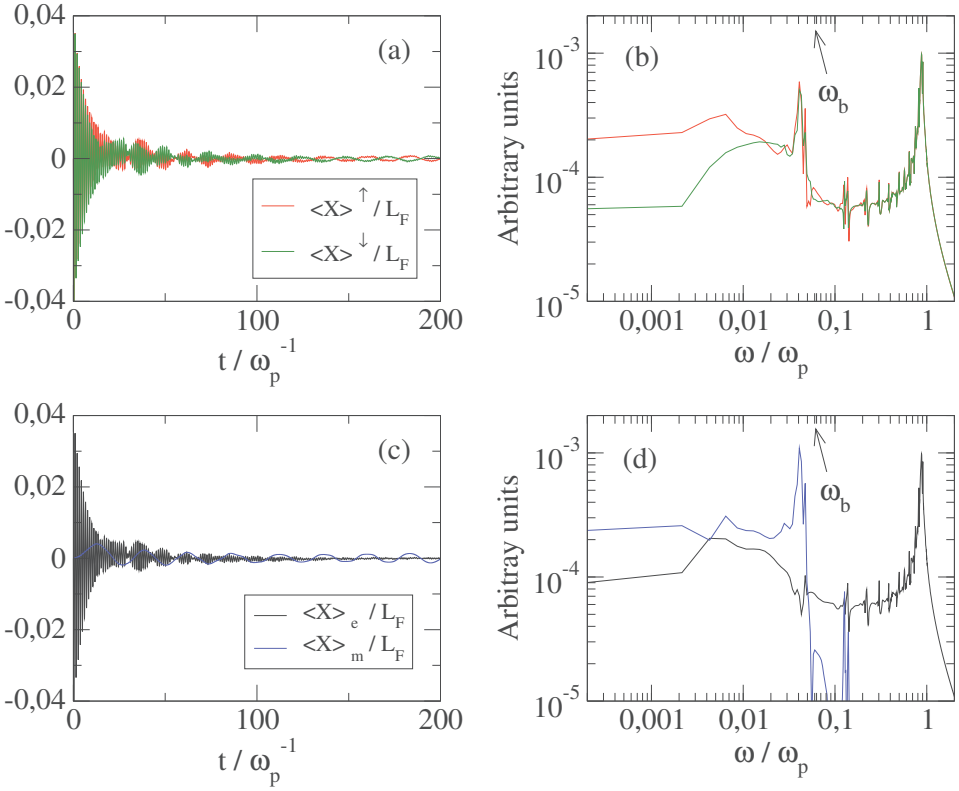

FIGURE 4.20: Simulations done on nickel films of size $L = 50\ L_{\mathrm{F}}$ and $\sigma = 1\ L_{\mathrm{F}}$ with the following numerical parameters : $N_x = 5000$, $N_v = 500$, $\delta t = T_p/20$. The electrons are excited with a velocity shift $\Delta v = 0.05\ v_{\mathrm{F}}$ on $f^{\uparrow}$ and $f^{\downarrow}$. In the plot (a), we draw the time evolution of both spin-up (red curve) and spin-down (green curve) dipoles . In the plot (c), we draw the time evolution of both electric (black curve) and magnetic (blue curve) dipoles. And in the plots (b) and (d), we draw the Fourier transform of each dipole.

the ballistic oscillations present in the magnetic dipole. Indeed in Fig. 4.20(d), we clearly see that the magnetic dipole is mainly oscillating at the ballistic frequency and there is no trace of any plasmon oscillations. On the same plot, we notice also that the situation is completely different for the electric dipole. The latter oscillates only at the plasma frequency and there is no trace of the ballistic frequency, as is the case for spinless electrons. Consequently, as the spin-up and spin-down distribution functions are linear combinations of f_0 and f_z, we observe both frequencies (plasma and ballistic) in the spin-up and spin-down dipoles, see Fig. 4.20(b). To be more precise, the magnetic dipole is not exactly oscillating at the ballistic frequency but at lower frequency. The reason is that the ballistic frequency does not take into account surface effects related to the parameter σ. More details about the formation of these ballistic oscillations will be given in this section, but before we will analyse the influence of finite size effects on the ballistic frequency. Such an analysis is done in Fig. 4.21, were we sketch the evolution of the low frequency component of the spin-up and spin-down dipoles as a function of the size of the film and we compare it to the theoretical values for the ballistic frequency. We study different film sizes:

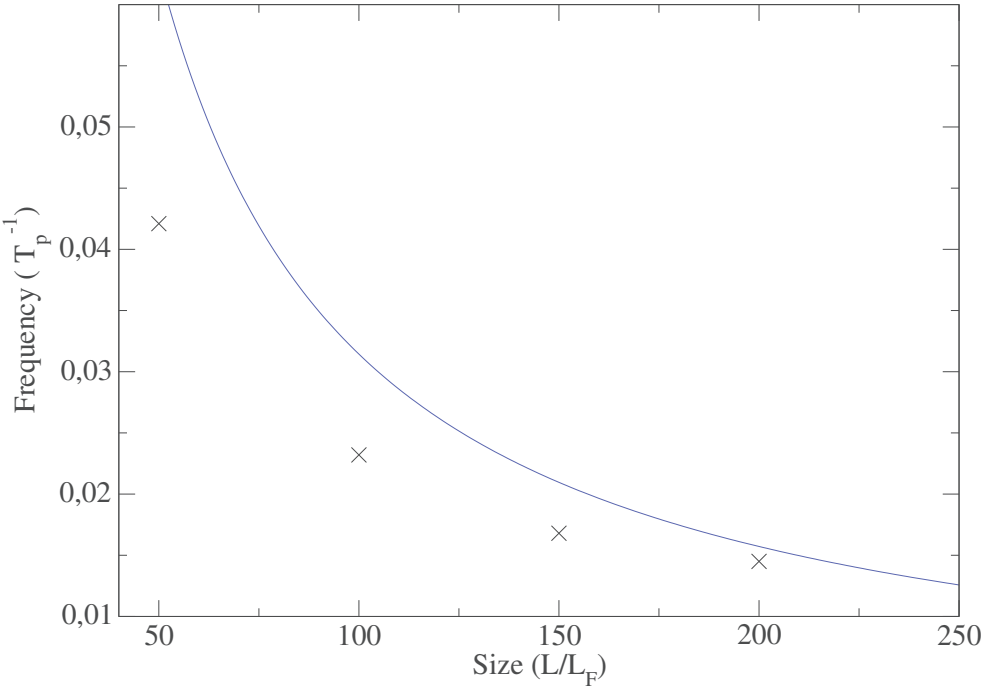

FIGURE 4.21: In this figure, we sketch the ballistic frequency obtained by numerical simulations (black cross) with nickel films of different sizes : $L = 50, 100, 150, 200\ L_{\mathrm{F}}$. The border of the film is always characterized by the same value of $\sigma = 1\ L_{\mathrm{F}}$. The blue line represents the theoretical value of the ballistic frequency : $\omega_b = (2L/v_{\mathrm{F}})^{-1}$.

$L = 50, 100, 150, 200\ L_{\mathrm{F}}$ and $\sigma = 1\ L_{\mathrm{F}}$. Surface effects are mainly proportional to the ratio between σ and L. We notice that the difference between the spin current frequency and the ballistic frequency increases with the increase of size effects, see Fig. 4.21 (until 50% for $\sigma/L = 1/50$). Therefore the finite size of the system, modelled by parameter σ, seems to play an important role in the formation of the magnetic dipole. This is also analysed in Fig. 4.22, where we plot the numerical ballistic frequencies obtained for two different cases. The first case (blue cross) corresponds to the previous one, i.e. thin films of different sizes and with fix values of σ. The second case (red cross) corresponds to a fix ratio between L and σ, i.e.: $L = 50\ L_{\mathrm{F}}, \sigma = 1\ L_{\mathrm{F}}$; $L = 100\ L_{\mathrm{F}}, \sigma = 2\ L_{\mathrm{F}}$; $L = 150\ L_{\mathrm{F}}, \sigma = 3\ L_{\mathrm{F}}$ and $L = 200\ L_{\mathrm{F}}, \sigma = 4\ L_{\mathrm{F}}$. For the second case, we notice that the ballistic frequency is a linear function of the size of the film. This kind of behaviour is a typical characteristic of ballistic phenomena.
Before going further we shall give a physical explanation for the creation of the magnetic dipole with an electric type of excitation. Let us consider the simplest kinetic model to describe the dynamics of an interacting spin polarized (in the z direction) electron gas. It is a reduction of the full spin-Vlasov model (4.23):

$$\frac{\partial f_0}{\partial t} + v_x \left(\partial_x f_0\right) - \frac{e}{m} E_x \left(\partial_{v_x} f_0\right) = 0, \tag{4.114}$$

$$\frac{\partial f_z}{\partial t} + v_x \left(\partial_x f_0\right) - \frac{e}{m} E_x \left(\partial_{v_x} f_z\right) = 0, \tag{4.115}$$

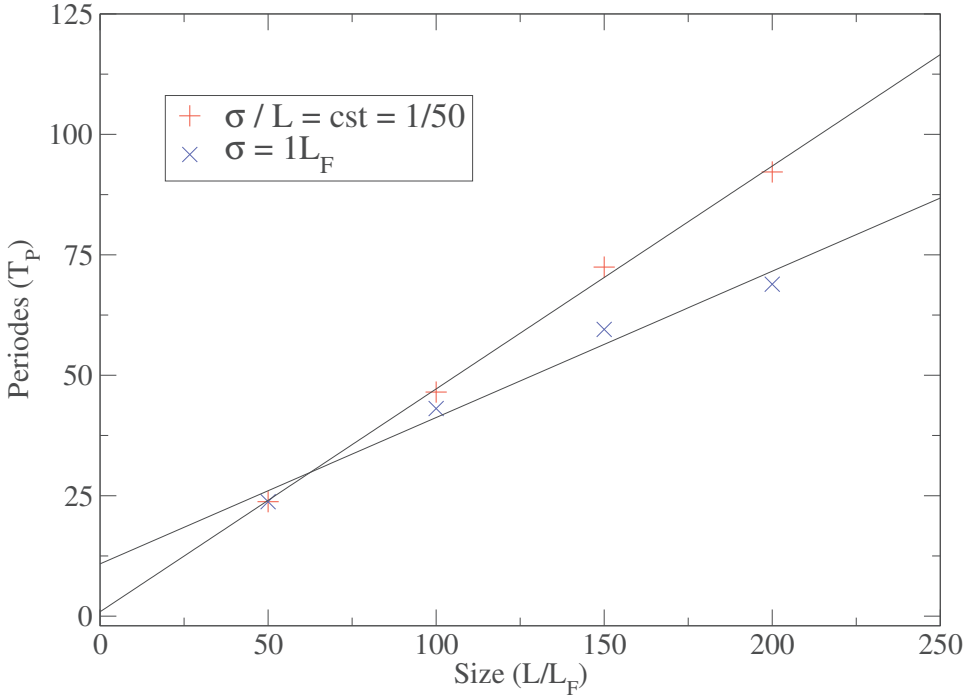

FIGURE 4.22: In this figure, we sketch the ballistic frequencies obtained by numerical simulations with nickel films of different sizes : $L = 50, 100, 150, 200\ L_{\mathrm{F}}$. For the blue crosses, the border of the film is always characterized by the same value of $\sigma = 1\ L_{\mathrm{F}}$. For the red crosses the value of σ is always equal to two per cent of the size of the film. The dashed lines are linear fits of the points.

where the electric field E_x is given by the Poisson equation (4.40).
With such a simple model, we still observe the creation of a magnetic dipole oscillating at the ballistic frequency. In Eqs. (4.114) and (4.115), we completely neglect the Zeeman interaction as well as exchange-correlation effects. The latter are thus not responsible of the magnetic dipole oscillations. We only keep the electrostatic interactions between the particles through the Poisson equation. Moreover we also suppressed the ion spin dynamics, but their influence is still visible in the electron ground state (spin polarized ground state). In this model, the charge distribution function of the electrons f_0 evolves independently of the magnetic distribution function f_z. The opposite is not true since the electric field E_x, present in both equations, is related to f_0 through the electron density $n = \int f_0\ dv$ in the Poisson equation. Therefore the electrons are moving in a self consistent way with respect to the Eq. (4.114) whereas the spin is simply transported with the electrons, Eq. (4.115), without having their own dynamics. This is the reason why the plasma frequency appears only in the electric dipole and not in the magnetic dipole.
For the ballistic oscillations the situation is more complex to understand. First we have seen that the oscillations of the magnetic dipole are due to ballistic electrons travelling back and forth in the film near the Fermi velocity. They are also strongly related to the properties of the density at the border of the film, characterized by the parameter σ, and to the magnetic properties of the ground state, since they were

not observed in non magnetic materials. We propose the following explanation to understand this phenomenon. In the ground state, the confinement potential felt by the spin-up and spin-down electrons is a bit different. This is illustrated in Fig. 4.9, where we clearly see that the confinement potential is deeper for the spin-up electrons than for the spin-down electrons. This is namely due to the exchange interaction between the electron and the ion spins which acts as a local magnetic field. Then, after the initial excitation (with an electric field) both spin-up and spin-down electrons are accelerated in the longitudinal direction (x) of the film, see Fig. 4.1. But due to the different confinement potentials, the spin-down electrons which are less confined will arrive on average at the border of the film before the spin-up electrons. At the border of the film the spin-down electrons are going to feel an electric field which will bring them back to the film. However, at the same time, the spin-up electrons reach the border of the film. They will feel an electric field different from that felt by the spin-down electrons, precisely because some of the latter are already present at the border. Thus because of electron-electron repulsion, the spin-up electrons will return to the center of the film more rapidly than the spin-down electrons. On the other side of the film, the opposite situation occurs. This explanation is illustrated in Fig. 4.18 and Fig. 4.19, where we clearly see that the centers of mass of the spin-up and spin-down electrons are more and more separated in space. This effect is amplified after each plasmon oscillation, until arriving at the situation where the two densities oscillate in phase opposition. All of these effects are electrostatic effects and are taken into account through the Poisson equation.

To summarize, to create an oscillating magnetic dipole at the ballistic frequency with an electric excitation, we need the three following ingredients. First a magnetic ground state for which the spin-up and the spin-down electrons are differently confined. Second, we need a finite system to create the spatial separation of the spin-up and spin-down dipoles. And finally, we need also to take into account the self-consistent electric field created by the electrons. If we suppress one of these ingredients, then the magnetic dipole disappears.

Now that we have a better understanding on the origin of this magnetic dipole, we shall perform complete simulations by solving the full spin-Vlasov model, Eqs. (4.23), with exchange correlation effects and with the Zeeman interaction. In all the previous simulations, we have excited the system with an initial velocity shift in the distribution functions. This kind of excitation is not realistic since it corresponds to the action of an instantaneous electric field at time $t = 0$. Such an excitation can be represented by a delta function in time and thus in the frequency domain as a constant function, meaning that we excite all the frequencies in the same way. We shall now consider more realistic excitations. With the recent development of ultra-fast optical techniques, one is able to produce laser pulses with a time duration of a few

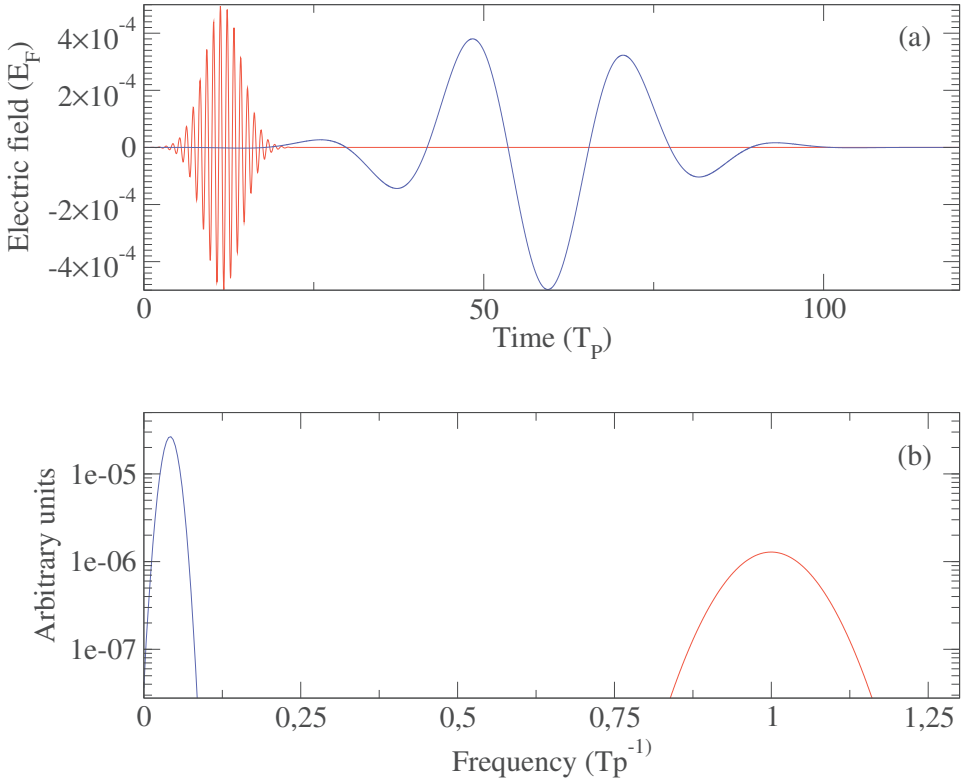

FIGURE 4.23: In this figure, we sketch in the upper part (a) the temporal profile of two laser pulses (4.116). We used the following parameters to characterized the electric field: $\Delta t = 1$ fs $\simeq 4\, T_p$, $\omega_l = \omega_p$ for the red curve and $\Delta t = 5$ fs $\simeq 20\, T_p$, $\omega_l = \omega_b$ for the blue curve. In both cases, the amplitude of the electric field is $E_0 \simeq 10^8$ V/m and $t_0 = 3\, \Delta t$. In the lower part (b), we sketch the Fourier spectrum of the two pulses.

femtosecond. Such laser pulses can be modelled by the following electric field:

$$\boldsymbol{E}(x) = \boldsymbol{E_0}(x) \exp\left[-\left(\frac{t-t_0}{\Delta t}\right)^2\right] \cos\left(\omega_l t\right), \tag{4.116}$$

where $\boldsymbol{E_0}$ is the amplitude of the laser, Δt is the time width of the pulse and ω_l is the central frequency of the pulse. The parameter t_0 corresponds to the time when the pulse reach its maximal amplitude. Here and in the following, we shall consider that the electric field is linearly polarized (in the x direction) and space independent, which is true if the wave length of the laser is much larger than the size of the film, i.e. $kL \ll 1$. Let us consider two different laser pulses. One with a central frequency equal to the plasma frequency and another one with a central frequency equal to the ballistic frequency. The time width of the pulses are respectively: $\Delta t = 1\ fs \simeq 4\, T_p$ and $\Delta t = 5\ fs \simeq 20\, T_p$. The temporal and frequency profiles of both pulses are sketched in Fig. 4.23. We clearly notice that the two pulses are well separated in the Fourier domain. Moreover the amplitude of the laser is relatively small ($E_0 \simeq 10^8 V/m$) in such a way that the system will be excited in the linear regime. Therefore we shall either excite the plasmon mode or the ballistic

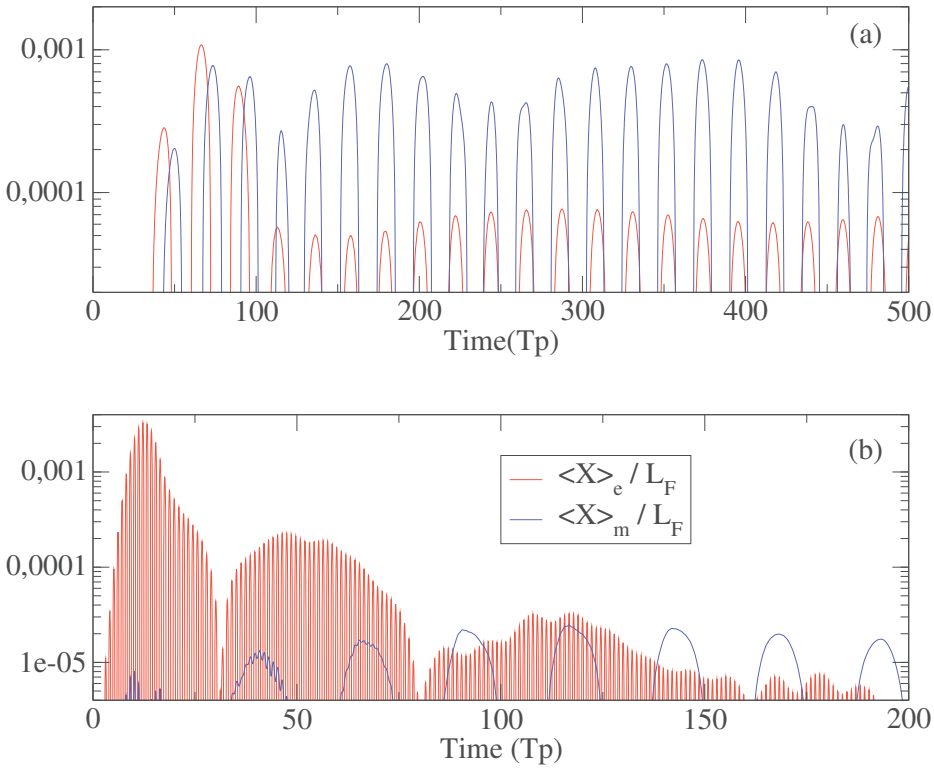

FIGURE 4.24: In this figure, we plot the electric (red curve) and the magnetic (blue curve) dipoles, normalized to the Fermi wave length), in the case of nickel films of size $L = 50\ L_{\mathrm{F}}$, $\sigma = 1\ L_{\mathrm{F}}$. In the upper part (a), the electrons are excited with a laser pulse with the following parameters: $\Delta t = 5$ fs $\simeq 20\ T_p$, $\omega_l = \omega_b$, $E_0 \simeq 10^8$ V/m and $t_0 = 3\ \Delta t$. In the lower part, the laser parameters are: $\Delta t = 1$ fs $\simeq 4\ T_p$, $\omega_l = \omega_p$, $E_0 \simeq 10^8$ V/m and $t_0 = 3\ \Delta t$.

mode. This type of excitation is completely different from the previous one (velocity kick), for which all modes where excited with the same amplitude.
In Fig. 4.24, we show the electric and the magnetic dipoles created by the above laser excitations. In the case where the laser frequency is equal to the ballistic frequency, we notice that a magnetic dipole is created and oscillates at the ballistic frequency. After the laser pulse disappeared (approximatively $100\ fs$, see Fig. 4.23) the magnetic dipole continues to oscillate at the ballistic frequency. An electric dipole is also created by the action of the pulse but rapidly decreases in amplitude. The electric dipole oscillates at the frequency of the laser pulse. In this picture, it is not so clear if the electric dipole oscillates at the laser frequency or at the ballistic frequency since they are equal. However, one can perform another simulation, where the two frequencies are a bit different. In that case, one would notice that the electric dipole oscillates at the laser frequency. That is probably the reason why it is drastically reduced after the laser pulse disappeared. In the case where the laser frequency is equal to the plasmon frequency, a different situation occurs. The electric dipole is excited by the laser pulse (which disappears after $20\ fs$) and then is damped in few plasma frequency trough the Landau damping. The magnetic dipole is not excited

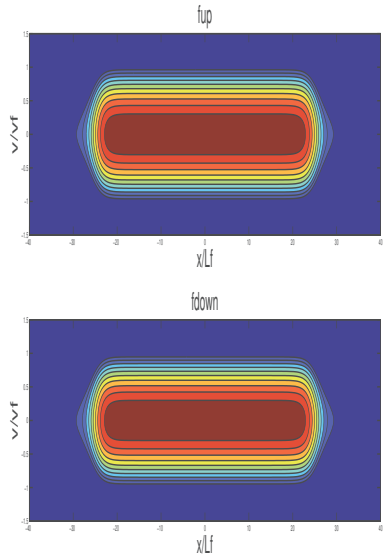

FIGURE 4.25: Ground state distribution functions, $f^{\uparrow}(x,v)$ (upper part) and $f^{\uparrow}(x,v)$ (lower part) for a nickel film of size $L = 50\ L_{\mathrm{F}}$ and $\sigma = 1\ L_{\mathrm{F}}$. The red and the blue colors represent, respectively, regions with high and low densities.

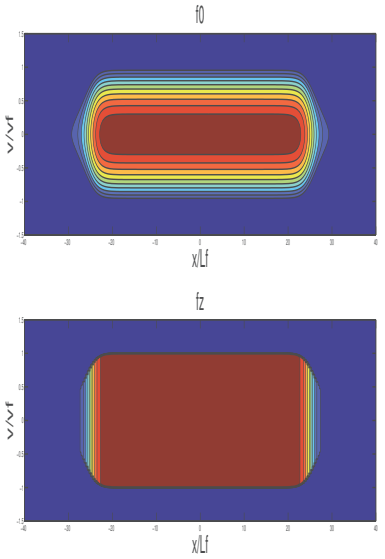

FIGURE 4.26: Ground state distribution functions, $f_0(x,v)$ (upper part) and $f_z(x,v)$ (lower part) for a nickel film of size $L = 50\ L_{\mathrm{F}}$ and $\sigma = 1\ L_{\mathrm{F}}$. The red and the blue colors represent, respectively, regions with high and low densities.

at all by the laser pulse.

Moreover we also notice that the ballistic modes have a much longer life time compared to the plasmon modes. This is illustrated in Fig. 4.20 (c) and in Fig. 4.24 (a) where we clearly see that the magnetic dipole persists on longer time scales than the electric dipole. Of course after sometimes, one should take into account dissipation effects such as spin flip processes, which would certainly affect the magnetic dipole. Nevertheless during the coherent dynamics, which occurs in the first hundred femtoseconds, the magnetic dipole is created and keeps oscillating. To explain this longer life time, we shall use an argument from plasma physics. It is well known in plasma physics that some special kind of distribution functions, called "water-bag", posses the property to be unaffected by the Landau damping [162]. A water-bag distribution function is a function which is constant in a given region of the phase space and zero everywhere else. By extension we expect that a function which is constant in a certain region of the phase phase space and which decreases rapidly to zero at the border of this region will have a week Landau damping. In Figs. 4.25 and 4.26, we sketch the ground state distribution functions $f^{\uparrow}$, $f^{\downarrow}$, f^{0} and f^{z} defined by the Eqs. (4.51)-(4.52). The distribution functions are plotted in the two dimensional phase space x and v_x. The spin-up and spin-down distribution functions appear to be the same (in reality they are slightly different). If we now look

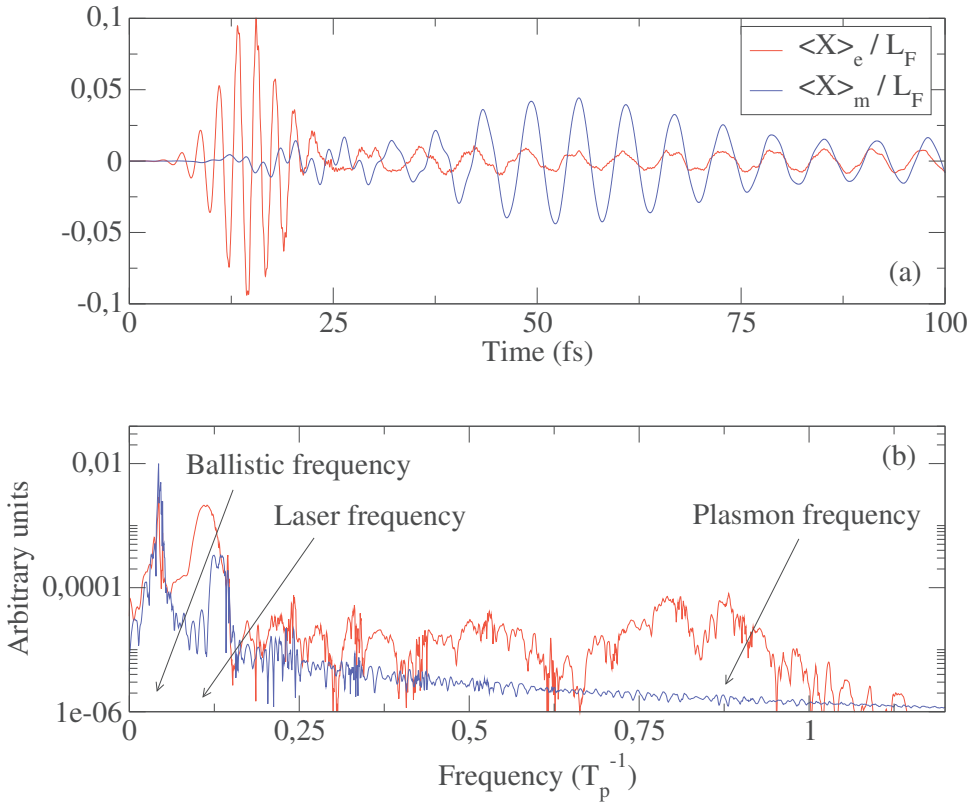

FIGURE 4.27: (a), electric (red curve) and the magnetic (blue curve) dipole (normalized to the Thomas-Fermi screening length) in the case of a film of nickel of size $L = 50\ L_{\mathrm{F}}$, $\sigma = 1\ L_{\mathrm{F}}$. The electrons are excited with a laser pulse with the following carcteristics: $\Delta t = 5$ fs, $\lambda_L = 800$ nm, $E_0 \simeq 10^{10}$ V/m and $t_0 = 3\ \Delta t$. (b), Fourier transform of both dipoles.

the distribution functions of the electron's charges f_0 and of the electron's spins f_z, we notice that they are very different. Indeed the distribution function f_0 (obtained by: $f_0 = f^{\uparrow} + f^{\downarrow}$) is similar to the spin-up and spin-down distributions, whereas the distribution f_z (obtained by: $f_z = f^{\uparrow} - f^{\downarrow}$) is similar to a water-bag distribution function. This can explain why the magnetic dipole, which is only related to the distribution function f_z, is not subjected to the Landau damping.

So far we have seen that we are able to create an oscillating magnetic dipole or spin current in ferromagnetic films using an electric excitation (laser pulse). The oscillations occurs at the ballistic frequency and are thus directly related to the size of the film. Moreover these oscillations have a life time longer than the plasmon oscillations because they are not subjected to the Landau damping. We also proposed an explanation of the physical mechanisms at the origin of these oscillations. To our knowledge, such phenomena was not discussed before in the literature. All the simulations were done with a weak laser power. We shall now check that this effect stays valid with larger incident laser powers.

In Fig. 4.27, we excite the system (nickel films of size $L = 50\ L_{\mathrm{F}}$, $\sigma = 1\ L_{\mathrm{F}}$) with a laser pulse in the visible domain at 800 nm, with a time width of $5\ fs$ and with

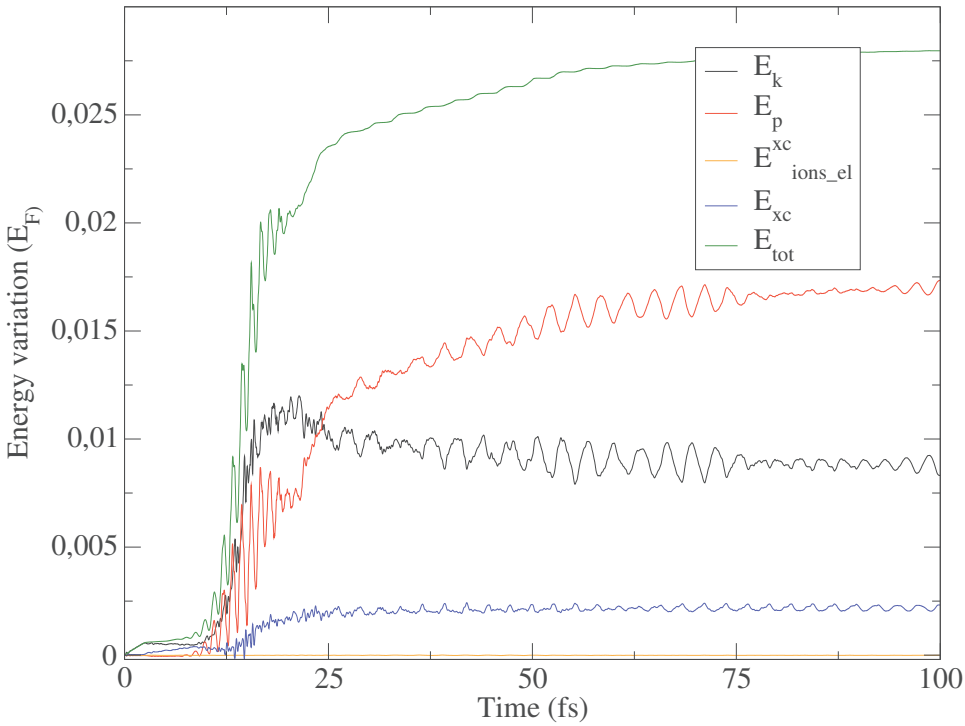

FIGURE 4.28: Time evolution of different electronic energies (normalized to the Fermi energy) corresponding to the simulation in Fig. 4.27.

an amplitude $E_0 \simeq 10^{10}$ V/m. The laser's amplitude is one hundred times stronger than those used in the linear regime, see Fig. 4.24. Roughly speaking that means we give ten thousand times more energy to the system. In the frequency domain this type of pulse cover a small region in the visible domain: $0.175 - 0.575$ PHz (Peta-Hertz) near the ballistic frequency $\omega_b \simeq 0.173$ PHz but far from the plasmon frequency $\omega_p \simeq 2.71$ PHz. In Fig. 4.27(a), we draw the time evolution of the electric and the magnetic dipole during one hundred femtoseconds. During the action of the pulse ($t < 25$ fs), we observe the creation of an electric dipole which oscillates at the laser frequency as it was the case in the linear regime. At the same time the magnetic dipole is created. Then after the laser pulse has disappeared, the magnetic and the electric dipoles continue to oscillates with similar amplitudes.
In Fig. 4.27(b), we give the Fourier transform of both dipoles. The magnetic dipole mainly oscillates at the ballistic frequency (after the pulse) and at the pulse frequency (during the pulse). The electric dipole oscillates at the laser frequency during the pulse, then after the pulse it oscillates at the ballistic and at the plasmon frequency. This can be seen in Fig. 4.27(a) where between $25 - 100$ fs, we see rapid oscillations (plasmon) superposed on large oscillations (ballistic). The fact that the frequency spectrum of the electric dipole contains the plasmon frequency is a signature of nonlinear effects. Indeed we do not excite the system at the plasma frequency, the latter is thus excited by nonlinear effects. We thus conclude that in the nonlinear regime the magnetic dipole (or the spin current) is still oscillating at the ballistic frequency. Moreover, after the laser pulse has disappeared, the electric dipole is

driven by nonlinear effects and oscillates in a combination of plasmon and ballistic frequencies.
We have also sketched in Fig. 4.28 the time evolution of the different energies (kinetic, potential, exchange-correlation and total) corresponding to the above nonlinear simulations. During the laser pulse $0 - 25$ fs all the energies are globally increasing which means that the laser pulse transfers some amount of energy to the system (approximatively $0.025\ E_{\mathrm{F}}$). After the pulse the energy is periodically convert from electron kinetic energy to electron potential energy. So, we again recover ballistic oscillations in the energy curves as it was the case for spinless simulations, see Fig. 4.15. The other energies do not vary significantly. We notice also that the total energy is not exactly constant after the pulse, this is probably due to numerical errors.

4.6 Conclusions and perspectives

In this chapter, we applied the spin-Vlasov equations to model the spin and charge dynamics in nickel thin films. We have seen that in order to construct a ferromagnetic ground state, one should make a distinction between localized and itinerant magnetism. In the case of nickel, we assumed that the itinerant magnetism is carried by the 4s electrons whereas the 3d electrons stay localized around the nucleus to form an ion spin. In our model (4.23), the itinerant electrons are described with the spin-Vlasov equations and the ion spins are described with a Landau-Lifshitz equation. Both magnetic moments (itinerant and localized) are coupled together with a Heisenberg exchange interaction with a coupling constant K. Moreover the ion spins are interacting together with an exchange constant J. K and J are the two main parameters of our model. the parameter J was determined by imposing that the magnetization goes to zero at the experimental Curie temperature. The parameter K was chosen to have the correct proportion of localized/itinerant magnetic moments at $T = 0$ K, according to DFT calculations. We have also seen, thanks to the linear analysis, that our model is able to convert spin-wave magnetic energy into kinetic energy of the itinerant electrons. This transfer of energy leads to a damping of the ion spin waves.
The main issue of this chapter was to study, with the spin-Vlasov model (4.23) coupled to a Landau-Lifshitz equation, the electron spin and the charge dynamics induced by a femtosecond laser pulse. Several studies [38, 39, 144] were done before but the authors studied only the charge dynamics. Taking into account the Zeeman interaction and spin dependent exchange-correlation effects, we were able to perform numerical simulations on the charge and the spin dynamics in thin films of nickel. Our main discovery was that, with an electric excitation, we are able to create an oscillating spin current (or an oscillating magnetic dipole) in addition to the usual electric dipole. While the latter oscillates at the plasma frequency, the spin

current oscillates at the ballistic frequency $\omega_b = (2L/v_{\rm F})^{-1}$ which is inversely proportional to the size of the film. For nickel films of size $L = 50\ L_{\rm F}$, the ballistic frequency $\omega_b = 0.173$ PHz is close to the Peta-Hertz regime. Therefore this ballistic mode can be excited with laser pulse in the visible range. Up to our knowledge this is something which was never before discussed in the literature. Moreover, we have seen that the spin current is not subjected to the Landau damping as it is the case for the electric dipole and thus has a much longer life time. We also proposed a physical explanation for the creation of this oscillating spin current. It relies on three ingredients: the finite size of the system, the self consistent electron-electron interactions and the magnetic properties of the electron ground state.
The present study could be extended in several ways:

- In this study, the $x - y$ components of the electron and ion spins remained weak. The magnetism was thus essentially collinear. Moreover we have always excited the system with electric excitations, we have never used external magnetic fields. A possibility for exploring non-collinear magnetism would be to prepare the system in a non-collinear stationary state. This could be done by launching a spin wave in the system, for instance with an oscillating magnetic field, before the arrival of the laser pulse. Then it would be interesting to see if the spin wave have an influence of the spin current generation or *vice versa*.

- It would also be interesting to study the electron charge and spin dynamics in more complex structures. For instance in bilayer systems, where a ferromagnetic film (nickel) is sticked on a non magnetic film (Gold). So, depending of the relative thickness of both film, it would be interesting to see if the spin current generation persists or not and how the latter is modified.

- In the present work, we only did numerical simulations in a 2 dimensional phase space (x, v_x). Indeed the electrons were only able to move in the transversal direction (x) of the film. It would be very interesting to extend the simulations to 4 dimensions (x, v_x, v_y, v_z). Then, it would be possible to correctly describe the spin-orbit interaction in a dynamical fashion. Even if the corresponding evolution equations would be classical (at least for the orbital dynamics), we would be able to see if it is possible to induce an ultra-fast demagnetization of the system with optical pulses, especially in the nonlinear regime. This would give us a better understanding of the physics contained in the spin-Vlasov equations (2.54)-(2.55). In particular, how the self-consistent electric and magnetic fields are able to enhance the spin-orbit interaction. The difficulties are mainly numerical, as the 2 dimensional simulations (x, v_x) require long simulation times, we have to parallelize our code. Otherwise it would be impossible to perform more than 2 dimensional simulations.
  Another solution could be to combined both kinetic and fluid models. For instance, the dynamics in the (x, v_x) phase space would be treated with kinetic

models such as the spin-Vlasov model (2.54)-(2.55). Whereas the dynamics in the (v_x, v_y) phase space would be described with a set of fluid equations. Such methods were recently used in plasma physics to model particle transport in a tokamak scrape-off layer [163].

Chapter 5

Variational approach to the quantum hydrodynamic models

This last chapter concerns the study of reduced models to describe the nonlinear charge dynamics of an ensemble of interacting electrons. In the previous chapters, we have seen how to include the spin in the electron dynamics. However the numerical simulations were done in the semiclassical limit, using a spin-Vlasov model. Thus the quantum effects on the orbital dynamic were completely neglected. The extension of these simulations in the quantum regime using the Wigner evolution equation is still a big challenge. Another alternative is to use quantum hydrodynamic models, that are an approximation of the Wigner equation and are valid in the long wavelength limit. Here we shall focus on the inclusion of quantum effects in the electronic dynamics but we will omit the spin dynamics. Hydrodynamic methods have been successfully used in the past to model the electron dynamics in molecular systems [45], metal clusters and nano-particles [46–48, 164], thin metallic films [49] and semiconductor quantum wells [52].
We shall use the quantum fluid model proposed by Manfredi in Ref. [68][1] :

$$\frac{\partial n}{\partial t} + \boldsymbol{\nabla}\cdot(n\boldsymbol{u}) = 0, \tag{5.1}$$

$$\frac{\partial \boldsymbol{u}}{\partial t} + \boldsymbol{u}\cdot\boldsymbol{\nabla}\boldsymbol{u} = \boldsymbol{\nabla}V_{\mathrm{H}} - \boldsymbol{\nabla}V_X - \boldsymbol{\nabla}V_{ext} - \frac{\boldsymbol{\nabla}P}{n} + \frac{1}{2}\boldsymbol{\nabla}\left(\frac{\boldsymbol{\nabla}^2\sqrt{n}}{\sqrt{n}}\right), \tag{5.2}$$

$$\boldsymbol{\nabla}^2 V_{\mathrm{H}} = 4\pi n, \tag{5.3}$$

where $n(\boldsymbol{r},t)$ is the electron density, $\boldsymbol{u}(\boldsymbol{r},t)$ the mean electron velocity, and $V_{\mathrm{H}}(\boldsymbol{r},t)$ the Hartree potential. Here, and in all the chapter, the equations are written in atomic units. The first equation (5.1) is the continuity equation and represents the conservation of the mass. The second equation (5.2) is an Euler type of equation, it gives the evolution of the current density with respect to the force acting on the system. The third equation (5.3) is the Poisson equation for the self-consistent Hartree potential V_{H}. In Eq. (5.2), $V_{ext}(\boldsymbol{r},t)$ is an external potential due to, for instance, the interaction with an external field or to a confinement potential. The latter can have different forms, in the Sec. 5.2 the confinement potential will be created by the ionic

[1] For more details about the derivation of this model, see Sec. 1.4

background, it will thus be taken into account in the Hartree potential. Whereas in the Sec. 5.3 it will be given by a non-parabolic and anisotropic well. $P(\boldsymbol{r},t)$ is a pressure term that close the set of the quantum hydrodynamic equations (5.1)-(5.3) one has to express the pressure as a function of the electronic density and the mean velocity[2]. In the next sections, we shall use the Fermi pressure of a 3D degenerated electron gas

$$P = \frac{(3\pi^2)^{2/3}}{5} n^{5/3}. \tag{5.4}$$

This is true if the temperature of the system is always much lower than the Fermi temperature. Finally, the last term in Eq. (5.2) is the so-called Bohm potential [94], which incorporates quantum effects to the lowest order. The Bohm potential is related to the so-called von Weizsäcker term in Thomas-Fermi theory and orbital-free DFT [165]. As in DFT, exchange effects can be modelled by a density-dependent effective potential

$$V_X[n(\boldsymbol{r},t)] = -\frac{1}{\pi}\left(3\pi^2 n\right)^{1/3} + \beta\left[2\,\frac{\boldsymbol{\nabla}^2 n}{n^{4/3}} - \frac{4}{3}\frac{\left(\boldsymbol{\nabla} n\right)^2}{n^{7/3}}\right], \tag{5.5}$$

where the first term is the local density approximation (LDA) and the other two terms are gradient corrections. The pre-factor β is a free parameter that we set equal to $\beta = 0.005$, which is a best-fit frequently used in atomic-structure calculations [166].

Although the quantum hydrodynamic equations are easier to solve numerically then the associated kinetic equations, it is still a considerable computational work to solve them. In this chapter, we will use a variational approach to simplify the quantum hydrodynamic equations. In the first section, we shall give a general overview of the variational approach applied to the quantum fluid model (5.1)-(5.3). The latter is based on a Lagrangian formulation and trial functions that characterize the matter density profile. Then, using this approach, we shall study in the Sec. 5.2 the nonlinear electron dynamics in metallic (Gold) nano-particles. We shall see that by irradiating a metallic nano-particle with an autoresonant chirped laser pulse, it is possible to drive the collective electron modes (surface plasmons) far into the nonlinear regime. This technique shall lead to a higher energy absorption and to a complete ionization of the nano-particle on short time scales ($\sim 100\,\mathrm{fs}$). In Sec. 5.3 we shall study, using the same approach, anharmonic and anisotropic effects in the nonlinear electronic dynamics.

[2] In general, the expression of the pressure can be a complicated function of the other fluid quantities, such examples are given in Sec. 1.4

5.1 Principle of the method

The quantum hydrodynamic equations (5.1)-(5.3) can be represented, without further approximations[3], by a Lagrangian density $\mathscr{L}_D(n, \theta, V_{\mathrm{H}})$, where the function $\theta(\boldsymbol{r}, t)$ is related to the average velocity, $\boldsymbol{u} = \boldsymbol{\nabla}\theta$. The expression for the Lagrangian density is as follows :

$$\begin{aligned}\mathscr{L}_D = n\left[\frac{1}{2}\left(\boldsymbol{\nabla}\theta\right)^2 + \frac{\partial\theta}{\partial t}\right] + \frac{1}{8n}\left(\boldsymbol{\nabla}n\right)^2 + \frac{3}{10}\left(3\pi^2\right)^{2/3} n^{5/3} \\ - \frac{3}{4\pi}\left(3\pi^2\right)^{1/3} n^{4/3} - \beta\frac{\left(\boldsymbol{\nabla}n\right)^2}{n^{4/3}} + nV_{\mathrm{ext}} - nV_{\mathrm{H}} - \frac{1}{8\pi}\left(\boldsymbol{\nabla}V_{\mathrm{H}}\right)^2 . \end{aligned} \tag{5.6}$$

By taking the standard Euler-Lagrange equations with respect to the three fields n, θ, and V_{H}, one recovers exactly the quantum hydrodynamic equations (5.1)-(5.3).
The development done thus far did not simplify the problem. In order to derive the tractable system of equations, one needs to specify a particular ansatz for the electron density. In other words, one has to find a mathematical function F that reproduce the correct electron density. In general the density has to be written as a function of N dynamical variables

$$n(\boldsymbol{r}, t) = F\left[\boldsymbol{r}, d_1(t), d_2(t), \cdots, d_N(t)\right] . \tag{5.7}$$

With such an assumption the time dependence of the electronic density is embedded in the dynamical variables $d_1(t), \cdots, d_N(t)$. The shape of the function F depends on the geometry of the problem and the dynamical variables correspond to the eigenmodes of the system. At this point, ab-inito calculations can be used to guide us in the research of the most realistic electronic density. For instance, the shape of the electronic density can be tuned to match electronic ground states founded by DFT methods. However nothing states that the assumption (5.7) holds when the system is driven far from its equilibrium state.
Such methods were first used to describe the many electron dynamics of semiconductor quantum wells [52]. The author modelled the confinement potential as an harmonic potential. In this case, they assume a Gaussian profile for the electron density. Moreover they introduced two time-dependent variables in the electron density $d(t)$ and $\sigma(t)$, that represent the center-of-mass (dipole motion) and the spatial dispersion of the electron gas (breathing motion), respectively. With such an assumption, the authors constraint the solution of the fluid models to be Gaussian functions. Nevertheless they were able to describe the dipole and the breathing dynamics of the electron gas through the variables $d(t)$ and $\sigma(t)$. In principle, one can imagine to construct more complicated density profiles to study for instance multipolar dynamics. However, as it will be showed below, the choice of the density is a

[3]This assertion is not completely true, indeed to construct the Lagrangian density we wrote the average velocity as deriving from a scalar potential $\boldsymbol{u} = \boldsymbol{\nabla}\theta$. This necessary implies that the average velocity field has a zero rotational.

critical requirement to operate the variational approach.
As we have seen, the heart of the method is to assume a mathematical expression of the electron density to write the Lagrangian density. Then, one is able to find the Lagrangian L of the system by integrating the Lagrangian density over the all space

$$L\left(d_1(t),\cdots,d_N(t),\dot{d_1}(t),\cdots,\dot{d_N}(t)\right)=\int \mathscr{L}_D\left(\boldsymbol{r},d_1(t),\cdots,d_N(t),\dot{d_1}(t),\cdots,\dot{d_N}(t)\right)d\boldsymbol{r}. \tag{5.8}$$

Having the Lagrangian of the system, one can use the Euler-Lagrange equation with respect to the different dynamical variables to obtain a set of N coupled differential equations (one for each dynamical variable)

$$\begin{cases} \ddot{d_1}(t) &= f_1\left(d_1(t),\cdots,d_N(t)\right), \\ \ddot{d_2}(t) &= f_2\left(d_1(t),\cdots,d_N(t)\right), \\ \vdots & \\ \ddot{d_N}(t) &= f_N\left(d_1(t),\cdots,d_N(t)\right). \end{cases} \tag{5.9}$$

Using the Variational approach, the very complicated N body electron dynamics is embedded into a set of differential equations. The latter could be easily solved with standard numerical methods (Runge-Kutta).
For practical applications, the variational method can be difficult to use. Indeed, to find the Lagrangian (5.8) one has to specify, in addition to the electron density, an analytical expression of the fields $\theta(\boldsymbol{r},t)$ and $V_{\mathrm{H}}(\boldsymbol{r},t)$ as functions of the dynamical variables. The field $\theta(\boldsymbol{r},t)$ is related to the mean velocity and should satisfy the continuity equation (5.1) and the field V_{H} should satisfy the Poisson equation (5.3). One insists on the fact that we have to find analytical expressions of θ and V_H so that the variational approach is beneficial to use. However this can be in practice difficult to perform and depends mostly on the mathematical expression we assumed for the electronic density, i.e. on the function F in Eq. (5.7). Nevertheless it is a useful and relatively safe procedure to obtain a mathematically treatable set of equations that can be solved either exactly or with minimal numerical effort. For instance, it was noted in [52] that, even for an approximative density profile, the resonant frequencies computed with the variational techniques are still very close to the exact ones.

5.2 High harmonic generation in Gold nano-particles

In this section, we shall apply the variational approach based on quantum hydrodynamic equations to study the electron dynamics in Gold nano-particles. The latter are metal clusters composed of a few numbers of metallic atoms, between 2 and 10^7. Large metal clusters represent a bridge between molecules and solids. As such, they often exhibit properties belonging to both of these classical disciplines and therefore

are of immense scientific and practical interest. For instance some properties of metal clusters are size dependent. A relatively complete set of results about metal clusters are given in Ref. [132].
On a fundamental point of view, small clusters are very interesting to study because we are able to perform numerical simulations using a relatively complete quantum treatment, for instance using the time-dependent density functional theory (TDDFT) [32, 33] or Wigner function methods [39, 56]. Moreover many body quantum effect have a big influence of the behaviour of such systems. Therefore it is interesting to compare the exact theory to the experience, in order to understand better this type of effect. However such theories are much difficult to simulate for large clusters. An other alternative is to use reduced models such as the quantum hydrodynamic models presented above Eqs. (5.1)-(5.3).
In a first part, using this approach, we shall derive a set of equations of motion to describe the electrons dynamics. In particular, we will focus on the two electronic modes the dipole modes and the breathing modes. Our results will be compared to general results about metal clusters theory [132, 167, 168]. In a second part, we shall study the dynamics of collective electron modes (surface plasmons) excited with laser pulses in the visible range. To drive the plasmon mode far into the nonlinear regime, we will namely use chirped pulses with slowly varying frequency. This is based on the process of autoresonance, which is a theory applicable to any oscillating systems. The purpose is to use a time dependent driving frequency to lock the instantaneous oscillator frequency to the instantaneous excitation frequency. Then on is able to strongly excite the system without using a strong external driving force. Autoresonant effects were observed in many different physical fields, for instance in atomic physics [169, 170], fluid dynamics [171], plasmas [172], nonlinear waves [173, 174] and planetary dynamics [175, 176]. Autoresonant excitations has been also successfully applied on several systems, such as charged antiparticles [177], the quantum pendulum [178], semiconductor quantum dots [179] and electron-positron clusters [48]. This method will allow us to excite the plasmon modes far into the nonlinear regime, leading to the emission of electromagnetic radiation with a power spectrum rich in high-order harmonics.

5.2.1 Application of the Variational approach

We consider spherical metal clusters composed of N ions and of N electrons (ions are assumed singly ionized). Typically N shall be on the order of the hundred of atoms. We describe the clusters in the Jellium approximation, i.e. we consider that ions are fixed and homogeneously distributed. Therefore we have

$$n_i = \begin{cases} n_0, & r < R \\ 0, & r > R \end{cases}, \tag{5.10}$$

where the ions density in the cluster is given by $n_0 = N/\left(\frac{4}{3}\pi R^3\right)$. The parameter R represents the radius of such clusters which is related to the number of ions and to the Wigner-Seitz radius r_s by $R = r_s N^{1/3}$. The ions are supposed to be fixed during the electron motion. This assumption is justified by the fact that there is a time scale separation between the ions and the electrons motion, which is given by the plasma frequency ω_p (1.5). Indeed considering a Gold cluster with a density of 10^{28} atoms per cubic meter, we obtain a typical time on the order of 1 femtosecond for electrons and 0.3 picosecond for ions. Therefore electrons move a hundred times faster than ions.
The model we shall use is the based on the quantum hydrodynamic equations (5.1)-(5.3) except that the electrons are not confined by a confinement potential $V_{\text{conf}}(\boldsymbol{r}, t)$ but by the ionic background (5.10). Therefore the quantum hydrodynamic model writes:

$$\frac{\partial n}{\partial t} + \boldsymbol{\nabla}\cdot(n\boldsymbol{u}) = 0, \tag{5.11}$$

$$\frac{\partial \boldsymbol{u}}{\partial t} + \boldsymbol{u}\cdot\boldsymbol{\nabla}\boldsymbol{u} = \boldsymbol{\nabla}V_{\text{H}} - \boldsymbol{\nabla}V_x - \frac{\boldsymbol{\nabla}P}{n} + \frac{1}{2}\boldsymbol{\nabla}\left(\frac{\boldsymbol{\nabla}^2\sqrt{n}}{\sqrt{n}}\right), \tag{5.12}$$

$$\boldsymbol{\nabla}^2 V_{\text{H}} = 4\pi\left(n - n_i\right), \tag{5.13}$$

where V_x and P are respectively the exchange potential (5.5) and the pressure term (5.4). The QHD model (5.11)-(5.13) can be can be derived from the following Lagrangian density (5.6)

$$\begin{aligned}\mathscr{L}_D = n\left[\frac{\partial S}{\partial t} + \frac{(\boldsymbol{\nabla}S)^2}{2}\right] + \frac{(\boldsymbol{\nabla}n)^2}{8n} + \frac{3}{10}\left(3\pi^2\right)^{2/3} n^{5/3} \\ -\frac{3}{4\pi}\left(3\pi^2\right)^{1/3} n^{4/3} - \beta\frac{(\boldsymbol{\nabla}n)^2}{n^{4/3}} - \frac{(\boldsymbol{\nabla}V_{\text{H}})^2}{8\pi}\left(n_i - n\right)V_{\text{H}}.\end{aligned} \tag{5.14}$$

Our purpose now is to derive, using the variational approach described in Sec. 5.1, a set of evolution equations for a small number of macroscopic quantities that characterize the electron density profiles. In metal clusters the density of electrons presents two important characteristics. The first is a decay of the electron density near the border of the cluster, it is a classical effect known as the spill-out. The second are oscillations of the electron density in the center of the cluster. The latter have a purely quantum origin and can be interpreted as Friedrich oscillations due to screening effects [180]. Keeping in mind that our hydrodynamic model is semi-classic, we will just include the spill-out effect in our model. Therefore we assume that the electron density has the following shape :

$$n(\boldsymbol{r}, t) = \frac{A}{1 + \exp\left[\left(\frac{s(\boldsymbol{r},t)}{\sigma(t)}\right)^3 - \left(\frac{R}{\sigma_0}\right)^3\right]}, \tag{5.15}$$

where A is chosen in order to normalize the density

$$A = \frac{3N}{4\pi\sigma^3}\left[\ln\left(1+\exp\left(\frac{R}{\sigma_0}\right)^3\right)\right]^{-1} \tag{5.16}$$

and s is a displaced radial coordinate $s(\boldsymbol{r},t) = \sqrt{x^2+y^2+(z-d(t))^2}$. We introduced two macroscopic dynamical variables in the density profile, namely the center of mass of the electron gas called $d(t)$ and the thickness of the spill-out effect called $\sigma(t)$. The first represents a dipole motion of the electron gas along the ion bulk. The second represents a breathing motion because it corresponds to oscillations of the electron gas size through the spill-out effect. We introduced the variable d to allow the electron gas to oscillate in the z direction in order to describe collective electron oscillations (surface plasmons). The restriction along one axis is permitted because the system is isotropic. The equilibrium case corresponds to $d = 0$ and

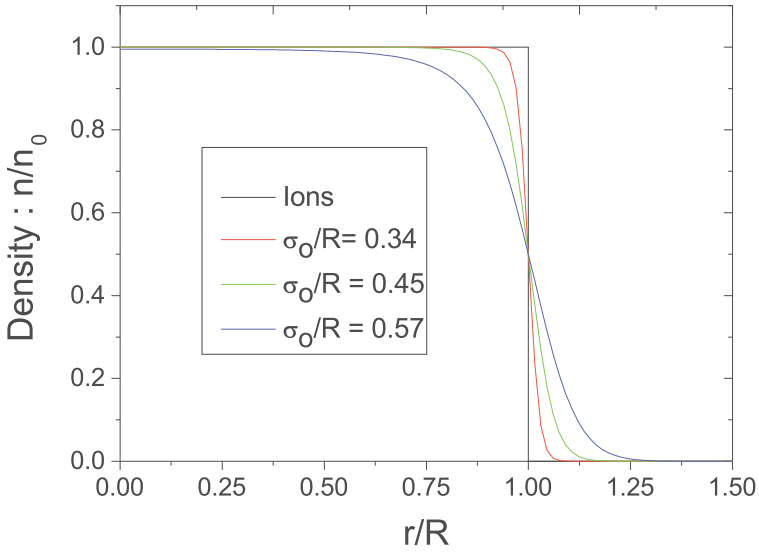

FIGURE 5.1: In this figure, we plot different electron densities in the case of a Gold clusters with 200 ions, the corresponding radius is $R = 17.60$ a.u. ($0.93\,\mathrm{nm}$). The black curve and the color curves correspond, respectively, to the ions (5.10) and the electrons (5.15) densities. The latter are given in the equilibrium case, i.e. for $\sigma = \sigma_0$ and $d = 0$, for different values of σ_0.

$\sigma = \sigma_0$. In Fig. 5.1, we sketched the electron and the ion equilibrium densities for different values of the parameter σ_0. Obviously for a given cluster, there is only one possible value of σ_0, we will see later how to determine it.
Of course, such an ansatz is not exact and may even differ significantly for small nano-particles from the electron density obtained, for instance, from DFT calculations, see Ref. [180]. Nevertheless, we shall have access to the electron dynamics thanks to the variables $d(t)$ and $\sigma(t)$.

To derive the equation of motion, we have to find the two other fields θ and V_{H} as a function of the dynamical variables $d(t)$ and $\sigma(t)$. Finding θ consist to search the average velocity of the electron gas $\boldsymbol{u}$ which is solution of the continuity equation. The Hartree potential corresponds to the solution of the Poisson equation, so it is fully determined by the two densities n and n_i and by the boundary conditions. One of the great advantages of the expression (5.15) is that we are able to find a simple expression for such quantities. Indeed, the continuity equation is solved with

$$\boldsymbol{u} = \frac{\dot{\sigma}}{\sigma}\left(x\widehat{x} + y\widehat{y}\right) + \left[\frac{\dot{\sigma}}{\sigma}\left(z-d\right) + \dot{d}\right]\widehat{z}, \tag{5.17}$$

which gives

$$\theta = \frac{\dot{\sigma}}{2\sigma}\left[x^2 + y^2 + (z-d)^2\right] + \dot{d}\left(z-d\right). \tag{5.18}$$

The Hartree potential is more complicated to find because we have to solve a Laplace equation. However, in our case we have just to find the gradient of V_{H}. Indeed the Lagrangian part containing the Hartree potential can be rewritten, using the Poisson equation, as

$$-\frac{(\boldsymbol{\nabla}V_{\mathrm{H}})^2}{8\pi} + (n_i - n)V_{\mathrm{H}} = \frac{(\boldsymbol{\nabla}V_{\mathrm{H}})^2}{8\pi} - \frac{\boldsymbol{\nabla}.(V_{\mathrm{H}}\boldsymbol{\nabla}V_{\mathrm{H}})}{4\pi}. \tag{5.19}$$

The last surface term will be irrelevant at least for decaying boundary conditions. So we need just to know $\boldsymbol{\nabla}V_{\mathrm{H}}$, which can be easily found using the following decomposition $V_{\mathrm{H}} = V_i + V_e$, where V_i and V_e are, respectively, the contribution due to the ions ($\boldsymbol{\nabla}^2 V_i = -4\pi n_i$) and the electrons ($\boldsymbol{\nabla}^2 V_e = 4\pi n$). They can be solved separately, using the spherical coordinates one obtains :

$$\frac{\partial V_i(r)}{\partial r} = \begin{cases} -\dfrac{N}{r_c^3}r, & r \leq r_c \\ \\ -\dfrac{N}{r^2}, & r > r_c \end{cases}, \tag{5.20}$$

and

$$s^2\frac{\partial V_e(s,t)}{\partial s} = \frac{N}{\ln(1+1/a)}\left[\frac{s^3}{\sigma^3} - \ln\left[1 + a\exp(s^3/\sigma^3)\right] + \ln(1+a)\right], \tag{5.21}$$

where we introduce the small parameter $a = \exp\left(-r_c^3/\sigma_0^3\right)$. The last equation is physically relevant for $s \to 0$ and for $s \to \infty$.
The next step is to integrate this Lagrangian density with respect to space in order to obtain the Lagrangian function L, see Eq. (5.22). In general it is a straightforward problem to integrate the Lagrangian density. However here many expressions can not be integrated easily and have to be evaluated numerically. The most difficult problem comes from the cross term $\int \boldsymbol{\nabla}V_e.\boldsymbol{\nabla}V_i d\boldsymbol{r}$, which apparently can only be

found in terms of a power series on the variables d/R. So the Lagrangian (5.22) will be not exact but it will be calculated up to $O(d^5/R^5)$. Skipping the details, which are given in appendix C, the result is

$$L = \frac{-1}{N}\int \mathscr{L}_D d\boldsymbol{r} = \frac{M(a)\dot{\sigma}^2}{2} - U(\sigma) + \frac{\dot{d}^2}{2} - \frac{\Omega_d^2(\sigma)d^2}{2} + K(\sigma)d^4, \tag{5.22}$$

where the fictitious mass

$$M(a) = -\frac{\Gamma(5/3)\mathrm{Li}_{5/3}(-1/a)}{\ln(1+1/a)}, \tag{5.23}$$

is given in terms of a Gamma function $\Gamma(5/3) \simeq 0.90$ and a Polylogarithm function $\mathrm{Li}_{5/3}(-1/a)$. The other terms in equation (5.22) are the pseudo-potential

$$U(\sigma) = \frac{f_B(a)}{\sigma^2} + \frac{N^{2/3}f_F(a)}{\sigma^2} - \frac{N^{1/3}f_X(a)}{\sigma} - \frac{\beta f_{X'}(a)}{N^{1/3}\sigma} + \frac{N f_{ee}(a)}{\sigma} - \frac{N f_{ei}(\sigma)}{r_c} \tag{5.24}$$

and the functions

$$\Omega_d^2(\sigma) = \frac{N}{r_c^3\ln(1+1/a)}\left[\frac{r_c^3}{\sigma^3} + \ln(1+a) - \ln\left[1 + a\exp(r_c^3/\sigma^3)\right]\right], \tag{5.25}$$

$$K(\sigma) = \frac{9Nr_c a}{40\ln(1+1/a)\sigma^6}\,\frac{\exp(r_c^3/\sigma^3)}{\left[1+a\exp(r_c^3/\sigma^3)\right]^2}, \tag{5.26}$$

which are both positive definite. The quantities f_B, f_F, f_X, $f_{X'}$, f_{ee} and f_{ei}, present

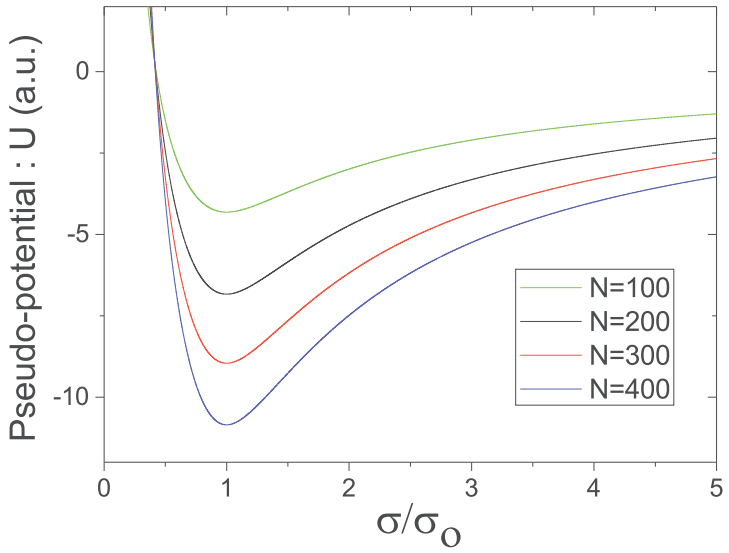

FIGURE 5.2: Plot of the pseudo-potential $U(\sigma)$ (5.24) for different nano-particle sizes.

in the pseudo-potential (5.24), are given explicitly in appendix C by (C.16), (C.18), (C.20), (C.22), (C.25) and (C.28). They are related respectively to the Bohm potential, Fermi pressure, exchange energy (LDA), gradient correction to the exchange energy (GGA), electron-electron interactions and the zero order electron-ion interactions, i.e for $d = 0$. All these functions are positive, as well as the fictitious mass $M(a)$, in accordance with the role played by the Bohm, Fermi and electron-electron terms which are repulsive, and by the exchange energy and the electron-ion terms which are attractive. The quantity $\Omega_d^2(\sigma)$ corresponds to the second order term in the development of the electron-ion interacting energy and $K(\sigma)$ to the fourth order. The first and the third terms in the Lagrangian (5.22) correspond to kinetic energies, while the second and the two last terms correspond to potential terms. The exact Lagrangian corresponding to (5.22) should include an infinite power series of the dynamical variable d. Only even terms must be present because the problem is symmetric according to the x, y plane. In (5.22) we only have the three first terms, we shall see that it is sufficient to describe non linear effects.
Using the Euler-Lagrange equation on (5.22), we obtain the following equations of motion :

$$\ddot{\sigma} = \frac{1}{M(a)}\left\{ -\frac{dU(\sigma)}{d\sigma} + \frac{3Nd^2}{2\sigma^4 \ln(1+1/a)} \frac{1}{1+a\exp(r_c^3/\sigma^3)} - \frac{27Nr_c a \exp(r_c^3/\sigma^3) d^4}{40\ln(1+1/a)\sigma^{10}} \right.$$
$$\left. \times \frac{\left[1-a\exp(r_c^3/\sigma^3)\right] r_c^3 + 2\left[1+a\exp(r_c^3/\sigma^3)\right]\sigma^3}{\left[1+a\exp(r_c^3/\sigma^3)\right]^3} \right\}, \tag{5.27}$$

$$\ddot{d} = -\Omega_d^2(\sigma) d + 4K(\sigma) d^3. \tag{5.28}$$

We end up with a set of two differential equations which are coupled to each other. As expected they describe two modes of oscillations, the dipole mode which is governed by (5.28) and related to the variable d. And the breather mode which is governed by (5.27) and related to σ. These two modes of oscillation were also found in Ref. [52].
The approximation made on the Lagrangian (5.22) has an impact only on the evolution equation for d. Therefore the evolution equation for σ is valid for all values of d and σ. Normally the equation governing the dipole motion should be composed of an infinite number of odd terms of the variable d. However we shall see in the Sec. 5.2.3 that it is sufficient to describe large dipole oscillations. The reason why we chose to developed the Lagrangian up to $O(d^5/r_c^5)$ appears clearly here, it is to have at least a non linear contribution for the dipole motion. Solutions of these differential equations are easily accessible numerically using for instance a Runge-Kutta algorithm.
In summary, we have reduced the formidable problem of the quantum electron dynamics in a metallic nano-particle to a simple set of two coupled differential equations, which can be easily solved even for large systems containing many electrons, where DFT methods are too costly. No assumptions of linearity were made so far,

so that Eqs. (5.27)-(5.28) can be used to study the nonlinear response (as long as d is not too large). Further, compared to simple "rigid sphere models" [181], our approach incorporates many more effects, including quantum nonlocality, spill-out, exchange, and (as shown later) correlations [182].

5.2.2 Steady state and linear response

N	r_0 (a.u.)	σ_0 (a.u.)	$\Omega_d(\sigma_0)$ (a.u.)	$\Omega_b(\sigma_0)$ (a.u.)
50	11.09	6.24	0.1793	0.2988
100	13.97	7.21	0.1821	0.3059
150	15.99	7.86	0.1835	0.3093
200	17.60	8.36	0.1843	0.3114
250	18.96	8.77	0.1848	0.3129
300	20.15	9.12	0.1852	0.3141
350	21.21	9.43	0.1856	0.3150
400	22.18	9.70	0.1859	0.3158
450	23.07	9.95	0.1861	0.3164

TABLE 5.1: The values calculated here correspond to Gold clusters. We give the equilibrium values of the dynamical variable σ for different clusters size and the associated resonant frequencies.

In order to validate the above model, we first present an analysis of the ground state and linear response of the system, for which well-established results, both theoretical and experimental, already exist. The ground state of the system is obtained by setting the time derivatives equal to zero in Eqs. (5.27)-(5.28). Equation (5.28) is satisfied automatically for $d = 0$ (i.e., the center of mass of the ions and the electrons should coincide). Setting $d = 0$ in Eq. (5.27), the stable equilibrium is the value σ_0 that minimizes the pseudopotential $U(\sigma)$, i.e. $U'(\sigma_0) = 0$ and $U''(\sigma_0) > 0$. In this case the probelm is a bit more complicated because the pseudo-potential U depends itself on the equilibrium value σ_0. Therefore, an iterative process can be applied to find σ_0, starting from a trial value of σ_0. Results for Gold clusters are given in Tab.5.1. We plot also the pseudo-potential as a function of σ for different clusters size in Fig. 5.2. As expected they have a minimum in $\sigma = \sigma_0$

In the linear response regime, one can identify two electronic modes, corresponding to oscillations of $\sigma(t)$ (breathing mode) and oscillations of $d(t)$ (dipole, or surface plasmon, mode). We first consider the breathing mode. Setting $d = 0$ in Eq. (5.27)

and expanding $U(\sigma)$ around σ_0 up to first order, we obtain $\ddot{\sigma} =\simeq \frac{1}{M(a)}\frac{d^2U}{d\sigma^2}(\sigma_0)\,(\sigma-\sigma_0)$. The linear breathing frequency is therefore

$$\Omega_b(\sigma_0) = \left[\frac{1}{M(a)}\frac{d^2U}{d\sigma^2}(\sigma_0)\right]^{1/2}. \tag{5.29}$$

which can be easily evaluated numerically. For the dipole mode, assuming that $\sigma = \sigma_0$ and $d \ll R$, Eq. (5.28) yields immediately the linear dipole frequency

$$\Omega_d(\sigma_0) = \sqrt{\frac{N}{r_c^3\ln(1+1/a)}\left[\frac{r_0^3}{\sigma_0^3}+\ln(1+a)\right]}. \tag{5.30}$$

For large nano-particles, the latter tends to the bulk Mie frequency [132,183] : $\omega_{Mie} = \frac{\omega_p}{\sqrt{3}}$ (where ω_p is the plasmon frequency (1.5)), as can be checked directly by taking the limit $R/\sigma \to \infty$.
In general, both the dipole and breather frequencies should depend on the size of the nano-particle in the following fashion [167,168,184]:

$$\Omega_{d,b}(N) = \Omega_\infty\left(1 - k_{d,b}N^{-1/3}\right), \tag{5.31}$$

where $k_{d,b}$ are positive constants, and Ω_∞ is equal to ω_{Mie} for the dipole mode and to ω_p for the breathing mode. Our model reproduces very well these scaling, as can be seen from Fig5.3. The extrapolation at $N \to \infty$ gives the correct Mie or plasmon frequency for the bulk. As it was mentioned above electron correlations

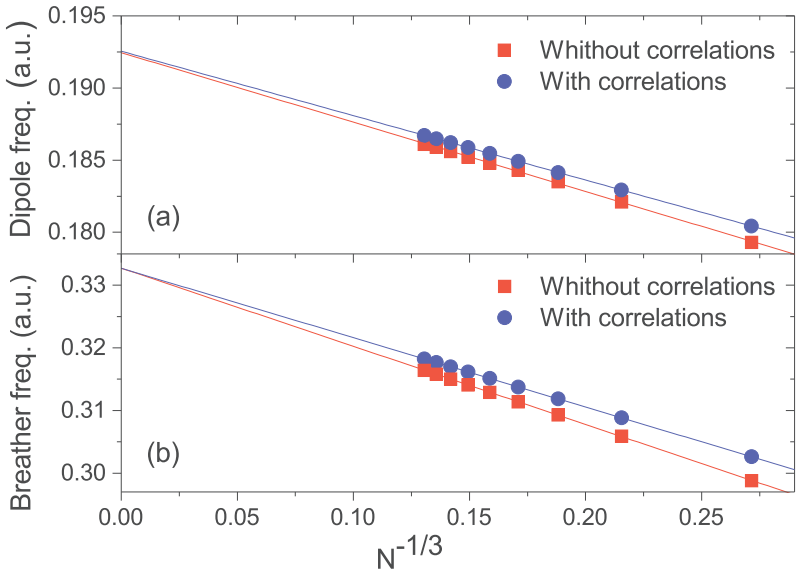

FIGURE 5.3: Linear dipole (a) and breathing (b) frequencies for gold nano-particles as a function of $N^{-1/3}$. Blue circles and red squares represent respectively the results with and without correlations. The straight lines are linear fits.

can be introduced through an appropriate functional of the density. Here, we use the functional proposed by Brey et al. [185], which yields the following correlation potential: $V_C = -\gamma \ln\left[1 + \delta n^{1/3}\right]$, with $\gamma = 0.03349$ and $\delta = 18.376$. This potential can be included in our Lagrangian formalism (details are given in appendix C). For all the cases we studied, the effect of the correlations was almost negligible, as can be seen from Fig. 5.3. Indeed, a quick estimate shows that the ratio between the exchange (LDA) and the correlation potentials is very small, $V_C/V_{X,LDA} \approx 0.084$. This is also in agreement with early results obtained with DFT and Hartree-Fock methods [186].
Now, we propose to do some numerical simulations in the linear regime in order to verify that we recover the corresponding frequencies for the dipole mode and the breather mode. We start with a configuration close to the equilibrium case, i.e. $d \simeq 0$ and $\sigma \simeq \sigma_0$, and we leave the system oscillating. We observe periodic oscillations for both modes, so we plot theirs frequencies spectrum in Fig.5.4. We find a intensity peak at 0.1841 a.u. for the dipole mode and a intensity peak at 0.3116 a.u. for the breather mode. This is very close to what was predicted in Tab.5.1 and thus validates our numerical simulations.

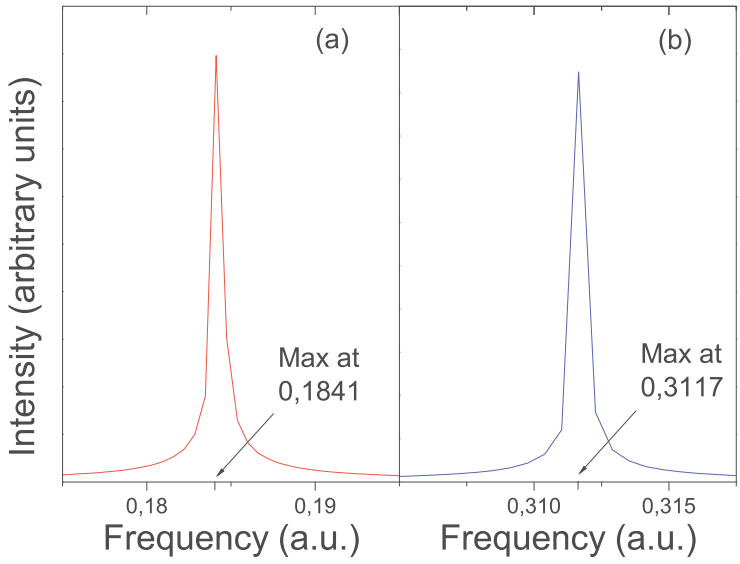

FIGURE 5.4: We plot the Fourier transform of the dipole (a) and breathing (b) modes obtained by numerical simulations on Gold nano-particles with $N = 200$. The electron density was exited by a small space shift of the electronic center of mass in order to stay in the linear regime.

5.2.3 Nonlinear response and autoresonant excitation

In this section we will present the autoresonance phenomena [66], we will see how it allows us to create large amplitude oscillations with a weak driving force. In

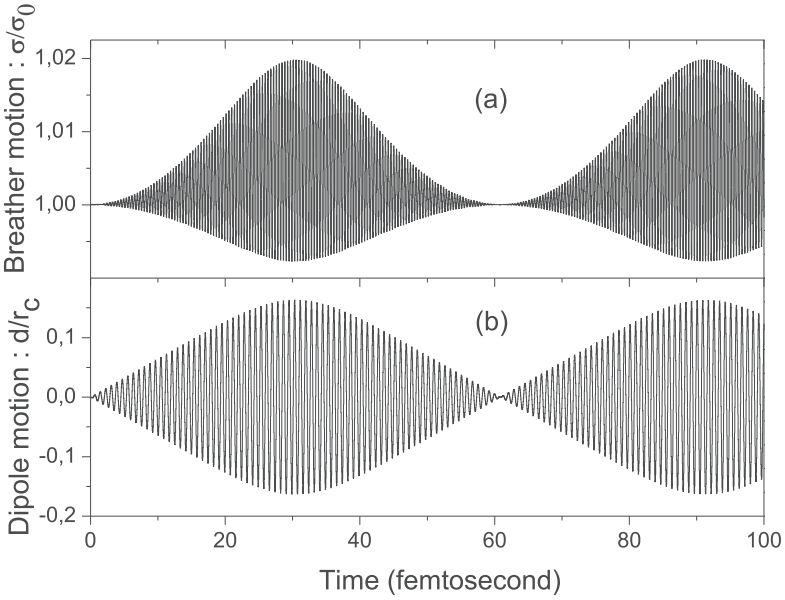

FIGURE 5.5: Numerical simulations done on Gold nano-particles with $N = 200$. The electrons are exited with a sinusoidal electric field (5.34) at the dipole frequency and with an excitation strength $\xi =$. In Fig. (a), we plot the time evolution of the breathing mode ($\sigma(t)$) and in Fig. (b) the time evolution of the dipole mode $d(t)$.

our case the driving force is a laser field, which create an oscillating electric field in the z direction : $\boldsymbol{E} = E_z \boldsymbol{u_z}$. Large amplitudes means that the electron gas will explore the nonlinear regime. However the equation for the dipole motion (5.28) is not necessarily valid in the nonlinear regime. The reason is that we developed the Lagrangian in terms of a power series on the variable d/R (up to the order five). Therefore we must first discuss the limits of this approximation. More precisely the equation of the dipole motion (5.28) can be rewritten as

$$\ddot{d} = -\frac{\partial V(d,\sigma)}{\partial d}, \tag{5.32}$$

where $V(d,\sigma)$ is the potential in which evolves the center of mass of the electron gas

$$V(d,\sigma) = \frac{\Omega_d^2(\sigma)}{2} d^2 - K(\sigma) d^4. \tag{5.33}$$

Since $K(\sigma)$ is always positive, this potential is attractive for values of d smaller than a certain critical length d_c, then it becomes repulsive. The latter behaviour is not a physical behaviour because fore large values of d the potential should behave like an attractive Colombian potential. Therefore we can estimate that our approximation is correct until the potential remains attractive, i.e. $d \ll d_c$. The critical length cannot be determined in advance because it depends on the values of $\sigma(t)$ and thus

changes in time. A mathematical analysis of the potential (5.33) shows us this critical length is at minimum equal to 65% of the cluster's size. Moreover this result does not change a lot with the number of particles. Therefore the model is considered as valid only if the center of mass of the electron gas is displaced on lengths below 65% of R, i.e. $d/R \ll 0.65$. In the simulations, the fact that σ oscillates a lot allows us to excite the electron gas on lengths close to 80% of the cluster size. This is sufficient to study the nonlinear regime.
In order to create large oscillations, we have to excite the system at the its resonant frequencies. Therefore to create dipole oscillations we shall apply a sinusoidal electric field E_z at the dipole frequency

$$E_z = \xi \cos\left(\Omega_d(\sigma_0)t\right), \tag{5.34}$$

where $\Omega_d(\sigma_0)$ is the frequency of the laser and ξ its amplitude.
The action of the laser field can be incorporated easily in the equation of motion. The interacting energy between the laser and the electron gas is equal to $\int nV d\boldsymbol{r}$, where V is the electric potential which corresponds to the electric field (5.34), thus $V = -zE_z$. Then, the new Lagrangian is obtained by adding this interacting energy to the previous Lagrangian

$$L = L_{old} - \frac{1}{N}\int -nzE_z dz = L_{old} + dE_z, \tag{5.35}$$

where L_{old} is the previous Lagrangian (5.22). This correction shall only change the equation of motion for d, we obtain

$$\ddot{d} + \Omega_d^2(\sigma)d = 4K(\sigma)d^3 - E_z. \tag{5.36}$$

Nonlinear simulations of the dipole and the breathing motions are showed in Fig.5.5. As expected the dipole oscillations grow rapidly and then decrease after some times. The physical reason is that, when the dipole frequency of the electron gas approaches the resonant frequency then the amplitudes of the oscillations become more and more important. The system thus enters in the nonlinear regime where the resonant frequencies become dependent of the oscillation's amplitudes. The consequence is that the instantaneous frequency of the system goes out of phase with its drive and we are not able to excite the system any more. For the breathing oscillations the same kind of physics happens. Consequently it seems impossible, with a simple sinusoidal excitation of the type (5.34), to create very large dipole oscillations without using a strong driving force. However we will see that it is possible using an autoresonant excitation.
The principle of an autoresonant excitation is to reduce slowly the frequency of the driving force such that the frequency of the system stays always in phase with its drive, see Ref. [66]. The variation of the frequency is supposed to be linear in time

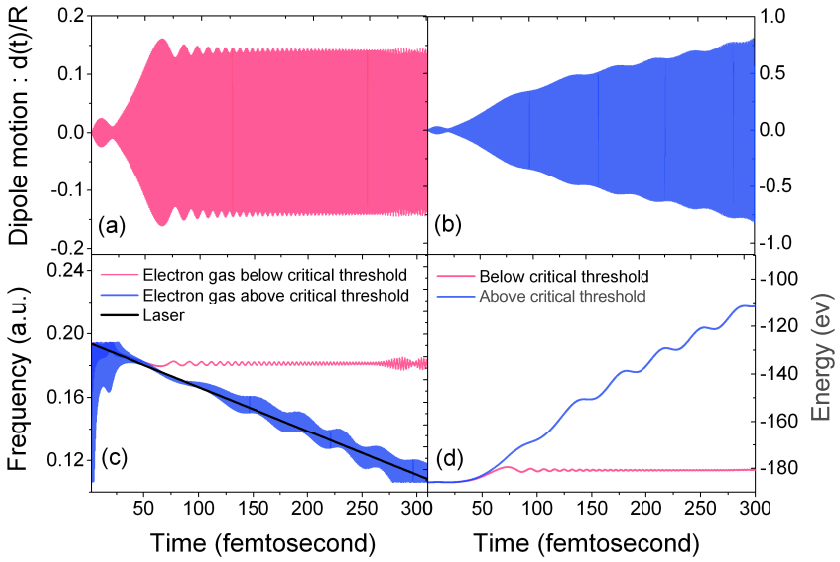

FIGURE 5.6: . Autoresonant excitation of a gold nano-particle with $N = 200$, for two values of the laser intensity, $I_0 = 4.5 \times 10^{10}\mathrm{W/cm^2}$ (below threshold, red curves) and $I_0 = 5.4 \times 10^{10}\mathrm{W/cm^2}$ (above threshold, blue curves). The top panels show the time evolution of the dipole $d(t)$ (a) below threshold and (b) above threshold. (c) Laser frequency (red straight line) and instantaneous dipole frequency of the electron gas for the below threshold (red) and above threshold (blue) cases. (d) Energy absorbed by the electron gas, for both cases.

with a rate $\alpha < 0$[4]. The linearity dependence of the frequency is assumed because, as we will see below, the phase locking process should be done in an adiabatic way. The autoresonant excitation can be thus written as

$$E_z = \xi \cos\left[\Omega_d(\sigma_0)\,(t - t_0) + \frac{1}{2}\alpha\,(t - t_0)^2\right], \tag{5.37}$$

where the time dependent frequency is

$$\omega(t) = \Omega_d(\sigma_0) + \alpha\,(t - t_0)\,. \tag{5.38}$$

We introduce the parameter t_0 such that at the time $t = t_0$ the instantaneous frequency of the laser field is equal to the resonant frequency of the dipole mode. This process is called autoresonant because, at any time, the nonlinear instantaneous frequency of the system should matches the frequency of its drive. The two fundamental parameters are the strength of the driving force ξ and the rate of variation of the laser frequency. α. Both can not be chosen arbitrarily, they have to satisfy a resonant condition. For $\alpha \ll \Omega_d^2$ and ξ above a certain threshold ξ_{th}, the instantaneous oscillator frequency becomes "locked" to the instantaneous excitation frequency, so that

[4]In principle the frequency chirp can also be positive, it depends on the local form of the confinement potential

the resonance condition is always satisfied. In that case, the amplitude of the oscillations grows indefinitely and without saturation, until of course some other effect kicks in. In Ref. [66], the authors found that in the case of a duffing equation, there is a critical threshold proportional to $\alpha^{3/4}$: $\xi_c \sim |\alpha|^{3/4}$ below which autoresonance no longer works. Therefore the amplitude can be arbitrarily small provided that the external frequency varies slowly enough. It is also mentioned that this relation stays valid for other type of systems which are not governed by a duffing equation, it thus seems to be a universal property of autoresonance processes.

In Fig. 5.6, we display the results of an autoresonant excitation of the electron gas, for two realistic (but still very modest) [187] values of the laser intensity $I_0 = \frac{1}{2}c\varepsilon_0|E_0|^2$ that are either below or above the autoresonant threshold. For an intensity $I_0 = 4.5 \times 10^{10}\mathrm{W/cm}^2$ (below threshold, Fig. 5.6a), the dipole oscillations grow initially and then saturate at a rather low level. Figure 5.6c shows the instantaneous laser frequency and the dipole frequency of the electron gas. The instantaneous frequency of the dipole motion is determined by using an Hilbert transform [188]. The two frequencies stay close together initially, but then diverge for the below-threshold case. In contrast, when $I_0 = 5.7 \times 10^{10}\mathrm{W/cm}^2$ (just above threshold), the amplitude of the dipole oscillations increases virtually without limits, reaching 80% of the size of the nano-particle (Fig. 5.6b). Thus, in practice, all the electrons have been ejected from the nano-particle (although they are still accounted for by our dynamical model) on a time scale of the order of a few hundred femtoseconds. The laser and the electron gas frequencies are locked in resonance during the entire duration of the simulation (Fig. 5.6c, blue line), which is the hallmark of the autoresonant excitation. This leads to strongly enhanced absorption of the laser energy by the nano-particle, as is evident from the plot of the total absorbed energy in Fig. 5.6d. It must be noted that, since we expanded the Lagrangian in d/R, the force acting on the dipole in Eq. (5.28) becomes repulsive for d exceeding a certain value $d_{\max}$ (which depends on σ), thus making the model invalid for $d > d_{\max}$.This value reaches its minimum for $\sigma \approx \sigma_0$, where $d_{\max} \simeq 0.65R$. We notice also that the system is driven far from its equilibrium state in a ultra shirt time scale, on the order of of a few picoseconds ($0.3\,\mathrm{ps}$). Here we reach an other limit of our model which is the Born-Oppenheimer approximation, i.e. that the ions are friezed during the electron motion. Indeed the ionic time scale is close to $0.3\,\mathrm{ps}$. Even with these limitations, our simulations constitute a clear proof of principle that strongly nonlinear plasmon modes can be excited using an autoresonant laser pulse of relatively low intensity.

We have also done simulations to verify the threshold power law ($\xi_c \sim |\alpha|^{3/4}$). We first fix the frequency chirp α to a given value and then we wary the laser intensity from until reaching the threshold value. Results are given in Fig.5.7, we correctly found that ξ scales as $\alpha^{3/4}$. Again this is a hallmark of an autoresonant process. Here the simulation were done over two orders of magnitude of the parameter α. We can not check for higher values of α because the corresponding critical electric field is too big, so the system does not remain confined in the attractive part of the

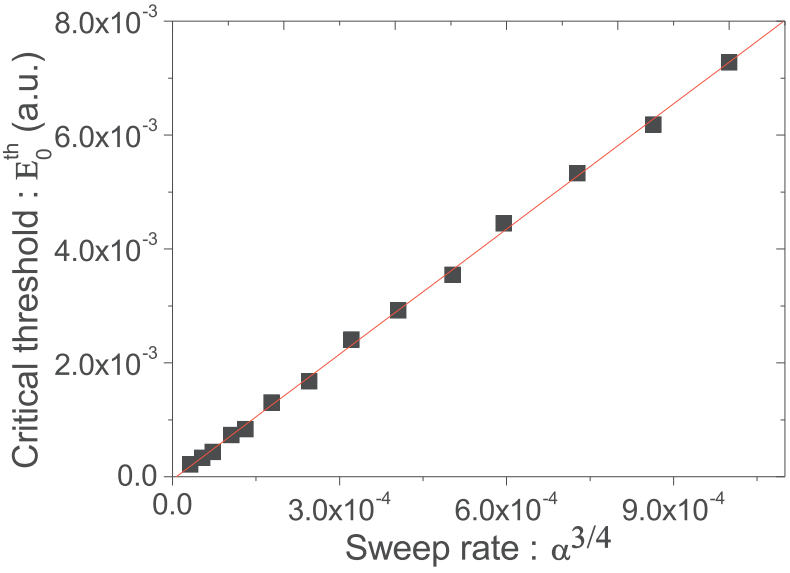

FIGURE 5.7: Critical threshold as a function of the frequency chirp (black square). The simulations were done on gold clusters with two hundred ions ($N = 200$). The red line is a linear fit.

potential before autoresonance occurs.

It is also interesting to compute the total power radiated by the electron gas, for cases above and below the critical threshold. Far from the nano-particle, the electron gas can be viewed as an electric dipole of charge $-Ne$ and displacement $d(t)$ oscillating along the z axis. In this case we can apply the Larmor formula [189] for the total radiated power :

$$P = \frac{e^2}{6\pi\epsilon_0 c^3}\ddot{d}(t). \tag{5.39}$$

Below threshold, the total power spectrum $P(\omega)$ is localized around the surface plasmon frequency (Fig. 5.8a). In contrast, the spectrum is rich in high-order harmonics in the above-threshold regime (Fig. 5.8b), for which the electron gas explores the nonlinear part of the confining potential [190]. Such difference in the observed spectrum could be used as an experimental signature to assess the effectiveness of the autoresonant excitation. High-harmonic generation is also a crucial issue for the production and shaping of attosecond laser pulses [191]. We showed that by irradiating a metallic nano-particle with an autoresonant chirped laser pulse, it is possible to drive the collective electron modes (surface plasmons) far into the nonlinear regime, leading to enhanced energy absorption and complete ionization of the nanoparticle on a time scale of the order of $100\,\mathrm{fs}$. Thanks to the autoresonant technique, the required laser intensity is rather modest ($\sim 10^{10}\ \mathrm{W/cm^2}$). Such enhanced absorbtion may be used, for instance, to improve the efficiency of nanoparticle-based radiotherapy [4].

The autoresonant mechanism is extremely flexible, since it requires no feedback as in

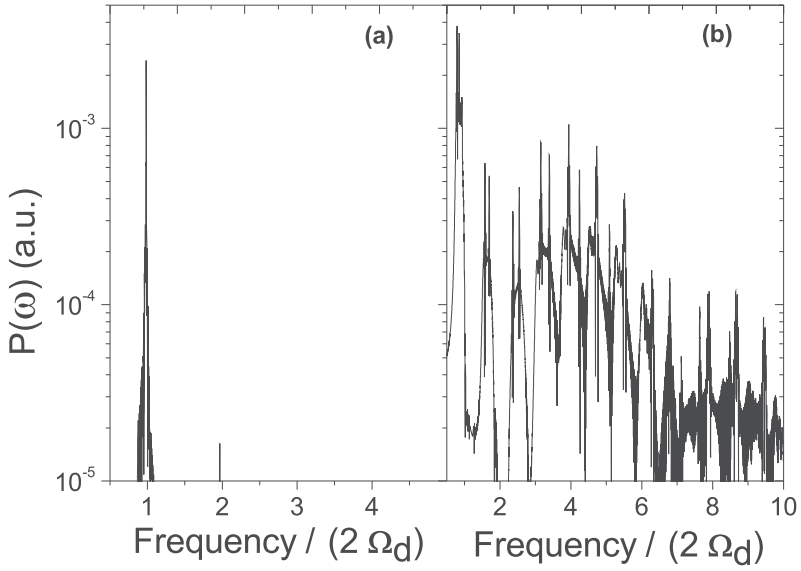

FIGURE 5.8: Frequency spectrum of the total radiated power (5.39) in a gold nano-particle with $N = 200$, for two cases, below the autoresonance threshold (a) and above the threshold (b). We used the same laser parameters as in Fig. 5.6.

usual control theory. Further, the laser does not need to be perfectly matched to the linear frequency (the only requirement is that the linear frequency be crossed during the excitation). This feature means that a whole assembly of nano-particles [192] could be excited autoresonantly, even if the they have different sizes and thus different plasmon resonances.

5.3 Non-linear electronic dynamics in a non-parabolic and anisotropic well

In the previous section, we study the nonlinear dynamics of an electron gas confined in an isotropic well (created by spherical nano-particles). We have seen that such systems can be used to generate high harmonics. This section deals with the nonlinear dynamics of a confined electron gas in a non-parabolic and anisotropic well.

Current technology allows the manipulation and control of the electron dynamics in small devices of nanometric size, such as semiconductor quantum dots and quantum wells. These devices have attracted considerable attention in the last few decades, among other reasons because of their potential use for quantum computing [193]. When the confining potential is perfectly parabolic, the electron response is dominated by the Kohn mode [194, 195], i.e., a rigid oscillation of the electron density at the characteristic frequency of the parabolic well. For nonparabolic confinement the situation is much more complex. When the excitation is small (linear

response), the Kohn mode may still be dominating. However, for larger excitation energies, the electrons may explore the anharmonic regions of the confining potential; in that case, the frequency spectrum of such nonlinear response becomes much more intricate, with the appearance of second- and higher-order harmonics. In addition to the effect of the anharmonicity of the confinement, the interparticle Coulomb interactions also contribute to the complexity of the spectral response.
At a mathematical level, this complexity arises because the center-of-mass and internal degrees of freedom can no longer be separated, as was shown in several studies that use powerful exact methods to model the quantum electron dynamics [196,197]. However, exact approaches are necessarily limited to a very small number of electrons. Although such few- or even single-electron systems can nowadays be realized in practice, in most practical situations a charged gas containing a great many electrons is involved. For quantum devices that contain with many electrons [27], self-consistent effects – arising from the Coulomb interactions between all the electrons – play a crucial role on the dynamics. Several theoretical and computational studies have investigated the linear and nonlinear electron response.
Here we shall use quantum hydrodynamic models to study the nonlinear electron dynamics. The QHD model can be further simplified by means of a variational approach [48] that expresses the QHD equations in terms of a Lagrangian density. With this method, it is possible to obtain a system of ordinary differential equations for a set of macroscopic quantities, such as the center of mass and the size of the electron gas. Although simple, the final equation still capture some of the most prominent features of the electron dynamics: (i) the self-consistent Coulomb interaction, (ii) quantum effects to lowest order, (iii) exchange and correlation effects in a DFT fashion, and (iv) the geometry of the confining well. Our main focus will be on the effect of the anharmonicity and the anisotropy of the potential well on the electron response.

5.3.1 Lagrangian of the system

The model we shall use is based on the quantum hydrodynamic equations (5.1)-(5.3) where the electrons are confined in an external potential. The latter is given by the sum of a harmonic and an anharmonic (but isotropic) part, whose relative strength is measured by the parameter $\zeta \geq 0$:

$$V_{\text{conf}} = \frac{1}{2}\left(k_1 x^2 + k_2 y^2 + k_3 z^2\right) + \zeta\left(x^2 + y^2 + z^2\right)^2 . \tag{5.40}$$

We chose this specific form for the anharmonic part of the confinement, so that it can be captured by a single parameter. In this section we shall use, unless otherwise specified, "semiconductor" atomic units (au). These are formally identical to standard au, but the electron mass m_e is replaced by the effective mass $m^* = 0.067 m_e$ and the vacuum dielectric constant ϵ_0 by its effective counterpart $\epsilon^* = 13\epsilon_0$.

In this system of units, length are normalized to an effective Bohr radius $a^* = 4\pi\epsilon^*\hbar^2/(m^*e^2) = 10.3\,\mathrm{nm}$, energy to an effective Hartree energy $E_H^* = \hbar^2/(m^*a^{*2}) = 10.8\,\mathrm{meV}$, frequency to $\omega^* = E_H^*/\hbar = 16.5\,\mathrm{THz}$, and time to $\tau^* = 1/\omega^* = 0.606\,\mathrm{ps}$. The elastic constants k_i of the harmonic potential in Eq. (5.40) are normalized to $k^* = 1.64 \times 10^{-5}\mathrm{J/m^2}$.
As before, we took the Pressure of a degenerated electron gas (5.4) and the exchange potential defined in Eq. (5.5). Then the QHD equations (5.1)-(5.3) can be represented by the following Lagrangian density:

$$\begin{aligned}\mathscr{L}_D = n\left[\frac{1}{2}\left(\boldsymbol{\nabla}\theta\right)^2 + \frac{\partial\theta}{\partial t}\right] + \frac{1}{8n}\left(\boldsymbol{\nabla}n\right)^2 + \frac{3}{10}\left(3\pi^2\right)^{2/3}n^{5/3} \\ - \frac{3}{4\pi}\left(3\pi^2\right)^{1/3}n^{4/3} - \beta\frac{\left(\boldsymbol{\nabla}n\right)^2}{n^{4/3}} + nV_{\mathrm{conf}} - nV_{\mathrm{H}} - \frac{1}{8\pi}\left(\boldsymbol{\nabla}V_{\mathrm{H}}\right)^2.\end{aligned} \tag{5.41}$$

In order to derive the tractable system of equations, one needs to specify a particular Ansatz for the electron density. Here, we take a Gaussian shape, which is a reasonable choice, as it is it the exact ground state solution when one neglects Coulomb interactions and the anharmonic part of the confinement. Thus we write:

$$n(\boldsymbol{r},t) = \frac{A}{\sigma_1\sigma_2\sigma_3}\exp\Big(-\frac{1}{2}\rho^2\Big), \tag{5.42}$$

where the prefactor $A = N/\left(2\pi\right)^{3/2}$ is obtained by fixing the total number of particles $N = \int n d\boldsymbol{r}$, and ρ is a displaced position variable

$$\rho(x,y,z,t) = \sqrt{\frac{1}{\sigma_1^2}\left(x-d_1\right)^2 + \frac{1}{\sigma_2^2}\left(y-d_2\right)^2 + \frac{1}{\sigma_3^2}\left(z-d_3\right)^2}. \tag{5.43}$$

Here, $d_i(t)$ and $\sigma_i(t)$ are time-dependent variables that represent respectively the center of mass and the size of the electron gas in each Cartesian direction.
We now need to express the other variables (θ and V_{H}) in terms of the electron density. The mean velocity $\boldsymbol{u}$ can be obtained exactly from the continuity equation (5.1). Its Cartesian components are:

$$u_i = \frac{\dot{\sigma}_i}{\sigma_i}\left(r_i - d_i\right) + \dot{d}_i, \tag{5.44}$$

where $r_i = (x,y,z)$. From the above expression we obtain

$$\theta = \sum_{i=1}^{3}\left(\frac{\dot{\sigma}_i}{2\sigma_i}(r_i-d_i)^2 + \dot{d}_i(r_i-d_i)\right). \tag{5.45}$$

For the self-consistent Hartree potential, we take the expression

$$V_{\mathrm{H}} = -4\pi\sqrt{\frac{\pi}{2}}\frac{A}{(\sigma_1\sigma_2\sigma_3)^{1/3}}\frac{\mathrm{erf}\left(\rho/\sqrt{2}\right)}{\rho}, \tag{5.46}$$

where erf is the error function. This expression constitutes an approximate solution of Poisson's equation (5.3), which becomes exact in the radially symmetric case ($\sigma_1 = \sigma_2 = \sigma_3$). Substituting the above expression for n, θ, and V_{H} into the Lagrangian density (5.41) and integrating over the entire space, we obtain the following Lagrangian function:

$$L[d_i, \sigma_i, \dot{d}_i, \dot{\sigma}_i] = \frac{1}{N}\int \mathscr{L}_D d\boldsymbol{r} = \frac{1}{2}\sum_{i=1}^{3}\left(\dot{\sigma_i}^2 + \dot{d_i}^2\right) - U(d_i, \sigma_i), \tag{5.47}$$

where a dot stands for differentiation with respect to time and $U(d_i, \sigma_i) = U_d(d_i) + U_\sigma(\sigma_i) + U_{d\sigma}(d_i, \sigma_i)$. The different potential terms read as:

$$U_d = \frac{1}{2}\sum_{i=1}^{3} k_i d_i^2, \tag{5.48}$$

$$U_\sigma = \frac{1}{2}\sum_{i=1}^{3} k_i\sigma_i^2 + \left(\sum_{i=1}^{3}\frac{1}{\sigma_i^2}\right)\left(\frac{1}{8} + \alpha_1 N\left[\sigma_1\sigma_2\sigma_3\right]^{1/3} - \alpha_2\,\beta\left[\frac{\sigma_1\sigma_2\sigma_3}{N}\right]^{1/3}\right) + \alpha_3\left[\frac{N}{\sigma_1\sigma_2\sigma_3}\right]^{2/3} - \alpha_4\left[\frac{N}{\sigma_1\sigma_2\sigma_3}\right]^{1/3}, \tag{5.49}$$

$$U_{d\sigma} = \zeta\left[\sum_{i=1}^{3}\left(3\sigma_i^4 + 6d_i^2\sigma_i^2 + d_i^4\right) + 2\sum_{i>k=1}^{3}\left(\sigma_i^2 + d_i^2\right)\left(\sigma_k^2 + d_k^2\right)\right], \tag{5.50}$$

and represent respectively the dipole motion (U_d), the breathing motion (U_σ), and the coupling between the dipole and breathing dynamics ($U_{d\sigma}$). Note that such coupling disappears for purely harmonic confinement ($\zeta = 0$). The various coefficient appearing in Eqs. (5.48)-(5.50) are given by:

$$\alpha_1 = \frac{2\pi}{3\sqrt{2}}(2\pi)^{-3/2} \approx 0.0940,$$
$$\alpha_2 = \frac{9}{4}\sqrt{3\pi} \approx 6.9075,$$
$$\alpha_3 = \frac{9}{50}\sqrt{\frac{3}{5}}\left(3\pi^2\right)^{2/3}\frac{1}{2\pi} \approx 0.2124,$$
$$\alpha_4 = \frac{9\sqrt{3}}{32\pi}\frac{\left(3\pi^2\right)^{1/3}}{\sqrt{2\pi}} \approx 0.1914.$$

Finally, the equations of motion of the system can be obtained from the Euler-Lagrange equations for L, and read as:

$$\ddot{d}_i = -\frac{\partial U_d}{\partial d_i} - \frac{\partial U_{d\sigma}}{\partial d_i}, \qquad \ddot{\sigma}_i = -\frac{\partial U_\sigma}{\partial \sigma_i} - \frac{\partial U_{d\sigma}}{\partial \sigma_i}. \tag{5.51}$$

As expected, in the case of harmonic confinement ($\zeta = 0$) the dipole and breathing modes are completely decoupled (Kohn's theorem [194, 195]).
We have thus reduced the complex problem of the dynamics of a multi-electron system to a relatively simple system of six coupled differential equations for the center of mass and size of the electron gas, which can be solved on a desktop computer using standard methods (e.g., Runge-Kutta). As noted in the introduction, this approximate system still incorporates such important effects as Coulomb interactions, quantum and exchange effects, as well as the effects of the geometry of the confining trap (anharmonicity and anisotropy). Also, no assumptions of linearity were made, so that Eqs. (5.51) can be used to study the nonlinear response of the electron gas.

5.3.2 Ground state and linear regime

Stationary states are obtained by setting $\ddot{d}_i = \ddot{\sigma}_i = 0$. For the dipole mode, the solutions are clearly $d_i = 0$. For the breathing mode, the equations of motions are those of a fictitious particle evolving in the external potential $U_\sigma + U_{d\sigma}$. The equilibrium solution $\sigma^{(0)}$ corresponds to the minimum of such potential and can be found by setting its first derivative to zero:

$$\left.\frac{\partial\left(U_\sigma + U_{d\sigma}\right)}{\partial \sigma_i}\right|_{d_i=0} = k_i\sigma_i - \frac{2}{\sigma_i^3}\left[\frac{1}{8} + \gamma_2 V^{1/3}\right] + q\frac{\gamma_2}{3}\left[\frac{V^{1/3}}{\sigma_i}\right] - \frac{2\gamma_1}{3}\left[\frac{V^{-2/3}}{\sigma_i}\right] + \frac{\gamma_3}{3}\left[\frac{V^{-1/3}}{\sigma_i}\right] + \zeta\left[12\sigma_i^3 + 4\sigma_i\left(\sum_{j\neq i}\sigma_j^2\right)\right] = 0, \tag{5.52}$$

where $V(t) = \sigma_x\sigma_y\sigma_z$ is the electron gas volume, $q = \sum_i \sigma_i^{-2}$, and the following additional parameters were defined $\gamma_1 = \alpha_3 N^{2/3}$, $\gamma_2 = \alpha_1 N - \alpha_2\beta N^{-1/3}$ and $\gamma_3 = \alpha_4 N^{1/3}$. In the most general case, it is not possible to obtain analytical solutions for the ground state and one has to resort to numerical methods. However, an analytical solution can be found in the case of isotropic confinement ($k_x = k_y = k_z \equiv k$) and in the limit of a large number of particles ($N \gg 1$). We found that the size of the electron gas scales as a power of the number of electrons N. The exponent varies according to whether the anharmonic part of the potential is included or not: $\sigma^{(0)} = \left(\frac{\alpha_1}{k}N\right)^{1/3}$ for $\zeta = 0$ (harmonic) and $\sigma^{(0)} = \left(\frac{\alpha_1}{20J}N\right)^{1/5}$ for $\zeta \neq 0$ (anharmonic). For harmonic confinement, the volume increases, as expected, as the total number of particles. For the anharmonic case, the increase with N is slower, reflecting the fact that the anharmonic term tends to further confine the electrons. Note that in this case the exponent is always $1/5$, irrespective of the value of ζ. These results were

confirmed by numerical simulations of the isotropic case obtained without making the large-N approximation (Fig. 5.9). Having found the ground state, it is possi-

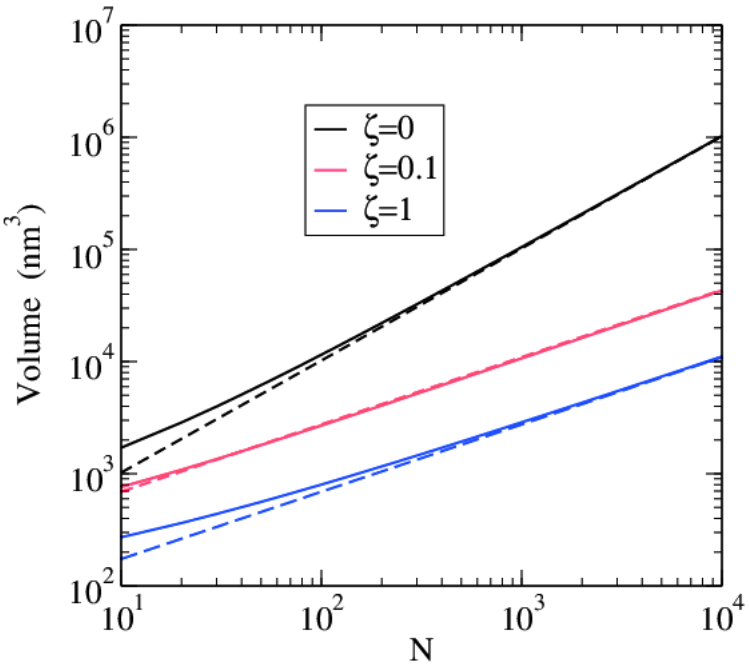

FIGURE 5.9: Volume of the electron gas as a function of the number of electrons N for an isotropic confinement and different values of the anharmonicity parameter ζ. The solid lines are solutions of Eq. (5.52), whereas the dashed lines are analytical solutions obtained in the $N \to \infty$ limit.

ble to compute the linear response frequencies of the system. In the most general case, there are six such frequencies, three of which correspond to the dipole (center-of-mass) modes Ω_d and three corresponding to the breathing modes Ω_σ. These frequencies are obtained by finding the eigenvalues of the Hessian matrix constructed out of the second derivatives of the potential

$$\mathcal{H} = \begin{pmatrix} \mathcal{H}_\sigma & 0 \\ 0 & \mathcal{H}_d \end{pmatrix}, \tag{5.53}$$

where

$$\mathcal{H}_\sigma = \left.\frac{\partial^2 U}{\partial \sigma_i \sigma_j}\right|_{d_i=0,\ \sigma_i=\sigma_i^{(0)}},$$
$$\mathcal{H}_d = \left.\frac{\partial^2 U)}{\partial d_i d_j}\right|_{d_i=0,\ \sigma_i=\sigma_i^{(0)}}$$

are symmetric ($\mathcal{H}_\sigma$) and diagonal ($\mathcal{H}_d$) 3×3 matrices.

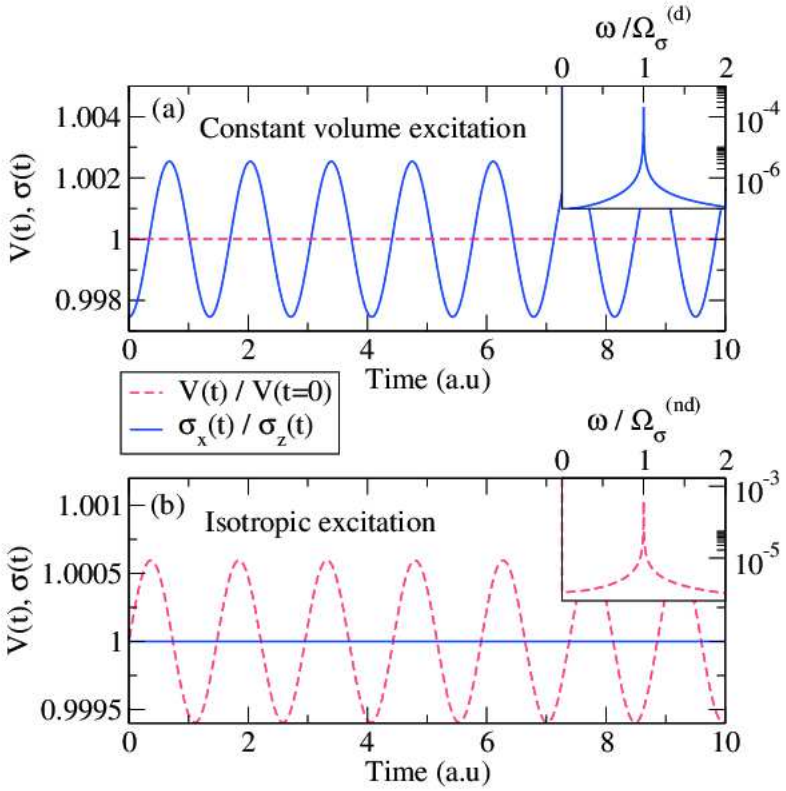

FIGURE 5.10: Simulations of the two breathing modes in the linear regime (small perturbations) for an isotropic case $k_x = k_y = k_z = 1$ with $N = 50$ and $\zeta = 0.1$. Top panel (a): degenerate mode at constant volume $V(t)$ and varying aspect ratio σ_x/σ_z; Bottom panel (b): non-degenerate mode at constant aspect ratio and oscillating volume. The insets show the Fourier transforms of the oscillating quantities, which peak at the expected degenerate ($\Omega_\sigma^{(d)}$) and non-degenerate ($\Omega_\sigma^{(nd)}$) frequencies.

The case of purely harmonic confinement is trivial, therefore we concentrate on the effect of anharmonicity. As an example, we focus on the case $\zeta = 0.05$. The numerically computed linear frequencies are given in Tab. 5.2 for different confinements (isotropic and anisotropic) and different numbers of particles. For an isotropic case ($k_1 = k_2 = k_3 = 1$) we obtain, as expected, a single value for the dipole frequency that is three times degenerate, but two values for the breathing frequencies, one of which is twice degenerate. These two breathing frequencies correspond to two distinguished modes. In the non-degenerate mode the volume $V(t)$ of the electron gas oscillates, whereas the aspect ratios σ_i/σ_j remain constant. This mode preserves the spherical symmetry of the equilibrium state and can be excited by perturbing the three σ_i in the same way. In contrast, for the twice-degenerate mode the volume stays constant whereas the ratios σ_i/σ_j oscillate at the corresponding frequency.

These modes are shown in Fig. 5.10. In the figure, we show numerical simulations of the full system obtained by perturbing the stationary ground state of a very small

N	k_1	k_2	k_3	Ω_σ/ω^*	Ω_d/ω^*
20	1	3	2	3.21 3.69 4.19	1.43 1.73 1.99
	1	1	2	3.17 3.32 3.76	1.46 (×2) 1.75
	1	1	1	3.14 3.34 (×2)	1.46 (×3)
50	1	3	2	3.63 4.15 4.64	1.60 2.10 1.87
	1	1	2	3.55 3.88 4.25	1.63 (×2) 1.89
	1	1	1	3.51 3.90 (×2)	1.65 (×3)
100	1	3	2	4.00 4.61 5.07	1.76 2.00 2.23
	1	1	2	3.92 4.38 4.70	1.79 (×2) 2.03
	1	1	1	3.89 4.40 (×2)	1.81 (×3)

TABLE 5.2: Dipole and breathing frequencies for various numbers of particles N and different geometries of the confinement. The anharmonicity constant is $\zeta = 0.05$ everywhere.

quantity: $\sigma_i(t=0) = \sigma_i^{(0)} + \delta_i$. In all cases, the dipole mode is not excited, i.e., $d_i(t=0) = 0$. In the top panel, we only excited the twice-degenerate mode by choosing the perturbations δ_i such that the volume is invariant: as expected, the volume stays constant during the linear evolution, while the various σ_i oscillate. In the bottom panel, we only excited the non-degenerate mode by taking $\delta_x = \delta_y = \delta_z$: here, the volume oscillate while the ratio $\sigma_x(t)/\sigma_z(t)$ remain constant.
In the case of isotropic confinement ($k_1 = k_2 = k_3 \equiv k$), analytical expressions for the dipole frequency Ω_d and for the degenerate ($\Omega_\sigma^{(d)}$) and non-degenerate ($\Omega_\sigma^{(nd)}$) breathing frequencies can be found in the large N limit. For harmonic confinement ($\zeta = 0$), one obtains the following expressions (which are actually exact for all values of N):

$$\Omega_d = \sqrt{k}, \quad \Omega_\sigma^{(nd)} = \sqrt{3k}, \quad \Omega_\sigma^{(d)} = \sqrt{6k}, \tag{5.54}$$

whereas for anharmonic confinement ($\zeta > 0$) in the large N limit:

$$\Omega_d = \left[(20\zeta)^{3/2}\,\alpha_1 N\right]^{1/5}, \quad \Omega_\sigma^{(nd)} = 5\left[(20\zeta)^{3/2}\,\alpha_1 N\right]^{1/5}, \quad \Omega_\sigma^{(d)} = \frac{34}{5}\left[(20\zeta)^{3/2}\,\alpha_1 N\right]^{1/5}. \tag{5.55}$$

Note that the presence of an anharmonic part in the confining potential introduces a dependence on the number of particle in the dipole frequency.
In Fig. 5.11, we show the dependence of the dipole frequency with the geometry of the trap (characterized by the parameter $k_\perp/k_z$, where $k_\perp \equiv k_x = k_y$) and the number of electrons. Note that when $k_\perp/k_z \ll 1$ the trap is "pancake shaped", while in the opposite case $k_\perp/k_z \gg 1$ it is "cigar shaped"; $k_\perp/k_z = 1$ denotes an isotropic trap. For isotropic confinement (Fig. 5.11, middle panel) the analytical expressions match closely the numerical results for $N \to \infty$. The anharmonicity introduces a

dependence of the dipole frequency with the number of electrons, with higher frequencies corresponding to larger N. The same trend is observed for a cigar-shaped trap (left panel) and a pancake-shaped trap (right panel). In these anisotropic traps, the longitudinal (parallel to z) and transverse ($\perp$) dipole frequencies of course do not coincide, but both still grow with N.

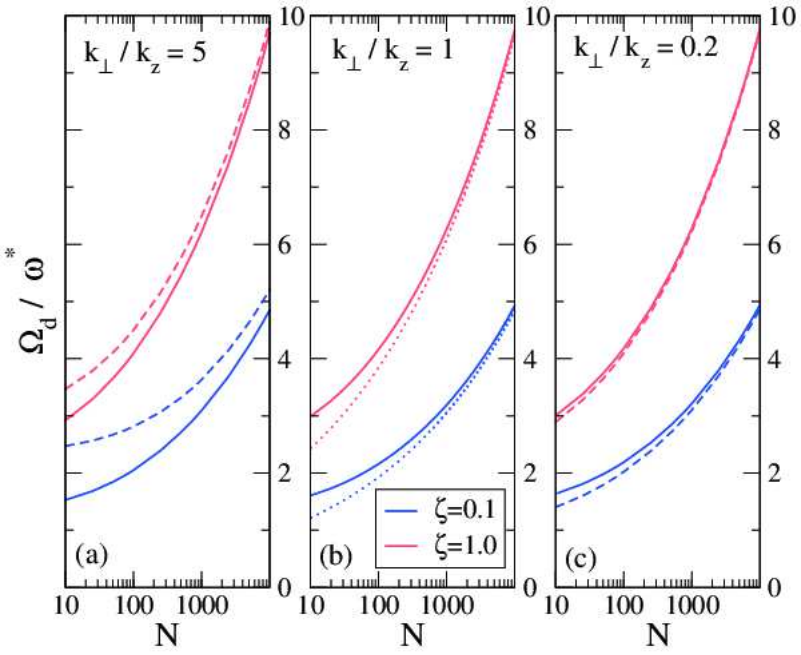

FIGURE 5.11: Dipole frequencies Ω_{d_z} (solid lines) and $\Omega_{d_\perp}$ (dashed lines) as a function of the number of electrons N for two values of the anharmonicity parameter, $\zeta = 0.1$ (blue) and $\zeta = 1$ (red). The left panel (a) corresponds to a cigar-shaped trap with $k_\perp > k_z$; the middle panel (b) to an isotropic trap ($k_\perp > k_z$); and the right panel (c) to a pancake shaped trap ($k_\perp < k_z$). In the isotropic case (b) the longitudinal and transverse dipoles coincide, and the dotted lines represent the analytical expressions of Eq. (5.55).

5.3.3 Nonlinear regime and harmonic generation

In the previous sections, we characterized the linear response of the electron dynamics by studying the eigenvalues of the linearized system of equations. Physically, the linear response corresponds to a weak excitation of the system and results in one or a few lines in the frequency spectrum. In order to trigger high harmonic generation (HHG), it is often necessary to probe the nonlinear response regime, typically by increasing the excitation.

HHG and Poincaré sections

In a first set of simulations in the nonlinear regime, we show that HHG is accompanied by some typical signatures of deterministic chaos in the dynamics. Here, we use Poincaré sections as evidence of chaotic behavior. We also point out that this type of study is feasible because our reduced mathematical model is a system of ordinary differential equations, which can be analyzed with the usual methods of classical Hamiltonian mechanics.
The method of Poincaré sections consists in choosing a two-dimensional cross-section (i.e., a plane) of the entire phase space (which, in our case, is six-dimensional) and recording the position on such plane each time that the representative point of the system crosses it. If the system is chaotic, then there is no correlations between the various points on the Poincaré section, and some finite 2D regions of the plane will be covered uniformly. In contrast, if the system is regular, i.e. periodic, the representative point of the system will pass through the same point after some time, and the Poincaré section will consist of isolated points or 1D lines on the plane.
In our case, we choose the (d_x, d_y) plane for the Poincaré section. Such plane divides the electron trap in two identical regions. In the forthcoming simulations we take $N = 50$ electrons and an anisotropic trap characterized by $k_\perp = 5$ and $k_z = 1$. We perturb the stationary ground state by suddenly changing the velocity of the dipole variable, i.e., by setting the initial conditions at $t = 0$: $\dot{d}_x = -\dot{d}_y = d_i = \delta$, with the perturbation amplitude δ varying between 0.01 and 3. The corresponding Poincaré sections are shown in Fig. 5.12. For $\delta = 0.01$ the system is clearly regular, as the Poincaré sections is basically an ellipse (this is due to the choice of the initial condition). By increasing δ, the central phase-space region starts filling up, first partially and in a regular way (Figs. 5.12)b-c) and then completely for $\delta = 3$ (Figs. 5.12)d). The homogeneous coverage of a finite phase-space area is a signature of chaotic behaviour.

It is interesting to check how the onset of chaos with increasing perturbation is reflected in the quantity $|\ddot{d}_z(\omega)|^2$, where $\ddot{d}_z(\omega)$ is the Fourier transform of the second derivative of the dipole coordinate $d_z(t)$. This quantity is related to the total power radiated by an electric dipole of charge $-Ne$ and displacement $d_z(t)$ oscillating along the z axis, given by the Larmor formula [189]: $P(t) = e^2/(6\pi\epsilon_0 c^3)|\ddot{d}(t)|^2$. The dipole power spectrum is shown in Fig. 5.13 for the same cases as in Fig. 5.12. As expected, the spectrum displays a single line at the dipole frequency when the excitation is weak ($\delta = 0.01$). Higher order harmonics start appearing at larger values of δ, which are at the origin of the multiperiodic motion observed in the corresponding Poincaré sections. Finally, for $\delta = 3$ the spectrum is nearly continuous, in agreement with the chaotic dynamics observed in Fig. 5.12.
The same transition to chaos accompanied by HHG was observed for a case where we keep the excitation constant ($\dot{d}_x(0) = -\dot{d}_y(0) = d_i(0) = \delta$, with $\delta = 1$) and increase the anharmonicity parameter from $\zeta = 0$ to $\zeta = 0.1$ (Figs. 5.14-5.15). In

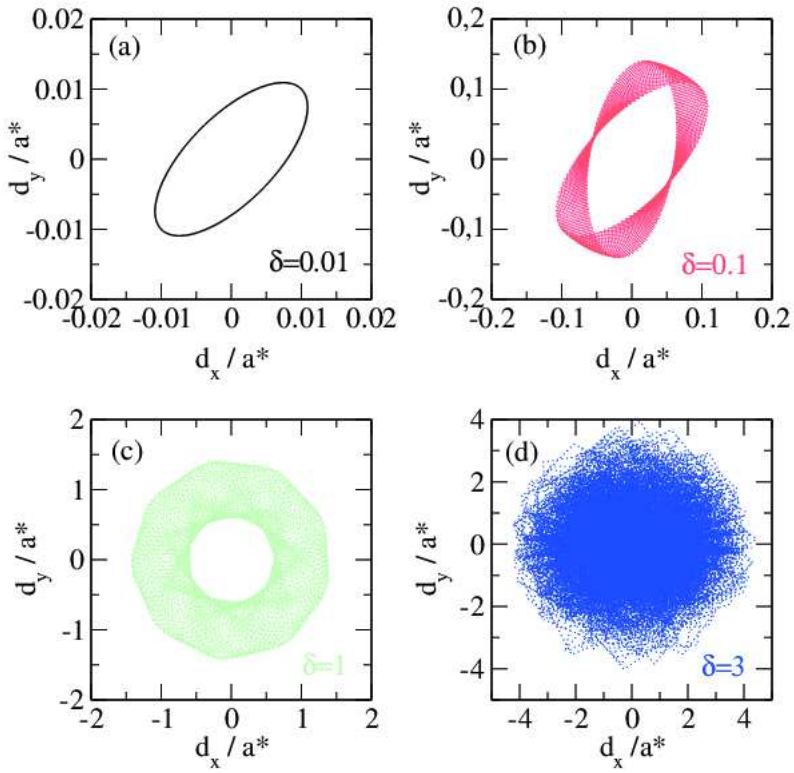

FIGURE 5.12: Poincaré sections in the plane (d_x, d_y) for different values of the initial excitation, $\dot{d}_x = -\dot{d}_y = d_i = \delta$, with $\delta = 0.01$ (a), 0.1 (b), 1 (c), and 3 (d). The simulations were performed for an anisotropic trap with $k_\perp = 5$ and $k_z = 1$, $N = 50$, and $\zeta = 0.01$.

order to observe some chaotic dynamics, an anharmonic term in the confinement is necessary – a purely harmonic oscillator is always integrable. A finite value of ζ introduces some coupling between the dipole and the breathing motions, which enlarges the available phase space and allows chaotic behavior. This chaotic behavior is displayed only when the system explores the nonparabolic regions of the confining trap. This can be achieved by either increasing the initial excitation (Figs. 5.12-5.13) or increasing the anharmonicty of the trap (Figs. 5.14-5.15). Finally, we note that a certain degree of anisotropy ($k_\perp = 5k_z$ in our case) was also required to observed such irregular motion.

HHG and resonant excitation

So far, we used a simple excitation for our nonlinear system, namely an initial velocity imparted on the dipole variables $\dot{d}_i(t = 0)$. In reality, the electron dynamics is usually triggered by electromagnetic (laser) pulses. We assume that the confined electron gas xis excited via an oscillating electric field directed along the z axis, $\mathbf{E} = E_z(t)\mathbf{e}_z$. The effect of the laser can be included by adding a term $E_z d_z$ to the lagrangian L. We consider three cases: (i) excitation at a nonresonant frequency, (ii) excitation at a resonant frequency, and (iii) excitation with chirp (autoresonance).

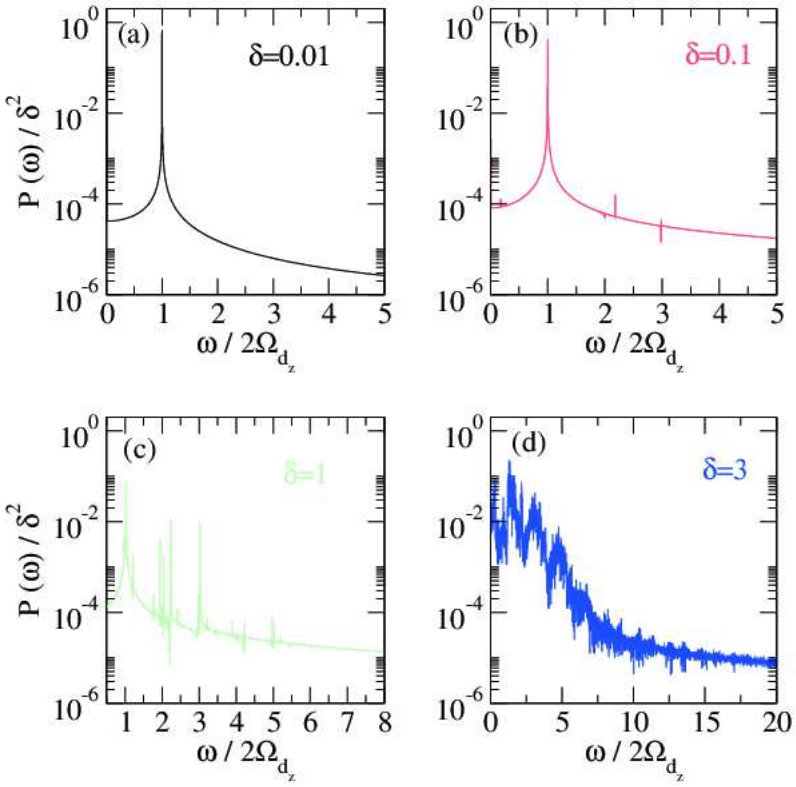

FIGURE 5.13: Power spectrum of the dipole $P(\omega)$ for different initial excitations δ, for the same case as in Fig. 5.12.

Note that the dipole linear resonant frequency is in the Tera-Hertz domain.
The results are shown in Fig. 5.16. For the first two cases, the excitation has the form $E_z(t) = E_0 \cos(\omega_0 t)$, where E_0 is the electric field amplitude of the electromagnetic wave. In all cases shown here, we took the same amplitude $E_0 = 0.01\,\mathrm{au}$, corresponding to $E_0 = 10^4\,\mathrm{V/m}$ in SI units. In the first case (green curves on the figure), ω_0 differs from the linear response frequency Ω_{d_z}. Being out of resonance, the system stays close to the linear regime: the oscillation amplitude remains small (Fig. 5.16a), small amount of energy is absorbed by the electron gas (Fig. 5.16b), and the power spectrum displays a single line at the dipole frequency (Fig. 5.16c). For resonant excitation $\omega_0 = \Omega_{d_z}$ (black curves), the oscillation amplitude and the absorbed energy initially increase, but then decrease again after some time. This is because the effective force acting on the dipole is not harmonic and the resonant frequency actually depends on the amplitude of the oscillations. When the amplitude grows and the system reaches the nonlinear regime, the fixed external frequency does no longer match the instantaneous resonant frequency (which differs from Ω_{d_z} in the nonlinear regime). The resulting power spectrum displays two lines corresponding to the linear frequency and the first harmonic.
Finally, we use an oscillating field with a chirped frequency: $E_z(t) = E_0 \cos\left(\omega_0 t + \frac{\alpha}{2} t^2\right)$, where α is the rate of variation of the laser frequency. This type of forcing is known

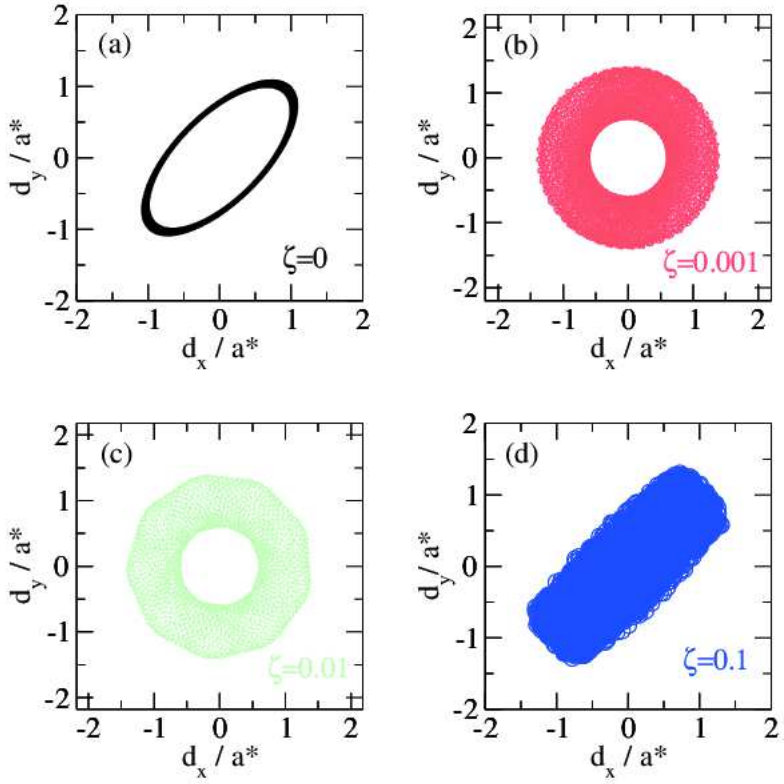

FIGURE 5.14: *Color online*. Poincaré sections in the plane (d_x, d_y) for different values of the anharmonicity parameter $\zeta = 0$ (a), 0.001 (b), 0.01 (c), and 0.1 (d). The simulations were performed for an anisotropic trap with $k_\perp = 5$ and $k_z = 1$, $N = 50$, and initial excitation $\delta = 1.0$.

as 'autoresonance' [66] and was applied in the past to many physical systems. Autoresonance occurs when a classical nonlinear oscillator is externally excited by an oscillating field with slowly varying frequency. For $|\alpha| \ll \Omega_d^2$ (adiabatic process) and E_0 above a certain threshold, the instantaneous oscillator frequency becomes "locked" to the instantaneous excitation frequency, so that the resonance condition is always satisfied. In that case, the amplitude of the oscillations grows indefinitely and without saturation, until of course some other effect becomes dominant. Usually the threshold behaves as $E_0^{\rm th} \sim |\alpha|^{3/4}$, so that the amplitude can be arbitrarily small provided that the external frequency varies slowly enough [66]. In order for autoresonance to work, the excitation frequency, which varies linearly in time as $\omega(t) = \omega_0 + \alpha t$, must cross at some point the resonant dipole frequency $\Omega_{d_z} = 20.07\,\mathrm{THz}$. Therefore, for this simulation we chose $\omega_0 = 18.45\,\mathrm{THz}$ and a chirp rate $\alpha = 3.03\,\mathrm{THz/ns}$. The resonant frequency is crossed around $t \approx 0.55\,\mathrm{ns}$, after which the autoresonant process starts being effective, as can be seen in Fig. 5.16. It is clear from Fig. 5.16 that the autoresonant excitation allows one to increase phenomenally the amplitude of the dipole oscillations and consequently the absorbed energy, which is roughly three times as large compared to the non chirped case. We stress that the excitation amplitude is the same for all cases. The power spectrum

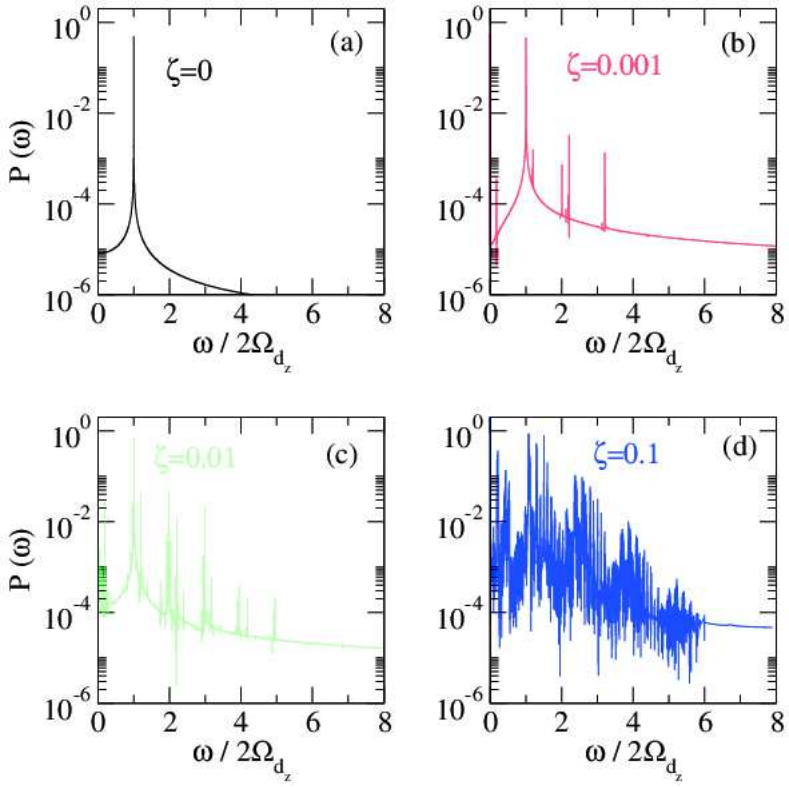

FIGURE 5.15: Power spectrum of the dipole $|d_z(\omega)|^2$ for different values of the anharmonicity parameter ζ, for the same case as in Fig. 5.14.

(Fig. 5.16c) displays several peaks for higher order harmonics (up to the third harmonic), with the first harmonic being roughly a factor of ten smaller that the linear mode. We also note that these spectral lines are unusually broad. This is probably due to the chirped excitation, which sweeps several frequencies around each harmonic. The important point is that, using a relatively weak excitation (which could be made even weaker by reducing the chirp rate α), one can induce significant energy absorption by the electron gas, accompanied by HHG at remarkably high levels.

Finally, in Fig. 5.17 we show the Poincaré sections for the three cases of nonresonant, resonant, and chirped excitation. Note that the relevant section here is not the (d_x, d_y) plane as before, because the dynamics now takes place essentially in the z direction (due to the fact that the forcing is along z). Instead, the relevant phase-space section is the plane $(d_z, \dot{d}_z)$, which is shown in Fig. 5.17. We note that the phase-space portraits become increasingly complex going from the nonresonant (a) to the chirped case (c). Nevertheless, even in the resonant and chirped excitation regimes, some regularities remain compared to the previous Poincaré sections. This is due to the fundamental difference between an autonomous system endowed with an initial condition (Figs. 5.12-5.15)and a time-dependent driven system (Figs. 5.16-5.17). The response of a driven system is generally dominated by the drive, which is what we see in Fig. 5.16, where the amplitude of the response changes dramatically

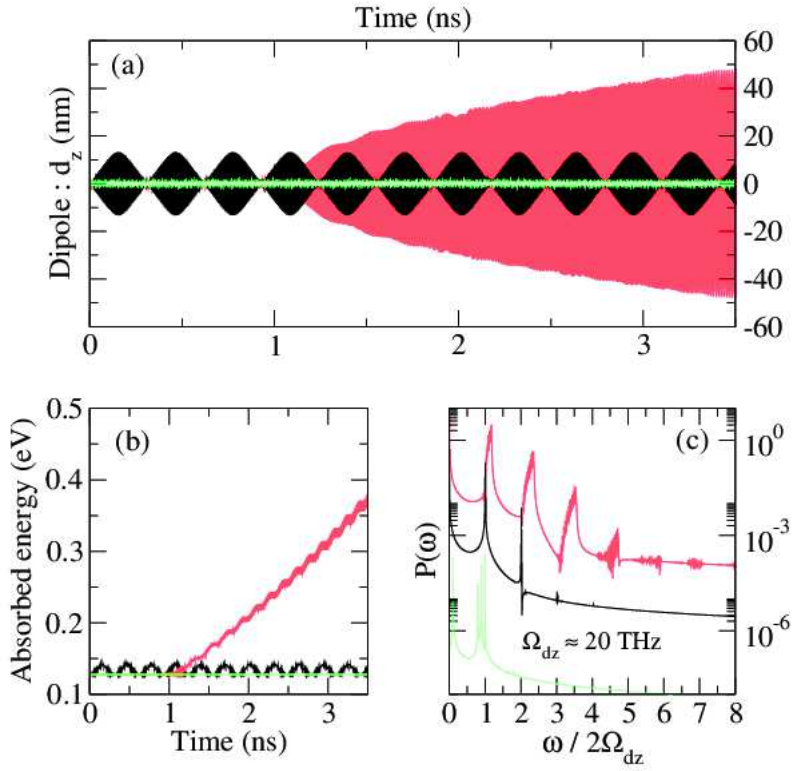

FIGURE 5.16: Laser excitation of the dipole response, for a trap with parameters: $k_\perp = 5$, $k_z = 1$, $N = 50$, $\zeta = 0.01$. The amplitude of the excitation is $E = 10^4\,\mathrm{V/m}$. We show the dipole ampitude $d_z(t)$ (a), the absorbed energy (b), and the power spectrum $|\ddot{d}(\omega)|^2$ (c), for three cases: nonresonant excitation at constant frequency (green curves), resonant excitation at constant frequency (black), and chirped excitation (red).

for the three cases. All in all, although the driven (resonant and chirped) systems explore uniformly a large fraction of the phase space [see Figs. 5.17(b) and 5.17(c)], they are less chaotic. This can also be seen from the difference between the power spectra, for instance comparing Fig. 5.13(d) with Fig. 5.16(c)(red line). In the latter case, although many harmonics are present, the spectrum is more regular than in the former.

In this work, our aim was to explore the possibility of high harmonic generation using nanometric system containing many electrons, such as semiconductor quantum dots and wells. With this purpose in mind, we constructed an effective model in the form of a dynamical system made of six coupled differential equations for the center of mass and the size of the electron gas. This effective model results from the application of a variational method to the equations of quantum hydrodynamics. The model was later applied to the dynamics of an electron gas in a nonparabolic and anisotropic well. Two main results were obtained. First, we showed that harmonic generation is accompanied by dynamical chaos in the equations of motion. The onset of chaos was quantified by the appearance of ergodic regions in some Poincaré sections. Second, we demonstrated that HHG can be efficiently achieved

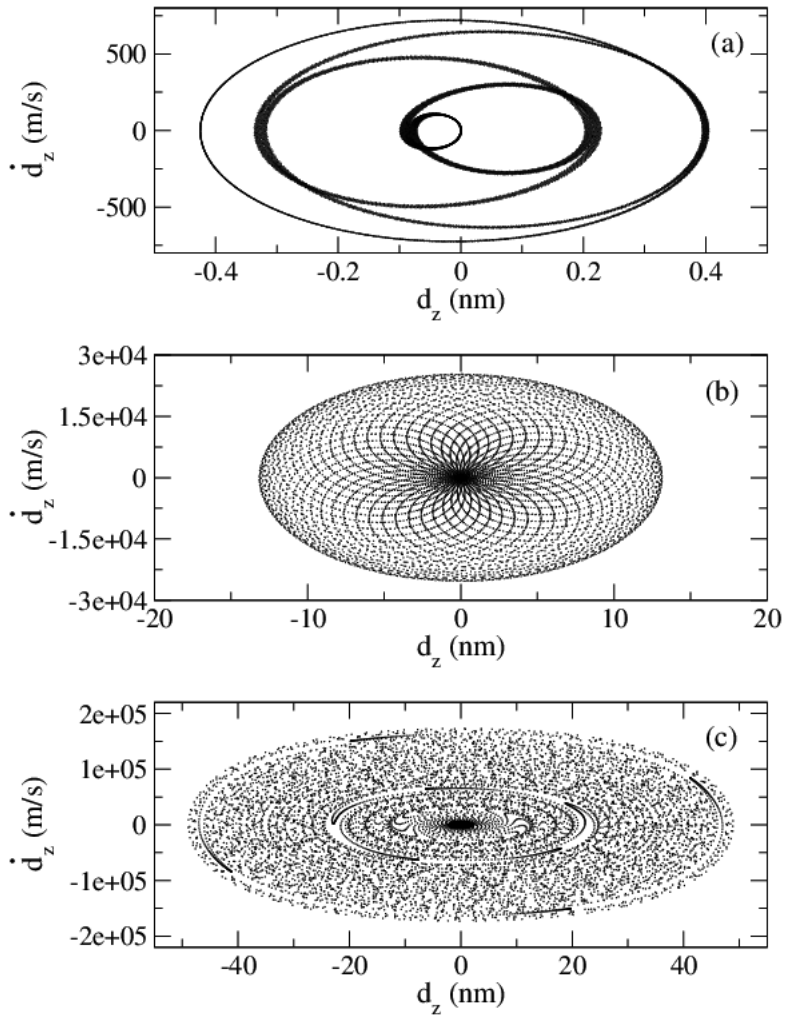

based

FIGURE 5.17: Poincaré sections in the $(d_z, \dot{d}_z)$ plane for the three cases of Fig. 5.16: nonresonant (a), resonant (b) and chirped excitation (c).

by exciting the system with a chirped laser pulse. This process, known as classical autoresonance, is capable of bringing the electrons into a strongly nonlinear regime, leading to the generation of high harmonics. Crucially, the autoresonance technique works well for relatively modest driving fields and does not require any fine tuning of the laser pulse.

5.4 Conclusions and perspectives

In this chapter we have used a variational approach, based on a Lagrangian formulation of quantum hydrodynamic equations, to model the nonlinear charge dynamics in metallic nano-structures. We have seen that the variational approach consists to restrict the solutions of the fluid equations by assuming a mathematical shape for the electronic density that depends on time dependent parameters. The latter represent the different dynamical modes of the system that we want to study (dipole

mode, breathing mode, etc.). This method has a great benefit, it provides a rapid access to the nonlinear electron dynamics including quantum effects (Bohm potential). The complicated many body quantum dynamics is embedded in a set of differential equations, where each equation holds for a particular mode of the system. However this method suffers from the following difficulties. First, we are generally limited to study systems with a simple geometry (spherical symmetry) for which it is possible to design a correct density shape. The latter can be inspired by ab-initio calculations (DFT). Secondly, to obtain the full Lagrangian density of the system one has also to specify a mathematical expression for the average velocity of the particles as well as for the Hartree potential. It is not always possible to perform the maths exactly and hence the variational approach cannot be used. In most of the case one has to work with few numbers of modes in order to perform the calculations.
In this chapter, we applied the variational approach on two different systems. The first systems are Gold nano-particles, we studied two well known oscillation modes the dipole and the breathing modes. We first validated the variational approach by comparing our results on the linear regime with the literature. Then we simulated the nonlinear dipole and breathing dynamics induced by optical excitations. To drive the plasmon mode far into the nonlinear regime we have used an autoresonant excitation. The latter is a chirped pulse with a slowly varying frequency. We have seen that under a specific condition, between the amplitude of the excitation and the variation rate of the laser frequency, it is possible to lock the instantaneous frequency of the system to the excitation frequency of the laser. Hence the system is driven far from its equilibrium configuration. The main advantage of using the autoresonance technique is that it works well for relatively modest driving fields and does not require any feed back on the laser pulse. We have thus created a nonlinear oscillating electric dipole and we have seen that the power spectrum radiated by this dipole is very rich in harmonics of the fundamental frequency (plasma frequency).
The second system is an electron gas trapped in an anharmonic and anisotropic well. In this study, we have seen that the electron dynamics becomes more and more complex and eventually fully chaotic when we increase the anharmonic component of the confining potential. This has been showed using the Poincaré sections. We have also showed that the appearance of chaotic behaviour is accompanied by the presence of higher-order harmonics in the electronic dipolar response. We have finally proved that using an autoresonant excitation the different harmonics as well as the phase-space trajectories present a clear signature of the chirped excitation. For instance the harmonics appearing in the spectrum are unusually broad.
The work done in this chapter is mainly a "proof-of-concept" that the autoresonant technique can be used to strongly excite a quantum electron gas and hence generate an electric field rich in high-order harmonics. The results obtained with our variational approach should be confirmed with more accurate calculations such as quantum hydrodynamic or TDDFT calculations. Moreover the studies performed

in this chapter can be extended to the following case:

- Firstly, it should be interesting to apply the variational approach on a system of two (or more) nano-particles. If they are far enough, the latter interact together with dipolar interactions. In this case, we shall obtain several sets of differential equations (one set for one nano-particle) coupled together through the dipolar interactions. Then, it shall be interesting to see the influence of this long-range interaction on the high-order harmonic generation. In the opposite case, where the two nano-particles are too close from each other, it is more complicated to use the variational approach. Namely because we completely lost the spherical symmetry of the system (even in the ground state). Moreover we have to find a density shape that allows overlaps of the two single nano-particle densities.

- Secondly, one should study in more details the formation of the different harmonics and namely the influence of the chirped excitation. The fact that the electrons are continuously in phase with the excitation field should give rise to a more coherent dynamics. For instance, it shall be interesting to see if we can modulate the shape of the different harmonics that appear in the radiated power spectrum, see Fig. 5.16.

- The variational approach should be also extended to the spin. In this case we first have to find a Lagrangian density that is equivalent to the fluid models constructed in Sec. 2.3. In Ref. [64, 198], the authors used a Lagrangian formulation of the Pauli equation. Those papers are a good starting point to think about a Lagrangian formulation of the fluid equations including the spin-orbit interaction. Such method should allows us to have access to the nonlinear charge and spin dynamics provided that we used a designing shape of the electron density and magnetization. Then it would be possible, using simple numerical methods, to study the nonlinear magnetization dynamics in an system of interacting electrons including self-consistent effects. We should also be able to study the influence of the external excitation (laser pulse) and the confinement potential on the spin dynamics.

Chapter 6

General conclusions and perspectives

In the first part of the thesis, composed by the first four chapters, we developed new phase-space models to study the spin and charge dynamics for an ensemble of interacting electrons. Phase-space methods can be applied in nanophysics to model the quantum or the classical dynamics of electrons confined in nano-structures. Spinless studies have been done in the past to study the electron dynamics in metallic nano-structures [32,89,96] both with the Wigner and the Vlasov equations. Here we addressed the situation, where the spin of the electrons cannot be neglected. We focused particularly on two spin effects, namely the Zeeman interaction and the spin-orbit coupling which are of most importance in many areas of physics. For instance in ultrafast spectroscopy the electron spin is strongly involved in the dynamics of the system, as it interacts with the incident laser field and with the self-consistent field generated by the electrons themselves. The methodology used to derive the different models can be easily generalized to describe other relativistic effects such as the Darwin term or the relativistic mass correction.

The first chapter is a general overview of different existing methods to treat a quantum system of interacting spineless electrons. Starting from the N-body Schrödinger equation, we have performed a mean field approximation to obtain the Hartree equation. Then we moved into the phase-space representation of quantum mechanics, the so-called Wigner representation. After having presented the Wigner formulation of quantum mechanics, we developed a gauge independent Wigner equation in order to describe magnetic interactions. Finally, we studied the semi-classical limit (Vlasov equation) as well as the fluid limit of the Wigner equations.

In the second chapter, we derived a four-component Wigner equation to describe the quantum dynamics of a system of spin-1/2 fermions including the Zeeman and the spin-orbit interaction. These equations coupled with the appropriate Maxwell equations form a self-consistent model to study the spin and the charge dynamics within the framework of the mean-field approximation. Exchange and correlation effects were added to our model, by means of some approximations, through an electric potential and a magnetic field that depend on the local electron density and

magnetization. Further, this model should not be limited to the linear response, as nonlinear effects are often important, especially for large incident laser powers. Then, from a semiclassical expansion at the order one in power of $\hbar$, we obtained a four-component Vlasov equation. The orbital part of the motion is classical, i.e. the particles follow classical phase-space trajectories, whereas the spin degrees of freedom are treated in a fully quantum fashion (two dimensional Hilbert space). From the numerical point of view, the spin-Vlasov equations are more tractable than the Wigner equations. Mainly because they are local in phase space in contrast to the Wigner equations which are typically non local. They constitute a relatively good approximation of the quantum version when the characteristic lengths are much larger than the de Broglie wavelength. Finally, the corresponding hydrodynamic equations were derived by taking velocity moments of the phase-space distribution functions. The spin-orbit interaction introduce some considerable changes in the hydrodynamic equation, we have namely seen that the charge and the spin current are modified in the presence of the spin-orbit coupling. As always the hydrodynamic equations need to be closed on the basis of some physical hypothesis. Several set of closed hydrodynamic equations with spin effects are proposed and can be used for applications.

In the third chapter, we used the Fourier and Laplace transforms to study the linear response of a spin polarized electron gas that is perturbed by a weak periodic excitation. We derived the dielectric function of a spin polarized electron gas with spin effects (Zeeman interaction and LSDA) and self-consistent effects (Hartree and Ampère). Then, using Maxwell-Boltzmann distribution functions, we found the plasma dispersion relation including spin effects. We have seen that the main spin effects on the plasma frequency originates from the spin dependent exchange interaction (LSDA). However, at the usual electron density and temperature of metallic nano-structures, these exchange effects are too weak to create appreciable changes of the plasma frequency.

In the fourth chapter, we applied the semiclassical spin-Vlasov model to simulate the electron spin and charge dynamics in nickel thin films. Our model is based on the distinction between localized and itinerant magnetism. In the case of nickel, we assumed that the itinerant magnetism is carried by the 4s electrons whereas the 3d electrons stay localized around the nucleus to form an ion spin. The itinerant electrons are described with the spin-Vlasov equations whereas the ion spins are modelled using a Landau-Lifshitz equation, see Eqs. (4.23). Both magnetic moments (itinerant and localized) are coupled together through an exchange interaction of Heisenberg type characterized by a coupling constant K. Moreover, the ion spins are interacting together with an exchange constant J. K and J are the two main parameters of our model. The latter were determined to obtain the experimental Curie temperature and the correct proportion of localized/itinerant

magnetic moments at $T = 0$ K. Then, we used this model to perform numerical simulations of the nonlinear charge and spin dynamics in nickel thin films. Several studies on the spinless electron dynamics in thin metallic films were done in previous works [38, 39, 144]. In our work, we take into account the Zeeman interaction and spin dependent exchange-correlation effects. Our main discovery was that, with an electric excitation, we are able to create an oscillating spin current (or an oscillating magnetic dipole) in addition to the usual electrical dipole. The electric excitation was modelled with a femtosecond laser pulse but without considering the magnetic field. While the electrical dipole oscillates at the plasma frequency, the spin current oscillates at a ballistic frequency $\omega_b = (2L/v_{\mathrm{F}})^{-1}$ which is inversely proportional to the size of the film. For nickel films of size $L = 50\ L_{\mathrm{F}}$, the ballistic frequency $\omega_b = 0.173$ PHz is in the visible range. To our knowledge this is something which was never before discussed in the literature. Moreover, we have seen that the spin current is not subjected to the Landau damping as it is the case for the electric dipole and thus has a much longer life time. We also proposed a physical explanation for the creation of this oscillating spin current. It relies on three ingredients: the finite size of the system, the self consistent electron-electron interactions and the magnetic properties of the electron ground state.

In the second part of the thesis (chapter five) we have used a variational approach, based on a Lagrangian formulation of quantum hydrodynamic equations, to model the nonlinear charge dynamics in metallic nano-structures. We have seen that the variational approach consists to restrict the solutions of the fluid equations by assuming a mathematical shape for the electron density that is a function of time dependent parameters. The latter represent the different dynamical modes of the system that we want to study (dipole mode, breathing mode, etc.). This method has the advantage of providing a rapid access to the nonlinear electron dynamics including quantum effects (Bohm potential). The complicated many body quantum dynamics is embedded in a set of differential equations, where each equation holds for a particular mode of the system. However this method suffers from the following difficulties. First, we are generally limited to study systems with a simple geometry (spherical symmetry) for which it is possible to design a correct density shape. The latter can be inspired by ab-initio calculations (DFT). Secondly, to obtain the full Lagrangian density of the system one has also to specify a mathematical expression for the average velocity of the particles as well as for the Hartree potential. It is not always possible to perform the maths exactly and hence the variational approach cannot be used. In most cases one has to work with few numbers of modes in order to perform the calculations.
We applied the variational approach to two different systems. The first systems are Gold nano-particles, we studied two well known oscillation modes the dipole and the breathing modes. We first validated the variational approach by comparing our

results on the linear regime with the existing literature. Then we simulated the nonlinear dipole and breathing dynamics induced by optical excitations. To drive the plasmon mode far into the nonlinear regime we have used an autoresonant excitation. The latter is a chirped pulse with a slowly varying frequency. We have seen that under a specific condition, between the amplitude of the excitation and the variation rate of the laser frequency, it is possible to lock the instantaneous frequency of the system to the excitation frequency of the laser. Hence the system is driven far from its equilibrium configuration. The main advantage of using the autoresonance technique is that it works well for relatively modest driving fields and does not require any feed back on the laser pulse. We have thus created a nonlinear oscillating electric dipole and we have seen that the power spectrum radiated by this dipole is very rich in harmonics of the fundamental frequency (plasma frequency). The second system is an electron gas trapped in an anharmonic and anisotropic well. In this study, we have seen that the electron dynamics becomes more and more complex and eventually fully chaotic when we increase the anharmonic component of the confining potential. This has been showed using the Poincaré sections. We have also showed that the appearance of chaotic behaviour is accompanied by the presence of higher-order harmonics in the electronic dipolar response. We have finally proved that using an autoresonant excitation the different harmonics as well as the phase-space trajectories present a clear signature of the chirped excitation. For instance the harmonics appearing in the spectrum are unusually broad.

Currently the spin-Vlasov solver that we developed is only capable to simulate the electron charge and spin dynamics in a reduced phase space (x, v_x). Here x is the direction of the applied electric field. Therefore, it is impossible to correctly describe the interaction between a magnetic field (internal or external) and the electrons. Indeed, a magnetic field applied in a given direction will necessarily create, according to the Lorentz force, an electron orbital motion in the perpendicular plane. However, the Zeeman interaction between a magnetic field and the electron spin is fully taken into account by our spin-Vlasov solver. Thus, we are able to perform non-collinear spin dynamics. It is also not possible to describe the spin-orbit interaction, since we need the three components of the velocity. An interesting perspective would be to extend our simulations to the entire velocity space, i.e. (x, v_x, v_y, v_z). Then, it would be possible to correctly describe the spin-orbit interaction in a dynamical fashion . It would be particularly interesting to study the nonlinear magnetization dynamics of a system of interacting electrons with spin effect (Zeeman and spin-orbit). This would give us a better understanding of the physics contained in the spin-Vlasov equations (2.54)-(2.55). In particular, how the self-consistent electric and magnetic fields are able to enhance the spin-orbit interaction. The difficulties are mainly numerical, as the 2 dimensional simulations (x, v_x) already require long simulation times, we have to parallelize our code. Otherwise it would be impossible to perform more than 2 dimensional simulations.

Another solution could be to combine both kinetic and fluid models. For instance, the dynamics in the (x, v_x) phase space would be treated with kinetic models such as the spin-Vlasov model (2.54)-(2.55). Whereas the dynamics in the (v_x, v_y) phase space would be described with a set of fluid equations. Such methods were recently used in plasma physics to model particle transport in a tokamak scrape-off layer [163].

An other perspectives would be to perform numerical simulations with the fluid models that we developed in the section 2.3. The main advantage of the fluid models is that they are less difficult to implement than the phase-space models. Indeed, since the fluid models are obtained by integrating the Wigner/Vlasov equations over the velocity space, the electron dynamics in nickel thin films would be a one dimensional problem (in the x direction). However as the fluid models are always approximations of the full phase-space models, it is not guaranteed that the solutions obtained are correct. Moreover, we have seen that the phase-space models conserve several physical quantities such as the mass, the total momentum, the total energy and the total angular momentum. It is not guaranteed that the fluid equations have the same conservation laws.

The variational approach should also be extended to incorporate the spin degrees of freedom. In this case, we first have to find a Lagrangian density that is equivalent to the fluid models constructed in Sec. 2.3. In Ref. [64, 198], the authors used a Lagrangian formulation of the extended Pauli equation (with the spin-orbit interaction). Those papers are a good starting point to think about a Lagrangian formulation of the fluid equations including the spin-orbit interaction. Then it may be possible to use a variational approach, such as in the chapter five, including spin effects (Zeeman and spin-orbit). Such method should allows us to have access to the nonlinear charge and spin dynamics provided that we used a designing shape of the electron density and magnetization. Then it would be possible, using simple numerical methods, to study the nonlinear magnetization dynamics in an system of interacting electrons including self-consistent effects. We should also be able to study the influence of the external excitation (laser pulse) and the confinement potential on the spin dynamics.

Appendix A

Derivation of the spin-Wigner equations in the presence of electromagnetic fields

The evolution equation of the density matrix in the case of an electron interacting with an electromagnetic field reads as

$$i\hbar\frac{\partial\widehat{\rho}}{\partial t}=\left[\widehat{\mathcal{H}},\widehat{\rho}\right],\quad\text{with}\quad\widehat{\rho}=\begin{pmatrix}\widehat{\rho}^{\uparrow\uparrow} & \widehat{\rho}^{\uparrow\downarrow}\\ \widehat{\rho}^{\downarrow\uparrow} & \widehat{\rho}^{\downarrow\downarrow}\end{pmatrix}\quad\text{and}\quad\widehat{\mathcal{H}}=\begin{pmatrix}\widehat{\mathcal{H}}^{\uparrow\uparrow} & \widehat{\mathcal{H}}^{\uparrow\downarrow}\\ \widehat{\mathcal{H}}^{\downarrow\uparrow} & \widehat{\mathcal{H}}^{\downarrow\downarrow}\end{pmatrix}. \tag{A.1}$$

In the forthcoming derivation, we shall include the Zeeman and the spin-orbit interaction. The four components of the Hamiltonian are as follows

$$\widehat{\mathcal{H}}^{\uparrow\uparrow}=\frac{\widehat{\mathbf{\Pi}}^2}{2m}+V(\widehat{\boldsymbol{R}})+\mu_B B_z(\widehat{\boldsymbol{R}})+\frac{\mu_B}{4mc^2}\left[E(\widehat{\boldsymbol{R}})\times\widehat{\mathbf{\Pi}}-\widehat{\mathbf{\Pi}}\times E(\widehat{\boldsymbol{R}})\right]_z, \tag{A.2}$$

$$\widehat{\mathcal{H}}^{\uparrow\downarrow}=\frac{\mu_B}{4mc^2}\left\{\left[E(\widehat{\boldsymbol{R}})\times\widehat{\mathbf{\Pi}}-\widehat{\mathbf{\Pi}}\times E(\widehat{\boldsymbol{R}})\right]_x-i\left[E(\widehat{\boldsymbol{R}})\times\widehat{\mathbf{\Pi}}-\widehat{\mathbf{\Pi}}\times E(\widehat{\boldsymbol{R}})\right]_y\right\}, \tag{A.3}$$

$$\widehat{\mathcal{H}}^{\downarrow\uparrow}=\frac{\mu_B}{4mc^2}\left\{\left[E(\widehat{\boldsymbol{R}})\times\widehat{\mathbf{\Pi}}-\widehat{\mathbf{\Pi}}\times E(\widehat{\boldsymbol{R}})\right]_x+i\left[E(\widehat{\boldsymbol{R}})\times\widehat{\mathbf{\Pi}}-\widehat{\mathbf{\Pi}}\times E(\widehat{\boldsymbol{R}})\right]_y\right\}, \tag{A.4}$$

$$\widehat{\mathcal{H}}^{\downarrow\downarrow}=\frac{\widehat{\mathbf{\Pi}}^2}{2m}+V(\widehat{\boldsymbol{R}})-\mu_B B_z(\widehat{\boldsymbol{R}})-\frac{\mu_B}{4mc^2}\left[E(\widehat{\boldsymbol{R}})\times\widehat{\mathbf{\Pi}}-\widehat{\mathbf{\Pi}}\times E(\widehat{\boldsymbol{R}})\right]_z. \tag{A.5}$$

In order to compute the phase-space functions corresponding to the above Hamiltonians, we apply the Weyl transformation described in Sec. 1.3 of the main paper. Here, we shall give the details of the Weyl transformation for the first term $\widehat{\mathcal{H}}^{\uparrow\uparrow}$.

First, we have to write the Hamiltonian (A.2) in a symmetric form

$$\begin{aligned}\widehat{\mathcal{H}}^{\uparrow\uparrow} &= \frac{\widehat{\mathbf{\Pi}}^2}{2m} + V(\widehat{\boldsymbol{R}}) + \mu_B B_z(\widehat{\boldsymbol{R}}) + \frac{\mu_B}{4mc^2}\epsilon_{ijz}\left(\frac{E_i(\widehat{\boldsymbol{R}})\widehat{\Pi_j}}{2} + \frac{\widehat{\Pi_j}E_i(\widehat{\boldsymbol{R}})}{2} + \frac{i\hbar}{2}\partial_j E_i\right) \\ &\quad - \frac{\mu_B}{4mc^2}\epsilon_{ijz}\left(\frac{\widehat{\Pi_i}E_j(\widehat{\boldsymbol{R}})}{2} + \frac{E_j(\widehat{\boldsymbol{R}})\widehat{\Pi_i}}{2} - \frac{i\hbar}{2}\partial_i E_j\right) \\ &= \frac{\widehat{\mathbf{\Pi}}^2}{2m} + V(\widehat{\boldsymbol{R}}) + \mu_B B_z(\widehat{\boldsymbol{R}}) + \frac{\mu_B}{4mc^2}\epsilon_{ijz}\left(\frac{E_i(\widehat{\boldsymbol{R}})\widehat{\Pi_j}}{2} + \frac{\widehat{\Pi_j}E_i(\widehat{\boldsymbol{R}})}{2} - \frac{\widehat{\Pi_i}E_j(\widehat{\boldsymbol{R}})}{2} - \frac{E_j(\widehat{\boldsymbol{R}})\widehat{\Pi_i}}{2}\right),\end{aligned} \tag{A.6}$$

where we used the following commutation relation: $\left[\widehat{\Pi_i}, F(\widehat{\boldsymbol{R}})\right] = -i\hbar\partial_i F(\boldsymbol{r})$. Then we replace all operators with their associated phase-space variables. By doing so, we obtain the phase-space functions associated to $\widehat{\mathcal{H}}^{\uparrow\uparrow}$:

$$H^{\uparrow\uparrow} = \frac{\boldsymbol{\pi}^2}{2m} + V + \mu_B B_z + \frac{\mu_B}{2mc^2}\left[\boldsymbol{E}\times\boldsymbol{\pi}\right]_z. \tag{A.7}$$

The phase-space functions for the other components of the Hamiltonian can be obtained through similar calculations:

$$H^{\uparrow\downarrow} = \mu_B\left(B_x - iB_y\right) + \frac{\mu_B}{2mc^2}\left(\left[\boldsymbol{E}\times\boldsymbol{\pi}\right]_x - i\left[\boldsymbol{E}\times\boldsymbol{\pi}\right]_y\right), \tag{A.8}$$

$$H^{\downarrow\uparrow} = \mu_B\left(B_x + iB_y\right) + \frac{\mu_B}{2mc^2}\left(\left[\boldsymbol{E}\times\boldsymbol{\pi}\right]_x + i\left[\boldsymbol{E}\times\boldsymbol{\pi}\right]_y\right), \tag{A.9}$$

$$H^{\downarrow\downarrow} = \frac{\boldsymbol{\pi}^2}{2m} + V - \mu_B B_z - \frac{\mu_B}{2mc^2}\left[\boldsymbol{E}\times\boldsymbol{\pi}\right]_z. \tag{A.10}$$

The equations of motion for the four Wigner functions are determined by Eq. (2.21) in the main text. Using this equation with the previous Hamiltonians (A.7)-(A.10), one obtains:

$$i\hbar\partial_t f_0 = \left[\frac{\boldsymbol{\pi}^2}{2m} + V, f_0\right]_\star^c + \mu_B\left[B_i, f_i\right]_\star^c + \frac{\mu_B}{2mc^2}\epsilon_{ijk}\left[E_i\pi_j, f_k\right]_\star^c, \tag{A.11}$$

$$\begin{aligned}i\hbar\partial_t f_k = &\left[\frac{\boldsymbol{\pi}^2}{2m} + V, f_k\right]_\star^c + \mu_B\left[B_k, f_0\right]_\star^c + \frac{\mu_B}{2mc^2}\epsilon_{ijk}\left[E_i\pi_j, f_0\right]_\star^c + i\mu_B\epsilon_{ijk}\left\{B_i, f_j\right\}_\star^A \\ &+ i\frac{\mu_B}{2mc^2}\epsilon_{lri}\epsilon_{ijk}\left\{E_l\pi_r, f_j\right\}_\star^A,\end{aligned} \tag{A.12}$$

where $\{A,B\}_\star^c = A\star B - B\star A$ and $\{A,B\}_\star^A = A\star B + B\star A$ denotes, respectively, the commutator and the anti-commutator. From the Eqs. (1.39)-(1.40) in the main text, we notice that the operators $\mathcal{L}$ and $\mathcal{L}_n$ commute with each other, so we can rewrite the Moyal product [Eq. (1.38) in the main text] in a more convenient way for the

calculations:

$$A(\boldsymbol{r},\boldsymbol{\pi})\star C(\boldsymbol{r},\boldsymbol{\pi})=\prod_{n=1}^{\infty}\exp\left(ie\sum_{n=1}^{\infty}\hbar^{n}\mathcal{L}_{n}\right)\exp\left(i\hbar\mathcal{L}\right)\left(A(\boldsymbol{r},\boldsymbol{\pi}),C(\boldsymbol{r},\boldsymbol{\pi})\right). \tag{A.13}$$

We will also use the following symmetry properties for the operators $\mathcal{L}$ and $\mathcal{L}_n$

$$\mathcal{L}^{n}\left(A,B\right)=(-1)^{n}\,\mathcal{L}^{n}\left(B,A\right),\quad \mathcal{L}_{n}^{m}\left(A,B\right)=(-1)^{nm}\,\mathcal{L}_{n}^{m}\left(B,A\right). \tag{A.14}$$

In order to develop Eqs. (A.11) and (A.12), we calculate separately the following five terms $\left[\frac{\boldsymbol{\pi}^2}{2m},f_0\right]_{\star}^{c}$, $[V,f_0]_{\star}^{c}$, $[E_i\pi_j,f_k]_{\star}^{c}$, $\{B_i,f_j\}_{\star}^{A}$ and $\{E_i\pi_j,f_k\}_{\star}^{A}$.

1. Term: $\left[\frac{\boldsymbol{\pi}^2}{2m},f_0\right]_{\star}^{c}$.
   From Eq. (1.38) in the main text, the above commutator reads as

$$\left[\frac{\boldsymbol{\pi}^2}{2m},f_0\right]_{\star}^{c}=\exp\left[i\hbar\mathcal{L}+ie\sum_{n=1}^{\infty}\hbar^{n}\mathcal{L}_{n}\right]\left[\left(\frac{\boldsymbol{\pi}^2}{2m},f_0\right)-\left(f_0,\frac{\boldsymbol{\pi}^2}{2m}\right)\right]. \tag{A.15}$$

   Let us develop the following quantity:

$$\begin{aligned}\exp\left(i\hbar\mathcal{L}\right)\left(f(\boldsymbol{r},\boldsymbol{\pi}),\frac{\boldsymbol{\pi}^2}{2m}\right)&=\sum_{n=0}^{\infty}\left(\frac{i\hbar}{2}\right)^{n}\frac{1}{n!}\left({}^{L}\partial_{i}{}^{R}\partial_{\pi_i}-{}^{R}\partial_{j}{}^{L}\partial_{\pi_j}\right)^{n}\left(f,\frac{\boldsymbol{\pi}^2}{2m}\right)\\&=\sum_{n=0}^{\infty}\sum_{p=0}^{n}\left(\frac{i\hbar}{2}\right)^{p}\frac{(-1)^{p}}{n!}\binom{n}{p}\left(\partial_{i_1\cdots i_{n-p}}^{n-p}\partial_{\pi_{j_1}\cdots\pi_{j_p}}^{p}f\right)\left(\partial_{\pi_{i_1}\cdots\pi_{i_{n-p}}}^{n-p}\partial_{j_1\cdots j_p}^{p}\frac{\boldsymbol{\pi}^2}{2m}\right),\end{aligned} \tag{A.16}$$

   where we used the following notation:

$$\partial_{i_1\cdots i_n}^{n}\partial_{\pi_{j_1}\cdots\pi_{j_p}}^{p}=\sum_{i_1\cdots i_n=1}^{3}\sum_{j_1\cdots j_p=1}^{3}\frac{\partial^{n}}{\partial r_{i_1}\cdots\partial r_{i_n}}\frac{\partial^{n}}{\partial\pi_{j_1}\cdots\partial\pi_{j_p}}, \tag{A.17}$$

   with $(r_1,r_2,r_3)=(x,y,z)$ and $(\pi_1,\pi_2,\pi_3)=(\pi_x,\pi_y,\pi_z)$.
   Eq. (A.16) differs from zero only if $p=0$, so one obtains:

$$\begin{aligned}\exp\left(i\hbar\mathcal{L}\right)\left(f(\boldsymbol{r},\boldsymbol{\pi}),\frac{\boldsymbol{\pi}^2}{2m}\right)&=\sum_{n=0}^{\infty}\left(\frac{i\hbar}{2}\right)^{n}\frac{1}{n!}\left(\partial_{\pi_{i_1}\cdots\pi_{i_n}}^{n}\frac{\boldsymbol{\pi}^2}{2m}\right)\partial_{i_1\cdots i_n}^{n}f\\&=\frac{\boldsymbol{\pi}^2}{2m}f+\frac{i\hbar}{2m}\pi_i\left(\partial_i f\right)-\frac{\hbar^2}{8m}\sum_{i=1}^{3}\left(\partial_i^2 f\right).\end{aligned} \tag{A.18}$$

   Using the symmetry properties (A.14) for the operator $\mathcal{L}$, one obtains:

$$\exp\left(i\hbar\mathcal{L}\right)\left(\frac{\boldsymbol{\pi}^2}{2m},f(\boldsymbol{r},\boldsymbol{\pi})\right)=\frac{\boldsymbol{\pi}^2}{2m}f-\frac{i\hbar}{2m}\pi_i\left(\partial_{x_i}f\right)-\frac{\hbar^2}{8m}\sum_{i=1}^{3}\left(\partial_{x_i}^2 f\right). \tag{A.19}$$

Injecting Eqs. (A.18) and (A.19) in Eq. (A.15) gives

$$\left[\frac{\boldsymbol{\pi}^2}{2m}, f_0\right]_\star^c = \frac{1}{2m}\prod_{n=1}^{\infty}\exp\left(ie\sum_{n=1}^{\infty}\hbar^n\mathcal{L}_n\right)\left(\pi_k^2, f\right) - \frac{1}{2m}\prod_{n=1}^{\infty}\exp\left(ie\sum_{n=1}^{\infty}\hbar^n\mathcal{L}_n\right)\left(f, \pi_k^2\right) - \frac{i\hbar}{2m}\prod_{n=1}^{\infty}\exp\left(ie\sum_{n=1}^{\infty}\hbar^n\mathcal{L}_n\right)\left(\pi_i, \partial_i f\right) - \frac{i\hbar}{2m}\prod_{n=1}^{\infty}\exp\left(ie\sum_{n=1}^{\infty}\hbar^n\mathcal{L}_n\right)\left(\partial_i f, \pi_i\right). \tag{A.20}$$

From Eq. (1.40) in the main text, the $\mathcal{L}_n$ operator contains at least one derivative in $\boldsymbol{\pi}$. Then, by developing the exponentials in power series of the operators $\mathcal{L}_n$ in Eq. (A.20), all the operators of order higher than $n = 2$ will give no contributions. Then Eq. (A.20) reduces to

$$\left[\frac{\boldsymbol{\pi}^2}{2m}, f_0\right]_\star^c = -\frac{i\hbar}{m}\left(\pi_i\partial_{x_i}f\right) + \frac{1}{2m}\left[ie\sum_{n=1}^{\infty}\hbar^n\mathcal{L}_n - \frac{e^2}{2}\left(\sum_{n=1}^{\infty}\hbar^n\mathcal{L}_n\right)^2\right]\left[\left(\pi_k^2, f\right) - \left(f, \pi_k^2\right)\right] + \frac{e\hbar}{2m}\left[\sum_{n=1}^{\infty}\hbar^n\mathcal{L}_n\right]\left[\left(\pi_i, \partial_i f\right) + \left(\partial_i f, \pi_i\right)\right]. \tag{A.21}$$

Using the symmetry properties (A.14) of the operator $\mathcal{L}_n$, one obtains:

$$\left[\frac{\boldsymbol{\pi}^2}{2m}, f_0\right]_\star^c = -\frac{i\hbar}{m}\left(\pi_i\partial_{x_i}f\right) + \frac{e\hbar}{m}\sum_{n=0}^{\infty}\hbar^{2n+2}\mathcal{L}_{2n+2}\left(\pi_i, \partial_{x_i}f\right) + \frac{ie}{m}\sum_{n=0}^{\infty}\hbar^{2n+1}\mathcal{L}_{2n+1}\left(\pi_k^2, f\right) - \frac{e^2}{m}\sum_{n=0}^{\infty}\sum_{p=0}^{\infty}\hbar^{2n+1}\hbar^{2p+2}\mathcal{L}_{2n+1}\mathcal{L}_{2p+2}\left(\pi_k^2, f\right), \tag{A.22}$$

where the second term on the right-hand side reads as

$$\sum_{n=0}^{\infty}\hbar^{2n+2}\mathcal{L}_{2n+2}\left(\pi_i, \partial_i f\right) = \frac{1}{\hbar}\sum_{n=0}^{\infty}\left(\frac{i\hbar}{2}\right)^{2n+3}\frac{\epsilon_{jlr}}{(2n+3)^2(2n+2)!}\left(\partial^{2n+1}_{x_{i1}\ldots x_{i_{2n+1}}}B_r\right){}^{L}\partial_{\pi_j}{}^{R}\partial_{\pi_l}$$
$$\sum_{p=1}^{2n+1}\binom{2n+3}{p}g(n,p)\,{}^{L}\partial_{\pi_{i1}}\cdots{}^{L}\partial_{\pi_{ip-1}}{}^{R}\partial_{\pi_{ip}}\cdots{}^{R}\partial_{\pi_{i_{2n+1}}}\left(\pi_i, \partial_i f\right),$$

with $g(n,p) = \left[\left(1-(-1)^p\right)(2n+3) - \left(1-(-1)^{2n+3}\right)p\right]$.
Only the term corresponding to $p = 1$ gives a nonzero contribution

$$\sum_{n=0}^{\infty}\hbar^{2n+2}\mathcal{L}_{2n+2}\left(\pi_i, \partial_i f\right) = -\frac{i\hbar}{2}\sum_{n=0}^{\infty}\left(\frac{\hbar}{2}\right)^{2n+1}\frac{(-1)^n(2n+2)}{(2n+3)!}\epsilon_{jlr}\left(\partial^{2n+1}_{i_1\ldots i_{2n+1}}B_r\right)\partial^{2n+1}_{\pi_{i_1}\cdots\pi_{i_{2n+1}}}\partial_{\pi_l}\left(\partial_j f\right). \tag{A.23}$$

By similar developments, the third and the fourth terms of Eq. (A.22) become

$$\sum_{n=0}^{\infty}\hbar^{2n+1}\mathcal{L}_{2n+1}\left(\pi_k^2,f\right)=-\hbar\pi_j\epsilon_{jlr}\sum_{n=0}^{\infty}\left(\frac{\hbar}{2}\right)^{2n}\frac{(-1)^n}{(2n+1)!}\left(\partial^{2n}_{i1\ldots i_{2n}}B_r\right)\partial^{2n}_{\pi_{i_1}\cdots\pi_{i_{2n}}}\left(\partial_{\pi_l}f\right), \tag{A.24}$$

$$\sum_{n,p=0}^{\infty}\hbar^{2n+1}\hbar^{2p+2}\mathcal{L}_{2n+1}\mathcal{L}_{2p+2}\left(\pi_k^2,f\right)=\frac{i\hbar^2}{2}\epsilon_{ijk}\epsilon_{ilr}\sum_{n,p=0}^{\infty}\left(\frac{\hbar}{2}\right)^{2n+2p+1}\frac{(-1)^n}{(2n+1)!}\frac{(-1)^p(2p+2)}{(2p+3)!}$$
$$\left(\partial^{2n}_{i1\ldots i_{2n}}B_r\right)\left(\partial^{2p+1}_{j_1\ldots j_{2p+1}}B_k\right)\partial^{2n}_{\pi_{i_1}\cdots\pi_{i_{2n}}}\partial^{2p+1}_{\pi_{j_1}\cdots\pi_{j_{2p+1}}}\partial_{\pi_j}\left(\partial_{\pi_l}f\right). \tag{A.25}$$

Injecting Eqs. (A.23), (A.24) and (A.25) into Eq. (A.22), one obtains:

$$\left[\frac{\boldsymbol{\pi}^2}{2m},f_0\right]_\star^c=-\frac{i\hbar}{m}\left[\left(\boldsymbol{\pi}+\tilde{\boldsymbol{\Delta\pi}}\right)\cdot\boldsymbol{\nabla}f\left(\boldsymbol{r},\boldsymbol{\pi},t\right)-e\left[\left(\boldsymbol{\pi}+\tilde{\boldsymbol{\Delta\pi}}\right)\times\tilde{\boldsymbol{B}}\right]_i\partial_{\pi_i}f\left(\boldsymbol{r},\boldsymbol{\pi},t\right)\right], \tag{A.26}$$

where we use the notation introduced by Serimaa et al. [87]:

$$\boldsymbol{\Delta}\widetilde{\boldsymbol{\pi}}=-i\hbar e\boldsymbol{\nabla}_{\boldsymbol{\pi}}\times\left[\int_{-1/2}^{1/2}d\tau\tau\boldsymbol{B}\left(\boldsymbol{r}+i\hbar\tau\boldsymbol{\nabla}_{\boldsymbol{\pi}}\right)\right],\quad\tilde{\boldsymbol{B}}=\int_{-1/2}^{1/2}d\tau\boldsymbol{B}\left(\boldsymbol{r}+i\hbar\tau\boldsymbol{\nabla}_{\boldsymbol{\pi}}\right). \tag{A.27}$$

2. Term: $[V,f_0]_\star^c$.

   This term is the same as in the unmagnetized case. Indeed, the $\mathcal{L}_n$ operators do not act on V since they contain at least one derivative in $\boldsymbol{\pi}$. Thus, one obtains:

$$\begin{aligned}
&[V,f_0]_\star^c=\exp\left(i\hbar\mathcal{L}\right)\left[\left(V,f_0(\boldsymbol{r},\boldsymbol{\pi})\right)-\left(f_0(\boldsymbol{r},\boldsymbol{\pi}),V\right)\right]\\
&=2i\sum_{n=0}^{\infty}\left(\frac{\hbar}{2}\right)^{2n+1}\frac{(-1)^n}{(2n+1)!}\left({}^{L}\partial_i{}^{R}\partial_{\pi_i}-{}^{R}\partial_j{}^{L}\partial_{\pi_j}\right)^{2n+1}\left(V,f_0(\boldsymbol{r},\boldsymbol{\pi})\right)\\
&=2i\sum_{n=0}^{\infty}\sum_{p=0}^{2n+1}\left(\frac{\hbar}{2}\right)^{2n+1}\frac{(-1)^{n+p}}{(2n+1)!}\binom{2n+1}{p}\left(\partial^{2n+1-p}_{i_1\cdots i_{2n+1-p}}\partial^{p}_{\pi_{j_1}\cdots\pi_{j_p}}V\right)\left(\partial^{2n+1-p}_{\pi_{i_1}\cdots\pi_{i_{2n+1-p}}}\partial^{p}_{j_1\cdots j_p}f_0\right).
\end{aligned} \tag{A.28}$$

   Only the contribution corresponding to $p=0$ survives, because V does not depend on $\boldsymbol{\pi}$. Thus:

$$[V,f_0]_\star^c=-i\hbar e\widetilde{\boldsymbol{E}}\cdot\boldsymbol{\nabla}_{\boldsymbol{\pi}}f_0, \tag{A.29}$$

where we have introduced the following quantity:

$$\tilde{\boldsymbol{E}} = \int_{-1/2}^{1/2} d\tau \boldsymbol{E}\left(\boldsymbol{r} + i\hbar\tau\boldsymbol{\nabla}_{\boldsymbol{\pi}}\right). \tag{A.30}$$

3. Term: $\epsilon_{ijk}\left[E_i\pi_j, f_k\right]_\star^c$.

We start by developing the following expression

$$\begin{aligned}\exp\left(\imath\hbar\mathcal{L}\right)\left(E_i\pi_j, f_k\right) &= \sum_{n=0}^{\infty}\left(\frac{i\hbar}{2}\right)^n \frac{1}{n!}\left({}^L\partial_k {}^R\partial_{\pi_k} - {}^R\partial_l {}^L\partial_{\pi_l}\right)^n \left(E_i\pi_j, f_k\right) \\ &= \sum_{n=0}^{\infty}\sum_{p=0}^{n}\left(\frac{i\hbar}{2}\right)^n \frac{(-1)^p}{n!}\binom{n}{p}\left(\partial^{n-p}_{i_1\cdots i_{n-p}}\partial^p_{\pi_{j_1}\cdots\pi_{j_p}}\pi_j E_i\right)\left(\partial^{n-p}_{\pi_{i_1}\cdots\pi_{i_{n-p}}}\partial^p_{j_1\cdots j_p} f_k\right).\end{aligned} \tag{A.31}$$

Only the terms with $p = 0$ or $p = 1$ survive, so that

$$\begin{aligned}\exp\left(\imath\hbar\mathcal{L}\right)\left(E_i\pi_j, f_k\right) = \pi_j \sum_{n=0}^{\infty}\left(\frac{i\hbar}{2}\right)^n \frac{1}{n!}\left(\partial^n_{\pi_{j_1}\cdots\pi_{j_n}} f_k\right)\left(\partial^n_{j_1\cdots j_n} E_i\right) \\ - \sum_{n=1}^{\infty}\left(\frac{i\hbar}{2}\right)^n \frac{1}{(n-1)!}\left(\partial^{n-1}_{\pi_{j_1}\cdots\pi_{j_{n-1}}}\partial_j f_k\right)\left(\partial^{n-1}_{j_1\cdots j_{n-1}} E_i\right).\end{aligned} \tag{A.32}$$

Then the Moyal product between $E_i\pi_j$ and f_k can be written as:

$$\left(E_i\pi_j\right)\star f_k = \prod_{p=1}^{\infty}\exp\left(ie\hbar^p\mathcal{L}_p\right)\exp\left(\imath\hbar\mathcal{L}\right)\left(E_i\pi_j, f_k\right) = \left[1 + ie\sum_{p=1}^{\infty}\hbar^p\mathcal{L}_p\right]\exp\left(\imath\hbar\mathcal{L}\right)\left(E_i\pi_j, f_k\right). \tag{A.33}$$

The last equality holds because the operator $\mathcal{L}_p$ acts one a phase-space function that is at most linear in $\boldsymbol{\pi}$. Then we only have to evaluate the following

quantity:

$$
\begin{aligned}
&ie\sum_{p=1}^{\infty}\hbar^{p}\mathcal{L}_{p}\left[\exp\left(\imath\hbar\mathcal{L}\right)\left(E_{i}\pi_{j},f_{k}\right)\right]\\
&=ie\sum_{n=0}^{\infty}\sum_{p=1}^{\infty}\hbar^{p}\left(\frac{i\hbar}{2}\right)^{n}\frac{1}{n!}\mathcal{L}_{p}\left(\pi_{j}\left(\partial^{n}_{j_{1}\cdots j_{n}}E_{i}\right),\left(\partial^{n}_{\pi_{j_{1}}\cdots\pi_{j_{n}}}f_{k}\right)\right)\\
&=ie\sum_{n=0}^{\infty}\sum_{p=1}^{\infty}\hbar^{p}\left(\frac{i\hbar}{2}\right)^{n}\frac{1}{n!}\left(\frac{i}{2}\right)^{p+1}\frac{\epsilon_{slr}}{(p+1)^{2}p!}\left(\partial^{p-1}_{i_{1}\cdots i_{p-1}}B_{r}\right)\left(\partial^{n}_{j_{1}\cdots j_{n}}E_{i}\right)\sum_{m=1}^{p}\binom{p+1}{m}g(p,m)\\
&\left(\partial^{m-1}_{\pi_{i_{1}}\cdots\pi_{i_{m-1}}}\partial_{\pi_{s}}\pi_{j}\right)\left(\partial^{p-m}_{\pi_{i_{m}}\cdots\pi_{i_{p-1}}}\partial^{n}_{\pi_{j_{1}}\cdots\pi_{j_{n}}}\partial_{\pi_{l}}f_{k}\right)\\
&=\frac{ie}{\hbar}\epsilon_{jlr}\sum_{n=0}^{\infty}\sum_{p=1}^{\infty}\left(\frac{i\hbar}{2}\right)^{n}\frac{1}{n!}\left(\frac{i\hbar}{2}\right)^{p+1}\frac{1}{(p+1)!}\left(\partial^{p-1}_{i_{1}\cdots i_{p-1}}B_{r}\right)\left(\partial^{n}_{j_{1}\cdots j_{n}}E_{i}\right)\\
&g(p,1)\left(\partial^{p-1}_{\pi_{i_{1}}\cdots\pi_{i_{p-1}}}\partial^{n}_{\pi_{j_{1}}\cdots\pi_{j_{n}}}\partial_{\pi_{l}}f_{k}\right),
\end{aligned}
$$

with $g(p,1)=2p$ if p is even and $g(p,1)=2(p+1)$ if p is odd. Hence one obtains:

$$
\begin{aligned}
&\left(E_{i}\pi_{j}\right)\star f_{k}=\sum_{n=0}^{\infty}\frac{\pi_{j}}{n!}\left(\frac{i\hbar}{2}\right)^{n}\left(\partial^{n}_{\pi_{j_{1}}\cdots\pi_{j_{n}}}f_{k}\right)\left(\partial^{n}_{j_{1}\cdots j_{n}}E_{i}\right)\\
&-\sum_{n=1}^{\infty}\left(\frac{i\hbar}{2}\right)^{n}\frac{1}{(n-1)!}\left(\partial^{n-1}_{\pi_{j_{1}}\cdots\pi_{j_{n-1}}}\partial_{j}f_{k}\right)\left(\partial^{n-1}_{j_{1}\cdots j_{n-1}}E_{i}\right)\\
&+\frac{ie}{\hbar}\epsilon_{jlr}\sum_{n=0}^{\infty}\sum_{p=1}^{\infty}\left(\frac{i\hbar}{2}\right)^{n}\frac{1}{n!}\left(\frac{i\hbar}{2}\right)^{p+1}\frac{1}{(p+1)!}\left(\partial^{p-1}_{i_{1}\cdots i_{p-1}}B_{r}\right)\left(\partial^{n}_{j_{1}\cdots j_{n}}E_{i}\right)g(p,1)\\
&\left(\partial^{p-1}_{\pi_{i_{1}}\cdots\pi_{i_{p-1}}}\partial^{n}_{\pi_{j_{1}}\cdots\pi_{j_{n}}}\partial_{\pi_{l}}f_{k}\right),
\end{aligned}
\tag{A.34}
$$

Using the symmetry identities (A.14), one obtains:

$$
\begin{aligned}
&f_{k}\star\left(E_{i}\pi_{j}\right)=\sum_{n=0}^{\infty}\frac{\pi_{j}}{n!}\left(\frac{-i\hbar}{2}\right)^{n}\left(\partial^{n}_{\pi_{j_{1}}\cdots\pi_{j_{n}}}f_{k}\right)\left(\partial^{n}_{j_{1}\cdots j_{n}}E_{i}\right)-\sum_{n=1}^{\infty}\left(\frac{-i\hbar}{2}\right)^{n}\frac{1}{(n-1)!}\\
&\left(\partial^{n-1}_{\pi_{j_{1}}\cdots\pi_{j_{n-1}}}\partial_{j}f_{k}\right)\left(\partial^{n-1}_{j_{1}\cdots j_{n-1}}E_{i}\right)+\frac{ie}{\hbar}\epsilon_{jlr}\sum_{n=0}^{\infty}\sum_{p=1}^{\infty}\left(\frac{i\hbar}{2}\right)^{n}\frac{(-1)^{n}}{n!}\left(\frac{i\hbar}{2}\right)^{p+1}\frac{(-1)^{p}}{(p+1)!}\\
&\left(\partial^{p-1}_{i_{1}\cdots i_{p-1}}B_{r}\right)\left(\partial^{n}_{j_{1}\cdots j_{n}}E_{i}\right)g(p,1)\left(\partial^{p-1}_{\pi_{i_{1}}\cdots\pi_{i_{p-1}}}\partial^{n}_{\pi_{j_{1}}\cdots\pi_{j_{n}}}\partial_{\pi_{l}}f\right),
\end{aligned}
\tag{A.35}
$$

Using Eqs. (A.34) and (A.35), one finally obtains:

$$
\begin{aligned}
&\frac{\epsilon_{ijk}}{i\hbar}\left[E_{i}\pi_{j},f_{k}\right]^{c}_{\star}=-\frac{1}{2}\left[\left(\boldsymbol{E}_{+}+\boldsymbol{E}_{-}\right)\times\boldsymbol{\nabla}\right]\cdot\boldsymbol{f}-\boldsymbol{\nabla}\left[\boldsymbol{\pi}\times\widetilde{\boldsymbol{E}}\right]_{k}\cdot\boldsymbol{\nabla}_{\pi}f_{k}\\
&+e\left[\widetilde{\boldsymbol{E}}\times\left[\widetilde{\boldsymbol{B}}\times\boldsymbol{\nabla}_{\pi}\right]\right]\cdot\boldsymbol{f}-\frac{1}{i\hbar}\left[\boldsymbol{\Delta}\widetilde{\boldsymbol{\pi}}\times\left(\boldsymbol{E}_{+}-\boldsymbol{E}_{-}\right)\right]\cdot\boldsymbol{f}.
\end{aligned}
\tag{A.36}
$$

The index $\pm$ means that the associated quantity is evaluated at a shifted position $\boldsymbol{r} \pm i\hbar\boldsymbol{\nabla}_{\boldsymbol{\pi}}/2$.

4. Term: $i\epsilon_{lri}\epsilon_{ijk}\left\{E_l\pi_r, f_j\right\}_\star^A$

   Using equation (A.34) and (A.35), one directly obtains:

$$\begin{aligned} i\epsilon_{lri}\epsilon_{ijk}\left\{E_l\pi_r, f_j\right\}_\star^A &= -i\left\{\left[(\boldsymbol{\pi}+\boldsymbol{\Delta}\widetilde{\boldsymbol{\pi}})\times(\boldsymbol{E}_+ + \boldsymbol{E}_-)\right]\times\boldsymbol{f}\right\}_k \\ &+ \frac{\hbar}{2}\left\{\left[(\boldsymbol{E}_+ - \boldsymbol{E}_-)\times\left(\boldsymbol{\nabla} - e\widetilde{\boldsymbol{B}}\times\boldsymbol{\nabla}_{\boldsymbol{\pi}}\right)\right]\times\boldsymbol{f}\right\}_k . \end{aligned} \tag{A.37}$$

5. Term: $i\epsilon_{ijk}\left\{B_i, f_j\right\}_\star^A$

   The calculation is very similar to that of the second item, i.e. for $\{V, f_0\}_\star^A$. The only difference is that we keep the even terms in Eq. (A.28) instead of the odd terms. Then one simply obtains :

$$i\epsilon_{ijk}\left\{B_i, f_j\right\}_\star^A = i\epsilon_{ijk}\left(\boldsymbol{B}_+ + \boldsymbol{B}_-\right)_i f_j. \tag{A.38}$$

Using the Eqs. (A.26), (A.29), (A.36), (A.37), (A.38), as well as the Eqs. (A.11), (A.12), we finally obtain the Wigner equation for an electron interacting with an electromagnetic field, including the Zeeman interaction and the spin-orbit coupling:

$$\begin{aligned} &\frac{\partial f_0}{\partial t} + \frac{1}{m}(\boldsymbol{\pi}+\boldsymbol{\Delta}\widetilde{\boldsymbol{\pi}})\cdot\boldsymbol{\nabla} f_0 - \frac{e}{m}\left[m\widetilde{\boldsymbol{E}} + (\boldsymbol{\pi}+\boldsymbol{\Delta}\widetilde{\boldsymbol{\pi}})\times\widetilde{\boldsymbol{B}}\right]_i \partial_{\pi_i} f_0 \\ &- \mu_B\boldsymbol{\nabla}\left(\widetilde{\boldsymbol{B}} - \frac{1}{2mc^2}\boldsymbol{\pi}\times\widetilde{\boldsymbol{E}}\right)_i \cdot\boldsymbol{\nabla}_{\boldsymbol{\pi}} f_i + \frac{\mu_B}{4mc^2}\left[(\boldsymbol{E}_+ + \boldsymbol{E}_-)\times\boldsymbol{\nabla}\right]\cdot\boldsymbol{f} \\ &- \frac{\mu_B e}{2mc^2}\left[\widetilde{\boldsymbol{E}}\times\left[\widetilde{\boldsymbol{B}}\times\boldsymbol{\nabla}_\pi\right]\right]\cdot\boldsymbol{f} - \frac{\mu_B}{2mc^2}\frac{i}{\hbar}\left[\boldsymbol{\Delta}\widetilde{\boldsymbol{\pi}}\times(\boldsymbol{E}_+ - \boldsymbol{E}_-)\right]\cdot\boldsymbol{f} = 0, \end{aligned} \tag{A.39}$$

$$\begin{aligned} &\frac{\partial f_k}{\partial t} + \frac{1}{m}(\boldsymbol{\pi}+\boldsymbol{\Delta}\widetilde{\boldsymbol{\pi}})\cdot\boldsymbol{\nabla} f_k - \frac{e}{m}\left[m\widetilde{\boldsymbol{E}} + (\boldsymbol{\pi}+\boldsymbol{\Delta}\widetilde{\boldsymbol{\pi}})\times\widetilde{\boldsymbol{B}}\right]_i \partial_{\pi_i} f_k \\ &- \mu_B\boldsymbol{\nabla}\left(\widetilde{\boldsymbol{B}} - \frac{1}{2mc^2}\boldsymbol{\pi}\times\widetilde{\boldsymbol{E}}\right)_k \cdot\boldsymbol{\nabla}_{\boldsymbol{\pi}} f_0 + \frac{\mu_B}{4mc^2}\left[(\boldsymbol{E}_+ + \boldsymbol{E}_-)\times\boldsymbol{\nabla}\right]_k f_0 \\ &- \frac{\mu_B e}{2mc^2}\left[\widetilde{\boldsymbol{E}}\times\left[\widetilde{\boldsymbol{B}}\times\boldsymbol{\nabla}_\pi\right]\right]_k f_0 - \frac{\mu_B}{2mc^2}\frac{i}{\hbar}\left[\boldsymbol{\Delta}\widetilde{\boldsymbol{\pi}}\times(\boldsymbol{E}_+ - \boldsymbol{E}_-)\right]_k f_0 \\ &- \frac{e}{2m}\left[\left(\boldsymbol{B}_+ + \boldsymbol{B}_- - \frac{1}{2mc^2}(\boldsymbol{\pi}+\boldsymbol{\Delta}\widetilde{\boldsymbol{\pi}})\times(\boldsymbol{E}_+ + \boldsymbol{E}_-)\right)\times\boldsymbol{f}\right]_k \\ &+ \frac{\mu_B}{2mc^2}\frac{i}{2}\left[\left((\boldsymbol{E}_+ - \boldsymbol{E}_-)\times\left(\boldsymbol{\nabla} - e\widetilde{\boldsymbol{B}}\times\boldsymbol{\nabla}_{\boldsymbol{\pi}}\right)\right)\times\boldsymbol{f}\right]_k = 0. \end{aligned} \tag{A.40}$$

Appendix B

Details on derivation of the fluid models using the MEP

B.1 Three-moment Fermi-Dirac closure

We begin by demonstrating the relation (2.95) between the equilibrium distribution $\mathcal{F}^{eq}$ and the component of the Hamiltonian $\mathcal{H}' = h'_0\sigma_0 + \boldsymbol{h'}\cdot\boldsymbol{\sigma'}$, where $h'_0 = m\left(\boldsymbol{v}-\boldsymbol{v_0}\right)^2/2 + \lambda_0$ and $\boldsymbol{h'} = \boldsymbol{\lambda_S}$. Developing the exponential as a power series in Eq. (2.86) (F–D) and inverting the associated matrix, we obtain

$$\begin{aligned}
\mathcal{F}^{\mathrm{eq}} &= a_0\left[\exp\left(\beta\mathcal{H}'\right)+1\right]^{-1}, \\
&= \left(\frac{m}{2\pi\hbar}\right)^3 \exp\left(\beta h'_0\right)\left[\cosh\left(\beta h'_0\right)\sigma_0 + \cosh\left(\beta|\boldsymbol{h'}|\right)\frac{\boldsymbol{h'}\cdot\boldsymbol{\sigma}}{|\boldsymbol{h'}|}\right]^{-1}, \\
&= \frac{a_0}{2}\frac{\left(\cosh\left(\beta|\boldsymbol{h'}|\right)+\exp^{-\beta h'_0}\right)\sigma_0 - \sinh\left(\beta h'_0\right)\left(\boldsymbol{h'}\cdot\boldsymbol{\sigma}\right)/|\boldsymbol{h'}|}{\left[\cosh\left(\beta h'_0\right)+\cosh\left(\beta|\boldsymbol{h'}|\right)\right]}.
\end{aligned}$$

In this case, we obtain the following expression for f_0^{eq} and f_i^{eq} :

$$f_0^{\mathrm{eq}} = a_0\frac{\cosh\left(\beta|\boldsymbol{h'}|\right)+\exp^{-\beta h'_0}}{\cosh\left(\beta h'_0\right)+\cosh\left(\beta|\boldsymbol{h'}|\right)} \quad \text{and} \quad f_i^{\mathrm{eq}} = -\frac{a_0\,\hbar}{2}\frac{\sinh\left(\beta|\boldsymbol{h'}|\right)h'_i/|\boldsymbol{h'}|}{\cosh\left(\beta h'_0\right)+\cosh\left(\beta|\boldsymbol{h'}|\right)}.$$

These expressions cannot be integrated analytically over the velocity space. To obtain a treatable model, we assume that the electron gas is at zero temperature, i.e. $\beta\to\infty$. We start by calculating the density

$$\begin{aligned}
n &= \lim_{\beta\to\infty}\int f_0^{eq}d\boldsymbol{v} = a_0\lim_{\beta\to\infty}\int\frac{e^{\beta|\boldsymbol{h'}|}+2e^{-\beta h'_0}}{e^{\beta h'_0}+e^{-\beta h'_0}+e^{\beta|\boldsymbol{h'}|}}d\boldsymbol{v} \\
&= a_0\lim_{\beta\to\infty}\left[\int\frac{1}{1+e^{\beta\left(h'_0-|\boldsymbol{h'}|\right)}+e^{-\beta\left(h'_0+|\boldsymbol{h'}|\right)}}d\boldsymbol{v} + 2\int\frac{1}{1+e^{2\beta h'_0}+e^{\beta\left(h'_0+|\boldsymbol{h'}|\right)}}d\boldsymbol{v}\right].
\end{aligned}$$

We call n_1 and n_2 respectively the limit for $\beta \to \infty$ of the first and the second integral in the above expression, such that $n = n_1 + n_2$. One can show that

$$
\begin{aligned}
n_1 &= 4\pi a_0 \lim_{\beta\to\infty} \int_0^{+\infty} \frac{v^2}{1+\exp[\beta\left(\frac{m}{2}v^2+\lambda_0-|\boldsymbol{\lambda^S}|\right)]+\exp[-\beta\left(\frac{m}{2}v^2+\lambda_0-|\boldsymbol{\lambda^S}|\right)]} dv \\
&= \begin{cases}
\frac{4\pi}{3}a_0\left[\frac{2}{m}\left(|\boldsymbol{\lambda^S}|-|\lambda_0|\right)\right]^{3/2} & \text{if} \quad 0<\lambda_0<|\boldsymbol{\lambda^S}| \\
0 & \text{if} \quad \lambda_0>|\boldsymbol{\lambda^S}| \\
\frac{4\pi}{3}a_0\left[\frac{2}{m}\left(|\boldsymbol{\lambda^S}|+|\lambda_0|\right)\right]^{3/2} & \text{if} \quad -|\boldsymbol{\lambda^S}|<\lambda_0<0 \\
\frac{4\pi}{3}a_0\left(\left[\frac{2}{m}\left(|\boldsymbol{\lambda^S}|+|\lambda_0|\right)\right]^{3/2}-\left[\frac{2}{m}\left(|\lambda_0|-|\boldsymbol{\lambda^S}|\right)\right]^{3/2}\right) & \text{if} \quad \lambda_0<-|\boldsymbol{\lambda^S}|
\end{cases} \\
n_2 &= 8\pi a_0 \lim_{\beta\to\infty} \int_0^{+\infty} \frac{v^2}{1+\exp^{2\beta\left(\frac{m}{2}v^2+\lambda_0\right)}+\exp^{\beta\left(\frac{m}{2}v^2+\lambda_0+|\boldsymbol{\lambda^S}|\right)}} dv \\
&= \begin{cases}
0 & \text{if} \quad \lambda_0>-|\boldsymbol{\lambda^S}| \\
\frac{8\pi}{3}a_0\left[\frac{2}{m}\left(|\lambda_0|-|\boldsymbol{\lambda^S}|\right)\right]^{3/2} & \text{if} \quad \lambda_0<-|\boldsymbol{\lambda^S}|
\end{cases}
\end{aligned}
$$

For $\boldsymbol{S}$ we obtain

$$
S_i = \lim_{\beta\to\infty}\int f_i d\boldsymbol{v} = -\frac{\hbar}{2}a_0\frac{\lambda_i^S}{|\boldsymbol{\lambda^S}|}\lim_{\beta\to\infty}\int \frac{e^{\beta|\boldsymbol{h'}|}}{e^{\beta h_0'}+e^{-\beta h_0'}+e^{\beta|\boldsymbol{h'}|}}d\boldsymbol{v} = -\frac{\hbar}{2}a_0\frac{\lambda_i^S}{|\boldsymbol{\lambda^S}|}n_1.
$$

In the case where $\lambda_0 > -|\boldsymbol{\lambda^S}|$, we have the following relation between $\boldsymbol{S}$ and n: $|\boldsymbol{S}| = \frac{\hbar}{2}n$. Comparing with Eq. (2.12), we notice that we are in the limit of pure states. If we consider the case where $\lambda_0 < -|\boldsymbol{\lambda^S}|$, we obtain

$$
\begin{aligned}
n &= \frac{4\pi}{3}a_0\left(\left[\frac{2}{m}\left(|\boldsymbol{\lambda^S}|+|\lambda_0|\right)\right]^{3/2}+\left[\frac{2}{m}\left(|\lambda_0|-|\boldsymbol{\lambda^S}|\right)\right]^{3/2}\right), \\
\boldsymbol{S} &= -\frac{\hbar}{2}a_0\frac{\boldsymbol{\lambda^S}}{|\boldsymbol{\lambda^s}|}\frac{4\pi}{3}\left(\left[\frac{2}{m}\left(|\boldsymbol{\lambda^S}|+|\lambda_0|\right)\right]^{3/2}-\left[\frac{2}{m}\left(|\lambda_0|-|\boldsymbol{\lambda^S}|\right)\right]^{3/2}\right), \\
\boldsymbol{u} &= \boldsymbol{v_0}.
\end{aligned}
$$

It is obvious that in this case we have $|\boldsymbol{S}| \leq \frac{\hbar}{2}n$, which is in agreement with Eq. (2.12) and corresponds to admissible physical solutions (quantum mixed states). We are now able to extract the following relation between the Lagrange multipliers and the fluid moments:

$$
|\lambda_0| \pm |\boldsymbol{\lambda^S}| = \left(\frac{2\pi\hbar}{m}\right)^2\frac{m}{2}\left(\frac{3}{8\pi}\right)^{2/3}\left(n \mp \frac{2}{\hbar}|\boldsymbol{S}|\right)^{2/3}.
$$

The next step is to calculate the pressure $P_{ij} = m\int v_i v_j f_0^{eq} d\boldsymbol{v} - mnu_i u_j$. By using parity arguments, we deduce that the pressure must be isotropic. Thus, we obtain

$$\begin{aligned}
P &= \frac{m}{3}\int \boldsymbol{v}^2 f_0^{eq} d\boldsymbol{v} - mn\boldsymbol{u}^2 \\
&= \frac{4\pi m}{3} a_0 \Bigg[\lim_{\beta\to\infty} \int_0^{+\infty} \frac{v^4}{1+\exp[\beta\left(\frac{m}{2}v^2+\lambda_0-|\boldsymbol{\lambda^S}|\right)]+\exp[-\beta\left(\frac{m}{2}v^2+\lambda_0-|\boldsymbol{\lambda^S}|\right)]} dv \\
&\quad +2\lim_{\beta\to\infty}\int_0^{+\infty} \frac{v^2}{1+\exp[2\beta\left(\frac{m}{2}v^2+\lambda_0\right)]+\exp[\beta\left(\frac{m}{2}v^2+\lambda_0+|\boldsymbol{\lambda^S}|\right)]} dv \Bigg] \\
&= \frac{4\pi m}{3}\frac{a_0}{5}\left(\left[\frac{2}{m}\left(|\boldsymbol{\lambda^S}|+|\lambda_0|\right)\right]^{5/2} + \left[\frac{2}{m}\left(|\lambda_0|-|\boldsymbol{\lambda^S}|\right)\right]^{5/2} \right) \\
&= \frac{\hbar^2}{5m}\frac{(3\pi^2)^{2/3}}{2}\left[\left(n-\frac{2}{\hbar}|\boldsymbol{S}|\right)^{5/3} + \left(n+\frac{2}{\hbar}|\boldsymbol{S}|\right)^{5/3}\right].
\end{aligned}$$

As to the spin current $J^S_{i\alpha} = \int v_i f_\alpha d\boldsymbol{v}$, we notice directly, again by parity arguments, that it factorizes as $J^S_{i\alpha} = u_i S_\alpha$.

B.2 Four-moments Maxwell-Boltzmann collinear closure

In this Appendix, we provide a proof of the relations (2.105)-(2.108) between the fluid moments and the Lagrange multipliers in the case of a Maxwell-Boltzmann distributions with four constraints of the moments, in the collinear approximation.

The equilibrium distribution function is given by Eqs. (2.86) and (2.101). We have

$$\mathcal{F}^{\mathrm{eq}} = \exp\left(-\beta\mathcal{H}'\right) = \exp\left(-\beta h'_0\right)\left[\cosh\left(-\beta h'_z\right)\sigma_0 + \sigma_z \sinh\left(-\beta h'_z\right)\right], \tag{B.1}$$

where h'_0 and h'_z are given by Eqs. (2.102)-(2.103). In order to simplify the notation, we introduce the following definitions: $\gamma_i = \lambda^J_{iz}$ and $J^S_{iz} = J^S_i$. We first compute the density

$$\begin{aligned}
n &= 2\int \exp\left(-\beta h'_0\right)\cosh\left(-\beta h'\right) d\boldsymbol{v} \\
&= e^{-\beta\left(\lambda_0+\lambda^S_z\right)}\int e^{-\frac{\beta m}{2}(\boldsymbol{v}-\boldsymbol{v_0})^2} e^{-\beta\boldsymbol{\gamma}\cdot\boldsymbol{v}} d\boldsymbol{v} + e^{-\beta\left(\lambda_0-\lambda^S_z\right)}\int e^{-\frac{\beta m}{2}(\boldsymbol{v}-\boldsymbol{v_0})^2} e^{\beta\boldsymbol{\gamma}\cdot\boldsymbol{v}} d\boldsymbol{v}.
\end{aligned}$$

Let us first define with I the following integral

$$I^0_{\pm}(v_{0_i},\gamma_i) = \int e^{-\frac{\beta m}{2}\left(v_i-v_{0_i}\right)^2} e^{\pm\beta\gamma_i v_i} dv_i = \Gamma^{1/3}(T) e^{\pm\beta\gamma_i v_{0_i}} e^{-\beta\gamma_i^2/2m}.$$

Therefore, we have

$$\begin{aligned} n &= e^{-\beta\left(\lambda_0+\lambda_z^S\right)} I_-^0(v_{0_x},\gamma_x) I_-^0(v_{0_y},\gamma_y) I_-^0(v_{0_z},\gamma_z) + e^{-\beta\left(\lambda_0-\lambda_z^S\right)} I_+^0(v_{0_x},\gamma_x) I_+^0(v_{0_y},\gamma_y) I_+^0(v_{0_z},\gamma_z) \\ &= 2\Gamma(T)\exp\left(-\beta\lambda_0\right)\exp\left(-\frac{\beta\boldsymbol{\gamma}^2}{2m}\right)\cosh\left[\beta\left(\lambda_z^S+\boldsymbol{\gamma}\cdot\boldsymbol{v_0}\right)\right]. \end{aligned} \tag{B.2}$$

The calculation for S_z is quite similar, and we obtain

$$S_z = \hbar\Gamma(T)\exp\left(-\beta\lambda_0\right)\exp\left(-\frac{\beta\boldsymbol{\gamma}^2}{2m}\right)\sinh\left[-\beta\left(\lambda_z^S+\boldsymbol{\gamma}\cdot\boldsymbol{v_0}\right)\right]. \tag{B.3}$$

The calculation of $\boldsymbol{u}$ is slightly different. Let us compute explicitly the component u_x (the generalization to the other components is then straightforward):

$$\begin{aligned} u_x &= \frac{2}{n}\int v_x e\left(-\beta h_0'\right)\cosh\left(-\beta|\boldsymbol{h'}|\right)d\mathbf{v} \\ &= \frac{1}{n}\left[e^{-\beta\left(\lambda_0+\lambda_z^S\right)}\int v_x e^{-\frac{\beta m}{2}(\boldsymbol{v}-\boldsymbol{v_0})^2} e^{-\beta\boldsymbol{\gamma}\cdot\boldsymbol{v}} d\boldsymbol{v} + e^{-\beta\left(\lambda_0-\lambda_z^S\right)}\int v_x e^{-\frac{\beta m}{2}(\boldsymbol{v}-\boldsymbol{v_0})^2} e^{+\beta\boldsymbol{\gamma}\cdot\boldsymbol{v}} d\boldsymbol{v}\right]. \end{aligned}$$

Defining the following integral

$$I_\pm^1(v_{0_i},\gamma_i) = \int v_i e^{-\frac{\beta m}{2}\left(v_i-v_{0_i}\right)^2} e^{\pm\beta\gamma_i v_i} dv_i = \Gamma^{1/3}(T) e^{\pm\beta\gamma_i v_{0_i}} e^{-\beta\gamma_i^2/2m}\left(v_{0_i}\pm\frac{\gamma_i}{m}\right),$$

we obtain

$$\begin{aligned} u_x &= \frac{e^{-\beta\left(\lambda_0+\lambda_z^S\right)}}{n}\left[I_-^1(v_{0_x},\gamma_x) I_-^0(v_{0_y},\gamma_y) I_-^0(v_{0_z},\gamma_z) + e^{2\beta\lambda_z^S} I_+^1(v_{0_x},\gamma_x) I_+^0(v_{0_y},\gamma_y) I_+^0(v_{0_z},\gamma_z)\right] \\ &= v_{0_x} - \frac{2S_z}{n\hbar m}\gamma_x. \end{aligned}$$

The generalisation to the other components gives

$$\boldsymbol{u} = \boldsymbol{v_0} + \frac{2S_z}{n\hbar m}\boldsymbol{\gamma}. \tag{B.4}$$

We finally compute the spin current, again starting from its x component:

$$\begin{aligned} J_x^S &= \hbar\int v_i\frac{h_\alpha'}{|\boldsymbol{h'}|}\exp\left(-\beta h_0'\right)\sinh\left(-\beta|\boldsymbol{h'}|\right)d\mathbf{v} \\ &= \frac{\hbar}{2}e^{-\beta\left(\lambda_0+\lambda_z^S\right)} I_-^1(v_{0_x},\lambda_{xz}^J) I_-^0(v_{0_y},\lambda_{yz}^J) I_-^0(v_{0_z},\lambda_{zz}^J) \\ &\quad -\frac{\hbar}{2}e^{-\beta\left(\lambda_0-\lambda_z^S\right)} I_+^1(v_{0_x},\lambda_{xz}^J) I_+^0(v_{0_y},\lambda_{yz}^J) I_+^0(v_{0_z},\lambda_{zz}^J) \\ &= v_{0_x} S_z - \frac{\hbar\gamma_x}{2m}n. \end{aligned}$$

The generalisation to the other components gives

$$J_i^S = v_{0_i} S_z - \frac{\hbar n}{2m} \gamma_i. \tag{B.5}$$

Inverting the relations (B.2)-(B.5), we obtain

$$\begin{cases} \gamma_i & = & \dfrac{2n\hbar m}{\hbar^2 n^2 + 4S_z^2} \left(S_z u_i - J_i^S \right), \\ v_{0_i} & = & \dfrac{1}{\hbar^2 n^2 + 4S_z^2} \left(\hbar^2 n^2 u_i + 4 S_z J_i^S \right), \\ e^{-\beta \lambda_0} & = & \dfrac{e^{\beta \gamma^2 / 2m}}{\Gamma(T)} \sqrt{\left(\dfrac{n}{2} \right)^2 - \left(\dfrac{S_z}{\hbar} \right)^2}, \\ \lambda_z^S & = & \dfrac{k_B T}{2} \ln \left(\dfrac{n - \frac{2|\boldsymbol{S}|}{\hbar}}{n + \frac{2|\boldsymbol{S}|}{\hbar}} \right) - \boldsymbol{\gamma} \cdot \boldsymbol{v_0}. \end{cases} \tag{B.6}$$

Appendix C

Details about the derivation of the variational approach applied to gold nano-particles

C.1 Derivation of the Lagrangian

The hydrodynamic equations

$$\frac{\partial n}{\partial t} + \nabla \cdot (n\mathbf{u}) = 0, \tag{C.1}$$

$$\frac{\partial \mathbf{u}}{\partial t} + \mathbf{u} \cdot \nabla \mathbf{u} = \nabla V_H - \nabla V_X - \frac{\nabla P}{n} + \frac{1}{2}\nabla\left(\frac{\nabla^2\sqrt{n}}{\sqrt{n}}\right), \tag{C.2}$$

can be derived from the following Lagrangian density

$$\begin{aligned}\mathcal{L} = n\left[\frac{\partial S}{\partial t} + \frac{(\nabla S)^2}{2}\right] + \frac{(\nabla n)^2}{8n} + \frac{3}{10}\left(3\pi^2\right)^{2/3} n^{5/3} \\ -\frac{3}{4\pi}\left(3\pi^2\right)^{1/3} n^{4/3} - \beta\frac{(\nabla n)^2}{n^{4/3}} - \frac{(\nabla V_H)^2}{8\pi} + (n_i - n)\, V_H.\end{aligned} \tag{C.3}$$

We assume that the electron density has the following form:

$$n(r,t) = \frac{A}{1 + \exp\left[\left(\frac{s}{\sigma(t)}\right)^3 - \left(\frac{R}{\sigma_0}\right)^3\right]}, \tag{C.4}$$

where $A = 3N/(4\pi\sigma^3)\left[\ln\left(1+\exp\left(R/\sigma_0\right)^3\right)\right]^{-1}$ is chosen to satisfy the normalization condition $\int n d\mathbf{r} = N$, and $s(t) = \sqrt{x^2 + y^2 + [z - d(t)]^2}$.

We first need to obtain an expression for the two other fields, S and V_H, as a function of the dynamical variables $d(t)$ and $\sigma(t)$. In order to determine $S(\mathbf{r}, t)$, or

equivalently the mean velocity $\mathbf{u}(\mathbf{r},t)$, we insert Eq. (C.4) into the continuity equation (C.1). This yields the exact solution

$$\mathbf{u} = \frac{\dot{\sigma}}{\sigma}\left(x\widehat{x} + y\widehat{y}\right) + \left[\frac{\dot{\sigma}}{\sigma}\left(z-d\right) + \dot{d}\right]\widehat{z}, \tag{C.5}$$

which gives

$$S = \frac{\dot{\sigma}}{2\sigma}\left[x^2 + y^2 + \left(z-d\right)^2\right] + \dot{d}\left(z-d\right), \tag{C.6}$$

where the dot stands for differentiation with respect to time.

In order to obtain the Hartree potential, we rewrite the last two terms in Eq. (C.3) as

$$-\frac{\left(\nabla V_H\right)^2}{8\pi} + \left(n_i - n\right)V_H = \frac{\left(\nabla V_H\right)^2}{8\pi} - \frac{\nabla\cdot\left(V_H\nabla V_H\right)}{4\pi}. \tag{C.7}$$

The last (divergence) term disappears upon integration over space for reasonable boundary conditions, so that only the gradient of V_H is required. We decompose the Hartree potential as $V_H = V_i + V_e$, where $V_{i,e}$ are the contributions due to the ions and the electrons respectively, which satisfy the equations: $\nabla^2 V_i = -4\pi n_i$ and $\nabla^2 V_e = 4\pi n$. Assuming spherical symmetry and integrating once in the radial coordinate, we find

$$\frac{\partial V_i(r)}{\partial r} = \begin{cases} -\dfrac{N}{R^3}r\,, & r \le R \\ \\ -\dfrac{N}{r^2}\,, & r > R \end{cases} \tag{C.8}$$

and

$$\begin{aligned} s^2\frac{\partial V_e(s,t)}{\partial s} \;=\; & \frac{N}{\ln(1+1/a)}\left\{\frac{s^3}{\sigma^3} - \ln\left[1 + a\exp(s^3/\sigma^3)\right]\right. \\ & \left. + \ln(1+a)\right\}, \end{aligned} \tag{C.9}$$

where we introduced the small parameter $a = \exp\left(-R^3/\sigma_0^3\right)$. Note that Eq. (C.9) is well-behaved both for $s \to 0$ and $s \to \infty$.

Having obtained the expressions for the fields n, S, and ∇V_H – given by Eqs. (C.4), (C.6), (C.8) and (C.9) – we may proceed to integrate the Lagrangian density (C.3) with respect to the radial variable in order to obtain the Lagrangian function

$L(d, \sigma, \dot{d}, \dot{\sigma})$:

$$\begin{aligned} L &= \frac{-1}{N}\int \mathcal{L} d\mathbf{r}, \\ &= -\underbrace{\frac{1}{N}\left[\int n\frac{\partial S}{\partial t}d\mathbf{r}\right]}_{A} + \underbrace{\frac{1}{2}\int n\left(\nabla S\right)^2 d\mathbf{r}}_{B} + \underbrace{\frac{1}{8}\int \frac{\left(\nabla n\right)^2}{n}d\mathbf{r}}_{C} \\ &\quad + \underbrace{\frac{3}{10}\left(3\pi^2\right)^{2/3}\int n^{5/3}d\mathbf{r}}_{D} - \underbrace{\frac{3}{4\pi}\left(3\pi^2\right)^{1/3}\int n^{4/3}d\mathbf{r}}_{E} \\ &\quad - \underbrace{\beta\int \frac{\left(\nabla n\right)^2}{n^{4/3}}d\mathbf{r}}_{F} + \underbrace{\frac{1}{8\pi}\int (\nabla V_H)^2 d\mathbf{r}}_{G} \\ &\quad - \underbrace{\frac{1}{4\pi}\int \nabla\cdot(V_H\nabla V_H)d\mathbf{r}}_{H}\Bigg]. \end{aligned} \tag{C.10}$$

The last integral (term H) is a surface term which is equal to zero if the Hartree electric field vanishes at infinity.

The first step is to express the quantities $\partial S/\partial t$, $(\nabla S)^2$ and $(\nabla n)^2$ as functions of the dynamical variables $d(t)$, $\sigma(t)$ and of the shifted radial coordinate s. The fields n and S are defined respectively by Eqs. (C.4) and (C.6). We obtain

$$\begin{aligned} \frac{\partial S}{\partial t} &= \frac{\ddot{\sigma}\sigma - \dot{\sigma}^2}{2\sigma^2}s^2 - \frac{\dot{\sigma}}{\sigma}\dot{d}\left(z-d\right) + \ddot{d}\left(z-d\right) - \dot{d}^2, \\ \left(\nabla S\right)^2 &= \left[\frac{\dot{\sigma}}{\sigma}\right]^2 s^2 + 2\frac{\dot{\sigma}}{\sigma}\left(z-d\right)\dot{d} + \dot{d}^2, \\ \left(\nabla n\right)^2 &= \frac{9a^2s^4}{A^2\sigma^6}\exp\left[\frac{2s^3}{\sigma^3}\right]n^4. \end{aligned}$$

Now, we are in a position to compute the integrals in the Lagrangian (C.10). We evaluate each term separately:

- Term A:

$$\begin{aligned} \int n\frac{\partial S}{\partial t}d\mathbf{r} &= \left[\frac{\ddot{\sigma}}{2\sigma} - \frac{\dot{\sigma}^2}{2\sigma^2}\right]\int ns^2 d\mathbf{r} + \left[\ddot{d} - \frac{\dot{\sigma}}{\sigma}\dot{d}\right] \\ &\quad \times \int n\left(z-d\right)d\mathbf{r} - \dot{d}^2\int n d\mathbf{r}, \\ &= \left[\frac{\ddot{\sigma}}{2\sigma} - \frac{\dot{\sigma}^2}{2\sigma^2}\right]\int ns^2 d\mathbf{r} - N\dot{d}^2. \end{aligned} \tag{C.11}$$

We used the symmetry properties of the electron density to obtain the above expression. We further compute

$$\begin{aligned}\int ns^2 d\mathbf{r} &= A\int \frac{s^2}{1+a\exp\left(s^3/\sigma^3\right)}d\mathbf{r},\\ &= 4\pi A\int_0^\infty \frac{X^4}{1+a\exp\left(X^3/\sigma^3\right)}dX,\\ &= N\sigma^2 M(a),\end{aligned} \tag{C.12}$$

where $M(a)$ is definesd as

$$M(a) = -\frac{\Gamma(5/3)\mathrm{Li}_{5/3}(-1/\mathrm{a})}{\ln(1+1/a)}.$$

Li is a polylogarithm function defined by

$$\mathrm{Li}_p(-1/a) = -\frac{1}{\Gamma(p)}\int_0^\infty \frac{X^{p-1}}{1+a\exp\left(X\right)}dX,$$

where $\mathrm{Re}(p) > 0$, $\mathrm{Im}(a) = 0$, and $1/a > -1$

Now we can inject Eq. (C.12) into Eq. (C.11) to obtain

$$\begin{aligned}\int n\frac{\partial S}{\partial t}d\mathbf{r} &= \frac{N}{2}M(a)\left(\ddot{\sigma}\sigma - \dot{\sigma}^2\right) - N\dot{d}^2,\\ &= \frac{N}{2}M(a)\left[\frac{d}{dt}\left(\sigma\dot{\sigma}\right) - 2\dot{\sigma}^2\right] - N\dot{d}^2,\\ &= -NM(a)\dot{\sigma}^2 - N\dot{d}^2,\end{aligned} \tag{C.13}$$

where we suppressed the total time derivative as it does not modify the equations of motion.

- Term B:

$$\begin{aligned}\frac{1}{2}\int n\left(\nabla S\right)^2 d\mathbf{r} &= \frac{1}{2}\left[\frac{\dot{\sigma}}{\sigma}\right]^2\int ns^2 d\mathbf{r} + \frac{\dot{\sigma}}{\sigma}\dot{d}\\ &\quad\times\int\left(z-d\right)nd\mathbf{r} + \frac{\dot{d}^2}{2}\int nd\mathbf{r},\\ &= \frac{N}{2}M(a)\dot{\sigma}^2 + \frac{N}{2}\dot{d}^2.\end{aligned} \tag{C.14}$$

- Term C:

$$\begin{aligned}\frac{1}{8}\int\frac{\left(\nabla n\right)^2}{n}d\mathbf{r} &= \frac{9\pi a^2 A}{2\sigma^6}\int_0^\infty \frac{X^6\exp\left(2X^3/\sigma^3\right)}{\left[1+a\exp\left(X^3/\sigma^3\right)\right]^3}dX,\\ &= \frac{Nf_B(a)}{\sigma^2},\end{aligned} \tag{C.15}$$

where f_B is defined as

$$f_B(a) = \frac{27a^2}{8\ln(1+1/a)} \int_0^\infty \frac{X^6 \exp(2X^3)}{[1+a\exp(X^3)]^3} dX. \tag{C.16}$$

- Term D:

$$\begin{aligned} \frac{3(3\pi^2)^{2/3}}{10} \int n^{5/3} d\mathbf{r} &= \frac{6\pi(3\pi^2)^{2/3}}{5} A^{5/3} \\ &\times \int_0^\infty \frac{X^2}{[1+a\exp(X^3/\sigma^3)]^{5/3}} dX, \\ &= \frac{N^{5/3} f_F(a)}{\sigma^2}, \end{aligned} \tag{C.17}$$

where f_F is defined as

$$\begin{aligned} f_F(a) &= \frac{6}{5}(3\pi)^{2/3} \left[\frac{3}{4\ln(1+1/a)}\right]^{5/3} \\ &\times \int_0^\infty \frac{X^2}{[1+a\exp(X^3)]^{5/3}} dX. \end{aligned} \tag{C.18}$$

- Term E:

$$\begin{aligned} \frac{3(3\pi^2)^{1/3}}{4\pi} \int n^{4/3} d\mathbf{r} &= \left(81\pi^2\right)^{1/3} A^{4/3} \\ &\times \int_0^\infty \frac{X^2}{[1+a\exp(X^3/\sigma^3)]^{4/3}} dX, \\ &= \frac{N^{4/3} f_X(a)}{\sigma}, \end{aligned} \tag{C.19}$$

where f_X is defined as

$$\begin{aligned} f_X(a) &= \left[\frac{9}{4\sqrt{\pi}\ln(1+1/a)}\right]^{4/3} \\ &\times \int_0^\infty \frac{X^2}{[1+a\exp(X^3)]^{4/3}} dX. \end{aligned} \tag{C.20}$$

- Term F:

$$\begin{aligned} \beta \int \frac{(\nabla n)^2}{n^{4/3}} d\mathbf{r} &= \frac{36\pi a^2 A^{2/3} \beta}{\sigma^6} \\ &\times \int_0^\infty \frac{X^6 \exp(2X^3/\sigma^3)}{[1+a\exp(X^3/\sigma^3)]^{8/3}} dX, \\ &= \frac{\beta N^{2/3}}{\sigma} f_{X'}(a), \end{aligned} \tag{C.21}$$

where $f_{X'}(a)$ is defined as

$$f_{X'}(a) = \left(\frac{4\pi}{3}\right)^{1/3} \frac{27a^2}{[\ln(1+1/a)]^{2/3}} \times \int_0^\infty \frac{X^6 \exp(2X^3)}{[1+a\exp(X^3)]^{8/3}} dX. \tag{C.22}$$

- Term G:

$$\frac{1}{8\pi}\int (\nabla V_H)^2 d\mathbf{r} = \frac{1}{8\pi}\left[\int (\nabla V_i)^2 d\mathbf{r} + \int (\nabla V_e)^2 d\mathbf{r} + 2\int \nabla V_i \cdot \nabla V_e d\mathbf{r}\right]. \tag{C.23}$$

The first integral in Eq. (C.23) does not contribute to the equations of motion because it does not depend on the dynamical variables d or σ. Let us evaluate the other two integrals separately:

$$\int (\nabla V_e)^2 d\mathbf{r} = \int \left[\frac{\partial V_e}{\partial s}\right]^2 d\mathbf{r} = \frac{8\pi N}{\sigma} f_{ee}(a), \tag{C.24}$$

where $f_{ee}(a)$ is defined as

$$f_{ee}(a) = \frac{1}{2\left[\ln(1+1/a)\right]^2}\int \frac{dX}{X^2}\left\{X^3 + \ln(1+a) - \ln\left[1+a\exp(X^3)\right]\right\}. \tag{C.25}$$

Let us call $I(d)$ the third integral in Eq. (C.23):

$$\begin{aligned} I(d) &\equiv \int \nabla V_e \cdot \nabla V_i \qquad (C.26)\\ &= \int \frac{\partial V_i}{\partial r}\frac{\partial V_e}{\partial s}\frac{1}{sr}(r^2 - zd) d\mathbf{r} \\ &= \frac{2\pi N}{\ln(1+1/a)}\int \frac{\partial V_i}{\partial r}\frac{r^2\sin\theta}{s^3}(r - d\cos\theta) \\ &\times \left\{\frac{s^3}{\sigma^3} - \ln\left[1+a\exp(s^3/\sigma^3)\right] + \ln(1+a)\right\} dr d\theta, \end{aligned}$$

where we used the expressions (C.8) and (C.9), and the angle θ is defined so that $z = r\cos\theta$. We cannot simplify the integral I because it does not possess spherical symmetry. The only way to proceed is to develop the variable $s = \sqrt{x^2+y^2+(z-d)^2}$ as a power series of d:

$$s = r - d\cos\theta + \frac{d^2\sin^2\theta}{2r} + O(d^3).$$

We find that I can be written in terms of a power series of d

$$I = \frac{4\pi N^2 f_{ei}(\sigma)}{R} - 2\pi N \Omega_d^2(\sigma) d^2 + 4\pi N K(\sigma) d^4 + \cdots , \tag{C.27}$$

where $f_{ei}(\sigma)$, $\Omega_d^2(\sigma)$ and $K(\sigma)$ are given by

$$\begin{aligned} f_{ei}(\sigma) &= \frac{1}{\ln(1+1/a)} \Bigg\{ \frac{\sigma^2}{R^2} \int_0^{R/\sigma} X \Big[X^3 + \ln(1+a) \\ &\quad - \ln\left(1 + a\exp\left(X^3\right)\right) \Big] dX + \frac{R}{\sigma} \int_{R/\sigma}^{\infty} \frac{dX}{X^2} \Big[X^3 \\ &\quad + \ln(1+a) - \ln\left(1 + a\exp\left(X^3\right)\right) \Big] \Bigg\}, \end{aligned} \tag{C.28}$$

$$\begin{aligned} \Omega_d^2(\sigma) &= \frac{N}{R^3 \ln(1+1/a)} \Bigg\{ \frac{R^3}{\sigma^3} + \ln(1+1/a) \\ &\quad - \ln\left[1 + a\exp(R^3/\sigma^3)\right] \Bigg\}, \end{aligned} \tag{C.29}$$

$$K(\sigma) = \frac{9NRa}{40\ln(1+1/a)\sigma^6} \frac{\exp(R^3/\sigma^3)}{\left[1 + a\exp(R^3/\sigma^3)\right]^2}. \tag{C.30}$$

The odd powers of d disappears, as expected, because the problem is symmetric with respect to the (x, y) plane, so that the equations should be unchanged if we change d with $-d$.

Injecting the results for the terms A–G into Eq. (C.10), we obtain the Lagrangian of the system up to fifth order in d:

$$L = \frac{-1}{N} \int \mathcal{L} d\mathbf{r} = \frac{M(a)\dot{\sigma}^2}{2} - U(\sigma) + \frac{\dot{d}^2}{2} - \frac{\Omega_d^2(\sigma) d^2}{2} + K(\sigma) d^4, \tag{C.31}$$

where the multiplicative factor $-(1/N)$ is introduced for convenience of notation and the pseudo-potential $U(\sigma)$ is defined as

$$\begin{aligned} U(\sigma) = \frac{f_B(a)}{\sigma^2} + \frac{N^{2/3} f_F(a)}{\sigma^2} - \frac{N^{1/3} f_X(a)}{\sigma} - \frac{\beta f_{X'}(a)}{N^{1/3}\sigma} \\ + \frac{N f_{ee}(a)}{\sigma} - \frac{N f_{ei}(\sigma)}{R}. \end{aligned} \tag{C.32}$$

The pseudo-potential $U(\sigma)$ is represented in Fig. 5.2.

The quantities f_B, f_F, f_X, $f_{X'}$, f_{ee} and f_{ei}, which appear in the pseudo-potential (C.32), are related respectively to the Bohm potential, Fermi pressure, exchange energy (LDA), gradient correction to the exchange energy, electron-electron and electron-ion Hartree interaction terms. All these functions are positive, in accordance with the role played by the Bohm, Fermi and electron-electron terms, which are repulsive, and by the exchange and the electron-ion terms, which are attractive.

The quantity $\Omega_d^2(\sigma)$ corresponds to the second order term in the development of the electron-ion interacting energy, whereas $K(\sigma)$ corresponds to the fourth order.

C.2 Correlation effects

So far, our model included exchange effects but no other type of correlations. In the framework of DFT, correlations can be introduced through an appropriate functional of the electron density. Here, we use the functional proposed by Brey et al. [185], which yields the following correlation potential

$$V_C = -\gamma \ln\left[1 + \alpha n^{1/3}\right], \tag{C.33}$$

with $\gamma = 0.03349$ and $\alpha = 18.376$. With this potential, the Euler equation becomes

$$\begin{aligned} \frac{\partial \mathbf{u}}{\partial t} + \mathbf{u}\cdot\nabla\mathbf{u} &= \nabla V_H - \nabla V_X - \nabla V_C - \frac{1}{mn}\nabla P \\ &\quad + \frac{\hbar^2}{2m^2}\nabla\left[\frac{\nabla^2\sqrt{n}}{\sqrt{n}}\right]. \end{aligned} \tag{C.34}$$

In order to include this correlation potential, the following term needs to be added to the Lagrangian density

$$\begin{aligned} \mathcal{L}_C &= -\frac{\gamma}{6\alpha^3}\left[-6\alpha n^{1/3} + 3\alpha^2 n^{2/3} - 2\alpha^3 n\right. \\ &\quad \left. +6\left(1+\alpha^3 n\right)\ln\left(1+\alpha n^{1/3}\right)\right]. \end{aligned} \tag{C.35}$$

This yields a new term in the integrated Lagrangian of the system:

$$\begin{aligned} L_C &= -\frac{1}{N}\int \mathcal{L}_C\, d\mathbf{r} \\ &= \frac{2\pi\gamma}{3\alpha^3 N}\Big[-6\alpha\bar{A}^{1/3}I_1\sigma^2 + 3\alpha^2\bar{A}^{2/3}I_2\sigma \\ &\quad -2\alpha^3 N + 6I_3(\sigma)\sigma^3\Big], \end{aligned} \tag{C.36}$$

where

$$\begin{aligned} \bar{A} &= A\sigma^3 = \frac{3N}{4\pi}\left[\ln\left(1+\exp\left(\frac{R}{\sigma_0}\right)^3\right)\right]^{-1}, \\ I_1 &= \int_0^\infty \frac{X^2}{\left[1+a\exp(X^3)\right]^{1/3}}dX, \\ I_2 &= \int_0^\infty \frac{X^2}{\left[1+a\exp(X^3)\right]^{2/3}}dX, \\ I_3(\sigma) &= \int_0^\infty X^2\left[1+\frac{B(X)^3}{\sigma^3}\right]\ln\left[1+\frac{B(X)}{\sigma}\right]dX, \end{aligned}$$

and

$$B(X) = \frac{\alpha \bar{A}^{1/3}}{\left[1 + a \exp\left(X^3\right)\right]^{1/3}}.$$

The resulting corrections can be incorporated in the pseudo-potential function $U(\sigma)$. The new terms are as follows

$$U_C(\sigma) = f_c \sigma^2 - f_{c'} \sigma - f_{c''} I_3(\sigma) \sigma^3, \tag{C.37}$$

where

$$\begin{aligned} f_c &= \frac{4\pi\gamma}{\alpha^2 N} \bar{A}^{1/3} I_1, \\ f_{c'} &= \frac{2\pi\gamma}{\alpha N} \bar{A}^{2/3} I_2, \\ f_{c''} &= \frac{4\pi\gamma}{\alpha^3 N}. \end{aligned}$$

Notice that the correlation effects only affect the equation for σ, but not the dipole. The properties of the ground state will also be modified, in particular the equilibrium value of the spill-out thickness σ_0.

C.3 Additional results

The following tables summarize the ground-state and linear-response results for gold nano-particles without correlations (Table C.1) and with correlations (Table C.2). Fig. 5.3 in the main text uses the data from these tables.

N	R	σ_0	Ω_d	Ω_b
50	11.09	6.24	0.1793	0.2988
100	13.97	7.21	0.1821	0.3059
150	15.99	7.86	0.1835	0.3093
200	17.60	8.36	0.1843	0.3114
250	18.96	8.77	0.1848	0.3129
300	20.15	9.12	0.1852	0.3141
350	21.21	9.43	0.1856	0.3150
400	22.18	9.70	0.1859	0.3158
450	23.07	9.95	0.1861	0.3164

TABLE C.1: Ground-state and linear-response parameters for gold nanoparticles of different sizes. All quantities are expressed in atomic units.

N	R	σ_0	Ω_d	Ω_b
50	11.09	6.07	0.1803	0.3026
100	13.97	7.0	0.1830	0.3089
150	15.99	7.61	0.1843	0.3118
200	17.60	8.09	0.1850	0.3138
250	18.96	8.48	0.1855	0.3154
300	20.15	8.81	0.1859	0.3162
350	21.21	9.1	0.1862	0.3170
400	22.18	9.37	0.1864	0.3175
450	23.07	9.6	0.1866	0.3182

TABLE C.2: Ground-state and linear-response parameters for gold nanoparticles of different sizes, including correlations. All quantities are expressed in atomic units.

Bibliography

[1] Mark I. Stockman. Nanoplasmonics: The physics behind the applications. *Physics Today*, 64(2):39–44, feb 2011.

[2] Antoine Moreau, Cristian Ciracì, Jack J. Mock, Ryan T. Hill, Qiang Wang, Benjamin J. Wiley, Ashutosh Chilkoti, and David R. Smith. Controlled-reflectance surfaces with film-coupled colloidal nanoantennas. *Nature*, 492(7427):86–89, dec 2012.

[3] Marie-Christine Daniel and Didier Astruc. Gold Nanoparticles: Assembly, Supramolecular Chemistry, Quantum-Size-Related Properties, and Applications toward Biology, Catalysis, and Nanotechnology. *Chem. Rev.*, 104:239–346, 2004.

[4] James F Hainfeld, Daniel N Slatkin, and Henry M Smilowitz. The use of gold nanoparticles to enhance radiotherapy in mice. *Phys. Med. Biol. Phys. Med. Biol*, 49(4904):309–315, 2004.

[5] Endo Tatsuro, Kerman Kagan, Nagatani Naoki, Hiepa Ha Minh, Kim Do-Kyun, Yonezawa Yuji, Nakano Koichi, and Tamiya Eiichi. Multiple Label-Free Detection of Antigen Antibody Reaction Using Localized Surface Plasmon Resonance Based Core Shell Structured Nanoparticle Layer Nanochip. 2006.

[6] Jonathan A. Scholl, Ai Leen Koh, and Jennifer A. Dionne. Quantum plasmon resonances of individual metallic nanoparticles. *Nature*, 483(7390):421–427, mar 2012.

[7] Yu Luo, A. I. Fernandez-Dominguez, Aeneas Wiener, Stefan A. Maier, and J. B. Pendry. Surface Plasmons and Nonlocality: A Simple Model. *Physical Review Letters*, 111(9):093901, aug 2013.

[8] M. S. Tame, K. R. McEnery, K. Özdemir, J. Lee, S. A. Maier, and M. S. Kim. Quantum plasmonics. *Nature Physics*, 9(6):329–340, jun 2013.

[9] Søren Raza, Nicolas Stenger, Shima Kadkhodazadeh, Søren V. Fischer, Natalie Kostesha, Antti-Pekka Jauho, Andrew Burrows, Martijn Wubs, and N. Asger Mortensen. Blueshift of the surface plasmon resonance in silver nanoparticles studied with EELS. *Nanophotonics*, 2(2):131–138, jan 2013.

[10] Metallic nanoparticles — Ninithi.com.

[11] C. Suárez, W. E. Bron, and T. Juhasz. Dynamics and Transport of Electronic Carriers in Thin Gold Films. *Physical Review Letters*, 75(24):4536–4539, dec 1995.

[12] J.-Y. Bigot, V. Halté, J.-C. Merle, and A. Daunois. Electron dynamics in metallic nanoparticles. *Chemical Physics*, 251(1):181–203, 2000.

[13] J-S. Lauret, C. Voisin, G. Cassabois, C. Delalande, Ph. Roussignol, O. Jost, and L. Capes. Ultrafast Carrier Dynamics in Single-Wall Carbon Nanotubes. *Physical Review Letters*, 90(5):057404, feb 2003.

[14] E. E. B. Campbell, K. Hansen, K. Hoffmann, G. Korn, M. Tchaplyguine, M. Wittmann, and I. V. Hertel. From Above Threshold Ionization to Statistical Electron Emission: The Laser Pulse-Duration Dependence of C 60 Photoelectron Spectra. *Physical Review Letters*, 84(10):2128–2131, mar 2000.

[15] R. Schlipper, R. Kusche, B. v. Issendorff, and H. Haberland. Thermal emission of electrons from highly excited sodium clusters. *Applied Physics A Materials Science & Processing*, 72(3):255–259, mar 2001.

[16] C. Voisin, D. Christofilos, N. Del Fatti, F. Vallée, B. Prével, E. Cottancin, J. Lermé, M. Pellarin, and M. Broyer. Size-Dependent Electron-Electron Interactions in Metal Nanoparticles. *Physical Review Letters*, 85(10):2200–2203, sep 2000.

[17] OV Salata. Applications of nanoparticles in biology and medicine. *Journal of nanobiotechnology*, 2(1):3, apr 2004.

[18] Leena Loomba and Tiziano Scarabelli. Metallic nanoparticles and their medicinal potential. Part II: aluminosilicates, nanobiomagnets, quantum dots and cochleates. *Therapeutic Delivery*, 4(9):1179–1196, sep 2013.

[19] Jérémy Butet, Julien Duboisset, Guillaume Bachelier, Isabelle Russier-Antoine, Emmanuel Benichou, Christian Jonin, and Pierre-Francois Brevet. Optical Second Harmonic Generation of Single Metallic Nanoparticles Embedded in a Homogeneous Medium. *Nano Letters*, 10(5):1717–1721, may 2010.

[20] H Singhal, R A Ganeev, P A Naik, A K Srivastava, A Singh, R Chari, R A Khan, J A Chakera, and P D Gupta. Study of high-order harmonic generation from nanoparticles. *Journal of Physics B: Atomic, Molecular and Optical Physics*, 43(2):025603, jan 2010.

[21] Jean-Yves Bigot, Mircea Vomir, and Eric Beaurepaire. Coherent ultrafast magnetism induced by femtosecond laser pulses. *Nature Physics*, 5(7):515–520, jul 2009.

[22] E. Beaurepaire, J.-C. Merle, A. Daunois, and J.-Y. Bigot. Ultrafast Spin Dynamics in Ferromagnetic Nickel. *Physical Review Letters*, 76(22):4250–4253, may 1996.

[23] K. Krieger, J. K. Dewhurst, P. Elliott, S. Sharma, and E. K. U. Gross. Laser-Induced Demagnetization at Ultrashort Time Scales: Predictions of TDDFT. *Journal of Chemical Theory and Computation*, 11(10):4870–4874, oct 2015.

[24] Maria Stamenova, Jacopo Simoni, and Stefano Sanvito. Role of spin-orbit interaction in the ultrafast demagnetization of small iron clusters. *Physical Review B*, 94(1):014423, jul 2016.

[25] M. Battiato, K. Carva, and P. M. Oppeneer. Superdiffusive Spin Transport as a Mechanism of Ultrafast Demagnetization. *Physical Review Letters*, 105(2):027203, jul 2010.

[26] M. Pereira and H. Wenzel. Interplay of Coulomb and nonparabolicity effects in the intersubband absorption of electrons and holes in quantum wells. *Physical Review B*, 70(20):205331, nov 2004.

[27] T. Müller, W. Parz, G. Strasser, and K. Unterrainer. Influence of carrier-carrier interaction on time-dependent intersubband absorption in a semiconductor quantum well. *Physical Review B*, 70(15):155324, oct 2004.

[28] C Guillon, P Langot, N Del Fatti, and F Vallée. Nonequilibrium electron energy-loss kinetics in metal clusters. *New Journal of Physics*, 5(1):13–13, feb 2003.

[29] M. Aeschlimann, M. Bauer, S. Pawlik, R. Knorren, G. Bouzerar, and K.H. Bennemann. Transport and dynamics of optically excited electrons in metals. *Applied Physics A: Materials Science & Processing*, 71(5):485–491, nov 2000.

[30] B. Rethfeld, A. Kaiser, M. Vicanek, and G. Simon. Ultrafast dynamics of nonequilibrium electrons in metals under femtosecond laser irradiation. *Physical Review B*, 65(21):214303, may 2002.

[31] David Pines and P. (Philippe) Nozières. *Theory of quantum liquids*. Addison-Wesley Pub. Co., Advanced Book Program, 1995.

[32] F. Calvayrac, P.-G. Reinhard, E. Suraud, and C.A. Ullrich. Nonlinear electron dynamics in metal clusters. *Physics Reports*, 337(6):493–578, 2000.

[33] T. V. Teperik, P. Nordlander, J. Aizpurua, and A. G. Borisov. Robust Subnanometric Plasmon Ruler by Rescaling of the Nonlocal Optical Response. *Physical Review Letters*, 110(26):263901, jun 2013.

[34] Uwe Schwengelbeck, Luis Plaja, Luis Roso, and Enrique Conejero Jarque. Plasmon-induced photon emission from thin metal films. *Journal of Physics B: Atomic, Molecular and Optical Physics*, 33(8):1653–1661, apr 2000.

[35] J Daligault and C Guet. Large amplitude femtosecond electron dynamics in metal clusters. *Journal of Physics A: Mathematical and General*, 36(22):5847–5855, jun 2003.

[36] S V Fomichev and D F Zaretsky. Vlasov theory of Mie resonance broadening in metal clusters. *Journal of Physics B: Atomic, Molecular and Optical Physics*, 32(21):5083–5102, nov 1999.

[37] D F Zaretsky, Ph A Korneev, S V Popruzhenko, and W Becker. Landau damping in thin films irradiated by a strong laser field. *Journal of Physics B: Atomic, Molecular and Optical Physics*, 37(24):4817–4830, dec 2004.

[38] G. Manfredi and P.-A. Hervieux. Finite-size and nonlinear effects on the ultrafast electron transport in thin metal films. *Physical Review B*, 72(15):155421, oct 2005.

[39] R Jasiak, G Manfredi, and P-A Hervieux. Quantum–classical transition in the electron dynamics of thin metal films. *New Journal of Physics*, 11(6):063042, jun 2009.

[40] D. T. Smithey, M. Beck, M. G. Raymer, and A. Faridani. Measurement of the Wigner distribution and the density matrix of a light mode using optical homodyne tomography: Application to squeezed states and the vacuum. *Physical Review Letters*, 70(9):1244–1247, mar 1993.

[41] Eric J. Heller. Wigner phase space method: Analysis for semiclassical applications. *The Journal of Chemical Physics*, 65(4):1289–1298, aug 1976.

[42] T. Dittrich, E. A. Gómez, and L. A. Pachón. Semiclassical propagation of Wigner functions. *The Journal of Chemical Physics*, 132(21):214102, jun 2010.

[43] Andrea Bertoni, Paolo Bordone, Rossella Brunetti, and Carlo Jacoboni. The Wigner function for electron transport in mesoscopic systems. *Journal of Physics: Condensed Matter*, 11(31):5999–6012, aug 1999.

[44] Fernando. Haas. *Quantum plasmas : an hydrodynamic approach*. Springer, 2011.

[45] Miroslaw Brewczyk, Kazimierz Rzazewski, and Charles W. Clark. Multielectron Dissociative Ionization of Molecules by Intense Laser Radiation. *Physical Review Letters*, 78(2):191–194, jan 1997.

[46] A. Domps, P.-G. Reinhard, and E. Suraud. Theoretical Estimation of the Importance of Two-Electron Collisions for Relaxation in Metal Clusters. *Physical Review Letters*, 81(25):5524–5527, dec 1998.

[47] Arup Banerjee and Manoj K. Harbola. Hydrodynamic approach to time-dependent density functional theory; Response properties of metal clusters. *http://dx.doi.org/10.1063/1.1290610*, 2000.

[48] Giovanni Manfredi, Paul-Antoine Hervieux, and Fernando Haas. Nonlinear dynamics of electron–positron clusters. *New Journal of Physics*, 14(7):075012, jul 2012.

[49] N. Crouseilles, P.-A. Hervieux, and G. Manfredi. Quantum hydrodynamic model for the nonlinear electron dynamics in thin metal films. *Physical Review B*, 78(15):155412, oct 2008.

[50] P. K. Shukla and B. Eliasson. Formation and Dynamics of Dark Solitons and Vortices in Quantum Electron Plasmas. *Physical Review Letters*, 96(24):245001, jun 2006.

[51] Padma K Shukla and B Eliasson. Nonlinear aspects of quantum plasma physics. *Physics-Uspekhi*, 53(1):51–76, jan 2010.

[52] F. Haas, G. Manfredi, P. K. Shukla, and P.-A. Hervieux. Breather mode in the many-electron dynamics of semiconductor quantum wells. *Physical Review B*, 80(7):073301, aug 2009.

[53] A. Puente, M. Casas, and Ll. Serra. A semiclassical approach to the ground state and density oscillations of quantum dots. *Physica E: Low-dimensional Systems and Nanostructures*, 8(4):387–397, 2000.

[54] Ll. Serra and A. Puente. Magnetic Thomas-Fermi-Weizsäcker model for quantum dots: A comparison with Kohn-Sham ground states. *The European Physical Journal D*, 14(1):77–81, apr 2001.

[55] O Morandi, P-A Hervieux, and G Manfredi. Ultrafast magnetization dynamics in diluted magnetic semiconductors. *New Journal of Physics*, 11(7):073010, jul 2009.

[56] O Morandi. Effective classical Liouville-like evolution equation for the quantum phase-space dynamics. *Journal of Physics A: Mathematical and Theoretical*, 43(36):365302, sep 2010.

[57] M. W. Thomas and R. F. Snider. Boltzmann equation and angular momentum conservation. *Journal of Statistical Physics*, 2(1):61–81, 1970.

[58] R. F. Snider and K. S. Lewchuk. Irreversible Thermodynamics of a Fluid System with Spin. *The Journal of Chemical Physics*, 46(8):3163–3172, apr 1967.

[59] J Zamanian, M Marklund, and G Brodin. Scalar quantum kinetic theory for spin-1/2 particles: mean field theory. *New Journal of Physics*, 12(4):043019, apr 2010.

[60] Jens Zamanian, Martin Stefan, Mattias Marklund, and Gert Brodin. From extended phase space dynamics to fluid theory. *Physics of Plasmas*, 17(10):102109, 2010.

[61] Felipe A Asenjo, Jens Zamanian, Mattias Marklund, Gert Brodin, and Petter Johansson. Semi-relativistic effects in spin-1/2 quantum plasmas. *New Journal of Physics*, 14(7):073042, jul 2012.

[62] Anton Arnold and Herbert Steinrück. The 'electromagnetic' Wigner equation for an electron with spin. *ZAMP Zeitschrift für angewandte Mathematik und Physik*, 40(6):793–815, nov 1989.

[63] Iwo Bialynicki-Birula. Relativistic Wigner functions. *EPJ Web of Conferences*, 78:01001, sep 2014.

[64] Anant Dixit, Yannick Hinschberger, Jens Zamanian, Giovanni Manfredi, and Paul-Antoine Hervieux. Lagrangian approach to the semirelativistic electron dynamics in the mean-field approximation. *Physical Review A*, 88(3):032117, sep 2013.

[65] A. M. Anile and O. Muscato. Improved hydrodynamical model for carrier transport in semiconductors. *Physical Review B*, 51(23):16728–16740, jun 1995.

[66] J. Fajans and L. Frièdland. Autoresonant (nonstationary) excitation of pendulums, Plutinos, plasmas, and other nonlinear oscillators. *American Journal of Physics*, 69(10):1096–1102, oct 2001.

[67] P. Drude. Zur Elektronentheorie der Metalle. *Annalen der Physik*, 306(3):566–613, 1900.

[68] G. Manfredi. How to model quantum plasmas. *Fields Institute Communications , (2005).*, Series 46:263–287, may 2005.

[69] Giovanni Manfredi and Jérôme Hurst. Solid state plasmas. *Plasma Physics and Controlled Fusion*, 57(5):054004, may 2015.

[70] Sergei V Vladimirov and Yu O Tyshetskiy. On description of a collisionless quantum plasma. *Physics-Uspekhi*, 54(12):1243–1256, dec 2011.

[71] Neil W. Ashcroft, N. David. Mermin, Franck. Biet, Hamid. Kachkachi, and Impr. Jouve). *Physique des solides*. EDP sciences, 2002.

[72] C Fourment, F Deneuville, D Descamps, F Dorchies, S Petit, O Peyrusse, B Holst, and V Recoules. Experimental determination of temperature-dependent electron-electron collision frequency in isochorically heated warm dense gold. *PHYSICAL REVIEW B*, 89, 2014.

[73] C. A. Ullrich, P.-G. Reinhard, and E. Suraud. Simplified implementation of self-interaction correction in sodium clusters. *Physical Review A*, 62(5):053202, oct 2000.

[74] D. R. Hartree. The Wave Mechanics of an Atom with a Non-Coulomb Central Field. Part I. Theory and Methods. *Mathematical Proceedings of the Cambridge Philosophical Society*, 24(01):89, jan 1928.

[75] J. C. Slater. The Theory of Complex Spectra. *Physical Review*, 34(10):1293–1322, nov 1929.

[76] V. Fock. Näherungsmethode zur Lösung des quantenmechanischen Mehrkörperproblems. *Zeitschrift für Physik*, 61(1-2):126–148, jan 1930.

[77] F. Villars. Adiabatic time-dependent Hartree-Fock theory in nuclear physics. *Nuclear Physics A*, 285(2):269–296, 1977.

[78] E.J. Baerends, D.E. Ellis, and P. Ros. Selfconsistent molecular Hartree-Fock-Slater calculations I. The computational procedure. *Chemical Physics*, 2(1):41–51, 1973.

[79] W. Kohn and L. J. Sham. Self-Consistent Equations Including Exchange and Correlation Effects. *Physical Review*, 140(4A):A1133–A1138, nov 1965.

[80] P. Hohenberg and W. Kohn. Inhomogeneous Electron Gas. *Physical Review*, 136(3B):B864–B871, nov 1964.

[81] R. O. Jones. Density functional theory: Its origins, rise to prominence, and future. *Reviews of Modern Physics*, 87(3):897–923, aug 2015.

[82] Erich Runge and E. K. U. Gross. Density Functional Theory for Time Dependent Systems. *Physical Review Letters*, 52(12):997–1000, mar 1984.

[83] E. Wigner. On the Quantum Correction For Thermodynamic Equilibrium. *Physical Review*, 40(5):749–759, jun 1932.

[84] H. Weyl. Quantenmechanik und Gruppentheorie. *Zeitschrift für Physik*, 46(1-2):1–46, 1927.

[85] Leon Cohen. *The Weyl Operator and its Generalization*. Springer Basel, Basel, 2013.

[86] J. E. Moyal, M. S. Bartlett, E. Wigner, N. H. McCoy, P. A. M. Dirac, H.J. Groenewold, and R. P. Feynman. Quantum mechanics as a statistical theory. *Mathematical Proceedings of the Cambridge Philosophical Society*, 45(01):99, jan 1949.

[87] O. T. Serimaa, J. Javanainen, and S. Varró. Gauge-independent Wigner functions: General formulation. *Physical Review A*, 33(5):2913–2927, may 1986.

[88] Kodi Husimi. Some Formal Properties of the Density Matrix. *Proceedings of the Physico-Mathematical Society of Japan. 3rd Series*, 22(4):264–314, 1940.

[89] R. Jasiak, G. Manfredi, and P.-A. Hervieux. Electron thermalization and quantum decoherence in metal nanostructures. *Physical Review B*, 81(24):241401, jun 2010.

[90] Robert N. Wilson, Walter I. Futterman, and John T. Yue. Derivation of the Vlasov Equation. *Physical Review A*, 3(1):453–470, jan 1971.

[91] R L Stratonovich. On The Statistical Interpretation of Quantum Theory. 5(32):1483–1495, 1957.

[92] M Müller. Product rule for gauge invariant Weyl symbols and its application to the semiclassical description of guiding centre motion. *Journal of Physics A: Mathematical and General*, 32(6):1035–1052, 1999.

[93] E. Madelung. Quantentheorie in hydrodynamischer Form. *Zeitschrift für Physik*, 40(3-4):322–326, mar 1927.

[94] David Bohm. A Suggested Interpretation of the Quantum Theory in Terms of "Hidden" Variables. I. *Physical Review*, 85(2):166–179, jan 1952.

[95] Zhenning Cai, Yuwei Fan, Ruo Li, Tiao Lu, and Yanli Wang. Quantum hydrodynamic model by moment closure of Wigner equation. *Journal of Mathematical Physics*, 53(10):103503, 2012.

[96] G. Manfredi, P.-A. Hervieux, Y. Yin, and N. Crouseilles. Collective Electron Dynamics in Metallic and Semiconductor Nanostructures. pages 1–44. Springer Berlin Heidelberg, 2010.

[97] Yu L Klimontovich and Viktor P Silin. the spectra of systems of interacting particles and collective energy losses during passage of charged particles through matter. *Soviet Physics Uspekhi*, 3(1):84–114, jan 1960.

[98] Yu. Tyshetskiy, S. V. Vladimirov, and R. Kompaneets. On kinetic description of electromagnetic processes in a quantum plasma. *Physics of Plasmas*, 18(11):112104, 2011.

[99] Ling-Hsiao Lyu. *Elementary Space Plasma Physics*. Taiwan, R.O.C., second edition, 2014.

[100] James E. Drummond. *Plasma physics*.

[101] G. Manfredi and F. Haas. Self-consistent fluid model for a quantum electron gas. *Physical Review B*, 64(7):075316, jul 2001.

[102] Walther Gerlach and Otto Stern. Der experimentelle Nachweis der Richtungsquantelung im Magnetfeld. *Zeitschrift für Physik*, 9(1):349–352, dec 1922.

[103] Leslie L. Foldy and Siegfried A. Wouthuysen. On the Dirac Theory of Spin 1/2 Particles and Its Non-Relativistic Limit. *Physical Review*, 78(1):29–36, apr 1950.

[104] Paul Strange. *Relativistic quantum mechanics : with applications in condensed matter and atomic physics*. Cambridge University Press, 1998.

[105] Y. Hinschberger and P.-A. Hervieux. Foldy–Wouthuysen transformation applied to the interaction of an electron with ultrafast electromagnetic fields. *Physics Letters A*, 376(6):813–819, 2012.

[106] Ritwik Mondal, Marco Berritta, Karel Carva, and Peter M. Oppeneer. Ab initio investigation of light-induced relativistic spin-flip effects in magneto-optics. *Physical Review B*, 91(17):174415, may 2015.

[107] Ritwik Mondal, Marco Berritta, and Peter M. Oppeneer. Relativistic theory of spin relaxation mechanisms in the Landau-Lifshitz-Gilbert equation of spin dynamics. *Physical Review B*, 94(14):144419, oct 2016.

[108] Luigi Barletti. Wigner Envelope Functions for Electron Transport in Semiconductor Devices. *Transport Theory and Statistical Physics*, 32(3-4):253–277, jan 2003.

[109] O Morandi and F Schürrer. Wigner model for quantum transport in graphene. *Journal of Physics A: Mathematical and Theoretical*, 44(26):265301, jul 2011.

[110] Mattias Marklund, Jens Zamanian, and Gert Brodin. Spin Kinetic Theory—Quantum Kinetic Theory in Extended Phase Space. *Transport Theory and Statistical Physics*, 39(5-7):502–523, mar 2010.

[111] Jérôme Hurst, Omar Morandi, Giovanni Manfredi, and Paul-Antoine Hervieux. Semiclassical Vlasov and fluid models for an electron gas with spin effects. *The European Physical Journal D*, 68(6):176, jun 2014.

[112] Giovanni Manfredi. Non-relativistic limits of Maxwell's equations. *European Journal of Physics*, 34(4):859–871, jul 2013.

[113] J. P. Perdew and Alex Zunger. Self-interaction correction to density-functional approximations for many-electron systems. *Physical Review B*, 23(10):5048–5079, may 1981.

[114] J Kubler, K H Hock, J Sticht, and A R Williams. Density functional theory of non-collinear magnetism. *Journal of Physics F: Metal Physics*, 18(3):469–483, mar 1988.

[115] F. G. Eich and E. K. U. Gross. Transverse Spin-Gradient Functional for Noncollinear Spin-Density-Functional Theory. *Physical Review Letters*, 111(15):156401, oct 2013.

[116] M. T. Entwistle, M. J. P. Hodgson, J. Wetherell, B. Longstaff, J. D. Ramsden, and R. W. Godby. Local density approximations from finite systems. *Physical Review B*, 94(20):205134, nov 2016.

[117] J. Zamanian, M. Marklund, and G. Brodin. Exchange effects in plasmas: The case of low-frequency dynamics. *Physical Review E*, 88(6):063105, dec 2013.

[118] L. H. Thomas. The Motion of the Spinning Electron. *Nature*, 117(2945):514–514, 1926.

[119] Andrzej Dragan and Tomasz Odrzygóźdź. A half-page derivation of the Thomas precession. *American Journal of Physics*, 81(8):631, 2013.

[120] G Brodin and M Marklund. Spin magnetohydrodynamics. *New Journal of Physics*, 9(8):277–277, aug 2007.

[121] Felipe A. Asenjo, Victor Muñoz, J. Alejandro Valdivia, and Swadesh M. Mahajan. A hydrodynamical model for relativistic spin quantum plasmas. *Physics of Plasmas*, 18(1):012107, 2011.

[122] Giuseppe Alì, Giovanni Mascali, Vittorio Romano, and Rosa Claudia Torcasio. A Hydrodynamic Model for Covalent Semiconductors with Applications to GaN and SiC. *Acta Applicandae Mathematicae*, may 2012.

[123] M Trovato and L Reggiani. Quantum hydrodynamic models from a maximum entropy principle. *Journal of Physics A: Mathematical and Theoretical*, 43(10):102001, mar 2010.

[124] Vittorio Romano. Non-parabolic band hydrodynamical model of silicon semiconductors and simulation of electron devices. *Mathematical Methods in the Applied Sciences*, 24(7):439–471, may 2001.

[125] G. Manfredi and M. R. Feix. Entropy and Wigner functions. *Physical Review E*, 62(4):4665–4674, oct 2000.

[126] Pierre Degond, Samy Gallego, Florian Méhats, and Christian Ringhofer. Quantum Hydrodynamic and Diffusion Models Derived from the Entropy Principle. pages 111–168. Springer Berlin Heidelberg, 2008.

[127] G Brodin, M Marklund, J Zamanian, and M Stefan. Spin and magnetization effects in plasmas. *Plasma Physics and Controlled Fusion*, 53(7):074013, jul 2011.

[128] Omar Morandi, Jens Zamanian, Giovanni Manfredi, and Paul-Antoine Hervieux. Quantum-relativistic hydrodynamic model for a spin-polarized electron gas interacting with light. *Physical Review E*, 90(1):013103, jul 2014.

[129] Lev Landau and Evguéni. Lifchitz. *Physique statistique*. Éd. Mir, 1994.

[130] A. A. Vlasov. On the oscillation properties of an electron gas. *Zh. Eksp. Teor. Fiz.*, 8:291–318, 1938.

[131] Lev Davidovich Landau. On the vibrations of the electronic plasma. *Zh. Eksp. Teor. Fiz.*, 10:25, 1946.

[132] Uwe Kreibig and Michael Vollmer. *Optical properties of metal clusters*. Springer, 1995.

[133] Yoochan Hong, Yong-Min Huh, Dae Sung Yoon, and Jaemoon Yang. Nanobiosensors Based on Localized Surface Plasmon Resonance for Biomarker Detection. *Journal of Nanomaterials*, 2012:1–13, 2012.

[134] Peter A. (Peter Andrew) Sturrock and Peter Andrew. *Plasma physics : an introduction to the theory of astrophysical, geophysical, and laboratory plasmas*. Cambridge University Press, 1994.

[135] O. Gunnarsson and B. I. Lundqvist. Exchange and correlation in atoms, molecules, and solids by the spin-density-functional formalism. *Physical Review B*, 13(10):4274–4298, may 1976.

[136] Burton D. Fried and Samuel Daniel Conte. *The plasma dispersion function : the Hilbert transform of the Gaussian*. Academic Press, 1961.

[137] P Kravanja, M Van Barel, O Ragos, M N Vrahatis, and F A Zafiropoulos. ZEAL: A mathematical software package for computing zeros of analytic functions. *Computer Physics Communications*, 124(124):212–232, 2000.

[138] William Jones and Norman H. (Norman Henry) March. *Theoretical solid state physics*. Dover Publications, 1985.

[139] Yue Yin, Paul-Antoine Hervieux, Rodolfo A. Jalabert, Giovanni Manfredi, Emmanuel Maurat, and Dietmar Weinmann. Spin-dependent dipole excitation in alkali-metal nanoparticles. *Physical Review B*, 80(11):115416, sep 2009.

[140] John F. Dobson. Electron gas boundary properties in non-neutral jellium (wide parabolic quantum well) systems. *Physical Review B*, 46(16):10163–10172, oct 1992.

[141] Jérôme Daligault. Landau damping and the onset of particle trapping in quantum plasmas. *Physics of Plasmas*, 21(4):040701, apr 2014.

[142] A Mushtaq and D B Melrose. Quantum effects on the dispersion of ion acoustic waves.

[143] Shane Rightley and Dmitri Uzdensky. Landau damping of electrostatic waves in arbitrarily degenerate quantum plasmas. *Physics of Plasmas*, 23(3):030702, mar 2016.

[144] G. Manfredi and P.-A. Hervieux. Vlasov simulations of electron dynamics in metallic nanostructures. *Computational Materials Science*, 35(3):327–331, 2006.

[145] Charles Kittel and Paul McEuen. *Introduction to solid state physics*, volume 8. Wiley, 1986.

[146] J. Stöhr. *MagnetismFrom Fundamentals to Nanoscale Dynamics*. Springer, 2006.

[147] L. D. Landau and E. M. Lifshitz. On the theory of the dispersion of magnetic permeability in ferromagnetic bodies. *Phys. Z. Sowietunion*, 8(153), 1935.

[148] R F L Evans, W J Fan, P Chureemart, T a Ostler, M O a Ellis, and R W Chantrell. Atomistic spin model simulations of magnetic nanomaterials. *Journal of physics. Condensed matter : an Institute of Physics journal*, 26(10):103202, mar 2014.

[149] Wolfgang Nolting and Anupuru. Ramakanth. *Quantum theory of magnetism*. Springer, 2008.

[150] M. A. Ruderman and C. Kittel. Indirect Exchange Coupling of Nuclear Magnetic Moments by Conduction Electrons. *Physical Review*, 96(1):99–102, oct 1954.

[151] C. Zener. Interaction Between the d Shells in the Transition Metals. *Physical Review*, 81(3):440–444, feb 1951.

[152] M. Lakshmanan. The fascinating world of the Landau–Lifshitz–Gilbert equation: an overview. *Philosophical Transactions of the Royal Society of London A: Mathematical, Physical and Engineering Sciences*, 369(1939), 2011.

[153] M. Lakshmanan, Th.W. Ruijgrok, and C.J. Thompson. On the dynamics of a continuum spin system. *Physica A: Statistical Mechanics and its Applications*, 84(3):577–590, 1976.

[154] Nammee Kim, H. Kim, J. W. Kim, S. J. Lee, and T. W. Kang. Numerical self-consistent field calculation of a ferromagnetic ZnMnO quantum well. *Physical Review B*, 74(15):155327, oct 2006.

[155] Bernard Diu. *Elements de physique statistique*. Hermann, 1989.

[156] Serigne Bira Gueye. The Exact Formulation of the Inverse of the Tridiagonal Matrix for Solving the 1D Poisson Equation with the Finite Difference Method. *Journal of Electromagnetic Analysis and Applications*, 06(10):303–308, 2014.

[157] C.Z Cheng and Georg Knorr. The integration of the vlasov equation in configuration space. *Journal of Computational Physics*, 22(3):330–351, 1976.

[158] Arbab Rahim, Carlo Ragusa, Bilal Jan, and Omar Khan. A mixed mid-point Runge-Kutta like scheme for the integration of Landau-Lifshitz equation. *Journal of Applied Physics*, 115(17):17D101, may 2014.

[159] Eric Fijalkow. A numerical solution to the Vlasov equation. *Computer Physics Communications*, 116(2):319–328, 1999.

[160] Francis Filbet, Eric Sonnendrücker, and Pierre Bertrand. Conservative Numerical Schemes for the Vlasov Equation. *Journal of Computational Physics*, 172(1):166–187, 2001.

[161] R. Courant, K. Friedrichs, and H. Lewy. On the Partial Difference Equations of Mathematical Physics. *IBM Journal of Research and Development*, 11(2):215–234, mar 1967.

[162] M. Navet and P. Bertrand. Multiple "water-bag" model and Landau damping. *Physics Letters A*, 34(2):117–118, 1971.

[163] David Coulette, Sever A Hirstoaga, and Giovanni Manfredi. Effect of collisional temperature isotropisation on ELM parallel transport in a tokamak scrape-off layer. *Plasma Physics and Controlled Fusion*, 58(8):085004, aug 2016.

[164] Cristian Ciracì, John B. Pendry, and David R. Smith. Hydrodynamic Model for Plasmonics: A Macroscopic Approach to a Microscopic Problem. *ChemPhysChem*, 14(6):1109–1116, apr 2013.

[165] D. Michta, F. Graziani, and M. Bonitz. Quantum Hydrodynamics for Plasmas - a Thomas-Fermi Theory Perspective. *Contributions to Plasma Physics*, 55(6):437–443, jun 2015.

[166] A. D. Becke. Density-functional exchange-energy approximation with correct asymptotic behavior. *Physical Review A*, 38(6):3098–3100, sep 1988.

[167] C. Bréchignac, Ph Cahuzac, J. Leygnier, and A. Sarfati. Optical response of large lithium clusters: Evolution toward the bulk. *Physical Review Letters*, 70(13):2036–2039, mar 1993.

[168] J. G. Aguilar, A. Mañanes, F. Duque, M. J. López, M. P. Iñiguez, and J. A. Alonso. Ionic vibrational breathing mode of metallic clusters. *International Journal of Quantum Chemistry*, 61(4):613–626, 1997.

[169] B. Meerson and L. Friedland. Strong autoresonance excitation of Rydberg atoms: The Rydberg accelerator. *Physical Review A*, 41(9):5233–5236, may 1990.

[170] Wing-Ki Liu, Binruo Wu, and Jian-Min Yuan. Nonlinear Dynamics of Chirped Pulse Excitation and Dissociation of Diatomic Molecules. *Physical Review Letters*, 75(7):1292–1295, aug 1995.

[171] L. Friedland. Control of Kirchhoff vortices by a resonant strain. *Physical Review E*, 59(4):4106–4111, apr 1999.

[172] J. Fajans, E. Gilson, and L. Friedland. Autoresonant (Nonstationary) Excitation of the Diocotron Mode in Non-neutral Plasmas. *Physical Review Letters*, 82(22):4444–4447, may 1999.

[173] Igor Aranson, Baruch Meerson, and Toshiki Tajima. Excitation of solitons by an external resonant wave with a slowly varying phase velocity. *Physical Review A*, 45(10):7500–7510, may 1992.

[174] L. Friedland and A. G. Shagalov. Excitation of Solitons by Adiabatic Multiresonant Forcing. *Physical Review Letters*, 81(20):4357–4360, nov 1998.

[175] R. Malhotra and R. Migrating planets. *Scientific American, Vol. 281, No. 3, p. 46 - 53*, 281:46–53, 1999.

[176] L Friedland. Migration timescale thresholds for resonant capture in the Plutino problem. *The Astrophysical Journal*, 547:75–79, 2001.

[177] G. B. et al. Andresen. Autoresonant Excitation of Antiproton Plasmas. *Physical Review Letters*, 106(2):025002, jan 2011.

[178] I Barth, L Friedland, O Gat, and A G Shagalov. Quantum versus classical phase-locking transition in a frequency-chirped nonlinear oscillator. *PHYSICAL REVIEW A*, 84, 2011.

[179] G. Manfredi and P.-A. Hervieux. Autoresonant control of the many-electron dynamics in nonparabolic quantum wells. *Applied Physics Letters*, 91(6):061108, aug 2007.

[180] Guillaume Weick. *Quantum dissipation and decoherence of collective excitations in metallic nanoparticles*. PhD thesis, 2006.

[181] M. Kundu and D. Bauer. Nonlinear Resonance Absorption in the Laser-Cluster Interaction. *Physical Review Letters*, 96(12):123401, mar 2006.

[182] Ruben Esteban, Andrei G. Borisov, Peter Nordlander, and Javier Aizpurua. Bridging quantum and classical plasmonics with a quantum-corrected model. *Nature Communications*, 3:825, may 2012.

[183] Gustav Mie. Beiträge zur Optik trüber Medien, speziell kolloidaler Metallösungen. *Annalen der Physik*, 330(3):377–445, 1908.

[184] Thomas Reiners, Christoph Ellert, Martin Schmidt, and Hellmut Haberland. Size Dependence of the Optical Response of Spherical Sodium Clusters. *Physical Review Letters*, 74(9):1558–1561, feb 1995.

[185] L. Brey, Jed Dempsey, N. F. Johnson, and B. I. Halperin. Infrared optical absorption in imperfect parabolic quantum wells. *Physical Review B*, 42(2):1240–1247, jul 1990.

[186] M. Madjet, C. Guet, and W. R. Johnson. Comparative study of exchange-correlation effects on the electronic and optical properties of alkali-metal clusters. *Physical Review A*, 51(2):1327–1339, feb 1995.

[187] M. Maier, G. Wrigge, M. Astruc Hoffmann, P. Didier, and B. v. Issendorff. Observation of Electron Gas Cooling in Free Sodium Clusters. *Physical Review Letters*, 96(11):117405, mar 2006.

[188] Jaideva C. Goswami and Albert E. Hoefel. Algorithms for estimating instantaneous frequency. *Signal Processing*, 84(8):1423–1427, 2004.

[189] John David Jackson. *Classical electrodynamics*. Wiley, 1999.

[190] J. Nappa, G. Revillod, I. Russier-Antoine, E. Benichou, C. Jonin, and P. F. Brevet. Electric dipole origin of the second harmonic generation of small metallic particles. *Physical Review B*, 71(16):165407, apr 2005.

[191] Ferenc Krausz and Misha Ivanov. Attosecond physics. *Reviews of Modern Physics*, 81(1):163–234, feb 2009.

[192] C. N. Ramachandra Rao, Giridhar U. Kulkarni, P. John Thomas, and Peter P. Edwards. Metal nanoparticles and their assemblies. *Chemical Society Reviews*, 29(1):27–35, 2000.

[193] P. et al. Zoller. Quantum information processing and communication. *The European Physical Journal D*, 36(2):203–228, nov 2005.

[194] Walter Kohn. Cyclotron Resonance and de Haas-van Alphen Oscillations of an Interacting Electron Gas. *Physical Review*, 123(4):1242–1244, aug 1961.

[195] John F Dobson. Harmonic-Potential Theorem: Implications for Approximate Many-Body Theories. 73(16), 1994.

[196] Tokuei Sako, Paul-Antoine Hervieux, and Geerd H. F. Diercksen. Distribution of oscillator strength in Gaussian quantum dots: An energy flow from center-of-mass mode to internal modes. *Physical Review B*, 74(4):045329, jul 2006.

[197] Sebastian Schröter, Paul-Antoine Hervieux, Giovanni Manfredi, Johannes Eiglsperger, and Javier Madroñero. Exact treatment of planar two-electron quantum dots: Effects of anharmonicity on the complexity. *Physical Review B*, 87(15):155413, apr 2013.

[198] Marcel Reginatto. Derivation of the Pauli equation using the principle of minimum Fisher information. *Physics Letters A*, 249(5):355–357, 1998.

UNIVERSITÉ DE STRASBOURG

Jérôme HURST

Ultrafast spin dynamics in ferromagnetic thin films

Résumé

Dans cette thèse, on s'intéresse à l'étude théorique et à la simulation numérique de la dynamique de charges et de spins dans des nano-structures métalliques. Ces dernières années la physique des nano-structures métalliques à connu un intérêt croissant, aussi bien d'un point de vue de la physique fondamental que d'un point de vue des applications technologiques. Il est donc essentiel d'avoir des modèles théoriques nous permettant de décrire correctement ce type d'objets. Cette thèse comporte deux études distinctes. Dans un premier temps on utilise un modèle semi-classique dans l'espace des phases afin d'étudier la dynamique de charges et de spins dans des films ferromagnétiques (Nickel). On décrit dans le même modèle le magnétisme itinérant et le magnétisme localisé. On montre qu'il est possible, en excitant le système avec un laser pulsé femtoseconde dans le domaine du visible, de créer un courant de spin oscillant dans la direction normal du film sur des temps ultra-rapides (femtoseconde). Dans un second temps on s'intéresse à la dynamique de charge d'électrons confinés dans des nano-particules d'Or ou bien encore par des potentiels anisotropes. On montre que de telles systèmes sont des candidats intéressant pour faire de la génération d'harmoniques.

Mots-clés : Dynamique de spin, magnétisme ultra-rapide, Méthode dans l'espace des phases, Équations de Wigner/Vlasov, Courant de spin, Dynamique non linéaire, Approche variationnelle, Génération d'harmoniques.

Résumé en anglais

In this thesis we focus on the theoritical description and on the numerical simulation of the charge and spin dynamics in metallic nano-structures. The physics of metallic nano-structures has stimulated a huge amount of scientific interest in the last two decades, both for fundamental research and for potential technological applications. The thesis is divided in two parts. In the first part we use a semiclassical phase-space model to study the ultrafast charge and spin dynamics in thin ferromagnetic films (Nickel). Both itinerant and localized magnetism are taken into account. It is shown that an oscillating spin current can be generated in the film via the application of a femtosecond laser pulse in the visible range. In the second part we focus on the charge dynamics of electrons confined in metallic nano-particles (Gold) or anisotropic wells. We show that such systems can be used for high harmonic generation.

Keywords : Spin dynamics, Ultrafast magnetism, Phase-space methods, Wigner/Vlasov equation, Spin current, Nonlinear dynamics, Variational approach, High harmonic generation.